PhD Thesis

School of Chemistry

Cardiff University

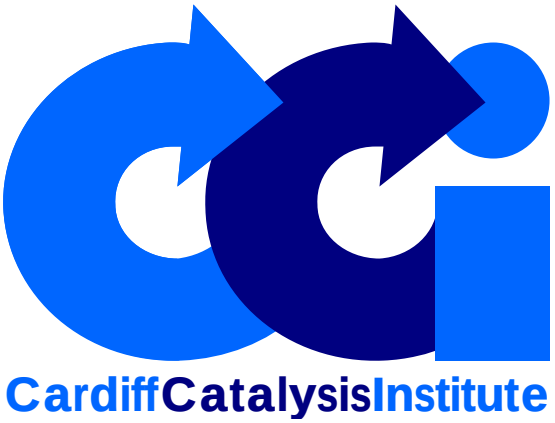

The Direct Synthesis of Hydrogen Peroxide Using Bimetallic, Gold and Palladium, Supported Catalysts

Thesis submitted in accordance with the requirements of the University of Cardiff for the degree of doctor in philosophy by:

Greg Shaw

2013

DECLARATION

This work has not been submitted in substance for any other degree or award at this or any other university or place of learning, nor is being submitted concurrently in candidature for any degree or other award.

Signed …… (candidate) Date ……

STATEMENT 1

This thesis is being submitted in partial fulfilment of the requirements for the degree of PhD

Signed …… (candidate) Date ……

STATEMENT 2

This thesis is the result of my own independent work/investigation, except where otherwise stated. Other sources are acknowledged by explicit references. The views expressed are my own.

Signed …… (candidate) Date ……

STATEMENT 3

I hereby give consent for my thesis, if accepted, to be available for photocopying and for inter-library loan, and for the title and summary to be made available to outside organisations.

Signed …… (candidate) Date ……

STATEMENT 4: PREVIOUSLY APPROVED BAR ON ACCESS

I hereby give consent for my thesis, if accepted, to be available for photocopying and for inter-library loans **after expiry of a bar on access previously approved by the Academic Standards & Quality Committee.**

Signed …… (candidate) Date ……

Summary

In this thesis the direct synthesis of hydrogen peroxide from hydrogen and oxygen using gold-palladium supported catalysts is described. The direct route presents a greener and sustainable alternative to the current industrial manufacture process. This work aims to meet industrial requirements set by Solvay® which would make the direct process industrially viable.

The drawback preventing the requirements being met is the reaction of hydrogen and oxygen over a catalyst can yield water as well as hydrogen peroxide. Once H_2O_2 is formed, it can be consumed by either reduction or decomposition. Thus, the rates of the subsequent reactions must be minimized to increase the selectivity and therefore H_2O_2 concentration to a desirable level. Aspects of the catalyst design and reaction variables have been studied over three results chapters.

Firstly, the thermal treatment conditions have been altered, ultimately producing a catalyst with no activity to the H_2O_2 consumption under standard conditions. Switching off H_2O_2 hydrogenation was concluded to be due to an increase in Pd^{2+}, isolating active Pd^0 species.

Secondly, active catalysts to both the synthesis and hydrogenation of H_2O_2 have been produced with no halide; the addition of halide has been shown to decrease hydrogenation activity while maintaining synthesis activity.

Finally, a biphasic solvent system and a constant flow of gases through the reaction medium have been examined in order to produce higher H_2O_2 concentrations. In the former case H_2O_2 is extracted *in-situ* from an immiscible organic phase. The production of a 3 wt% H_2O_2 solution highlights the potential of such a system. In the latter case a semi-continuous flow reactor is utilised increasing the H_2O_2 concentration up to *ca.* 1 wt% (from *ca.* 0.2 wt%). The reactor allowed H_2 selectivity and H_2O concentration to be measured as a function of time, thus providing greater insight into catalyst activity.

Acknowledgements

I would like to express my gratitude to Professor Graham Hutchings, my research supervisor, who not only provided me with this opportunity, but gave invaluable guidance, encouragement and useful critiques throughout this research work.

I would also like to thank Dr. Jennifer Edwards, for her advice and assistance throughout my three years of laboratory work and during the writing of this thesis. My grateful thanks are also extended to Dr. Albert Carley and Dr. David Morgan for their help with extensive X-ray photoelectron analysis; the team at Lehigh University in particular Professor Chris Kiely and Dr. Qian He who provided the electron microscopy characterisation; and Dr. Pelham Hawker, Dr. David Harrison and Dr. Jacob Moulijn for their useful and constructive recommendations on this project. I gratefully acknowledge all the staff in the chemistry department at Cardiff University who have helped with all enquires and allowed this project to run smoothly.

I wish to acknowledge Solvay® for their support and contribution to this project. My special thanks are extended to all the staff and students at Solvay NOH who helped me greatly during a 6 month secondment to Brussels, in particular Jean-Pierre Ganhy for his extensive guidance and support.

I would like to express my appreciation to all the students, postdocs and staff in the CCI for their constant help and suggestions throughout this work. Special thanks goes to Dr. Simon Kondrat and Dr. Peter Medizak for their assistance and guidance during the physical grinding work; and all of the *'hydrogen peroxide team'*, Dr Marco Piccinini, James Pritchard, Simon Freakley, Yingyu Wang and Adeeba Akram.

Last but not least I would like to thank all of my family and friends who I will always be indebted to for the love and support they have provided, without them this wouldn't have been possible.

CONTENTS

- CHAPTER ONE -

Introduction

1.1 General Introduction

The existence of a new force, which was called a 'catalytic force', was first published in a report, in 1836, by J. J. Berzelius.[1] While creating a report summarising the progress of the whole of chemistry, for the Stockholm Academy of Sciences, he reviewed a number of earlier findings on chemical change in both heterogeneous and homogeneous systems. He was able to show that these could be rationally co-ordinated by the introduction of a new concept which he called catalysis. He summarised his ideas on catalysis as a new force by writing:

''It is, then, proved that several simple or compound bodies, soluble and insoluble, have the property of exercising on other bodies an action very different from chemical affinity. By means of this action they produce, in these bodies, decompositions of their elements and different recombinations of these same elements to which they remain indifferent.''

Some of the early work which was summarised by Berzelius was done by a French scientist called Louis Jacques Thénard.[1] He observed that a chemical substance can speed up a chemical reaction without itself, at the end of the reaction, being chemically changed. This became clear as he researched the decomposition of hydrogen peroxide in the presence of various solids. He also found that the action of metals in bringing about decomposition became more vigorous as the metal was reduced to a finer state of subdivision.

Thénard had previously discovered the existence of hydrogen peroxide in 1818 when he was working on the reaction of barium peroxide with nitric or hydrochloric acid.[2] The following thesis concentrates on the synthesis of hydrogen peroxide directly from H_2 and O_2, by catalysis, with a view to making its production 'greener' and as a result increasing its contribution to 'Green Chemistry'.

1.1.1 Green Chemistry

Green chemistry, also known as sustainable chemistry, is the design, manufacture and application of chemical products that reduce or eliminate the use or generation of substances that are hazardous to human health and the environment. It is a science-based non-regulatory, economically driven approach toward sustainable development that has grown substantially since the concept fully emerged in the 1990's.[3] Today, the following 12 Principles of Green Chemistry developed by Paul Anastas and John, C., Warner,[4] are used as a guideline and criteria by chemical scientists.

1. **Prevention** – It is better to prevent waste than to treat or clean up waste after it has been created.
2. **Atom Economy** – Synthetic methods should be designed to maximise the incorporation of all materials used in the process into the final product.
3. **Less Hazardous Chemical Synthesis** – Wherever practicable, synthetic methods should be designed to use and generate substances that possess little or no toxicity to human health and the environment.
4. **Designing Safer Chemicals** – Chemical products should be designed to affect their desired function while minimising their toxicity.
5. **Safer Solvents and Auxiliaries** – The use of auxiliary substances (e.g. solvents, separation agents, etc) should be made unnecessary wherever possible and innocuous when used.
6. **Design for Energy Efficiency** – Energy requirements of chemical processes should be recognised for their environmental and economic impacts and should be minimised. If possible, synthetic methods should be conducted at ambient temperature and pressure.
7. **Use of Renewable Feedstock's** – A raw material or feedstock should be renewable rather than depleting whenever technically and economically practicable.
8. **Reduce Derivatives** – Unnecessary derivatisation (use of blocking groups, protection /de-protection, temporary modification of physical/chemical processes) should be

minimised or avoided if possible, because such steps require additional reagents and can generate waste.

9. **Catalysis** – Catalytic reagents (as selective as possible) are superior to stoichiometric reagents.

10. **Design and Degradation** – Chemical products should be designed so that at the end of their function they break down into innocuous degradation products and do not persist in the environment.

11. **Real – Time anyalysis for Pollution Prevention** – Analytical methodologies need to be further developed to allow for real-time, in process monitoring and control prior to the formation of hazardous substances.

12. **Inherently Safer Chemistry for Accident Prevention** – Substances and the form of a substance used in a chemical process should be chosen to minimise the potential for chemical accidents, including releases, explosions and fires.

In 2005, Ryoji Noyori[5] (Nobel laureate in chemistry, 2001) identified three key developments in green chemistry: (1) use of supercritical carbon dioxide as green solvent; (2) using aqueous hydrogen peroxide for clean oxidations and (3) use of hydrogen in asymmetric synthesis.

1.2 Catalysis

Today catalysis is defined as the acceleration (or deceleration) of a chemical reaction due to the presence of a catalyst. Where a catalyst is a substance that increases the rate of a chemical reaction (k) by reducing the activation energy (E_a), but which is left unchanged chemically at the end of the reaction. The catalyst lowers the activation energy of the reaction by providing an alternative path that avoids the slow, rate determining step of the un-catalysed reaction. The rate constant of such a reaction can be expressed using the Arrhenius rate law:

$$k = Ae^{-E_a/RT}$$

R - molar gas constant

T - absolute temperature

A - pre-exponential factor

E_a - activation energy

k - rate constant

Biological catalysts called enzymes are at the pinnacle of catalytic power and all synthetic catalysts strive to emulate them. For example, splitting hydrogen and oxygen from water using conventional electrolysis techniques requires considerable amounts of electrical energy. But green plants produce oxygen from water efficiently using a catalytic technique powered by sunlight, a process that is part of photosynthesis and so effective that it is Earth's major source of oxygen.

Formation of byproducts in various sectors of the chemical industry makes current processes non-environmentally benign. The fine chemical and pharmaceutical sectors have a very high impact on the environment and human life, due to the utilisation of conventional multistep syntheses based on using stiochiometric reagents producing large amounts of organic or

inorganic wastes. This is highlighted later in this introduction when dealing with the current manufacture of hydrogen peroxide.

In order to minimise such problems, chemical processes based on reagents need to be replaced by more catalytic dependent routes. Depending upon the phase in which a catalyst exists, it is classified in two types,

Homogeneous catalysis - all the substances are in one single phase; typically everything will be a gas or a single liquid phase.

Heterogeneous catalysis - here the catalyst is in a different phase to the reactants; normally the catalyst is a solid and the reactants are either a gas or liquid.

Catalysis has played a major role in improving quality of life by offering environmentally benign processes for the manufacture of various chemical products in day to day life. Catalysis is a multidisciplinary science that serves a broad range of applications covering speciality, fine, intermediate, and life science chemicals. About 85-90 % of industrial processes are based on catalysis, 80 % of which utilise heterogeneous catalysts.

Heterogeneous catalysts, which are the focus of this report, have a distinct advantage over homogeneous catalysts of easy recovery and recycling. Although colloidal catalysis is sometimes described as heterogeneous catalysis, this thesis does not deal with this topic and will concentrate on metal supported heterogeneous catalysts.

1.2.1 Heterogeneous Catalysts

The availability of bonding sites on the catalyst makes the catalytic process possible. This provides a lower energy pathway for molecules to rearrange their bonds in the breaking and reforming that is required for a chemical reaction, Figure 1.1. In the gas phase the activation energy, $?E_a$, is high largely because energy has to be expended to break bonds, before bond making begins. On the surface, however, the reacting molecules are anchored during the process, always keeping this bonding which stabilises the intermediates in the reaction.

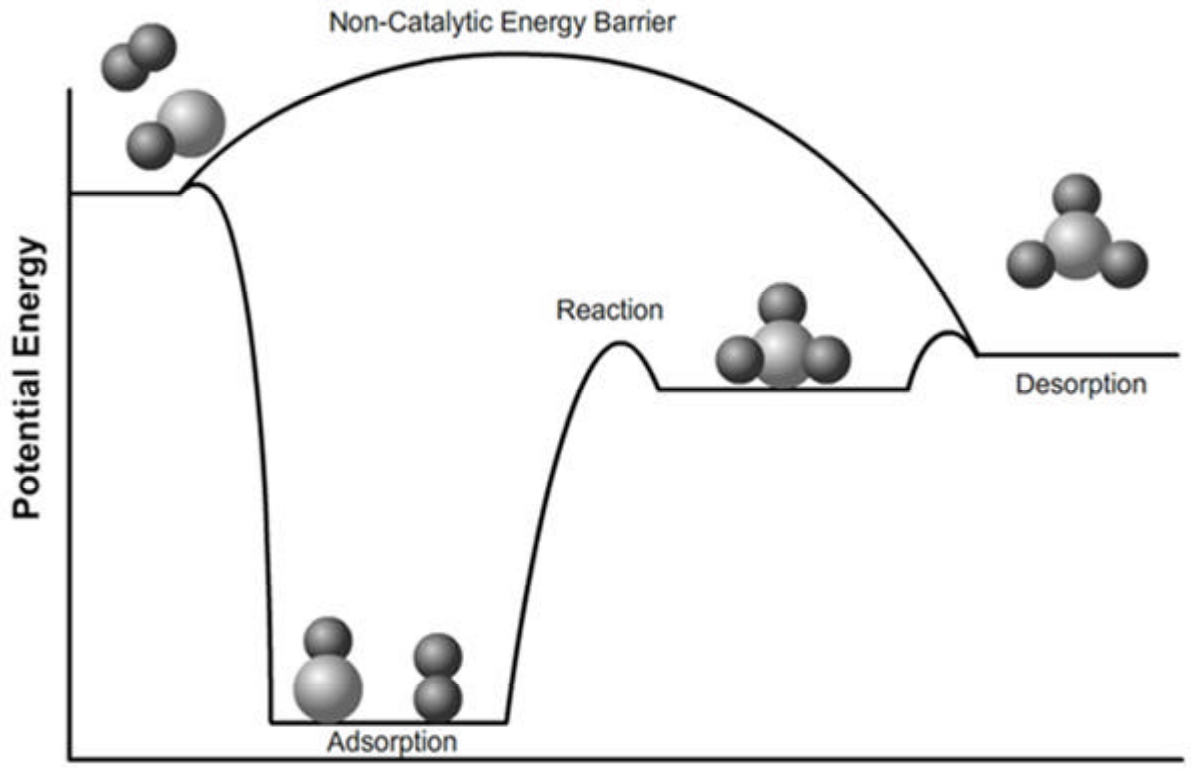

Figure 1.1 - The simplified energetics associated with a catalytic reaction. [6]

The result is that the activation barriers are generally lower than for the un-catalysed process and the reaction is kinetically accelerated. A catalyst, then, enhances reaction rates by lowering activation barriers, speeding the approach to equilibrium, but does not affect the equilibrium concentrations.

A high activity catalyst often requires a large active surface area and thus small particles, i.e. a high dispersion of the active phase. Because small particles, especially small metal particles, tend to sinter at relatively low temperatures, they are generally affixed to a pre-formed support which allows higher dispersion. Catalyst supports are thermally stable and maintain a specific surface area up to high temperatures. Suitable and frequently used supports are metal oxides and carbon, all being compounds with high melting and decomposition temperatures. With these supports other important (physical) features like texture (specific surface area, pore size distribution and pore volume), density and mechanical strength can be established.

A complication is that catalyst particles must have prescribed size and shape to be applicable in a specific reactor and/or to be removable from the liquid-phase by filtration or

centrifugation. Due to this, a large specific surface area can only be attained when support bodies are highly porous, which might conflict with the desired mechanical strength of the texture. Moreover, narrow and long pores might hinder transport of reactants which generally is undesirable. Furthermore, a high porosity might bring along a decreased mechanical strength causing the formation of fines and loss of expensive catalytic material.

With most catalysed reactions the combined chemical properties of the active phase and the support bring about the catalytic functionality. But even when the support material only serves as a vehicle for keeping the catalytically active species separated, these species have to interact in some degree and in some way with the support. And due to this interaction, which nature is often still unknown, the catalytic performance strongly depends on a complex mix-up of contributions of the morphology and dispersion of the active particles and, with metal catalysts, with the electronic properties of the metal.[7, 8]

The main catalysts used in this thesis are based on supported Au and Pd nano-particles.

1.2.2 Preparation of Heterogeneous Catalysts

The preparation of heterogeneous catalysts, complex ensembles of nano-scale active particles consisting of several thousand atoms, fixed onto a support, is complex even when the active site/features required are known. Catalyst preparations can be divided into two classes;

- The support and the metal precursor are formed at the same time – co-precipitation
- The metal precursor is added to a pre-formed support – impregnation, precipitation, reduction, physical mixing etc.

This thesis concentrates on the second class of preparation and minor adjustments of the preparation can significantly influence the delicate balance of conflicting demands: a high activity, a high selectivity and a long lifetime.

1) The concentration of the metal precursor in solution
2) The ratio of its volume and concentration to the mass of the support
3) The type of support
4) The temperature
5) The pH

6) The nature of the base or acid used to change the pH if necessary
7) The time
8) The method of filtration, washing, and drying
9) The conditions of calcination
10) External conditions e.g. light, humidity, temperature etc

Specific preparations of bimetallic catalysts active for the direct synthesis of H_2O_2 are highlighted in section 1.6; however it is important to briefly look at solvated precursors and suitable adsorption sites on the support surface (oxides and carbon).

Metal cations in water lead to the formation of covalent bonds between the central metal cation and the water ligands, charge transfer then promotes hydrolysis. The nature of the species formed with changing pH has been reasonably well studied for gold and palladium compounds.[16]

$$xM^{+}(aq) + yH_2O \rightleftharpoons M_x(OH)_{y(aq)}^{(xn-y)+} + yH^{+}(K_{xy})$$

For example, Gold at high pH has been found to completely hydrolyse;

$$[AuCl_4]^{-} + 4H_2O \rightleftharpoons [Au(OH)_4]^{-} + 4H^{+} + 4Cl^{-}$$

In view of the surface chemistry of the oxidic and carbon supports cationic or anionic metal precursor ions have to be available in a pH range of ~3 to ~9.

Oxides are widely used as pre-formed supports due to their high thermal stability. The surfaces of most oxides are hydroxylated or become hydroxylated upon contact with water. The nature of these sites can be identified by IR spectroscopy.[9, 10] Generally, when dispersed in aqueous solutions the surface of mineral amphoteric oxide particles, such as silica and alumina, become charged; primarily basic OH groups will be involved in reaction (1) and acidic hydroxyl in reaction (2);

(1) $M\text{-}OH + H^{+} \rightleftharpoons M\text{-}OH_2^{+}$

(2) $M\text{-}OH \rightleftharpoons M\text{-}O^- + H^+$

Where M = Si, Ti, Ce etc.

From the above equations it follows that the pH will influence the nature as well as the concentration of the charged surface. The pH value at which the net surface charge (surface and layer around the particle) is zero is referred to as the iso-electric point (IEP). At pH values above the IEP the surface is negatively charged and will adsorb cations, such as $Pd(NH_3)_4^{2+}$. Below the IEP the surface will be positively charged and anionic species, like $PdCl_4^-$, can adsorb.[11]

In addition to oxide materials, carbon supports are very important in catalysis as they have a high surface area (500-1200 m^2/g), low cost and relatively high chemical inertness. However, even after activation, carbon contains a large range of elements in various concentrations, such as hydrogen, oxygen, sulphur and even metal containments which can affect reproducibility/activity of catalysts. The texture of activated carbon is also extremely complex since it involves macro-pores, meso-pores as well as micro-pores.[12-14]

The precise nature of the surface species is not entirely established, it can vary between carbon type and even batches. In general, oxygen containing surface groups are believed to be the most important groups influencing the surface characteristics and adsorption behaviour of activated carbon.[15, 16] Several carbon-oxygen groups have been identified, Figure 1.2.[17]

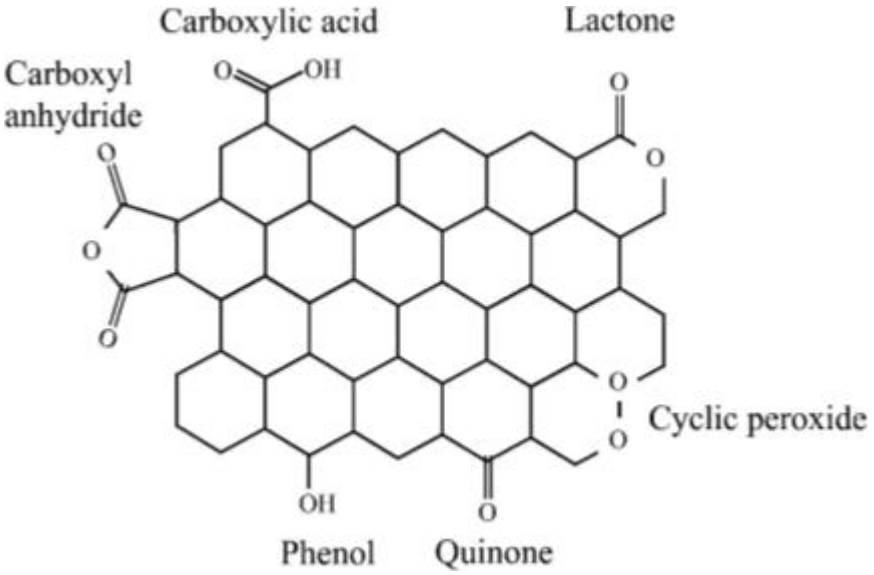

Figure 1.2 - Different types of oxygen containing surface groups on activated carbon.[17]

1.3 Hydrogen peroxide

Hydrogen peroxide is a clear, colourless liquid which is completely miscible with water. It is the simplest peroxide containing a single oxygen-oxygen bond. It has a skewed structure with a dihedral angle of 111.5° in the gas phase, Figure 1.3, which minimises repulsion between the lone pairs and O-H bond pairs. In the liquid and solid state the angle is affected by hydrogen bonding.[2]

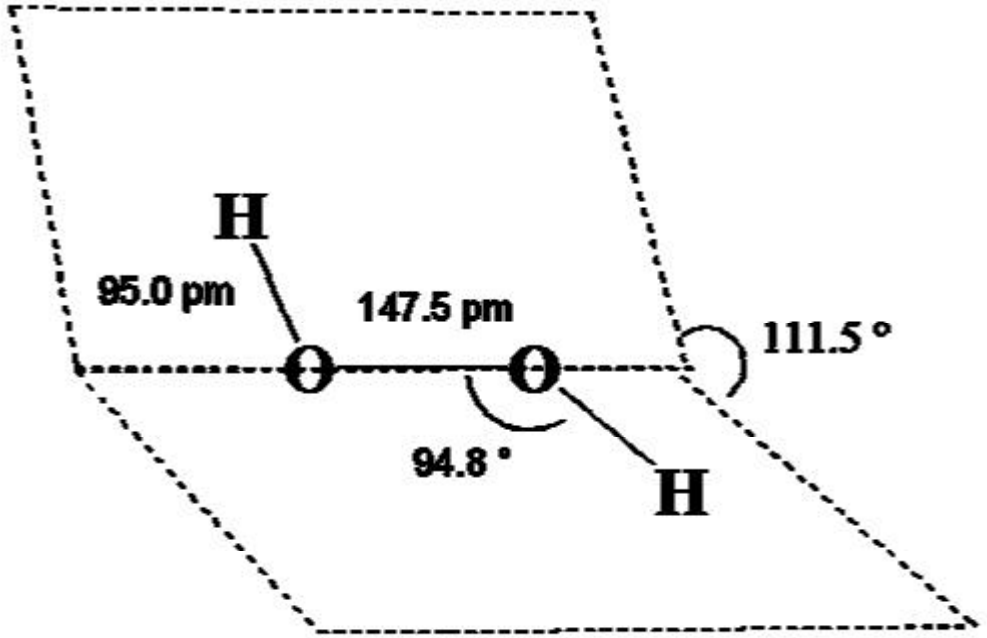

Figure 1.3 - Hydrogen peroxide in the gas phase highlighting the skewed angle and bond lengths.[2]

Compared to water, the energy content of hydrogen peroxide is much higher, seen from the heats of formations for water and H_2O_2.[18]

1) $H_2 + ½ O_2 \longrightarrow H_2O$?H = -286 kJmol^{-1}
2) $H_2 + O_2 \longrightarrow H_2O_2$?H = -188 kJmol^{-1}

The decomposition of hydrogen peroxide produces water, gaseous oxygen and heat (100.4 kJ mol^{-1}). The rate of decomposition can be controlled by the temperature and concentration of

the peroxide, as well as on the presence of impurities and stabilisers. Since the activation energy for the cleavage of the oxygen-oxygen bond is rather low ($?H = -71$ kJ mol^{-1}), traces of many substances can start the reaction, including most of the transition metals and their compounds, as well as certain organic compounds.[19] Although H_2O_2 will oxidise some reactions unaided, for faster reactions the addition of an activating agent, such as Fentons reagent,[20] is required.

Hydrogen peroxide is a strong, versatile oxidant, which can oxidise a broad variety of inorganic and organic substrates in liquid phase reactions. It is effective over the whole pH range, with high oxidation potential,

$$\text{Acidic} - H_2O_2 + 2H^+ + 2e^- \longrightarrow 2H_2O \quad (E^0 = 1.763 \text{ eV at pH 0})$$

$$\text{Alkaline} - H_2O_2 + 2OH^- \longrightarrow 2H_2O + 2O_2 + 2e^- \quad (E^0 = 0.878 \text{ eV at pH 14})$$

H_2O_2 possesses both nucleophillic and electrophillic properties. In alkaline solution H_2O_2 dissociates forming a perhydroxyl anion, HO^-, which is a powerful nucleophile reacting readily with a number of compounds including aldehydes and electron deficient olefins. In a highly acidic medium H_2O_2 can be protonated, forming $H_3O_2^+$, which is crucial to its use in wastewater treatment where it has the ability to reduce chlorine and hypochlorite. This electorphillic form can also be utilised for phenol hydroxylation.[21]

1.3.1 Applications

H_2O_2 decomposes to give only water and oxygen as the only reaction products, making it an environmentally safe oxidising agent for many large-scale applications, such as pulp and paper bleaching, textile applications, detergent applications, wastewater treatment, and chemical oxidation processes, Figure 1.4.

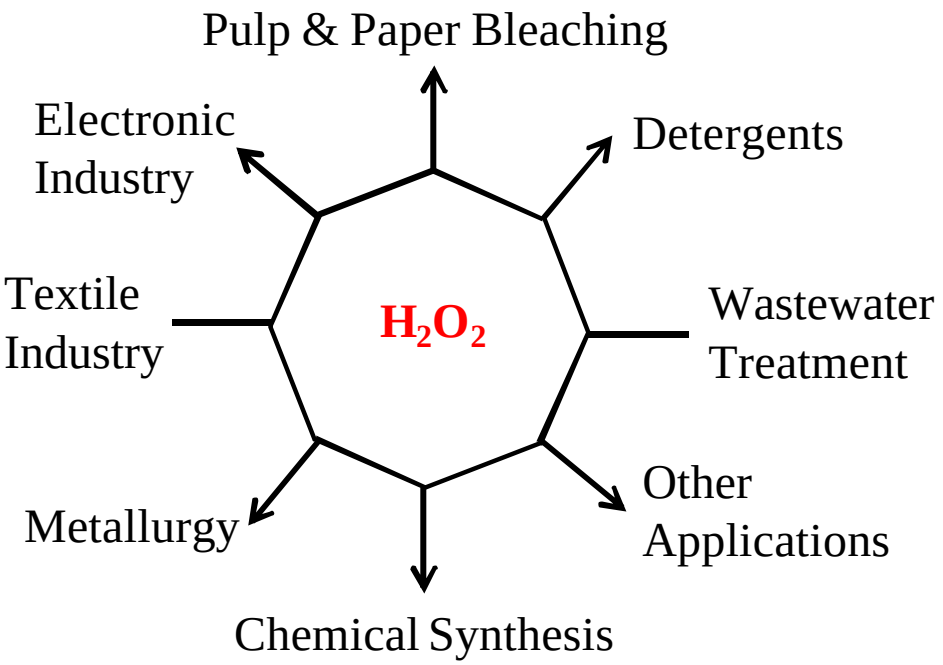

Figure 1.4 - Principal uses of hydrogen peroxide[21]

One of the most important applications is currently its use in pulp and paper bleaching,[22, 23] as well as for treatment of wastewaters and a variety of industrial wastes.[24] It has advantages over traditional chlorine and chlorine-containing bleaches and oxidants, such as sodium hypochlorite and sodium hydrochlorite, in that it is suitable for continuous processing, has no severe toxicity or effluent problems and is noncorrosive. The formation of the perhydroxyl anion, a nucleophile intermediate, is important for bleaching as it's responsible for the oxidation of chromophores in lignin through the cleavage of side chains.

Hydrogen peroxide is also used as a source of hydroxyl radicals which is the second most powerful oxidant after fluorine. They occur from single electron transfer reactions in the presence of an initiator, such as metals, enzymes (catalase) or heat. Generally, radicals produce more negative effects (delignification) than positive effects in the bleaching process,[23] however, are useful for more complex advanced oxidation processes.[25]

For processes in the fine chemical industry, operated using molecular oxygen, the presence of di-radical triplet states can potentially initiate homogeneous, non-catalysed background reactions in addition to the target reaction. Hence significant demand exists for green, atom-efficient, singlet-state oxygen donors, such as hydrogen peroxide. H_2O_2 can be employed

either directly or following transformation into a peroxocarboxylic acid, leading to an economically viable synthesis route for the manufacture of many organic and inorganic chemicals.

The potential of including hydrogen peroxide in large volume chemical synthesises has been recognised following the commercialisation of the integrated HPPO (hydrogen peroxide-propylene oxide) process, in which the hydrogen peroxide required for the epoxidation is produced on site. BASF and Dow Chemical opened a joint-venture pilot plant in Antwerp in 2008 with a yearly capacity of producing about $2x10^5$ metric tons.[26] In Japan, an increase in the consumption of hydrogen peroxide has stemmed from the commercialisation of Sumitomo's route to caprolactam.[27]

1.3.2 Manufacturing

In a rapidly expanding market the annual world production of hydrogen peroxide, currently *c.a.* 2.2 million metric tons[23] growing at roughly 10 % per annum, however, it is forecast to reach 4.67 million metric tons by 2017, mainly due to its demand in large scale chemical synthesis.[28]

H_2O_2 was first obtained on an industrial scale via a wet chemical process by treating barium peroxide with nitric acid. However, the high production costs limited H_2O_2 application. This was followed by large-scale production of hydrogen peroxide by electrolysis which can be traced back to Meidinger in 1895.[29] This proved to be an economically viable process for the production of highly concentrated solutions of hydrogen peroxide of high purity and stability. However, on-site electrochemical production of H_2O_2 for industrial applications requires a production method with higher reaction rates, higher efficiency and lower costs.

Currently, the anthraquinone oxidation (AO) process accounts for >95% hydrogen peroxide production worldwide. This industrial process was first developed by Hans – Joachim Riedl and Georg Pfliederer, in 1939,[30] with the first production plant being introduced by IG Farben-industrie in Germany in the 1940's. Since then significant improvements have been made in each of the four major steps: hydrogenation, oxidation, hydrogen peroxide extraction and treatment of the working solution. This has made the process more efficient and able to gain very high yields of peroxide per cycle at concentrations as high as 70 wt%.

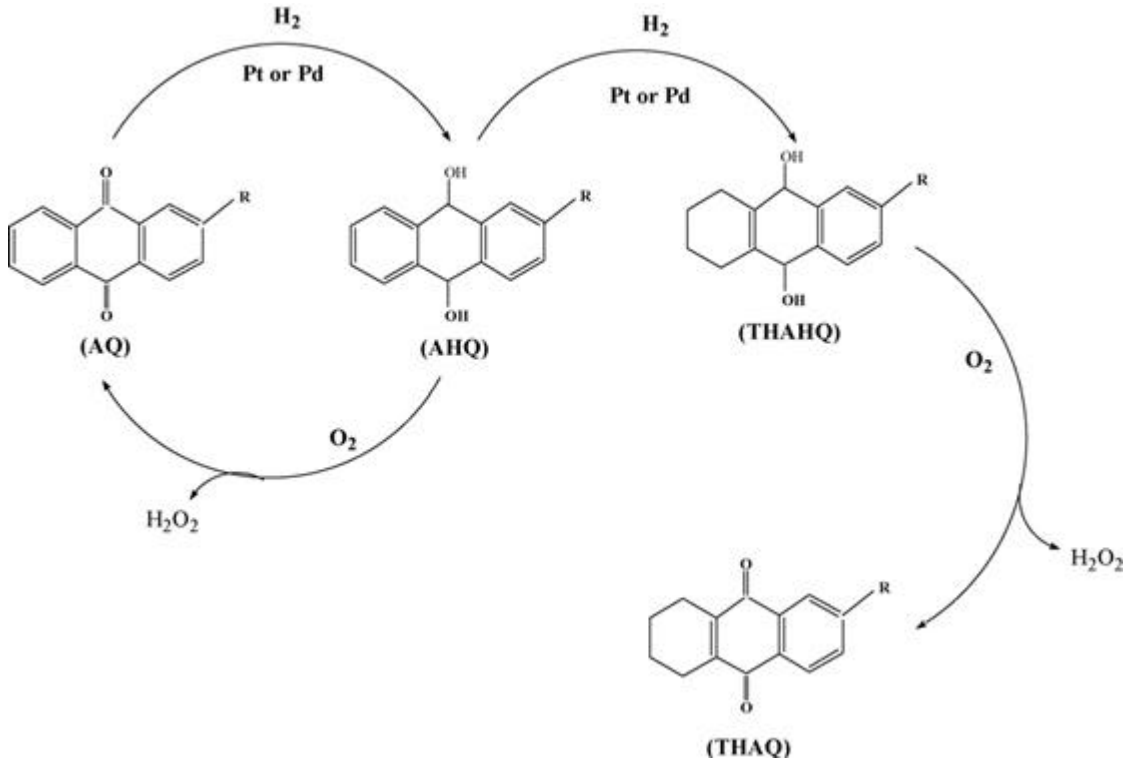

Figure 1.5 - Synthesis of H_2O_2 via anthraquinone auto-oxidation reactions.[31]

Firstly the working solution, 2-alkylanthraquinone (AQ) (usually 2-ethyl, 2-tert-buyl or 2-amylanthraquinone) in an appropriate solvent/s, is hydrogenated over a nickel or palladium based catalyst,[32, 33] to the corresponding anthraquinol or anthrahydroquinone (AHQ). The AHQ undergoes further hydrogenation to yield the corresponding tetrahydroanthrahydroquinone (THAHQ), Figure 1.5. This process is carried out under relatively mild conditions, normally temperatures of 40-50 ^{o}C and a hydrogen partial pressure of up to 4 bar are utilised. This step has two serious drawbacks: excessive hydrogenation and rapid deactivation.[31]

The solution containing the AHQ and THAHQ is separated from the hydrogenation catalyst and oxidised, usually by air, to regenerate the corresponding AQ and tetrahydroanthraquinone (THAQ) and equimolecular amounts of hydrogen peroxide. The oxidation is carried out non-catalytically by bubbling air through the solution at 30-60^{o}C and near atmospheric pressure. The reaction occurs by means of a well-documented free-radical mechanism, Figure 1.6.[21]

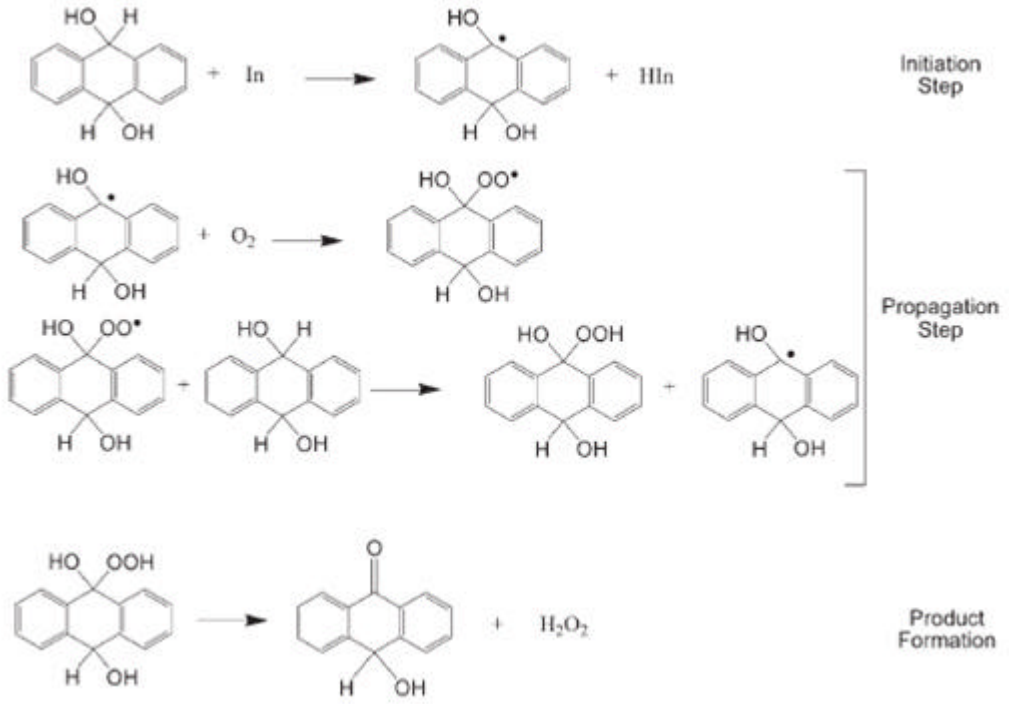

Figure 1.6 - H_2O_2 synthesis by the anthrahydroquinone oxidation reaction.[21]

Hydrogen peroxide can be stripped from the working solution by different methods, but those most generally used involve extraction with demineralised water to produce a crude solution that is usually between 25 - 45 wt% H_2O_2. Efficient extractors can recover more than 95% of H_2O_2 from the working solution.[31]

The aqueous hydrogen peroxide is then distilled to remove impurities and increase the concentration to meet commercial grades. The final solution is usually marketed as aqueous solutions at concentrations of 35, 40 and 70 wt% H_2O_2, with an added stabiliser (ppm level) and should be stored at low temperatures.[31]

The advantages of the AO process is not only the very high yields of H_2O_2 per cycle but also the H_2O_2 is produced continuously under relatively mild conditions (low temperatures and pressures) and direct contact between H_2 and O_2 is avoided. However, it is only commercially viable on a large scale (>$40x10^3$ tons per year) and entails many drawbacks. A series of side reactions can occur in this process which leads to a net consumption of athraquinone, which requires continual removal and regeneration of the working solution and hydrogenation catalyst. Cross-contamination between the water and organic working

solution during the recovery of the H_2O_2 product, by liquid-liquid extraction, is also a major problem. [31]

Most importantly there are safety concerns associated with the transportation of an unstable highly concentrated product from a central site to point of use. The fact that an environmentally friendly oxidant is manufactured in a non-environmentally friendly manner when general applications require 3-8 wt% H_2O_2 has prompted research and development into small-scale and widespread synthesis routes with improved efficiency to manufacture hydrogen peroxide at a lower market value. As such, there exists considerable interest in the development of a direct synthesis process to produce H_2O_2 from H_2 and O_2 gases using palladium based catalysts.

1.4 Emerging alternatives

1.4.1 Direct synthesis of hydrogen peroxide using Pd catalysts

Until very recently predominately supported Pd catalysts have been used in the direct synthesis of H_2O_2. Since the first patent by Henkel and Weber in 1914,[34] which utilised a Pd catalyst, it has been known that Pd is effective, for the liquid-phase hydrogenation of O_2 by H_2 to form H_2O_2.

However, two major drawbacks have prevented the process from an industrial application being accomplished. Firstly, due to safety issues H_2/O_2 mixtures need to be outside the flammability limits (5-95 v/v% for H_2 in O_2), H_2 concentrations less than 5 vol% H_2 are typically used. Secondly, Pd catalysts that are shown to be active for the direct H_2O_2 synthesis pathway are also active for the unwanted side reaction shown in Figure 1.7.

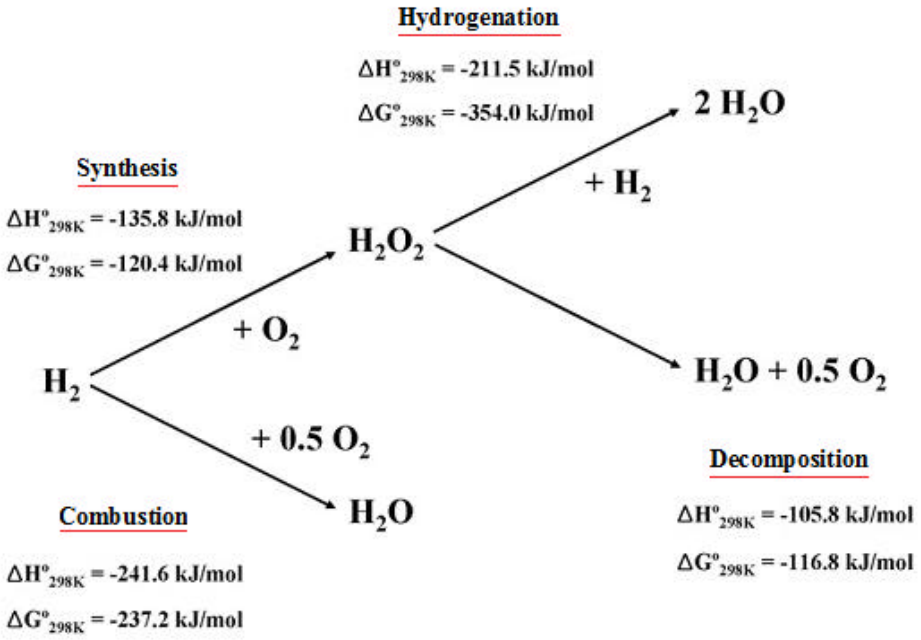

Figure 1.7 - Reactions involved in the direct production of H_2O_2.

All these reactions are thermodynamically favourable and highly exothermic, however, H_2O_2 is an intermediate and selectivity towards H_2O_2 is severely limited by the consecutive

decomposition and hydrogenation of H_2O_2. This is borne out by the heat contents (? H) and the free energy values (?G) shown in Figure 1.7. Factors that can influence the rate of H_2O_2 decomposition/hydrogenation are listed below.

- Catalyst design - hydrophobicity of catalyst etc
- Reaction conditions - H_2/O_2 ratio in feed, reaction time, catalyst amount, etc
- Reaction medium
- Presence of acids (i.e. H^+ ions)
- Presence of halide ions in reaction medium and/or catalyst
- Oxidation state of Pd in catalyst
- Presence of a second metal in Pd catalyst

Most of the research on the direct H_2O_2 synthesis concentrates on the catalyst design, where different metals or combination of metals and supports were studied to minimise the unwanted reactions. However, in addition to designing a suitable catalyst, the unwanted reactions can also be minimised acting on the operating conditions, but kinetics and mass transfer limitations must be known. Recently, contributions on the kinetics are growing in the literature.[35-42] The main efforts have been spent to rationalise the effect of different reaction conditions on the catalyst and to develop models to study the actual mechanism, for further optimisation of selectivity and production rate. However, results are difficult to compare mainly because of the different catalyst preparations, reactor designs and reaction conditions involved.

It has generally been accepted the rate determining step in the liquid-phase direct H_2O_2 synthesis is the dissociation of H_2. Taking into account the findings of a reaction variables investigation comparing the effect of different H_2/O_2 ratios and total reaction pressures, Hutchings and Moulijn[43] proposed a kinetic scheme for the production of hydrogen peroxide (steps 1-5) and for the parallel combustion and consecutive hydrogenation/decomposition of hydrogen peroxide (steps 6-10, which consider the dissociative adsorption of O_2), where * denotes a vacant site on the catalyst surface[43].

.

1. $H_2 + 2^* \rightarrow 2H^*$

2. $O_2 + * \rightarrow O_2^*$

6. $O_2 + 2^* \rightarrow 2O^*$

7. $O^* + H^* \rightarrow OH^* + *$

3. $H^* + O_2^* \rightarrow OOH^* + *$

4. $OOH^* + H^* \rightarrow H_2O_2^* + *$

5. $H_2O_2^* \rightarrow H_2O_2 + *$

8. $OH^* + H^* \rightarrow H_2O^* + *$

9. $H_2O^* \rightarrow H_2O + *$

10. $H_2O_2^* + * \rightarrow H_2O^* + O^*$

Therefore the rate of H_2O_2 production will strongly depend on the overall rate of mass transfer of the gaseous reactants to the catalyst surface. Water is the most desirable solvent considering its availability, cost and non-toxicity, however, the addition of alcohol improves the solubility of hydrogen and oxygen,[44] and thus the rate of H_2O_2 production.[45]

Since H_2O_2 is highly likely to decompose in the presence of a catalyst, it is often recommended to add a mineral acid to the reaction medium to stabilise the produced peroxide. With Pd-only catalysts, the presence of H^+ ions in the reaction medium has been found to be crucial for achieving higher H_2O_2 selectivity and productivity by inhibiting H_2O_2 decomposition.[46-50] However, high quantities of acid are undesirable since it may create problems related to catalyst stability and corrosion of reactor materials; with the dissolution of active substances (metals) into the reaction medium.

The specific role of H^+ ions in the catalytic path towards H_2O_2 formation is still not completely clear. In separate studies, Choudary[46] and Abate[51] postulated the H^+ ions plays a significant role in the elementary ionic and free radical reactions. Whereas Liu and Lunsford,[52] proposed H^+ have an indirect role in H_2O_2 formation, perhaps by influencing the electronic state of the palladium surface.

The catalysts activity towards the decomposition/hydrogenation of H_2O_2 can also be inhibited by adding halide ions to the reaction medium, causing an increase in the H_2O_2 selectivity. The halide ions can be added to the reaction medium as an alkali metal salt (Na, K or Cs salt) or in the form of a halogen acid (HCl, HBr or HI). Gosser *et al.*[53] disclosed that the presence of Cl^- or Br^- ions in an acidified reaction medium is important for improving both H_2O_2 productivity and selectivity. Whereas others have shown that although the addition of halide improves the selectivity the H_2 conversion is decreased.[42, 49, 54, 55]

The presence of iodide ions was detrimental to the catalysts activity and KF improved hydrogen conversion the most, however the reverse effect existed for H_2O_2 selectivity, indicating fluoride ions promote side and consecutive reaction pathways. The halide effects in the Pd-catalysed direct H_2O_2 synthesis can be correlated with the a or p donation ability of

halogens, which increases down the group (F<Cl<Br<I). The Pd-halide interaction was found to modify the electronic environment of Pd in the catalyst.[46]

Choudhary *et al*.[46, 56] indicated the presence of halide ions alone is not enough for promoting the selective oxidation of H_2 to H_2O_2 in the direct synthesis. However when halide ions (Cl^- or Br^-) were present together with H^+ ions, the selectivity for H_2O_2 formation was improved significantly. In general, when oxoacids (H_3PO_4, H_2SO_4 or HNO_3) in water were utilised very little H_2O_2 was formed. Whereas when halogen acids (HCl or HBr) were found to drastically improve the H_2O_2 selectivity while maintaining H_2O_2 synthesis rates. However, the use of the oxoacid, phosphoric acid (at a concentration <0.3 $moldm^{-3}$) in conjunction with halide, was recommended due to phosphate ions stabilising the H_2O_2 formed during reaction.[56] The combined halide and acid is thought to inhibit the dissociative chemisorption of dioxygen on the catalyst surface stabilising the formed peroxide which increases selectivity.

An optimum concentration of halide and H^+ is crucial for achieving the maximum H_2O_2 yield in the direct synthesis. Excess causes indiscriminate blocking of catalytic active sites, inhibiting the H_2 conversion and thereby decreasing the net formation of H_2O_2 in the direct synthesis.[54]

The presence of halide ions together with H^+ ions in a reaction medium may cause the reaction medium to become strongly corrosive towards the catalyst and even the metallic reactor materials, particularly stainless steel. Not only may these form active homogeneous catalysts that could promote the side reactions[57, 58] but isolation of H_2O_2 and catalyst recovery from the complex reaction mixture is a difficult task. This has limited the use of halogen promoters in acidic liquid reaction medium for the purpose of improving H_2O_2 yield/selectivity.

Colloidal palladium may be considered as a homogeneous catalytic system for the direct synthesis of H_2O_2. Dissanayake and Lunsford[57, 58] found the presence Pd^0/Pd^{2+} in a steady state (the overall composition of Pd^0/Pd^{2+} does not change dramatically over time), to be active for the direct synthesis of H_2O_2. A concentrated HCl (0.1-1.0M) reaction medium, together with O_2, led to dissolution of Pd from a Pd^0/SiO_2. There was a linear relationship between colloid concentration and H_2O_2 formation. Although a colloidal Pd system is highly interesting at a fundamental level, it is not suitable from a commercial perspective since the management of a Pd colloid would be a difficult task on a large scale.

To eliminate the need for corrosive halide in the reaction medium, incorporation of halide ions into the catalyst has been investigated. This was achieved by directly impregnating the halide ions into the supported Pd catalyst or *via* the deposition of halide ions onto the support prior to the deposition of Pd.[47, 54] An improvement in catalyst performance for the direct H_2O_2 synthesis was observed, however, the stability of the catalysts wasn't investigated. Impregnating preformed Au-Pd supported catalysts with bromide was shown to destabilise the supported metal causing it to leach into the reaction medium.[59]

The effect of the palladium oxidation state in the direct H_2O_2 synthesis has been investigated by many research groups. Choudhary et al.[60-62] have claimed that a PdO catalyst is more suitable than a Pd^0 catalyst, owing to its higher selectivity for the H_2O_2 formation. On the other hand, other scientists, including Thompson and co-workers[44], Chinta and Lunsford,[42] and Burch and Ellis[49] have claimed that higher H_2O_2 productivity and selectivity can be obtained with Pd^0 catalysts.

1.4.2 Electrolysis / fuel cells

A promising alternative is the production of hydrogen peroxide with inexpensive fuel cells, which unlike electrolytic devices do not require electrical energy. The electrochemical reduction of O_2 in acidic and alkaline media proceeds through two pathways which are mainly determined by the electrocatalyst and electrode potential: four electron reduction of O_2 into H_2O and two-electron reduction into H_2O_2.

$$O_2 + 4H^+ + 4e^- \longrightarrow 2H_2O$$

$$O_2 + 2H_2O + 2e^- \longrightarrow H_2O_2 + 2OH^-$$

The most promising results have been obtained by Yamanaka *et al.*[63-65] who have reported the H_2O_2 could be synthesised with selectivity of 93 % using a fuel-cell system. In this fuel-cell system, Pt and carbon were used for H_2 activation and H_2O_2 synthesis and a cation membrane (viz. Nafion) was used for preventing the diffusion of H_2O_2. Recent efforts have been made to develop a non-precious metal based system due to its high cost. Although the synthesis set up can be considered to be a green process it's still far away from being used for commercial exploitations.

1.4.3 Plasma

H_2O_2 can be synthesised from hydrogen and oxygen mixtures by plasma and other physical methods. The activation of H_2 and O_2 molecules in non-equilibrium plasma by dielectric barrier discharge gives quite high yields and selectivities of H_2O_2. This can be considered a green process and the optimum H_2/O_2-plasma mixtures are outside the explosive regime. However, this depends strongly on the reactor configuration.[66]

1.4.4 Supercritical CO_2

Supercritical CO_2 (Sc-CO_2) is becoming an important commercial and industrial solvent due to its low toxicity and environmental impact. It has been investigated using both homogeneous[67, 68] and heterogeneous[69, 70] catalysis. The synthesis of H_2O_2 from H_2 and O_2 in supercritical CO_2 is advantageous since both O_2 and H_2 are miscible with Sc-CO_2, which favours in reducing or even eliminating the mass transfer resistance. However, the disadvantage is the rate of H_2O_2 decomposition is too rapid at temperatures above the critical temperature (Tc = 31.1^oC) for this reaction medium to be beneficial.[71, 72]

1.5 Gold Catalysis

Gold is a fascinating metal that has long been used for its beauty. The chemical inertness of bulk gold has made it an important metal with high monetary value which is readily traded. two key discoveries came in the early eighties that predicted and subsequently demonstrated that nano-particulate gold can be an effective catalyst, superior to other metals.[73, 74]

- Graham Hutchings working in industrial laboratories for ACSI Ltd, in 1982, predicted that gold would be the best catalyst for acetylene hydrochlorination. Hutchings observations were published in 1985 and from subsequent experimental research this was found to be the case.[73]

- In 1982 Haruta et.al prepared ‘composite’ oxides of gold with a variety of transition metals by coprecipitation with a view to investigate their hydrogen oxidation activity. Later that year, he discovered that these gold materials were much more active for CO oxidation than for hydrogen oxidation and that they were still active even at -76°C.[74]

Although, prior to these studies there were reports of gold's activity, most notably Bond *et al.*[75] reported, in 1973, the hydrogenation of olefins over supported gold catalysts; these were the first studies that showed gold to be the best catalyst. It wasn't until a decade later, the mid 1990's, after the commercialisation of gold catalysts as an odour eater in 1992 that interest in gold as a catalyst really flourished. Supported gold nano-particles were implemented in rest rooms in Japan where they were utilised to oxidise the decomposition of odour compounds, especially ammonia and trimethylamine, at room temperature. Here the focus is on supported gold in catalysis but it also fascinates material scientists, surface and synthetic chemists and theoreticians in great numbers.

Since gold catalysts have been investigated for an extensive range of reactions, which have been reviewed by Hutchings and Hashmi,[76] a selection of important reactions using Au supported catalysts is discussed in the following sections.

1.5.1 Carbon Monoxide Oxidation

The oxidation of CO is a very important within both industrial and academic sectors. CO emissions within exhaust gases of petrol and diesel engine vehicles as well as industrial processes is of great burden to the environment and human health, and control of CO is of paramount importance (respirators for the removal of CO in toxic environments). For a simple reaction that has been studied by many, there are still many unresolved issues in the literature which are subject to continued debate, including the nature of the active site and although several mechanisms have been proposed its puzzling mechanism still hasn't been resolved.

Haruta *et al.* discovered that Au nanoparticles deposited on oxide supports were extremely active for the oxidation of CO at temperatures as low as -70 ^{o}C. Generally the active catalysts are thought to comprise of gold nano-particles (2-4 nm in diameter) on a suitable oxide support (e.g. ferric oxide or titania), prepared by precipitation.[77]

Bond and Thompson[78] have investigated the reaction mechanism and proposed that peripheral cationic gold is responsible for the activation of di-oxygen in the catalytic process. Kung *et al.*[79] reported mechanistic proposals in agreement with Bond-Thompson using the interface between small gold nanoparticles and the support as the key to the reaction. However, it is still unclear whether Au^{3+} or Au^{0} is the active form of gold.

Hutchings *et al.*[80] showed that Au^{3+} in Au/Fe_2O_3 was an important component of very active catalysts for the oxidation of CO. In accordance with this study, in a later paper Flytzani-Stephanopoulos *et al.*[81, 82] demonstrated that Au^{3+} was an important factor in obtaining high activity water gas shift catalyst based on Au added by deposition precipitation onto nanocrystalline 10 % La-doped CeO_2 (~5 nm). The catalysts were subsequently leached with 2 % NaCN removing 90 % of the gold and surprisingly, the catalytic activity was not only retained it was significantly enhanced.

A quantum size effect of the very small Au particles has been proposed by Goodman[83] and subsequently Boyen[84] concluded that Au particle size containing 55 atoms, which are 1.4 nm in diameter, are the most stable and active towards CO oxidation. Norskav *et al.*[85] showed by using DFT calculations the activation of CO was energetically favoured on Au particles with 10 atoms.

1.5.2 Hydrochlorination of Acetylene

The prediction by Hutchings in the 1980's that Au would be the best catalyst for the hydro-chlorination of acetylene to vinyl chloride, led to the industrial synthesis of vinyl acetate[86] and vinyl chloride[73, 87, 88] being performed based on gold catalysis. Production of vinyl chloride, which monometallic gold supported catalysts are the most active, is an important intermediate for the production of PVC (polyvinyl chloride).

Previously, vinyl chloride was produced using $HgCl_2$ supported on carbon; however, it was extremely toxic and suffered from a high deactivation rate. A study by Shinoda, highlighted a wide range of metal chloride catalysts supported on carbon were active for the reaction. However, a correlation based on the electron affinity of the metal cation divided by the metal valence was not useful for a prediction of the most active. Hutchings[73] reasoned that the reaction was not a one-electron process, as defined by the electron affinity, but was more likely to involve the 2 electrons of ethyne and hence, as most of the cations in the data set were divalent; the standard electrode potential was more viable parameter with which to correlate the data. On this basis it was predicted that Au would be the best catalyst for this reaction. In fact $AuCl_3$/carbon prepared by wetness impregnation with $HAuCl_4$ solution was found to be three times more active than traditional $HgCl_2$/carbon. Moreover, $AuCl_3$/carbon deactivated much less rapidly. Subsequent ^{197}Au M?ssbauer spectroscopy[87] clearly

demonstrated how this process was due to reduction of Au^{3+} to Au^{0}. Remarkably, gold catalysed acetylene hydro-chlorination is very selective with a selectivity >99.9 % to the vinyl chloride monomer.

1.5.3 Alkene Epoxidation

The epoxidation of propene to propyloxide (PO) using Au catalysts is not only significant to this thesis due to nanocrystaline metallic golds high activity, but also through the link of the reaction with H_2O_2 production, known as the Hydrogen Peroxide-Propylene Oxide (HPPO) process. PO is an important commodity chemical widely used for the production of polyurethane and polyols.

Haurta *et al.*[89-91] first demonstrated the potential of supported gold catalysts for the epoxidation of propene with dioxygen in the presence of H_2 as a sacrificial reductant. H_2 permits activation of oxygen at relatively low temperatures allowing the selective oxidation to occur, increased temperature results in a decrease in selectivity. They utilised a Au/TiO_2 catalyst prepared by the deposition precipitation method with intimate contact between Au nanoparticles (2-5 nm) and the TiO_2 support being responsible for the catalytic activity.

Although initial selectivities were low, improvements were made using different titanium-containing supports. Most studies concentrate on TS-1 as a support, which is a ZSM-5 type molecular sieve with MFI structure that has an outstanding ability to catalyse various oxidation reactions with aqueous H_2O_2 as the primary oxidant, such as the selective epoxidation of propene to PO.[92] Moulijin *et al.*[93] showed that a Au/TS-1 catalyst could to be very selective for the formation of PO. Mechanistic studies showed the important role of gold in the formation of the bidentate peroxy species as an intermediate.[94] Carefully tuning of the gold loading in particular is important to achieve high selectivities.[95]

Interestingly, Hughes *et al.*[96] have shown that sacrificial H_2 is not essential for the epoxidation of alkenes and very high selectivities can be achieved using catalytic amounts of peroxides to initiate the oxidation of alkenes with O_2.

1.5.4 Alcohol Oxidation

The selective oxidation of alcohols to chemical intermediates represents an important reaction in the production of fine chemicals. Platinum and palladium have been found to be very active for the oxidation of a large number of substrates, however they have low selectivity to the desired aldehydes or carboxylic acids.

Prati, Rossi and co-workers[97-104] have demonstrated that catalysts based on Au/C systems were effective for alcohol oxidation including diols such as ethane-1,2-diol (ethylene glycol). These studies have been extended to the oxidation of sugars, and similar high activities for the oxidation of glucose and glycerol have been observed. This is significant environmentally due to the increasing production of glycerol in the last decade, as the main by-product in the synthesis of bio-diesel.

Interestingly, in studies of the mechanism of glucose oxidation to gluconic acid using colloidal gold it has been postulated that hydrogen peroxide may be formed *in-situ*, however it decomposes before forming a critical concetration, due to the basic nature of the reaction medium, to efficiently compete with O_2 as the oxidant.[105]

Another significant advance in this area came from Corma and co-workers[106-109] who showed that Au/CeO_2 is active for the selective oxidation of alcohols to aldehydes and ketones as well as oxidation aldehydes to acids under relatively mild solvent-less conditions, in the presence of O_2. Stabilisation of a reactive peroxy intermediate by the Au/CeO_2 catalyst is thought to be responsible for the activity observed.

1.5.5 Direct Synthesis of Hydrogen Peroxide

Hutchings and co-workers were the first to show that gold catalysts were effective for the direct reaction.[71] However, the key discovery was the observation that the direct synthesis was significantly enhanced by using Au/Pd alloys supported on alumina compared to the monometallic counterparts, Au and Pd.[72] Bond and co-workers have highlighted that gold has a unique ability in forming stable, hydroperoxy, OOH species (an intermediate in the direct H_2O_2 synthesis), compared to Pd and Pt which are efficient with respect to dissociating the oxygen-oxygen bond.

1.6 Bimetallic catalysts

Besides the development of monometallic catalysts, a new set of catalysts prepared by mixing two metal components within a single catalyst, known as bimetallic or alloy catalysts have recently been investigated. Pioneering work by Sinfelt[110-112] led to their introduction in the area of petroleum refineries. After this discovery, a number of bimetallic catalysts have been reported for a range of reactions including oxidation,[113-115] hydrogenation,[116-118] hydrogenolysis,[119, 120] and reforming[121, 122] reactions. The properties of bimetallic catalysts are significantly different from their monometallic analogues because of what is often termed as 'synergistic' effects between the two metals, causing an enhancement in catalytic stabilities, activities and selectivities.

Bimetallic catalysts can be prepared in similar ways to the monometallic catalysts, however, due to the presence of the second metal component the complexity of the preparation method and final structure of the nano-particles increases. This leads them to be of interest for not only their catalytic activity but also from a materials science perspective.[123] Here the focus is on the preparation and influence of bimetallic Au-Pd nano-particles supported catalysts on the direct synthesis of hydrogen peroxide.

The enhancement observed by the addition of Au to Pd, has been postulated to be due to two alloy effects, i.e. ensemble and ligand effects. The ensemble effect is a dilution of surface Pd by Au. With increasing surface Au coverage, contiguous Pd ensembles disappear and isolated Pd ensembles form, and even cause the formation of highly active surface sites, e.g. isolated Pd pairs. The disappearance of contiguous Pd ensembles also switches off side reactions catalysed by these sites. The ligand effects are electronic perturbation of Pd by Au, via direct charge transfer or by affecting bond lengths, the ligand effects cause the Pd d band to be more filled, moving the d-band centre from the Fermi level. Both cause Pd to bind the reactants and products more weakly increasing selectivity.[124]

1.6.1 Direct Synthesis of Hydrogen Peroxide Using Au-Pd Catalysts (Cardiff)

Hutchings et al. discovered Au/Al_2O_3 was active for the liquid-phase direct synthesis of hydrogen peroxide. Its activity was relatively low compared to the monometallic Pd analogue. However, the most important discovery was the improved activity and selectivity

of Au-Pd catalysts, prepared by the impregnation of Al_2O_3 with Au and Pd simultaneously, compared to Pd/Al_2O_3.[71, 72]

Initial investigations used supercritical CO_2 (sc-CO_2) as the solvent. However, in subsequent experiments, due to high H_2O_2 decomposition rates in the sc-CO_2 reactions, a methanol-water solvent was utilised without the addition of promoters. The reactions were performed in a three-phase system (catalyst-solid, solvent-liquid, and reagents-gas) in a sealed stainless steel autoclave. The effect of reaction conditions on the direct H_2O_2 synthesis, have previously been studied.[125, 126] The total reaction pressure and the methanol-water solvent composition had profound effects on the rate of H_2O_2 synthesis, as both parameters affected the amount of H_2 available, in the solvent, for the reaction to take place. However, as expected, the reaction temperature, the H_2/O_2 molar ratio and the reaction time also had significant effects. By fine tuning of the parameters very high reaction rates for the synthesis of H_2O_2 were achieved with Au-Pd alloy catalysts.

Interestingly, Au-Pd/TiO_2 catalysts effective for low-temperature CO oxidation prepared by deposition precipitation (DP) were inactive for the direct H_2O_2 synthesis, whereas impregnation materials showed the opposite trend.[127] It was concluded that this activity was due to the particle size distribution and the nano-particle morphology. DP produced Au particles of the correct size (< 5 nm) to be active for CO oxidation and relatively large Au nano-crystals (*ca.* 25 nm), present on the impregnation Au/TiO_2, are active for selective hydrogenation of O_2 to H_2O_2.

It was shown that by using a simple impregnation method and by choosing the proper calcination temperature, highly efficient, stable Au-Pd/TiO_2 catalysts could be synthesised for the direct H_2O_2 synthesis. Catalysts calcined at lower temperature achieved higher H_2O_2 synthesis rates however this rate decreased upon re-use, shown to be due to the leaching of active components from the support surface. Detailed scanning transmission electron microscopy (STEM)-X-ray energy dispersive spectroscopy (XEDS) studies[128] showed that increasing the calcination temperature is crucial not only to achieve catalyst stability but also the development of Au_{core}-Pd_{shell} structures from random alloys. Furthermore, a bimodal distribution of metal particles was found, the majority of which were in the 2-10 nm regime with a minority of much larger particles, 35-80 nm in size. In agreement with the STEM-XEDS findings, x-ray photoelectron spectroscopy (XPS) revealed a significant surface Pd enrichment, as PdO, in the Au-Pd particles, indicating the development of the core shell

structure after heat treatment. A calcination temperature of 400 ^{o}C produced a stable Au-Pd/TiO_2 catalyst with a catalytic activity (64 $mol_{H2O2}kg_{cat}^{-1}h^{-1}$; 0.12 wt% H_2O_2), that was a factor of 2 and 9 higher than the corresponding Pd and Au monometallic catalysts respectively.[127]

In subsequent studies,[129-133] the effect of the support identity was carefully studied and it was found that carbon-based catalysts showed the lowest H_2O_2 hydrogenation and decomposition activity, whereas oxide supports such as TiO_2,[127, 133] CeO_2,[134] Fe_2O_3,[135] Al_2O_3, [136] SiO_2,[130] and MgO[132] showed much lower productivity.

Microstructural analysis of Au-Pd/C catalysts indicated a bimodal particle size distribution and the existence of homogeneous Au-Pd alloys in comparison to the core shell structures on oxide supports. The morphology of the particles on carbon and oxide supports are highlighted in the High Angle Annular Dark Field (HAADF) images with statistical analysis of the XEDS to produce the red-green-blue (RGB) images shown in Figure 1.8.[131] (Details of the XEDS technique utilised were detailed by Kiely *et al.*[137])

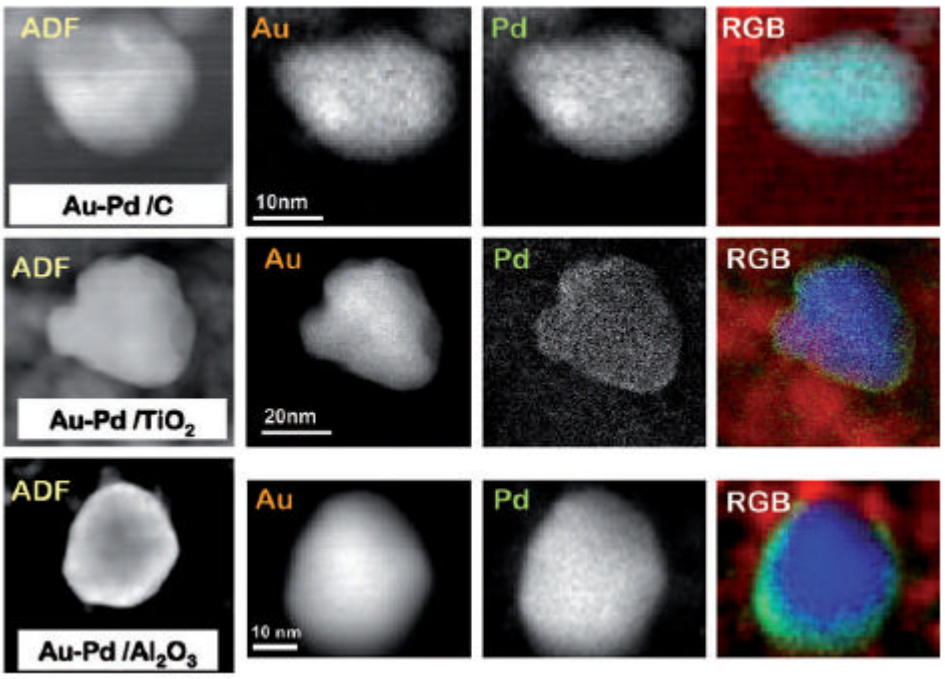

Figure 1.8 – HAADF images, and Au - Pd RGB overlap maps (Au = Blue: Pd = Green) for 2.5 wt% Au-2.5 wt% Pd/C, TiO_2 and Al_2O_3 catalysts prepared by wet impregnation and calcined in static air (400^{o}C, 3 h). (Aqua particle is a homogneous alloy).[131]

However, it was concluded that this activity trend was not only related to the morphology of the Au-Pd particles but also to the isoelectric point of the support as indicated in Figure 1.9. A general observation was made that acidic supports such as carbon and silica having low isoelectric points showed better catalytic performance, than basic supports. [132]

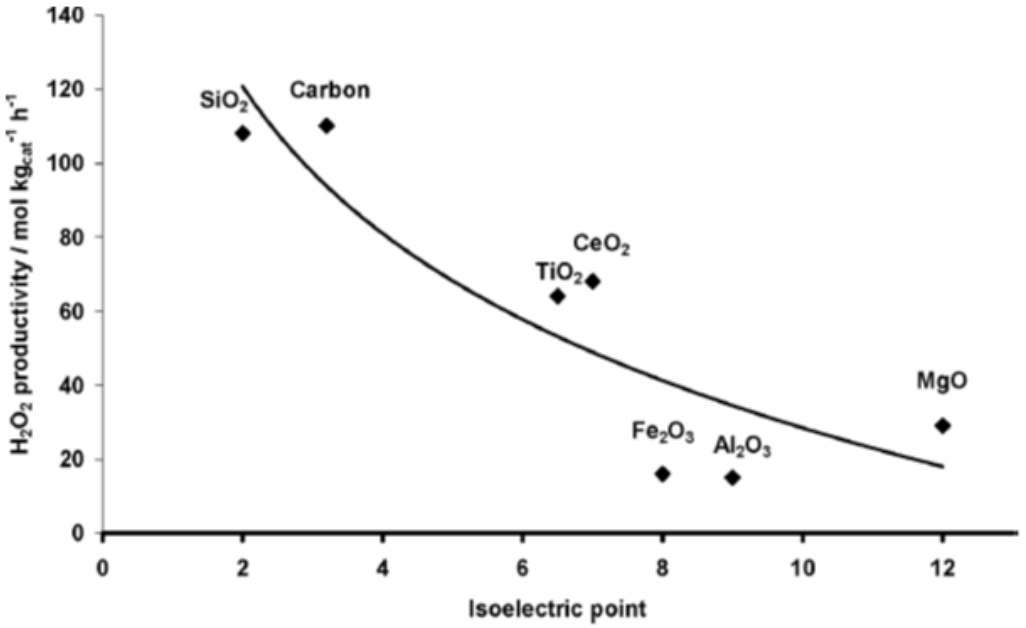

Figure 1.9 - H_2O_2 productivity over Au-Pd catalysts as a function of the isoelectric point of the support.[132]

This has recently been highlighted in a study into using Cs-containing heteropolyacid Au-Pd catalysts, which were considerably more effective in achieving H_2O_2 yields in the absence of acid or halide additives than previously reported catalysts. These materials also showed superior H_2O_2 synthesis activity under challenging conditions (ambient temperature, water-only solvent and CO_2-free reaction gas).[138]

Due to the consistently large improvements of H_2O_2 activity obtained using carbon supports, Hutchings *et al.* focused on further optimising Au-Pd bimetallic catalysts using carbon as the chosen support. They showed that a simple acid pre-treatment of an activated carbon support prior to the deposition of Au-Pd random alloy particles could yield a very significant improvement in the yield of H_2O_2 produced. This treatment resulted in a 'switching-off' of the hydrogen peroxide hydrogenation route, to allow hydrogen selectivities greater than 95%.[139] The same acid pre-treatment of titania produced a Au-Pd/TiO_2 sample with

improved H_2O_2 productivity with lowered H_2O_2 hydrogenation, however, it was not switched off.[140]

STEM-XEDS analysis of the acid and non-acid treated Au-Pd/C samples showed that in both cases all the particles were homogenous Au-Pd alloys, but a significant difference was found in the size distribution of the alloy particles. The acid pre-treatment favoured the formation of a greater number fraction of the smallest Pd-rich alloy particles, at the expense of the larger Au-rich particles, Figure 1.10. Therefore, an improvement of the Au dispersion in the bimetallic alloy particles was achieved by increasing the number of smaller Au-Pd nano-particles. This coupled with a selective decoration/blocking of specific active sites on the support were concluded to be responsible for the hydrogenation/decomposition of H_2O_2. Increase in H_2O_2 productivity was due to the formation of a larger number of smaller active alloy nanoparticles and the preferential blockage of the active H_2O_2 hydrogenation sites on the support.[139]

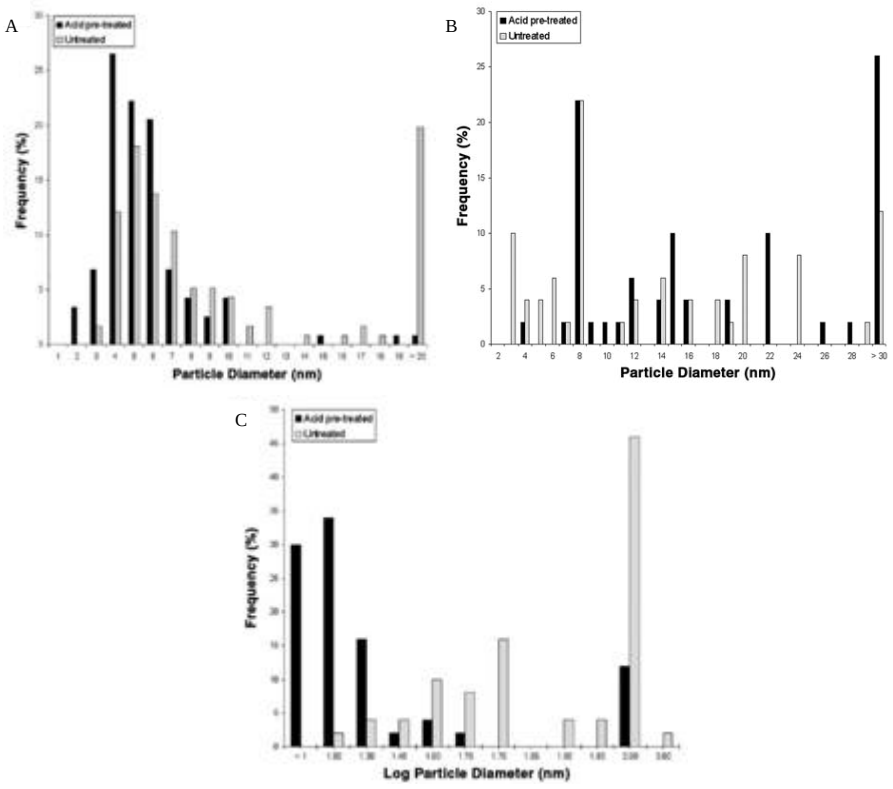

Figure 1.10 - The particle size distribution of; (A) alloy particles for untreated and acid pre-treated Au-Pd/carbon catalysts, (B) Pd particle size for untreated and acid pre-treated pure Pd/carbon catalysts, and (C) Au particles for the untreated and acid pre-treated pure Au/carbon catalysts.[139]

Further experiments by the same group utilised a colloidal method, sol-immobilisation, for the synthesis of Au-Pd nano-particles supported on carbon. This technique synthesised bimetallic Au-Pd colloids via sequential addition and reduction of the metals in the presence of a stabiliser, followed by immobilising the sols on carbon. These Au-Pd catalysts prepared were more active for the direct H_2O_2 synthesis than analogous impregnation catalysts. This was attributed to the significantly smaller mean particle size, particle size distribution, and predominately metallic oxidation state of the former materials.[141] It was also confirmed by changing the Au/Pd ratios that 1:1 by wt Au-Pd catalysts were the most active.[142]

The particle morphology was tuned using sol immobilisation to study the effect of random alloys versus core-shell structures on Au-Pd/C for the direct H_2O_2 synthesis, while maintaining a narrow particle size distribution. Instead of adding the Au and Pd salts simultaneously in the stabilising solution and reducing them together, it is also possible to reduce the metal salts sequentially.[143] Hutchings *et al.* concluded homogeneous alloy particles to be the most active for direct H_2O_2 synthesis and, contrary to previous conclusions,[131] that ultra-small Au-Pd nano-particles may not be the optimal catalyst structure for this demanding synthesis.[143] Although, sol-immobilisation catalysts achieved high initial yields, they were found to only be useful as 'model' catalysts due to high H_2O_2 hydrogenation rates and lack of stability.

Very recently Sankar *et al.*[144] have reported a stabilizer-ligand free synthesis method for producing supported gold-palladium nanoalloys with exceptionally high catalytic activity and stability for the direct synthesis of hydrogen peroxide. This method involves an 'anion-excess' modification of the conventially used impregnation methodology for preparing these catalysts. They demonstrated that by adding an excess of chloride anions during the synthesis of Au-Pd nanoalloy catalysts using $HAuCl_4$ and $PdCl_2$ as metal precursors, superior control over the particles size distribution and composition could be achieved without the need to add any stabilising ligands such as PVP or PVA. 1 wt%Au-Pd/TiO_2 catalysts were prepared by this modified impregnation method which had higher activity compared to analogus catalysts prepared by conventional impregnation and sol immobilisation methods. It was also demonstrated that more of the gold was in nanoscale alloy particles rather micron scale monometallic Au particles as was found for conventional impregnation. When the dried sample was calcined (static air atmosphere), a Au_{core}-Pd_{shell} nanoparticles were achieved, whereas, when it was reduced in a dilute hydrogen atmosphere homogeneous random Au-Pd alloys were obtained. The reduced homogeneous alloys were more catalytically active

compared to the core-shell structures. It should be noted reduction of the sample was required to induce stability and enable the catalyst to be reusable; this was concluded to be due to the removal of the majority of excess chloride.[144]

1.6.2 Direct Synthesis of Hydrogen Peroxide Using Bimetallic Catalysts (Other research groups)

Ishihara *et al.* reported that a 1wt% Au/SiO_2 catalyst tested in the absence of halide promoters exhibited promising H_2O_2 synthesis activity (with 30 % H_2 selectivity) compared to Pt, Pd or Ag/SiO_2 catalysts where no hydrogen peroxide was formed. The addition of 1 wt% Pd to Au/SiO_2 gave improved rates of H_2O_2 synthesis, with maximum yield reported using a Pd:Au weight ratio of 82:18.[145]

Strukul et al. have examined bimetallic palladium-gold catalysts supported on zirconia and ceria for the direct synthesis of hydrogen peroxide under very mild (1 bar and 20 ^oC) and non-explosive conditions. Monometallic gold catalysts were completely inactive, while the addition of gold to palladium improved both the productivity and the selectivity of the process. They also showed pre-treatment with hydrogen and oxygen improved the catalytic performance further.[146]

In 1989, Gosser *et al.* gained a patent for hydrogen peroxide production by direct combination of hydrogen and oxygen using platinum-palladium/Al_2O_3 catalysts. They used a colloidal method to deposit Pt-Pd on to a preformed Pt/Al_2O_3 catalyst, and found a Pt:Pd ratio of about 0.02 to about 0.2, to be beneficial for the direct H_2O_2 synthesis. However, harsh reaction conditions were utilised (138 ^oC).[147]

Lunsford *et al.* utilised a solvent system of ethanol, that contained H_2SO_4 and halide ions (Cl^- or Br^-) to show the addition of only 5 atom% Pt to a 0.5 wt% Pd resulted in a 2.5-fold increase in the rate of peroxide formation with only a small decrease in selectivity. The authors conclude the increase in rate was due to an electronic modification between Pt and the halide increasing hydrogen activation.[148]

Choudhary *et al.*[149] studied the effect of metal additives, Au, Pt, Rh and Ru, on a preformed 2.5%Pd/ZrO_2 for the direct synthesis of H_2O_2. They found the H_2O_2 yield passed through a maximum at *ca.* 0.02 wt%Au and then decreased slightly with increase in the Au

concentration. Although a similar effect was observed in the case of Pt, Au was found to be a superior promoter. Addition of Rh and Ru was found to be detrimental for the H_2O_2 yields; these results were explained in terms of increased H_2O_2 decomposition activity and/or enhanced H_2 to H_2O reaction activity in their presence.

1.7 Aims and objectives

The aim of this research is to produce hydrogen peroxide directly from H_2 and O_2 by heterogeneous catalysis in which the percentage produced is sufficiently high to make the process economically, environmentally and industrially viable and as a result replace the AO process currently used. The parameters required to achieve this have been identified by Solvay® as $[H_2O_2]$ = 8 wt% with H_2 selectivity > 90 %.

The objectives to reach this aim are as follows.

1. Study and record previous work in this field as the process develops.
2. Vary the heat treatment and preparation of the catalysts with a view of obtaining the most active sites for hydrogen peroxide production.
3. Identify the sites/components of the catalyst that are active for the unwanted subsequent H_2O_2 hydrogenation and decomposition pathways which lead to the destruction of the formed H_2O_2.
4. Develop a biphasic solvent system and investigate its potential, for producing high H_2O_2 concentrations, by varying reaction conditions.
5. Develop a semi-continuous flow reactor, enabling reagent H_2 selectivity to be calculated to give greater insight into a catalyst's activity.
6. Draw a conclusion to find if the aim was met and suggest further work.

1.8 References

1. J. J. Berzelius, *Edinburgh New Philosophical Journal*, 1836, **XXI**, 223.
2. C. W. Jones, in *Applications of Hydrogen Peroxide and Derivatives*, ed. J. H. Clark, Royal Society of Chemistry, Editon edn., 1999, pp. p1-36.
3. T. A. Paul, G. H. Lauren and C. W. Tracy, in *Green Chemical Syntheses and Processes*, American Chemical Society, Editon edn., 2000, vol. 767, pp. 1-6.
4. P. T. Anastas and J. C. Warner, *Green Chemistry: Theory and Practice*, Oxford University Press, New York, 1998.
5. R. Noyori, *Chemical Communications*, 2005, 1807-1811.
6. M. Bowker, *The Basis and Applications of Heterogeneous Catalysis*, Oxford University Press, Oxford, 1998.
7. A. Y. Stakheev and L. M. Kustov, *Applied Catalysis A: General*, 1999, **188**, 3-35.
8. B. L. Mojet, J. T. Miller, D. E. Ramaker and D. C. Koningsberger, *Journal of Catalysis*, 1999, **186**, 373-386.
9. I. V. Babich, Y. V. Plyuto, A. D. Van Langeveld and J. A. Moulijn, *Applied Surface Science*, 1997, **115**, 267-272.
10. J. A. R. Van Veen, *Journal of Colloid and Interface Science*, 1988, **121**, 214-219.
11. J. P. Brunelle, in *Studies in Surface Science and Catalysis*, ed. P. G. P. J. a. G. P. B. Delmon, Elsevier, Editon edn., 1979, vol. Volume 3, pp. 211-232.
12. F. Rodríguez-reinoso, *Carbon*, 1998, **36**, 159-175.
13. Z. Hu and E. F. Vansant, *Carbon*, 1995, **33**, 561-567.
14. H. F. Stoeckli, *Carbon*, 1990, **28**, 1-6.
15. C. Moreno-Castilla, A. n. F. Pérez-Cadenas, F. J. Maldonado-Hódar, F. Carrasco-Marín and M. A. Lillo-Ródenas, *Carbon*, 2003, **41**, 1157-1167.
16. M. L. Toebes, J. M. P. van Heeswijk, J. H. Bitter, A. Jos van Dillen and K. P. de Jong, *Carbon*, 2004, **42**, 307-315.
17. L. A. Langley, D. E. Villanueva and D. H. Fairbrother, *Chemistry of Materials*, 2005, **18**, 169-178.
18. N. N. Greenwood and A. Earnshaw, *Chemistry of the Elements: Second Edition*, Elsevier's Science & Technology, Burlington, 1997.
19. A. Hiroki and J. A. LaVerne, *The Journal of Physical Chemistry B*, 2005, **109**, 3364-3370.
20. N. S. S. Martinez, J. F. Fernández, X. F. Segura and A. S. Ferrer, *Journal of Hazardous Materials*, 2003, **101**, 315-322.
21. J. M. Campos-Martin, G. Blanco-Brieva and J. L. G. Fierro, *Angewandte Chemie International Edition*, 2006, **45**, 6962-6984.
22. H. U. Süss and N. F. Nimmerfroh, HYDROGEN PEROXIDE IN CHEMICAL PULP BLEACHING.
23. R. Hage and A. Lienke, *Angewandte Chemie International Edition*, 2006, **45**, 206-222.
24. P. C. Vandevivere, R. Bianchi and W. Verstraete, *Journal of Chemical Technology & Biotechnology*, 1998, **72**, 289-302.
25. C. B. Chidambara Raj and H. Li Quen, *Chemical Engineering Science*, 2005, **60**, 5305-5311.
26. D. BASF, SOLVAY, *BASF, Dow, Solvay partnership breaks new ground with innovative HPPO technology in Antwerp*.
27. *US6265574 Pat.*, 2001.
28. I. Global Industry Analysts, *Hydrogen Peroxide Market Report*, 2012.
29. H. Meidinger, *Ann. Chem. Pharm.*, 1853, **88**.
30. *CA 382467 Pat.*, 1939.
31. C. Samanta, *Applied Catalysis a-General*, 2008, **350**, 133-149.
32. R. Edvinsson Albers, M. Nyström, M. Siverström, A. Sellin, A. C. Dellve, U. Andersson, W. Herrmann and T. Berglin, *Catalysis Today*, 2001, **69**, 247-252.

33. Y. Hou, Y. Wang, F. He, S. Han, Z. Mi, W. Wu and E. Min, *Materials Letters*, 2004, **58**, 1267-1271.
34. *US 1108752 Pat.*, 1914.
35. Y. Voloshin, R. Halder and A. Lawal, *Catalysis Today*, 2007, **125**, 40-47.
36. T. Deguchi and M. Iwamoto, *Journal of Catalysis*, 2011, **280**, 239-246.
37. T. Inoue, M. A. Schmidt and K. F. Jensen, *Industrial & Engineering Chemistry Research*, 2007, **46**, 1153-1160.
38. Y. Voloshin and A. Lawal, *Chemical Engineering Science*, 2010, **65**, 1028-1036.
39. P. Biasi, N. Gemo, J. R. Hernández Carucci, K. Eränen, P. Canu and T. O. Salmi, *Industrial & Engineering Chemistry Research*, 2012, **51**, 8903-8912.
40. T. Deguchi and M. Iwamoto, *Industrial & Engineering Chemistry Research*, 2011, **50**, 4351-4358.
41. P. Biasi, P. Canu, F. Menegazzo, F. Pinna and T. O. Salmi, *Industrial & Engineering Chemistry Research*, 2012, **51**, 8883-8890.
42. S. Chinta and J. H. Lunsford, *Journal of Catalysis*, 2004, **225**, 249-255.
43. E. Ntainjua N, J. K. Edwards, A. F. Carley, J. A. Lopez-Sanchez, J. A. Moulijn, A. A. Herzing, C. J. Kiely and G. J. Hutchings, *Green Chemistry*, 2008, **10**, 1162-1169.
44. V. V. Krishnan, A. G. Dokoutchaev and M. E. Thompson, *Journal of Catalysis*, 2000, **196**, 366-374.
45. *US 7105143 B2 Pat.*, 2006.
46. V. R. Choudhary and C. Samanta, *Journal of Catalysis*, 2006, **238**, 28-38.
47. C. Samanta and V. R. Choudhary, *Applied Catalysis A: General*, 2007, **326**, 28-36.
48. V. R. Choudhary, P. Jana and S. K. Bhargava, *Catalysis Letters*, 2008, **125**, 296-301.
49. R. Burch and P. R. Ellis, *Applied Catalysis B-Environmental*, 2003, **42**, PII S0926-3373(0902)00232-00231.
50. J. H. Lunsford, *Journal of Catalysis*, 2003, **216**, 455-460.
51. S. Abate, G. Centi, S. Melada, S. Perathoner, F. Pinna and G. Strukul, *Catalysis Today*, 2005, **104**, 323-328.
52. Q. S. Liu and J. H. Lunsford, *Applied Catalysis a-General*, 2006, **314**, 94-100.
53. , US 4832938, 1989.
54. C. Samanta and V. R. Choudhary, *Applied Catalysis A: General*, 2007, **330**, 23-32.
55. V. R. Choudhary and P. Jana, *Applied Catalysis A: General*, 2007, **329**, 79-85.
56. V. R. Choudhary, C. Samanta and P. Jana, *Applied Catalysis A: General*, 2007, **317**, 234-243.
57. D. P. Dissanayake and J. H. Lunsford, *Journal of Catalysis*, 2002, **206**, 173-176.
58. D. P. Dissanayake and J. H. Lunsford, *Journal of Catalysis*, 2003, **214**, 113-120.
59. E. Ntainjua N, M. Piccinini, J. C. Pritchard, Q. He, J. K. Edwards, A. F. Carley, J. A. Moulijn, C. J. Kiely and G. J. Hutchings, *ChemCatChem*, 2009, **1**, 479-484.
60. A. G. Gaikwad, S. D. Sansare and V. R. Choudhary, *Journal of Molecular Catalysis A: Chemical*, 2002, **181**, 143-149.
61. V. Choudhary, A. Gaikwad and S. Sansare, *Catalysis Letters*, 2002, **83**, 235-239.
62. V. R. Choudhary, S. D. Sansare and A. G. Gaikwad, *Catalysis Letters*, 2002, **84**, 81-87.
63. K. Otsuka and I. Yamanaka, *Electrochimica Acta*, 1990, **35**, 319-322.
64. I. Yamanaka, T. Onizawa, S. Takenaka and K. Otsuka, *Angewandte Chemie International Edition*, 2003, **42**, 3653-3655.
65. I. Yamanaka, T. Hashimoto, R. Ichihashi and K. Otsuka, *Electrochimica Acta*, 2008, **53**, 4824-4832.
66. J. Zhou, H. Guo, X. Wang, M. Guo, J. Zhao, L. Chen and W. Gong, *Chemical Communications*, 2005, 1631-1633.
67. D. Hâncu, J. Green and E. J. Beckman, *Industrial & Engineering Chemistry Research*, 2002, **41**, 4466-4474.
68. D. Hancu and E. J. Beckman, *Green Chemistry*, 2001, **3**, 80-86.

69. Q. Chen and E. J. Beckman, *Green Chemistry*, 2007, **9**, 802-808.
70. E. J. Beckman, *Green Chemistry*, 2003, **5**, 332-336.
71. P. Landon, P. J. Collier, A. J. Papworth, C. J. Kiely and G. J. Hutchings, *Chemical Communications*, 2002, 2058-2059.
72. P. Landon, P. J. Collier, A. F. Carley, D. Chadwick, A. J. Papworth, A. Burrows, C. J. Kiely and G. J. Hutchings, *Physical Chemistry Chemical Physics*, 2003, **5**, 1917-1923.
73. G. J. Hutchings, *Journal of Catalysis*, 1985, **96**, 292-295.
74. M. Haruta, T. Kobayashi, H. Sano and N. Yamada, *Chemistry Letters*, 1985, **16**, 405-408.
75. G. C. Bond, P. A. Sermon, G. Webb, D. A. Buchanan and P. B. Wells, *Journal of the Chemical Society, Chemical Communications*, 1973, 444b-445.
76. A. S. K. Hashmi and G. J. Hutchings, *Angewandte Chemie International Edition*, 2006, **45**, 7896-7936.
77. M. Haruta, N. Yamada, T. Kobayashi and S. Iijima, *Journal of Catalysis*, 1989, **115**, 301-309.
78. G. Bond and D. Thompson, *Gold Bulletin*, 2000, **33**, 41-50.
79. H. H. Kung, M. C. Kung and C. K. Costello, *Journal of Catalysis*, 2003, **216**, 425-432.
80. N. A. Hodge, C. J. Kiely, R. Whyman, M. R. H. Siddiqui, G. J. Hutchings, Q. A. Pankhurst, F. E. Wagner, R. R. Rajaram and S. E. Golunski, *Catalysis Today*, 2002, **72**, 133-144.
81. M. B. Boucher, S. Goergen, N. Yi and M. Flytzani-Stephanopoulos, *Physical Chemistry Chemical Physics*, 2011, **13**, 2517-2527.
82. Q. Fu, H. Saltsburg and M. Flytzani-Stephanopoulos, *Science*, 2003, **301**, 935-938.
83. M. Valden, X. Lai and D. W. Goodman, *Science*, 1998, **281**, 1647-1650.
84. H. G. Boyen, G. Kästle, F. Weigl, B. Koslowski, C. Dietrich, P. Ziemann, J. P. Spatz, S. Riethmüller, C. Hartmann, M. Möller, G. Schmid, M. G. Garnier and P. Oelhafen, *Science*, 2002, **297**, 1533-1536.
85. N. Lopez and J. K. Nørskov, *Journal of the American Chemical Society*, 2002, **124**, 11262-11263.
86. M. Chen, D. Kumar, C.-W. Yi and D. W. Goodman, *Science*, 2005, **310**, 291-293.
87. B. Nkosi, M. D. Adams, N. J. Coville and G. J. Hutchings, *Journal of Catalysis*, 1991, **128**, 378-386.
88. B. Nkosi, N. J. Coville and G. J. Hutchings, *Applied Catalysis*, 1988, **43**, 33-39.
89. M. Haruta, *Nature*, 2005, **437**, 1098-1099.
90. T. Hayashi, K. Tanaka and M. Haruta, *Journal of Catalysis*, 1998, **178**, 566-575.
91. M. Haruta and M. Daté, *Applied Catalysis A: General*, 2001, **222**, 427-437.
92. T. A. Nijhuis, T. Visser and B. M. Weckhuysen, *The Journal of Physical Chemistry B*, 2005, **109**, 19309-19319.
93. T. A. Nijhuis, B. J. Huizinga, M. Makkee and J. A. Moulijn, *Industrial & Engineering Chemistry Research*, 1999, **38**, 884-891.
94. T. A. Nijhuis, T. Q. Gardner and B. M. Weckhuysen, *Journal of Catalysis*, 2005, **236**, 153-163.
95. C. Qi, T. Akita, M. Okumura, K. Kuraoka and M. Haruta, *Applied Catalysis A: General*, 2003, **253**, 75-89.
96. M. D. Hughes, Y.-J. Xu, P. Jenkins, P. McMorn, P. Landon, D. I. Enache, A. F. Carley, G. A. Attard, G. J. Hutchings, F. King, E. H. Stitt, P. Johnston, K. Griffin and C. J. Kiely, *Nature*, 2005, **437**, 1132-1135.
97. L. Prati and M. Rossi, *Journal of Catalysis*, 1998, **176**, 552-560.
98. S. Biella, L. Prati and M. Rossi, *Journal of Catalysis*, 2002, **206**, 242-247.
99. L. Prati and F. Porta, *Applied Catalysis A: General*, 2005, **291**, 199-203.
100. L. Prati and G. Martra, *Gold Bulletin*, 1999, **32**, 96-101.
101. M. Comotti, C. D. Pina, R. Matarrese, M. Rossi and A. Siani, *Applied Catalysis A: General*, 2005, **291**, 204-209.
102. F. Porta, L. Prati, M. Rossi, S. Coluccia and G. Martra, *Catalysis Today*, 2000, **61**, 165-172.
103. F. Porta, L. Prati, M. Rossi and G. Scari, *Journal of Catalysis*, 2002, **211**, 464-469.

104. C. Della Pina, E. Falletta, L. Prati and M. Rossi, *Chem Soc Rev*, 2008, **37**, 2077-2095.
105. M. Comotti, C. Della Pina, E. Falletta and M. Rossi, *Advanced Synthesis & Catalysis*, 2006, **348**, 313-316.
106. A. Abad, C. Almela, A. Corma and H. García, *Tetrahedron*, 2006, **62**, 6666-6672.
107. A. Corma and M. E. Domine, *Chemical Communications*, 2005, 4042-4044.
108. A. Abad, P. Concepción, A. Corma and H. García, *Angewandte Chemie International Edition*, 2005, **44**, 4066-4069.
109. A. Corma and H. Garcia, *Chemical Society Reviews*, 2008, **37**, 2096-2126.
110. J. H. Sinfelt, J. L. Carter and D. J. C. Yates, *Journal of Catalysis*, 1972, **24**, 283-296.
111. J. H. Sinfelt, *Journal of Catalysis*, 1973, **29**, 308-315.
112. J. L. Carter, G. B. McVinker, W. Weissman, M. S. Kmak and J. H. Sinfelt, *Applied Catalysis*, 1982, **3**, 327-346.
113. M. Dhakad, D. Fino, S. S. Rayalu, R Kumar, A. Watanabe, H. Haneda, S. Devotta, T. Mitsuhashi and N. Labhsetwar, *Topics in Catalysis*, 2007, **42-43**, 273-276.
114. S. Murahashi, T. Naota and N. Hirai, *The Journal of Organic Chemistry*, 1993, **58**, 7318-7319.
115. X. Peng, Q. Pan and G. L. Rempel, *Chemical Society Reviews*, 2008, **37**, 1619-1628.
116. P. Lu, T. Teranishi, K. Asakura, M. Miyake and N. Toshima, *The Journal of Physical Chemistry B*, 1999, **103**, 9673-9682.
117. S. Hermans, R. Raja, J. M. Thomas, B. F. G. Johnson, G. Sankar and D. Gleeson, *Angewandte Chemie International Edition*, 2001, **40**, 1211-1215.
118. R. M. Navarro, B. Pawelec, J. M. Trejo, R. Mariscal and J. L. G. Fierro, *Journal of Catalysis*, 2000, **189**, 184-194.
119. E. P. Maris, W. C. Ketchie, M. Murayama and R. J. Davis, *Journal of Catalysis*, 2007, **251**, 281-294.
120. A. M. Ruppert, K. Weinberg and R. Palkovits, *Angewandte Chemie International Edition*, 2012, **51**, 2564-2601.
121. T. Conant, A. M. Karim, V. Lebarbier, Y. Wang, F. Girgsdies, R. Schlögl and A. Datye, *Journal of Catalysis*, 2008, **257**, 64-70.
122. J. Zhang, H. Wang and A. K. Dalai, *Journal of Catalysis*, 2007, **249**, 300-310.
123. M. Sankar, N. Dimitratos, P. J. Miedziak, P. P. Wells, C. J. Kiely and G. J. Hutchings, *Chemical Society Reviews*, 2012, **41**, 8099-8139.
124. F. Gao and D. W. Goodman, *Chem Soc Rev*, 2012, **41**, 8009-8020.
125. M. Piccinini, E. Ntainjua N, J. K. Edwards, A. F. Carley, J. A. Moulijn and G. J. Hutchings, *Physical Chemistry Chemical Physics*, 2010, **12**, 2488-2492.
126. M. Piccinini, J. K. Edwards, J. A. Moulijn and G. J. Hutchings, *Catalysis Science & Technology*, 2012, **2**, 1908-1913.
127. J. K. Edwards, B. E. Solsona, P. Landon, A. F. Carley, A. Herzing, C. J. Kiely and G. J. Hutchings, *Journal of Catalysis*, 2005, **236**, 69-79.
128. A. A. Herzing, A. F. Carley, J. K. Edwards, G. J. Hutchings and C. J. Kiely, *Chemistry of Materials*, 2008, **20**, 1492-1501.
129. J. K. Edwards, A. Thomas, B. E. Solsona, P. Landon, A. F. Carley and G. J. Hutchings, *Catalysis Today*, 2007, **122**, 397-402.
130. J. K. Edwards, A. Thomas, A. F. Carley, A. A. Herzing, C. J. Kiely and G. J. Hutchings, *Green Chemistry*, 2008, **10**, 388-394.
131. J. K. Edwards, A. F. Carley, A. A. Herzing, C. J. Kiely and G. J. Hutchings, *Faraday Discussions*, 2008, **138**, 225-239.
132. N. N. Edwin, J. K. Edwards, A. F. Carley, J. A. Lopez-Sanchez, J. A. Moulijn, A. A. Herzing, C. J. Kiely and G. J. Hutchings, *Green Chemistry*, 2008, **10**, 1162-1169.
133. J. C. Pritchard, Q. He, E. N. Ntainjua, M. Piccinini, J. K. Edwards, A. A. Herzing, A. F. Carley, J. A. Moulijn, C. J. Kiely and G. J. Hutchings, *Green Chemistry*, 2010, **12**, 915-921.

134. E. N. Ntainjua, M. Piccinini, J. C. Pritchard, J. K. Edwards, A. F. Carley, C. J. Kiely and G. J. Hutchings, *Catalysis Today*, 2011, **178**, 47-50.
135. J. K. Edwards, B. Solsona, P. Landon, A. F. Carley, A. Herzing, M. Watanabe, C. J. Kiely and G. J. Hutchings, *Journal of Materials Chemistry*, 2005, **15**, 4595-4600.
136. B. E. Solsona, J. K. Edwards, P. Landon, A. F. Carley, A. Herzing, C. J. Kiely and G. J. Hutchings, *Chemistry of Materials*, 2006, **18**, 2689-2695.
137. A. A. Herzing, M. Watanabe, J. K. Edwards, M. Conte, Z. R. Tang, G. J. Hutchings and C. J. Kiely, *Faraday Discussions*, 2008, **138**, 337-351.
138. E. N. Ntainjua, M. Piccinini, S. J. Freakley, J. C. Pritchard, J. K. Edwards, A. F. Carley and G. J. Hutchings, *Green Chemistry*, 2012, **14**, 170-181.
139. J. K. Edwards, B. Solsona, E. N. N, A. F. Carley, A. A. Herzing, C. J. Kiely and G. J. Hutchings, *Science*, 2009, **323**, 1037-1041.
140. J. K. Edwards, E. Ntainjua N, A. F. Carley, A. A. Herzing, C. J. Kiely and G. J. Hutchings, *Angewandte Chemie International Edition*, 2009, **48**, 8512-8515.
141. J. A. Lopez-Sanchez, N. Dimitratos, P. Miedziak, E. Ntainjua, J. K. Edwards, D. Morgan, A. F. Carley, R. Tiruvalam, C. J. Kiely and G. J. Hutchings, *Physical Chemistry Chemical Physics*, 2008, **10**, 1921-1930.
142. J. Pritchard, L. Kesavan, M. Piccinini, Q. He, R. Tiruvalam, N. Dimitratos, J. A. Lopez-Sanchez, A. F. Carley, J. K. Edwards, C. J. Kiely and G. J. Hutchings, *Langmuir*, 2010, **26**, 16568-16577.
143. R. C. Tiruvalam, J. C. Pritchard, N. Dimitratos, J. A. Lopez-Sanchez, J. K. Edwards, A. F. Carley, G. J. Hutchings and C. J. Kiely, *Faraday Discuss*, 2011, **152**, 63-86; discussion 99-120.
144. M. Sankar, Q. He, M. Morad, J. Pritchard, S. J. Freakley, J. K. Edwards, S. H. Taylor, D. J. Morgan, A. F. Carley, D. W. Knight, C. J. Kiely and G. J. Hutchings, *ACS Nano*, 2012, **6**, 6600-6613.
145. T. Ishihara, Y. Ohura, S. Yoshida, Y. Hata, H. Nishiguchi and Y. Takita, *Applied Catalysis A: General*, 2005, **291**, 215-221.
146. F. Menegazzo, P. Burti, M. Signoretto, M. Manzoli, S. Vankova, F. Boccuzzi, F. Pinna and G. Strukul, *Journal of Catalysis*, 2008, **257**, 369-381.
147. , 1989.
148. Q. Liu, J. C. Bauer, R. E. Schaak and J. H. Lunsford, *Applied Catalysis A: General*, 2008, **339**, 130-136.
149. V. R. Choudhary, C. Samanta and T. V. Choudhary, *Applied Catalysis A: General*, 2006, **308**, 128-133.

- CHAPTER TWO -

Experimental

In this chapter the standard procedures for the preparation of catalysts and reaction conditions for the direct H_2O_2 synthesis and benzyl alcohol oxidation are described. Changes to these conditions have been highlighted during the thesis when studying certain aspects. The characterisation techniques used to analyse the prepared catalysts are also described.

2.1 Catalyst Preparation

Important Note: 2.5 wt%-2.5 wt% Pd represents the bimetallic catalyst composition that has been found to be the most active for direct H_2O_2 synthesis. If not specified otherwise, the abbreviation "Au-Pd" indicates a 2.5 wt% Au- 2.5 wt% Pd composition has been used.

2.1.1 Impregnation

Pd-only, Au-only and Au-Pd bimetallic catalysts were synthesised via impregnation of various preformed supports; titania (TiO_2, P25, Degussa), activated carbon (C, Darco G60, Aldrich), silica (SiO_2, matrex 60, Fisher) ceria (CeO_2, Nano-grade, Aldrich). 2.5 wt% Au-2.5 wt% Pd supported catalyst (1 g) was prepared using the following standard procedure. $HAuCl_4.6H_2O$ solution (2.04 ml), extracted from a readymade solution (12.25 g Au dissolved in water (1000 ml)), and $PdCl_2$ (0.0417 g) were weighed accurately into a vial. The solution was stirred (400 rpm) and heated (80°C) until the $PdCl_2$ had dissolved forming a homogeneous solution. The appropriate support (0.95g) was added to the solution and stirred (400 rpm) until a paste with minimal water was formed, (this has proved to be the crucial step when producing Au-Pd / TiO_2 catalysts[1]). The resultant material was placed in an oven (110 ºC, 16 hours), before being calcined in static air (400 ºC, 3 hours, 20 ºC/min).

Monometallic Au and Pd were synthesised using the same protocol with appropriate amounts of $PdCl_2$ or $HAuCl_4.6H_2O$ solution and support. A minimal amount of HCl in deionised water was required to dissolve $PdCl_2$ for preparation of the Pd-only catalysts.

2.1.2 Physical Grinding

Pd-only, Au-only and Au-Pd bimetallic catalysts were synthesised via grinding of metal acetates with various preformed supports; titania (TiO_2, P25, Degussa), activated carbon (C, Darco G60, Aldrich), silica (SiO_2, matrex 60, Fisher) ceria (CeO_2, Nano-grade, Aldrich). 2.5 wt% Au-2.5 wt% Pd supported catalyst (1 g) was prepared using the following standard procedure. Palladium acetate (0.0474 g) and gold acetate (0.0526 g) were added to the selected support (0.95 g) and the mixture was ground in a pestle and mortar (10 mins). The resultant material was heated (350 ^oC, 2 hours, 20 ^oC/min) under flowing Helium.

2.1.3 Support Pre-treatment

Acid washing the support prior to impregnating with Au and Pd has been shown to decrease the final materials activity towards the hydrogenation pathway of H_2O_2 [2, 3]. In the case of carbon (acid washed activated carbon (AwC, Darco G60, Aldrich)) the path can be switched off completely using the following standard procedure.

Support (5 g) was washed with HNO_3 (150 ml, 2 wt%), filtered and washed with an excess of water until the pH was neutral. The resulting material was dried (110 °C, 16 hours) before being used for catalyst preparation.

2.2 Direct Synthesis of Hydrogen Peroxide - Batch reactor

Catalytic tests were performed using a Parr Instruments stainless steel autoclave (Figure 2.1) with a nominal volume of 100 ml and a maximum working pressure of 2000 psi. However, for convenience a Teflon liner was used reducing the volume to *ca.*75 ml.

The autoclave was equipped with an overhead mechanical stirrer (0-2000 rpm) and provision for measurement of temperature and pressure. The desired temperature was maintained with a cooling jacket. Two pre-mixed gas cylinders (5 %H_2 / CO_2 and 25 %O_2 / CO_2 supplied by BOC) were connected.

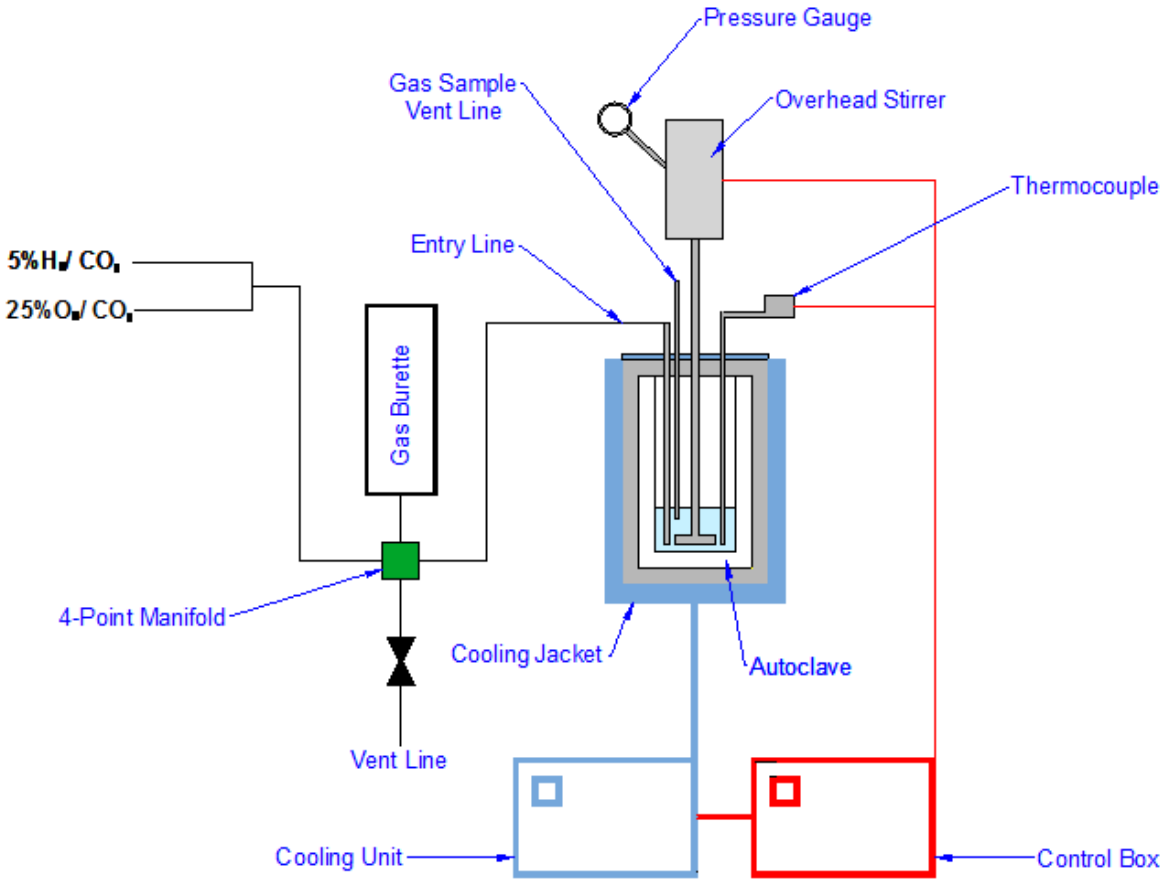

Figure 2.1 – Schematic of batch reactor

2.2.1 Standard Direct H_2O_2 Synthesis Conditions

Typically, the autoclave was charged with the catalyst (0.01 g), solvent (5.6 g CH_3OH and 2.9 g H_2O), purged three times with 5 %H_2/CO_2 (100 psi) and then filled with 5% H_2/CO_2 (420 psi) and 25 %O_2/CO_2 (160 psi) to give a hydrogen to oxygen ratio of 1:2 at a total working pressure of 580 psi. Stirring (1200 rpm) was commenced on reaching the desired temperature (2 °C). Standard experiments were carried out for 30 minutes. H_2O_2 yield was determined by titration of aliquots of the final filtered solution with acidified $Ce(SO_4)_2$ solution (*ca.*$8x10^{-3}$ M), using ferroin as indicator. $Ce(SO_4)_2$ solution was standardised against $(NH_4)_2Fe(SO_4)_2.6H_2O$. The error level, calculated from repeat experiments, was ± 2 molH_2O_2 $kg_{cat}^{-1}h^{-1}$ in all cases.

2.2.2 Standard H_2O_2 Hydrogenation and Decomposition Conditions

To test catalysts for H_2O_2 hydrogenation, the autoclave was charged with the catalyst (0.01 g) and a solution containing 4wt% H_2O_2 (5.6 g CH_3OH, 2.22 g H_2O and 0.68 g 50 wt% H_2O_2), purged three times with 5 %H_2/CO_2 (100 psi) and then filled with 5 %H_2/CO_2 (420 psi). Stirring (1200 rpm) was commenced on reaching the desired temperature (2 °C). Standard experiments were carried out for 30 minutes. The amount of hydrogenated H_2O_2 was determined before and after by titrating aliquots with acidified $Ce(SO_4)_2$ solution (*ca.*$8x10^{-3}$ M), using ferroin as indicator. Standardised as indicated in section 2.2.1.

The hydrogenation reaction described measures the catalysts activity towards H_2O_2 hydrogenation and decomposition. In order to evaluate the catalysts activity towards H_2O_2 decomposition only, 5 %H_2/CO_2 is omitted and 25 %O_2/CO_2 is utilised.

2.2.3 Evaluation of Catalyst Stability

The autoclave was charged with the catalyst (0.05 g), solvent (5.6 g CH_3OH and 2.9 g H_2O), purged three times with 5% H_2/CO_2 (100 psi) and then filled with 5% H_2/CO_2 (420 psi) and 25% O_2/CO_2 (160 psi) to give a total pressure of 580 psi. Stirring (1200 rpm) was commenced on reaching the desired temperature (2 ºC), and experiments were carried out for 30 minutes. After filtration, the catalyst was then dried in the oven (110 ºC, 2 h). Used catalyst (0.01 g) was tested using the standard H_2O_2 synthesis reaction conditions (section 2.2.1).

2.2.4 Direct H_2O_2 Synthesis Using Organic Solvents

In chapter 5 reactions were carried out using higher chain alcohols creating a two-phase reaction medium. The reaction conditions were the same as above however reactions were run at room temperature (*ca.*25 °C), to prevent the reaction medium freezing, and the solvent composition has been varied when studying certain aspects.

2.3 Direct Synthesis of Hydrogen Peroxide - Semi-Continuous Flow Reactor

In chapter 6, catalytic tests under a continuous flow of gas were performed inside a modified batch reactor, as shown in Figure 2.2, with a nominal volume of 100 ml and a maximum working pressure of 2000 psi.

Three flow meters with the possibility to regulate the rate of gas flow were installed. A mixing chamber with an internal volume of 150µm was positioned in order to make a homogenous combination of the three gases. At the exit of the reactor a back pressure regulator was installed; it controlled the inlet pressure by balancing an adjustable spring force against the inlet gas flow, making it possible to work with a fixed pressure inside the autoclave. Finally a gas chromatographer (GC-14 B SHIMADZU) was installed on line to measure the concentration of gases coming out of the reactor.

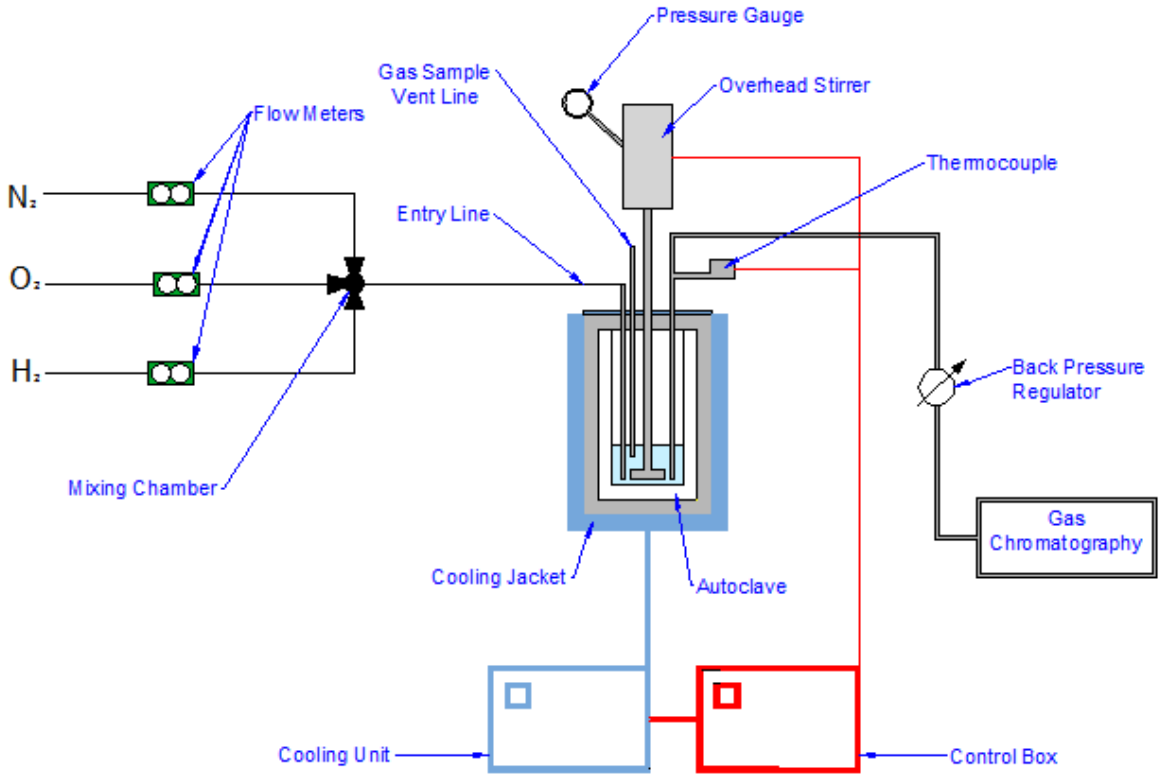

Figure 2.2 - Modified batch reactor with facility to flow the reactant gases continuously.

2.3.1 Standard Direct H_2O_2 Synthesis Conditions

The autoclave was charged with catalyst (0.02 g) and solvent (17 ml CH_3OH). Pre-mixed gas was injected inside the autoclave (N_2 180 ml min^{-1}, O_2 14 ml min^{-1} and H_2 7ml min^{-1}), in order to have a mixture of 89.5 %N_2, 7 %O_2, 3.5 %H_2. The H_2 concentration was monitored using the online GC, until the pressure (580 psi) and temperature (2 ^oC) was obtained. When the H_2 concentration stabilised the stirring (1200 rpm) was started (t=0). Throughout the reaction (30 min), the gas concentrations were recorded every 6 minutes. The gas was evacuated and the solution filtered to separate the catalyst. The concentration of H_2O_2 was determined calorimetrically at ?=410 nm after mixing a aliquot (*ca.*0.1 g) of the reaction medium with $TiCl_4$ in 2M H_2SO_4 (25 ml). Water concentration has been determined using Karl-Fischer titration in certain studies.

2.3.2 Product Analysis

2.3.2.1 UV-Visible Spectroscopy (UV-Vis)

Spectroscopy is a fundamental technique that allows quantification of the amount of radiation absorbed or emitted by a sample, based on the interaction of light with matter. In particular, UV-Vis spectroscopy concerns the absorption of emission of electromagnetic radiation in the ultraviolet or visible spectral region, ranging from 10-400 nm and 400-780 nm respectively. The radiation emitted by a light source is passed through a monochromator that selects one single wavelength and then focuses it on the sample. When light passes over the sample some energy will be absorbed causing molecules to undergo electronic transition from a lower energy state to one of higher energy. The signal is converted by a detector (usually a photomultiplier) that produces an electric signal when a photon strikes it. There are two different ways of describing the amount of radiation absorbed by a sample;

- Transmittance (T) is defined as the fraction of the initial radiation that crosses the sample, however, is more commonly recorded as the *percent transmittance*.

$$T = P/P_0$$

P = irradiance, energy per second per unit of the light beam

- Absorbance (A) is defined as;

$$A = \log(P_0/P) = -\log T$$

Absorbance is most commonly used as, according to the Beer-Lambert law, the electromagnetic radiation absorbed by the species is proportional to its concentration;

$$A = e.[c].l$$

[c] = concentration of the sample

e = molar extinction co-efficient

l = path length of the sample cell

The sample solution (between 0.2 and 5 ml) was mixed with a pre-prepared solution of $TiCl_4$ in 2M H_2SO_4 (25ml) and further diluted in a volumetric flask (100 ml) using water. The transmittance was measured at a wavelength of 410 nm (using a JASCO UV/Vis/NIR V-570 spectrophotometer) against a reagent blank and compared with a calibration curve as shown in Figure 2.3.

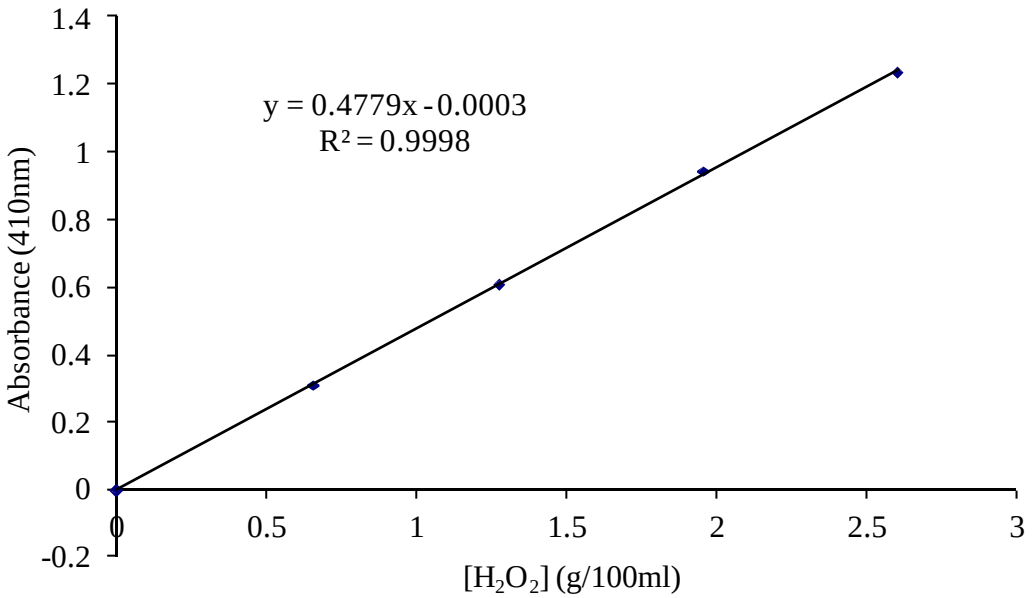

Figure 2.3 – Calibration of UV-Vis spectrometer with known concentrations of H_2O_2.

2.3.2.2 Karl Fischer Titration

The general reactions behind Karl Fischer titration consume water and iodine in a 1:1 ratio as follows:

$$ROH + SO_2 + RN \longrightarrow (RNH)^{+} SO_3R$$

$$(RNH)^{+} SO_3R + I_2 + H_2O + 2RN \longrightarrow (RNH)^{+} SO_4R + 2(RNH)I$$

Where RN = Base

In order to assure a stoichiometric course of the Karl Fischer titration, certain fundamental requirements must be met and several potential interferences must be avoided. The choice of working medium and pH range are the most critical considerations. Methanol is the preferred choice of working medium as it allows for a rapid and stoichiometric course of reaction. Most samples dissolve easily in methanol and it gives a sensitive and reliable indication of the end point. However, the direct H_2O_2 synthesis reactions are run with methanol as solvent, therefore a methanol free working medium was required. Research carried out by E. Scholz[4] revealed that other alcohols capable of improving the titre stability of the reagent such as ethanol, 2-propanol or methoxyethanol can be substituted for methanol.

A one-component titrating agent is used for the volumetric Karl Fischer titration. It contains all the reactants: iodine, sulphur dioxide and the bases imidazole and 2-methylimidazole, dissolved in diethyleneglycol monoethyl ether (DEGEE). Using 2-methylimidazole in addition to imidazole improves the stability and eliminates the formation of crystals, which can interfere with the performance of the titration. The concentration of the titrating agent was accurately calibrated using a Hydranal® Water Standard 10.0.

The volumetric Karl Fischer method was performed on a TitroLine KF where the titrating agent was accurately added through a piston burette. The standard procedure was as follows;

- The burette was filled with the titrating agent (Hydranal®-Composite 5),
- The working medium (Hydranal®-CompoSolver E) was added to the titration vessel,
- The working medium was titrated to dryness with the titrating agent,
- Sample was added (between 0.1 – 1 g depending on expected water concentration)
- The water concentration was determined through titration.

The volumetric method is used for the detection of the endpoint: An alternating current is applied to a pair of indicator electrodes. The voltage difference thus generated decreases drastically if traces of iodine are present. This fact is used to detect the endpoint of the titration.

2.3.2.3 Gas Chromatography

The exit gas was analysed by online gas chromatography (GC-14 B SHIMADZU). Manual injections were made at certain time intervals, so that a detailed profile of the composition of the exhaust gases could be obtained as a function of time. This allowed analysis of the catalytic performance of the catalyst during the reaction.

The injection valve of the GC was equipped with a six ways valve and two positions as shown in Figure 2.4.

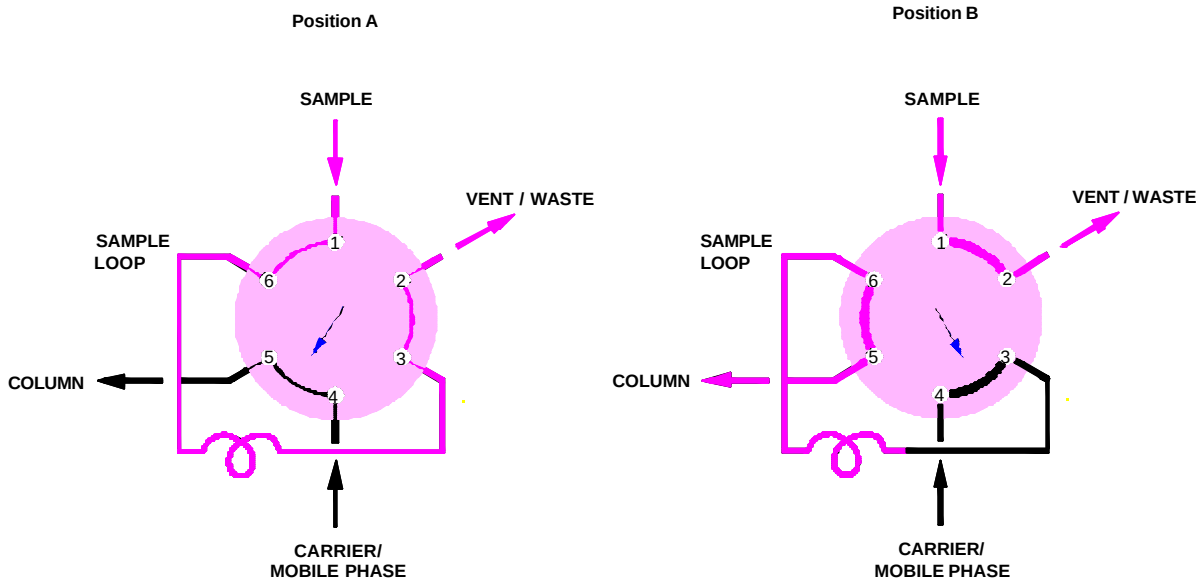

Figure 2.4 - Schematic of six way valve in two positions, A bypassing the GC, B after sample injection

The sample loop (0.375 ml) is constantly filled with the reactor effluent mixture. When an injection takes place, the carrier gas (Ar) injects the gases contained in the sample loop into the column molecular sieve, MS-5A. The GC was kept at constant temperature (100 ^{o}C) and the retention times are shown in Table 2.1.

Table 2.1 - Retention times observed for un-reacted gases during the direct H_2O_2 synthesis.

Eluted product	**Retention time (min)**
Hydrogen	0.524
Oxygen	1.438
Nitrogen	2.859

A thermal conductivity detector (TCD) was used for the detection and quantification of the un-reacted gases. The TCD produces a signal, the signal is plotted and an elution peak is obtained for each product. A TCD detects the difference between the heat capacities of a reference gas flow (carrier gas, Ar) and the sample gas flow (reactor products plus carrier gas). Differences in the heat capacities of different compounds mean that the results need to be corrected with a response factor (RF). The RF's for the TCD were obtained from calibration with 2 %H_2/N_2 and compressed air (oxygen content taken to equal 21 %). The peaks are integrated and the numeric value of each integrated peak is divided by the relative response factor of the compound. The result is the true response values. The true response values are proportional to the composition of the mixture, further calculations (as shown in Chapter Five) lead to the values of conversion and selectivity for a specific catalytic test.

2.4 Benzyl Alcohol Oxidation

2.4.1 Background

The catalytic oxidation of benzyl alcohol under free solvent conditions has been chosen as an appropriate model reaction for exploring the catalytic performance of the catalysts in chapter 4, at higher temperatures (140 ^oC). Not only has it been chosen due to its high reactivity in the presence of Au-Pd catalysts but also because of the existence of a complex reaction network as shown in Figure 2.5.

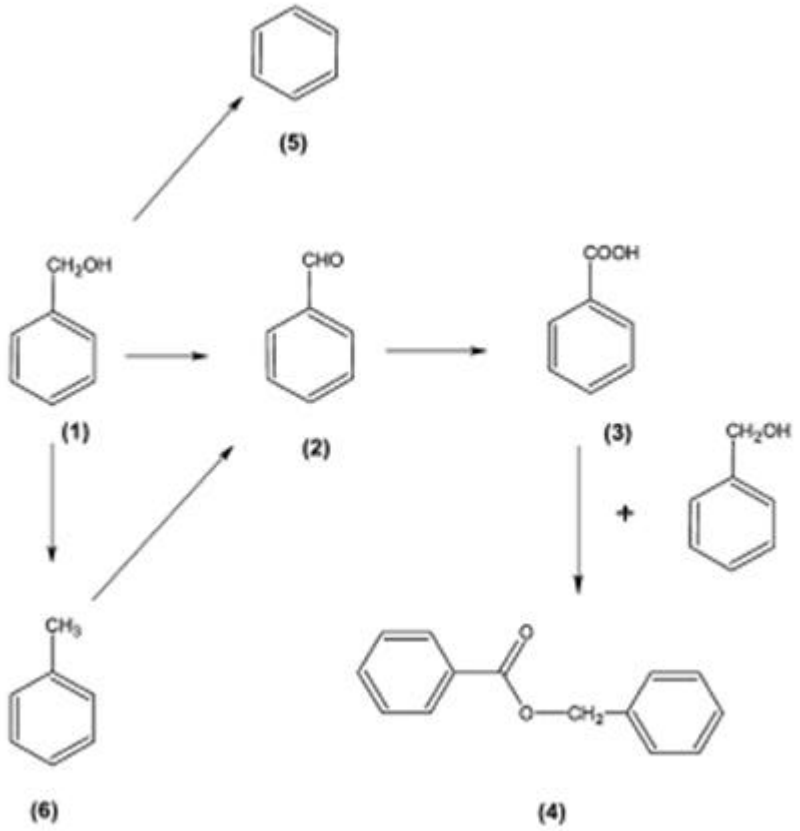

Figure 2.5 - General reaction pathway for benzyl alcohol oxidation: (1) benzyl alcohol; (2) benzaldehyde; (3) benzoic acid; (4) benzyl benzoate; (5) benzene; (6) toluene.[5]

The target product of benzyl alcohol oxidation is benzaldehyde, however other products e.g toluene, benzene, benzoic acid and benzyl benzoate can form depending on the reaction conditions and the nature of the catalyst used.[5-8] These by-products are likely to be the outcome of side reactions due to hydrogenolysis (toluene formation), decarbonylation (benzene) and esterification reaction pathways (benzyl benzoate), Figure 2.5. Two pathways were identified as the sources of the principal product, benzaldehyde: the first reaction pathway involved the direct catalytic oxidation of benzyl alcohol to benzaldehyde by O_2, while the second reaction pathway involved disproportionation of two molecules of benzyl alcohol to produce equimolar benzaldehyde and toluene.[9] Subsequent research has concentrated on controlling the disproportionation reaction in order to improve the selectivity to benzaldehyde,[10, 11] e.g. by choosing an appropriate support for Au-Pd such as MgO.[10]

Previously it has been demonstrated that Au-Pd catalysts active for selective oxidation of benzyl alcohol can be used for the selective oxidation of a broad range of alcohols.[12]

2.4.2 Standard Procedure

Catalyst testing was performed using an Autoclave Engineers stainless steel autoclave (Autoclve Engineers Inline MagneDrive III) with a nominal volume of 100 ml and a maximum working pressure of 2000 psi.

The vessel was charged with Benzyl alcohol (40 ml) and catalyst (0.025g). The autoclave was then purged 3 times with oxygen leaving the vessel at the desired pressure. The pressure was maintained constant throughout the experiment; as the oxygen was consumed in the reaction it was replenished. The stirrer speed (1500 rpm) was started and the reaction mixture was raised to the required temperature (140°C). Samples from the reactor were taken periodically (every 30 min) *via* a sampling pipe, ensuring that the volume purged before sampling was higher than the tube volume. An aliquot of the reaction mixture (0.5 ml) was diluted with mesitylene (0.5 ml) which is used as an internal standard and analysed by gas chromatography (GC-Varian 3800) using a CP-Wax column.

2.4.3 Product Analysis

The samples taken every 30 minutes were analysed by gas chromatography (GC-Varian 3800). An auto sampler 8400 was used to inject the samples (5.0 µl); each sample run took approximately 30 minutes. This allowed analysis of the catalytic performance of the catalyst during the reaction.

Samples were injected into the GC using a six-port valve (Figure 2.4). Separation of the reactants and products was done on a CP-Wax-S2 column (column pressure 5.0 psi, column flow 8.4 ml min^{-1}) using Argon as the carrier gas. The sample delivery program was built in conjunction with the temperature program (oven 250 ^{o}C) to get good separation of the reactants and products along with acceptable retention times as shown in Table 2.2.

Table 2.2 - Retention times observed for the products of benzyl alcohol oxidation, un-reacted benzyl alcohol and the internal standard mesitylene.

Eluted product	**Retention time (min)**
Benzene	1.852
Toluene	2.401
Mesitylene	3.934
Benzaldehyde	6.029
Benzyl alcohol	8.233
Benzoic acid	11.711
Benzbenzoate	12.465

A flame ionization detector (FID) was used for the detection and quantification of the products and un-reacted benzyl alcohol. The FID produces ions from burning the sample gas which will contain the hydrocarbons in turn as they are eluted. These ions are detected using a metal collector, which is biased, with a high direct current voltage. The current across the collector is proportional to the rate of ionisation which in turn depends upon the concentration of the hydrocarbon in the sample gas. The signal received from the GC was processed with Varian Star 4.5 software and with the aid of an electronic datasheet a quick analysis of the products is performed.

The GC was calibrated for analysis by injecting known amounts of reactants and products. The response factor (RF) is taken from the gradient of the calibration chart. The peak areas of each product corresponded to a specific concentration, determined by dividing the counts of each product by the corresponding response factor (RF) multiplied by the mesitylene count of the sample. Further calculations lead to the values of conversion and selectivity for a specific catalyst test. Mass balances were in the range of 95-105 % and the reaction data in the following work were reproducible with an error level of less than 5 %. Turn over frequency (TOF) was determined by assuming all the metal in the catalyst was active; moles of benzyl alcohol converted per kg metal per hour.

2.5 Characterisation Techniques[13-16]

The techniques briefly described in this section are vital in investigating the nano-scale materials used for heterogeneous catalysis, and go some way to explaining the catalytic activities observed.

2.5.1 Thermo-Gravimetric Analysis (TGA)

Thermal-gravimetric analysis (TGA) allows the measurement of weight changes of a material resulting from chemical reactions, decomposition, solvent and water evolution, and oxidation, as a function of increasing temperature or time. During the current work TGA is utilised to determine decomposition temperatures.

A Setaram TGA/Differential Thermal Analysis (DTA) was used to perform TGA. The instrument consists of a furnace which is mechanically connected to an analytical balance. The microbalance used is extremely sensitive; capable of detecting weight changes as small as 0.1 µg. When a sample is placed in the sample pan, the beam that supports the sample pan deflects. A detector measures the deflection with an optical sensor and uses current to return the beam to its original position. The amount of current used is a direct measure of the weight on the beam. The current is amplified and the signal is displayed as a percentage of total sample weight.

The sample pan was filled with sample (5-15 mg). The furnace was flushed with nitrogen and the inert atmosphere was maintained throughout the analysis. The weight change was recorded over a temperature range of 30 - 400 ^{o}C with a ramping rate of 5 ^{o}Cmin^{-1}.

2.5.2 X-Ray Diffraction (XRD)

X-ray diffraction (XRD) is used to characterise crystalline materials and determine their bulk structure. XRD allows the identification of crystalline phases, but cannot detect phases with crystallite size lower that *ca.*5 nm.

2.5.2.1 Background

X-ray diffraction experiments require an X-ray source, a sample, and a detector to pick up the diffracted X-rays. X-rays for diffraction experiments are normally produced by bombarding a metal target, often Cu or Mo, with a beam of electrons emitted from a heated filament. The incident electron beam will ionise electrons from the K-shell (1s) of the target atoms, and X-rays are emitted as the resultant vacancies are filled by electrons from the L (2p) or M (3p) levels (Figure 2.6A). This gives rise to intense Ka and Kß lines (Figure 2.6B).

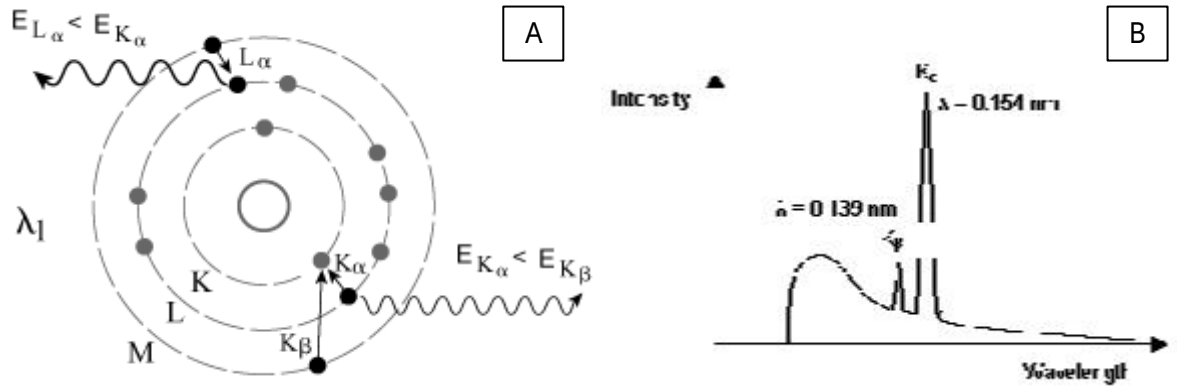

Figure 2.6 – A) Diagram illustrating the principles of electrons from outer shells filling the inner electron holes; causing the emission of x-rays, B) X-ray emission spectrum, showing characteristic Ka and Kß lines.

A monochromatic beam of wavelength, ?, can then be selected by reflecting an X-ray beam from a crystal monochromator according to the Bragg equation (Figure 2.7). Alternatively a filter may be used.

X-rays are scattered by their interaction with atomic electrons, and interference takes place between X-rays scattered form different parts of an atom. Powder samples have an infinite number of randomly orientated crystallites. When X-rays strike the sample, each set of lattice planes *hkl* will scatter them at the appropriate 2? angle, according to the Bragg equation.

$$n\lambda = 2d \sin\theta$$

Figure 2.7 - Bragg's law, where n is an integer, ? is the X-ray wavelength, d is the particular lattice plane spacing and ? is the Bragg diffraction angle.

When Bragg's law is satisfied, the reflected beams interfere constructively and a diffracted beam is produced, the angle of reflection is equal to the angle of incidence (Figure 2.8). If the angle of incidence does not satisfy Bragg's law, the reflected beams are out of phase and destructive interference occurs; hence the Bragg equation represents the condition for diffraction to take place.

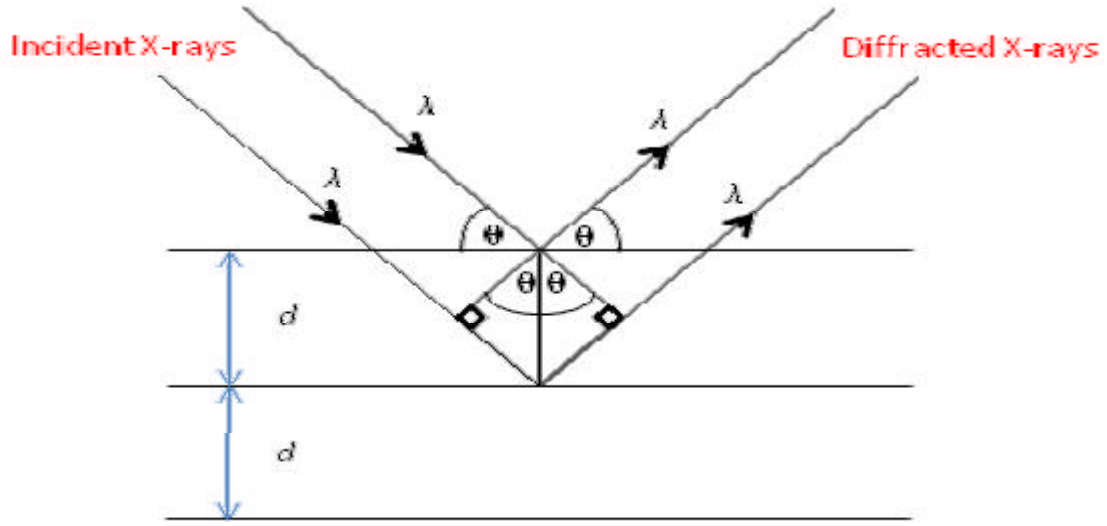

Figure 2.8 - Reflection of the incident beam at Bragg's angle, ?.

Since all possible orientations of crystallite should be present, a cone of scattering will be given at each Bragg angle. Each cone can be intercepted and analysised using the Debye-Scherrer X-ray powder method[17].

Limited information can be gained about the crystallite sizes according to the Debye-Scherrer equation (Figure 2.9). This is limited as particles under ca.5nm are too small to diffract the incident X-ray to a large enough angle to be measured.

$$B = \frac{0.893\lambda}{d \cos\theta}$$

Figure 2.9 – Debye-Scherrer equation, where B is the broadening of the diffraction peak, ? is the X-ray wavelength, d is the crystallite size and ? is the Bragg angle of diffraction.

2.5.2.2 Procedure

Investigation of the bulk of the materials was performed using powder X-ray diffraction (XRD) on a (?-?) PANalytical X'pert Pro powder diffractometer using a CuKa radiation source operating at 40 KeV and 40 mA. Standard analysis was performed using a 40 minute run with a back filled sample. Diffraction patterns of phases were identified using the International Centre for Diffraction Data (ICDD). Diffraction patterns were analyzed using full pattern refinement, with background functions, zero shift and pseudo-Voigt profile functions. Reference crystal structure profiles were provided by the inorganic crystal structure database[18].

2.5.3 Electron Microscopy (EM)

Electron microscopy (EM) provides a range of high resolution image modes used to characterise nanostructures. The resolution is such that it has the ability to image a single atom[19, 20]. From studying such images comments can be made about the topology of the material and a detailed particle distribution can be determined. When linked with an X-ray energy dispersive spectroscopy (XEDS) detector it has the ability to provide elemental composition and electronic structure.

2.5.3.1 Background

An incident high energy beam of electrons (formed by thermionic emission, often from a tungsten electrode) interacts with the sample surface in a variety of ways, some of which are shown in Figure 2.10. The electrons are scattered by the atomic potentials of the atom in the sample and broadly speaking the degree of scattering increases with atomic

number. In contrast to X-rays and neutrons, the scattering of electrons by matter is very strong and diffraction of electrons is feasible with gaseous samples.

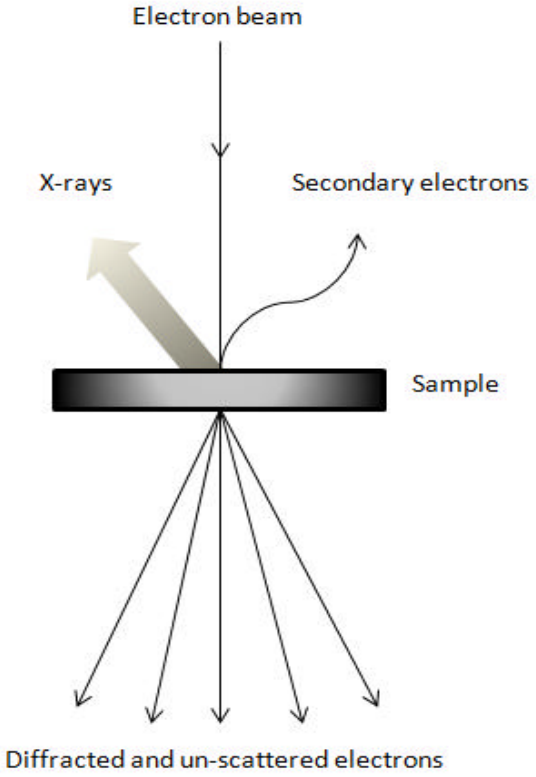

Figure 2.10 - The interaction of an electron beam with a sample

The low-energy (<50eV) secondary electrons emitted from the surface of the sample provide the basis for scanning electron microscopy (SEM). The electron beam can be concentrated to a small probe (say 20A diameter) that may be deflected across the sample in a raster fashion using scanning coils. The secondary electrons can be detected above the sample, and an image showing the intensity of secondary electrons emitted can be displayed. Heavier elements scatter the electrons more efficiently so show up brighter in the image (Z-contrast imaging[21]). The image is also dependent on the samples orientation as parts of the surface facing the detector appear brighter than surfaces facing away.

Imaging using secondary electrons, SEM, can produce images to a resolution of approximately 5nm however it is highly desirable to examine individual nanostructures with atomic level sensitivity. This requires a more sophisticated instrument, based on high

resolution transmission electron microscopy (TEM), where higher signal levels and better spatial resolution are available by detecting transmitted electrons. With a great deal of care and a good electron microscope it is possible to obtain images with atomic resolution, however the clarity is reduced.

The diffracted and un-scattered electrons form the basis for the conventional TEM[22] imaging mode. The diffraction pattern formed can be transformed directly into an image by magnetic lenses. A bright field (BF) image includes the transmitted beams so the holes appear bright, whereas a dark field (DF) image excludes the transmitted beams. Single-crystal diffraction patterns can be obtained by appropriately orientating a thin sample (approximately 1µm thick or less). Using the high magnification of the instrument individual crystallites can be selected from the sample and produce single crystal diffraction patterns which can be transformed into an image.

Scanning transmission electron microscopy (STEM) works on the same principle as conventional SEM, by forming a focused beam of electrons that is scanned over the sample, however thin samples are used so that transmission modes of imaging are also available. STEM has multiple detectors, providing a different and complimentary image of the sample. The advantage over standard transmission electron microscopy (TEM) is that radiation is reduced because the beam is not stationary. However it should be noted that many materials still will not survive the high vacuum in the microscope and the intense electron beam necessary for lattice imaging[13].

When an EM is coupled with XEDS, high resolution chemical analysis of the solids can be achieved. The bombardment of a sample with electrons gives rise to the emission of characteristic X-rays from the elements in the sample (see Figure 2.6); these can be detected and sorted into different energies using an energy dispersive detector. The intensity of the X-ray emission lines can be used to give quantitative chemical analysis. For example in Figure 2.11 point (left) and line (right) XEDS analysis modes have been used to prove the existence of a core shell morphology for a 40 nm Au-Ag ligand protected nano-particle.[23] Analytical work is restricted to elements with Z>10 on most instruments because the emissions from light elements are usually absorbed by the detector window. As the atomic number Z of the target element increases, the energy of the characteristic emissions increases and the wavelength decreases.

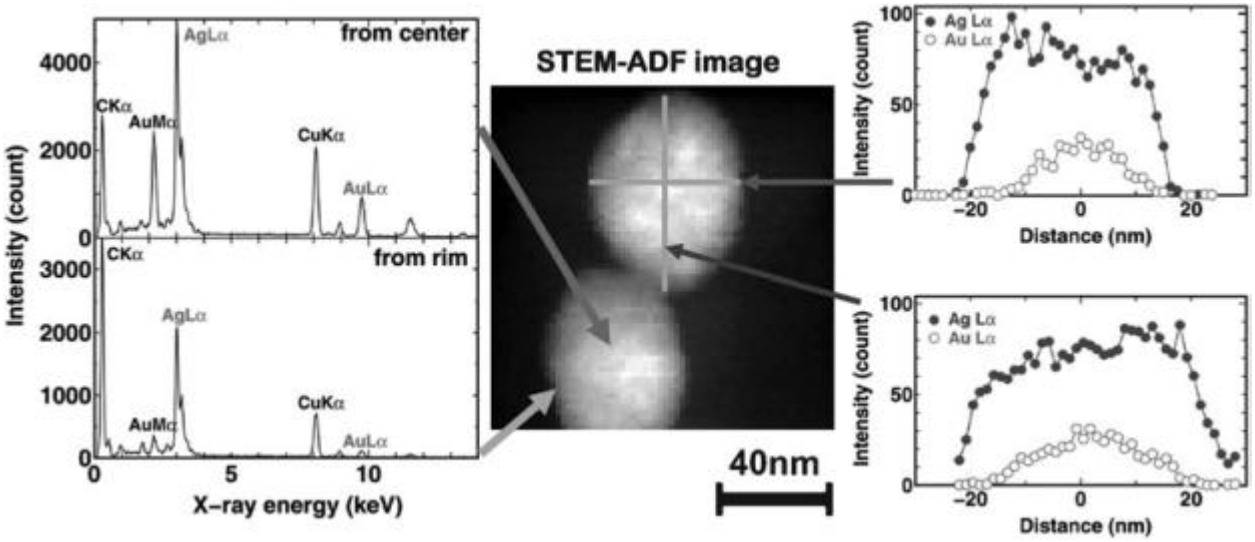

Figure 2.11 – Point XEDS spectra taken from the centre and edge of the Au-Ag nano-particle (Left) imaged in HAADF mode (centre) and the corresponding Ag I_8 and Au I_8 linescan profiles taken across the diameter of the same Au-Ag nano-particle (Right).[23]

2.5.3.2 Procedure

Samples were prepared for electron microscopy analysis by dispersing the powders in high-purity ethanol and allowing a drop of the solution to dry on a 300-mesh, Cu-supported lacey carbon film (SPI). All the scanning transmission electron microscopy (STEM) – high-angle annular dark field (HAADF) images were treated with a light low pass filter using a 3 x 3 kernel to decrease the high frequency noise. The JEOL 2000FX TEM/STEM was equipped with a Thermo Scientific Inc Si(Li) detector for X-ray energy dispersive spectroscopy (XEDS) analysis. Spectra were acquired with a total acquisition time of 120s. Spectrum images were acquired using a pixel dwell of 800ms. Multi-variate statistical analysis (MSA) of the XEDS data cubes was carried out utilising the MSA plug-in for Digital Micrograph.

2.5.4 X-ray Photoelectron Spectroscopy (XPS)

X-ray Photoelectron Spectroscopy (XPS) is a surface analysis technique (1-10 nm deep into the sample) giving information on the chemical and electronic state of the elements present at the surface of the material. Interpreting the data collected can indicate the concentration and composition of the elements. The basic principles, which are based on the photoelectric effect, are described in this section.

2.5.4.1 Background

When a sample is irradiated with x-rays an atom absorbs a photon of energy causing a core or valence electron with binding energy E_b to be ejected with a quantised kinetic energy E_{max}; this is based on the photoelectric effect as shown by Figures 2.12 and 2.13.

$$E^{K}_{Max} = h\nu - \Phi$$

Figure 2.12 - Photoelectric equation, E_{max} = maximum kinetic energy of the emitted electron, h? = energy of the incident X-ray, h is Planck's constant and ? is the frequency of the incident ray in Hertz. F is the work function; the energy, equal to the E_b, required to eject the photoelectron.

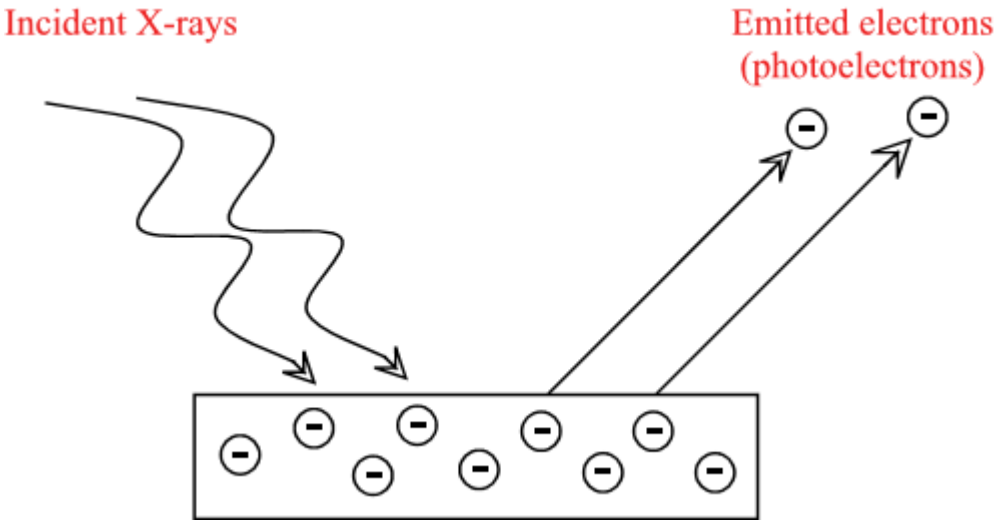

Figure 2.13 - Diagrammatic representation of the photoelectric effect.

Photoemission data shows kinetic energy of the photoelectron corresponding to the orbital from which the electron has been emitted. Binding energy of a photoelectron contains information on both the chemical state of the atom before photo ionisation (the initial state) and on the core-ionised atom left behind after the emission of an electron (the final state). However, it is often correct to interpret binding energy shifts as being the initial state.

A spectrometer detects the number of electrons being emitted and their kinetic energy. Each element has its own unique characteristic binding energies, which creates a 'fingerprint' spectrum of peaks. Different oxidation states can be identified as they cause the peaks on the spectra to shift slightly, due to changes in binding energies.

As XPS is a surface sensitive technique it can also recognise how well particles are dispersed over a support. When the particles are small almost all atoms are at the surface, covering the support to a large extent. This gives a high intensity from the particles, but a relatively low intensity from the support. Concentrations of the elements can be calculated when assuming a model structure first.

2.5.4.2 Procedure

XPS analysis was carried out using a Kratos Axis Ultra-DLD spectrometer employing a monochromatic AlKa X-ray source (75-120 W) and analyzer pass energies of 160 eV (for survey scans) or 40 eV (for detailed scans). Samples were mounted using double sided adhesive tape and analysised under ultra high vacuum (UHV) (<5x10-10 Torr). Binding energies were referenced to the C(1s) binding energy of adventitious carbon contamination which was taken to be 284.7eV.

2.6 References

1. J. C. Pritchard, Q. He, E. N. Ntainjua, M. Piccinini, J. K. Edwards, A. A. Herzing, A. F. Carley, J. A. Moulijn, C. J. Kiely and G. J. Hutchings, *Green Chemistry*, 2010, **12**, 915-921.
2. J. K. Edwards, E. Ntainjua N, A. F. Carley, A. A. Herzing, C. J. Kiely and G. J. Hutchings, *Angewandte Chemie International Edition*, 2009, **48**, 8512-8515.
3. J. K. Edwards, B. Solsona, E. N. N, A. F. Carley, A. A. Herzing, C. J. Kiely and G. J. Hutchings, *Science*, 2009, **323**, 1037-1041.
4. E. Scholz, *Fresenius' Zeitschrift für analytische Chemie*, 1983, **314**, 567-571.
5. J. A. Lopez-Sanchez, N. Dimitratos, P. Miedziak, E. Ntainjua, J. K. Edwards, D. Morgan, A. F. Carley, R. Tiruvalam, C. J. Kiely and G. J. Hutchings, *Physical Chemistry Chemical Physics*, 2008, **10**, 1921-1930.
6. P. Miedziak, M. Sankar, N. Dimitratos, J. A. Lopez-Sanchez, A. F. Carley, D. W. Knight, S. H. Taylor, C. J. Kiely and G. J. Hutchings, *Catalysis Today*, 2011, **164**, 315-319.
7. J. Pritchard, L. Kesavan, M. Piccinini, Q. He, R. Tiruvalam, N. Dimitratos, J. A. Lopez-Sanchez, A. F. Carley, J. K. Edwards, C. J. Kiely and G. J. Hutchings, *Langmuir*, 2010, **26**, 16568-16577.
8. N. Dimitratos, J. A. Lopez-Sanchez, D. Morgan, A. F. Carley, R. Tiruval am, C. J. Kiely, D. Bethell and G. J. Hutchings, *Physical Chemistry Chemical Physics*, 2009, **11**, 5142-5153.
9. S. Meenakshisundaram, E. Nowicka, P. J. Miedziak, G. L. Brett, R. L. Jenkins, N. Dimitratos, S. H. Taylor, D. W. Knight, D. Bethell and G. J. Hutchings, *Faraday Discussions*, 2010, **145**, 341-356.
10. M. Sankar, E. Nowicka, R. Tiruvalam, Q. He, S. H. Taylor, C. J. Kiely, D. Bethell, D. W. Knight and G. J. Hutchings, *Chemistry – A European Journal*, 2011, **17**, 6524-6532.
11. E. Cao, M. Sankar, E. Nowicka, Q. He, M. Morad, P. J. Miedziak, S. H. Taylor, D. W. Knight, D. Bethell, C. J. Kiely, A. Gavriilidis and G. J. Hutchings, *Catalysis Today*.
12. D. I. Enache, J. K. Edwards, P. Landon, B. Solsona-Espriu, A. F. Carley, A. A. Herzing, M. Watanabe, C. J. Kiely, D. W. Knight and G. J. Hutchings, *Science*, 2006, **311**, 362-365.
13. A. K. Cheetham and P. Day, *Solid State Chemistry Techniques*, Oxford Science, Oxford.
14. G. A. Somorjai and Y. Li, *Introduction To Surface Chemistry And Catalysis, Second Edition.*, John Wiley & Sons, New Jersey, 2010.
15. P. Atkins and J. d. Paula, *Elements of Physical Chemistry, Fourth Edition*, Oxford University Press, 2005.
16. M. Bowker, *The Basis and Applications of Hetrogeneous Catalysis*, Oxford University Press, Oxford, 1998.
17. H. P. Klug and L. E. Alexander, *X-ray diffraction procedures for polycrystalline and amorphous materials*, John Wiley and Sons, New York, 1974.
18. J. I. C. f. D. Data, 1984.
19. P. M. Voyles, J. L. Grazul and D. A. Muller, in *Ultramicroscopy*, Netherlands, Editon edn., 2003, vol. 96, pp. 251-273.
20. Y. Zhu, H. Inada, K. Nakamura and J. Wall, in *Nat Mater*, England, Editon edn., 2009, vol. 8, pp. 808-812.
21. S. J. Pennycook, *Philosophical Transactions of the Royal Society A.*, 2009, **367**, 3709-3733.
22. G. Thomas and M. J. Goringe, *Transmission electron microscopy of materials*, Wiley-Interscience, New York, 1979.
23. A. A. Herzing, M. Watanabe, J. K. Edwards, M. Conte, Z. R. Tang, G. J. Hutchings and C. J. Kiely, *Faraday Discussions*, 2008, **138**, 337-351.

- CHAPTER THREE -

The Effect of Heat Treatment Conditions on Catalytic Activity

3.1 Introduction

Catalysts have been prepared by impregnation and their activity towards the direct synthesis and hydrogenation of hydrogen peroxide under standard conditions are described and discussed. Experimental procedures are outlined in chapter 2.

The activity and stability of the catalyst depends not only on the method of preparation, but also on the conditions used for the subsequent thermal treatment.[1-4] After impregnation, many catalysts require calcination and/or a reduction stage to render the adsorbed metal species active. Thermal treatments may take the form of low-temperature drying operations (up to 150 ^{o}C) simply to remove water, although decomposition of some species are known to occur within this temperature range. Treatment temperatures between 150 ^{o}C and 500 ^{o}C are principally used to decompose the adsorbed species to the metal or metal oxide. Edwards et al.[5] have shown an un-calcined (dried at 110^{o}C for 16h-only) Au-Pd/TiO_2 catalyst prepared by impregnation has the highest activity for the direct H_2O_2 synthesis; however, it is not stable with both metals leaching from the TiO_2 surface during use. In order to stabilise the catalyst for subsequent uses, calcination at 400 ^{o}C for 3 h is crucial.

Compared to monometallic counterparts[6-8] bimetallic Au-Pd catalysts are highly active for the direct synthesis of H_2O_2; however, the origin of the active site is a topic currently under hot debate. The direct catalytic oxidation of H_2 with O_2 over an active catalyst will preferentially form water rather than H_2O_2. This is mainly because the catalysts which are active for H_2O_2 production could also facilitate the depletion of H_2O_2 formed *via* further hydrogenation and/or decomposition. However, a recent key discovery[9] has been that an acid pre-treatment of the support prior to the deposition of the metals, produces catalysts with higher activity towards H_2O_2 synthesis and lower activity towards the hydrogenation of H_2O_2, compared to catalysts prepared with an un-treated support. In the case of an acid pre-

treatment of activated carbon, the Au-Pd impregnated material produced has no activity towards the hydrogenation of H_2O_2 under standard conditions.[10]

Within this chapter the dependence of the calcination temperature on stabilising and switching off the hydrogenation of Au-Pd supported by acid-treated carbon (AwC) has been investigated. Detailed X-ray photoelectron spectroscopy (XPS) and Scanning transmission electron microscopy (STEM) of the materials has highlighted a number of key aspects which could be responsible for the effect in activity observed.

A series of carefully controlled reduction – oxidation treatments have also been utilised to elucidate the dependence of the Pd oxidation state on the activity of the catalyst towards H_2O_2 formation.

Note – The procedure for acid pre-treatment of the support has been described in section 2.1.3. Au-Pd = 2.5 %Au- 2.5 %Pd. The following reaction conditions have been utilised;

(a) Hydrogen Peroxide Synthesis catalyst (10 mg), 5% H_2/CO_2 (420 psi), 25% O_2/CO_2 (160psi), 5.6g MeOH and 2.9 H_2O as solvent, 2 ^oC, 1200 rpm, 30 minutes.

(b) Hydrogen Peroxide Hydrogenation catalyst (10 mg), 5% H_2/CO_2 (420 psi), 5.6g MeOH, 2.22 H_2O and 0.68g 50 wt% H_2O_2 as solvent, 2 ^oC, 1200 rpm, 30 minutes.

3.2 The Effect of Calcination Temperature on Au-Pd/Acid-Washed Carbon (AwC)

3.2.1 Direct H_2O_2 Synthesis and Hydrogenation

A series of Au-Pd/acid pre-treated activated carbon (AwC) catalysts, were calcined under static air at a variety of temperatures. The resultant materials were used for the direct synthesis of H_2O_2 and their stability was determined through re-use tests.

Table 3.1 - H_2O_2 synthesis activity of Au-Pd/AwC that were calcined at different temperatures.

Heat treatment[a]	**Productivity ($molH_2O_2kg_{cat}^{-1}h^{-1}$)**		**Hydrogenation ($molH_2O_2kg_{cat}^{-1}h^{-1}$)**
	Initial activity	***Re-use activity***	
Dried 120 °C	212	101	736
Calcined 200 °C	180	106	617
Calcined 300 °C	174	124	546
Calcined 350 °C	-	-	279
Calcined 400 °C	160	160	0

[a.] All catalysts were dried in air at 120 °C and then calcined for 3 h in static air at the temperature indicated

Table 3.1 shows that the material dried at 120 ^oC and not calcined has the highest activity of 212 $mol_{H2O2}kg_{cat}^{-1}h^{-1}$ on initial use; however upon re-use this activity falls by over a half to 101 $mol_{H2O2}kg_{cat}^{-1}h^{-1}$. This material is also the most active towards the hydrogenation of H_2O_2, destroying 736 $mol_{H2O2}kg_{cat}^{-1}h^{-1}$ under standard conditions, corresponding to a 36% consumption of the initial 4 wt% H_2O_2 present in the solution.

Increasing the calcination temperature decreases the catalysts activity towards the direct H_2O_2 synthesis; however, the loss in activity upon re-use is proportionally less. The hydrogenation rate also decreases with increasing calcination temperature.

A calcination temperature of 400 ^oC produces a material that retains all its initial activity, 160 $mol_{H2O2}kg_{cat}^{-1}h^{-1}$. Calcination at 400$^oC$ is also crucial to switch off the catalysts activity towards the H_2O_2 hydrogenation pathway. This would suggest that different sites on the catalyst are active for the H_2O_2 synthesis and hydrogenation.

The Au-Pd/AwC catalyst calcined at 350^oC still had considerable activity towards H_2O_2 hydrogenation (279 $mol_{H2O2}kg^{-1}h^{-1}$). A possibility for such a narrow temperature range is that a temperature >350 is required to decompose the metal chloride precursors completely. This binds the Au-Pd metal nano-particles to the surface and destroys/covers up active species for the H_2O_2 hydrogenation pathway.

3.2.2 X-Ray Photoelectron Spectroscopy (XPS)

The unused Au-Pd/AwC catalysts, which have been calcined at different temperatures, were analysed by XPS.

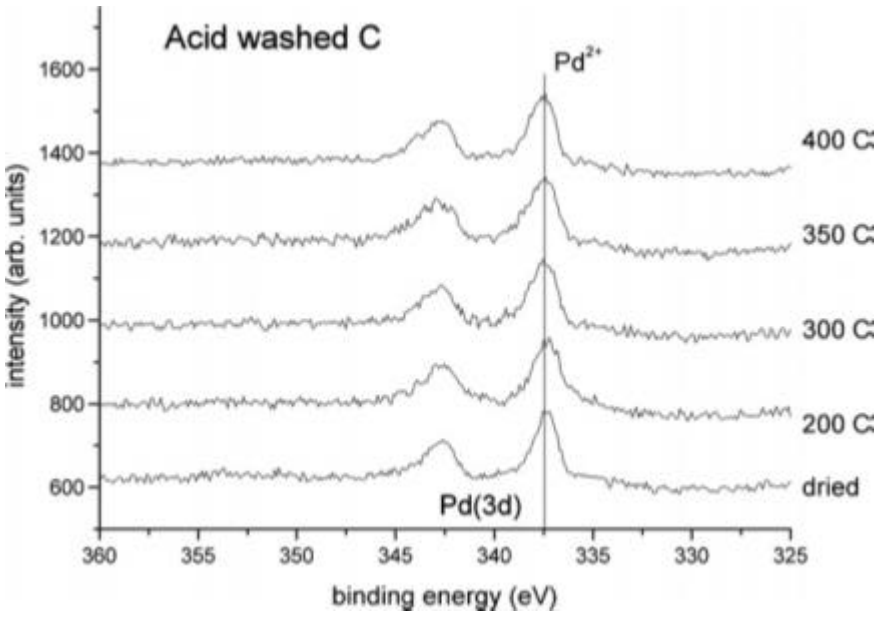

Figure 3.1 - Pd(3d) spectra observed for the Au-Pd/AwC catalysts calcined at the temperatures indicated.

Table 3.2 - Quantified XP data for the Au-Pd/AwC catalysts that were calcined at different temperatures.

Molar ratios	**Pd/Au**	**(Pd + Au)/C (x100)**	**Cl/C (x100)**	**Pd^{2+} (%)**
Acid pre-treated (°C)				
Dried 120°C	2.7	0.44	0.71	>90
Calcined 200°C	3.8	0.45	0.61	>90
Calcined 300°C	4.3	0.46	0.51	>90
Calcined 350°C	4.1	0.41	0.44	>90
Calcined 400°C	4.2	0.50	0.42	>90

The Pd (3d) spectra (Figure 3.1) and quantified X-ray photoelectron data (Table 3.2) indicate that Pd^{2+} species are predominant (=90 %) on the acid pre-treated support, for all calcination

temperatures. The Pd/Au ratio significantly increases when the catalyst is calcined at all temperatures utilised compared to the baseline material (dried only). This observation could in principle reflect the formation of core-shell type particles[8], as seen previously on a titania support[5]; however, detailed electron microscopy analysis, presented later, shows that this is not the case. Therefore, it is postulated that the variation in Pd/Au ratio is due to changes in the relative sizes of the Pd and Au nano-particles.

The corresponding Au(4f) and Cl(2p) spectra for the Au-Pd/AwC catalysts, are shown in Figure 3.2.

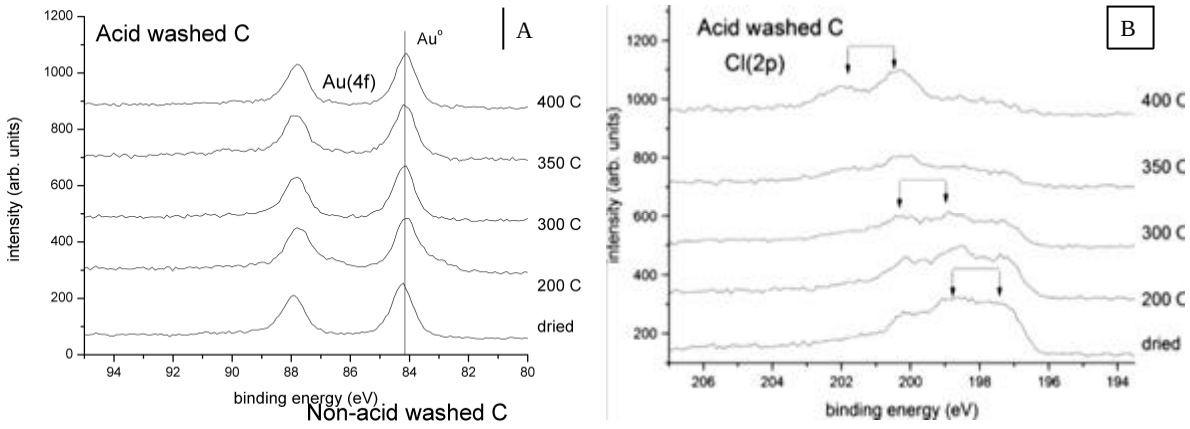

Figure 3.2 – XPS spectra observed for Au-Pd/AwC catalysts, calcined at the temperatures indicated. (A) Au(4f), (B) Cl(2p).

Firstly, looking at the Au(4f) spectra in figure 3.2A, there is no obvious affect on Au oxidation state or intensity in the Au-Pd/AwC catalysts calcined at different temperatures. This is as expected and highlights the characteristics of the difference in standard reduction potentials (E_0) of Au^{3+} and Pd^{2+} cations, 1.50 and 0.92 respectively.

The Cl(2p) spectra in figure 3.2B, shows the presence of chloride on the AwC surface at all calcination temperatures. The Cl signal is due to residual chlorine from the two metal precursors, aurochloric acid and palladium chloride, used to prepare the catalysts. Three doublets, which are indicated, are present in the spectra. The higher binding energy doublet (corresponding to a more ionic, negatively charged Cl^{X-} species) dominates after calcination at 400 ^{o}C. This indicates that increasing the calcination temperature causes an electronic

modification. A weaker chloride signal as calcination temperature increases is due to the loss of chloride from the surface as the metal chloride precursor oxidises.

3.2.3 Electron Microscopy (EM)

To determine the Au and Pd distribution as a function of calcination temperature, the unused Au-Pd/AwC catalysts, were analysed by scanning transmission electron microscopy (STEM), Figure 3.3.

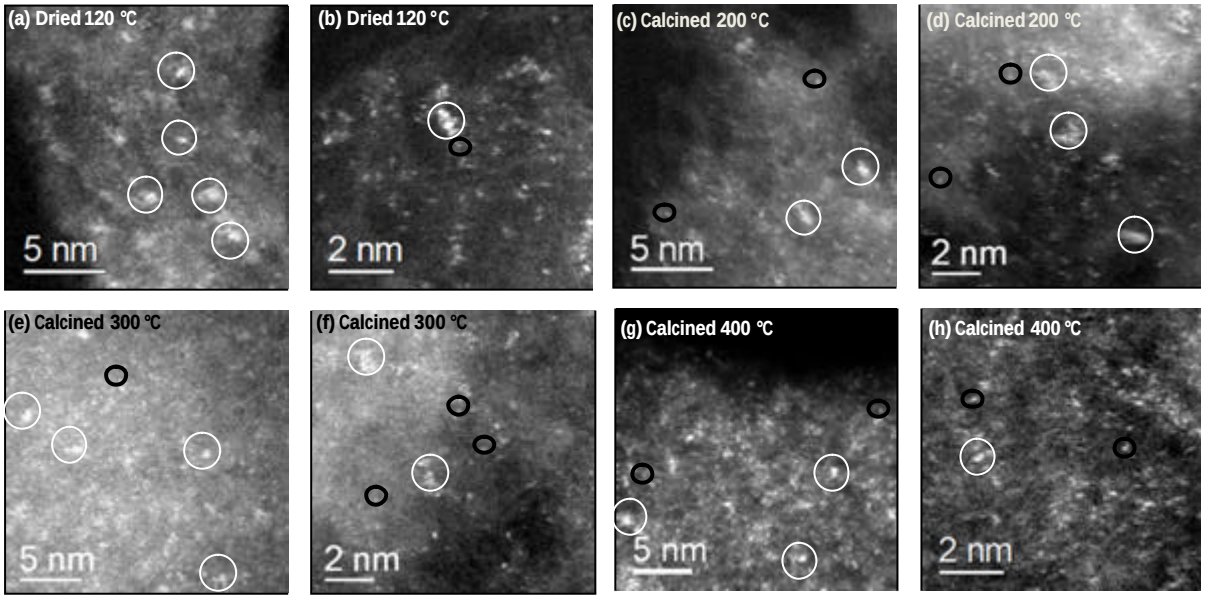

Figure 3.3 - Representative STEM-HAADF images of Au-Pd/AwC catalysts calcined at different temperatures.

As expected, in all samples highly dispersed Pd metal species, namely sub-nm clusters and single atoms, were found over all the acid pre-treated acid carbon support. In comparison to the baseline catalyst (dried only), the population of sub-nm clusters appeared to decrease progressively as the calcination temperature was increased. The calcination process appears to aid in dispersing the sub-nm clusters into atomically dispersed species. However, the differences between the morphology of samples with increasing calcination were subtle.

It was not possible to directly determine the chemical identity of the sub-nm species and isolated atoms, in the Au-Pd/AwC samples. Atomic level Z-contrast measurements were not effective due to the rough nature of the support which leads to complicating height variations between neighbouring metallic species. However, a previous study by Edwards et al.[11] of monometallic Au and Pd supported on untreated activated carbon showed that Pd tends to be more highly dispersed than Au for catalysts prepared using this impregnation route. This leads to the suggestion that in the bimetallic system the atomically dispersed species are mainly Pd intermixed with a dilute concentration of atomically dispersed Au.

3.2.4 Discussion

In order to stabilise a Au-Pd/AwC catalyst prepared using impregnation, calcination in static air at 400^{o}C for 3h is required. Calcination at 400^{o}C is also critical to the catalysts activity towards the hydrogenation pathway being switched off under the reaction conditions utilised. These are two key traits a catalyst material would require for the direct H_2O_2 synthesis to become viable at an industrial level.

However, explaining why these activity traits are only observed for the material calcined at 400^{o}C proves difficult. Below is a summary of the trends observed in surface composition and activity towards H_2O_2 synthesis, with increasing calcination temperature:

- H_2O_2 synthesis activity decreases
- H_2O_2 hydrogenation activity decrease, with hydrogenation switching off at 400 ^{o}C
- Catalyst stability increases, with stability being achieved at 400 ^{o}C
- Chloride concentration decreases and we observe more ionic, negatively charged Cl^{x-} species
- Pd/Au ratio increases for temperatures up to 300 ^{o}C then stabilises at a value of around 4.2
- Improved overall metal dispersion

The detailed XPS and STEM measurements highlighted a number of trends in the surface composition, with increasing calcination temperature, which could be responsible for the catalytic activity observed individually or simultaneously. This makes it difficult to identify the crucial feature/s required to switch off H_2O_2 hydrogenation.

The activity trends indicate that the effect of calcination temperature is a trade off between the activity of the catalyst and its stability. Unstable catalysts indicate that active components are leaching into the reaction mixture[5]; these could be forming active homogeneous catalysts which are producing a 'false' activity result. Dissanayake and Lunsford[12, 13] found there is a linear relationship between colloid palladium concentration and H_2O_2 formation. Although a homogeneous catalytic system of colloidal Pd is highly interesting at a fundamental level, it is not suitable from a commercial perspective since the management of the colloid would be a difficult task.

The modification of chloride species with calcination temperature in Figure 3.2B can be linked with decomposition/oxidation of the metal chloride precursor and an interaction between the chloride species with activated carbon. Simonov *et al.*[14] studied H_2PdCl_4 adsorption onto graphite-like carbon supports, identifying two competitive adsorption pathways.

The first, involved reduction of Pd (based on the high reducing power of carbon) close to the exterior of carbon particles, forming electropositive C^+ holes on the carbon surface. The Cl^- anions compensate the charge through the formation of an electric double layer on the carbon surface. If this is occurring, in this case, the reduced Pd is quickly oxidised at the temperatures used as >10% Pd^0 was found by XPS on the acid washed activated carbon of all catalysts.

The second, involved $PdCl_2$ forming p-complexes with C=C fragments of the carbon network. During drying weakly bonded $PdCl_2$ migrate along the surface to form more stable small clusters. The centres of agglomeration were found to be the surface steps due to their high adsorption potential. It can be assumed that increasing the calcination temperature oxidises the strongly bound Pd-complexes, releasing Cl^- to further interact with the carbon support. The breaking up of the complexes may be a reason why the dispersion of the Pd^{2+} nano-particles increases with increasing calcination temperature, as seen in the STEM images.

The effect that chloride has on the direct synthesis of H_2O_2 has been linked previously to a decrease in H_2O_2 hydrogenation activity, however it is complicated by the presence of H^+ ions and leaching of active metal species into the reaction medium.[15, 16] Therefore to investigate further, a chloride free 'baseline' catalyst is required a preparation technique to produce a halide free catalyst is called physical grinding is investigated in Chapter Four.

Another observation is the Pd/Au ratio is higher for the calcined samples compared to the dried only material. This represents an important discovery with higher Pd/Au ratio with the palladium in a Pd^{2+} oxidation state is linked with switching off H_2O_2 hydrogenation of the Au-Pd/AwC calcined at 400^{o}C. However, it is clear that this alone has little to do with the observed effects on hydrogenation activity and catalyst re-usability, as there are no significant changes in Pd/Au ratio between samples calcined at 200 and 400 ^{o}C. Samples calcined at 200 ^{o}C still have significant activity towards H_2O_2 hydrogenation. The reason for this could be the migration of all $PdCl_2$-complexes to the step sites being complete at 200 ^{o}C and increasing the temperature serves to increase oxidation/decomposition of the complexes.

The change of Pd oxidation state with calcination temperature is inconclusive from the results reported so far as Pd^{2+} species predominant (>90 %) for all Au-Pd/AwC catalysts calcined at all temperatures. Detecting changes in the Pd oxidation state are complicated by the presence of the Au ($4d_{5/2}$) component under the Pd (3d) envelope making it difficult to accurately assign the contribution of each state when Pd^{2+} species are predominant (>90 %).

3.3 The Effect of Pd Oxidation State on Direct H_2O_2 Synthesis

3.3.1 Background

The effect of the Pd oxidation state in the direct synthesis of H_2O_2 has been investigated by many research groups, when using monometallic Pd supported catalysts, with little agreement. Choudary et al.[17-19] have claimed that a PdO catalyst is more suitable than a Pd^0 catalyst, owing to its higher selectivity, increasing H_2O_2 yield for the direct synthesis.

Interestingly, separate studies[20-22] have demonstrated that supported PdO catalysts are more selective but less active than the corresponding Pd^0 catalysts in the direct H_2O_2 synthesis. The higher H_2O_2 selectivity of a PdO catalyst compared with the corresponding Pd^0 catalyst is attributed to the lower H_2O_2 decomposition/hydrogenation activity of the PdO catalyst. This is mostly attributed to the higher propensity of H_2O_2 to adsorb on the Pd^0 surface as compared to the PdO surface.

On the other hand, other researchers, including Thompson and co-workers[23], Chinta and Lunsford[24], and Burch and Ellis[25], have claimed that higher H_2O_2 productivity and selectivity can be obtained with Pd^0 catalysts.

The oxidation of surface/sub-surface Pd^0 and/or partial oxidation of bulk Pd^0 to PdO in the supported Pd^0 catalysts has been claimed to promote the H_2O_2 productivity[17]. Oxidation/ partial oxidation can be achieved by treating a Pd^0 catalyst with an oxidising agent, such as perchloric acid, hydrogen peroxide, nitrous oxide, oxygen or air. However, the increase in the H_2O_2 yield/ selectivity has been found to be small[17].

Melada et al.[26] used a combination of reduction and oxidation treatments to achieve higher catalytic activity/selectivity for direct H_2O_2 synthesis. They demonstrated that pre-treatment of a supported PdO catalyst with 5%H_2/Ar, reduced the PdO phase to Pd^0 (partially or completely). Using Temperature Programmed Reduction (TPR) it was shown that different Pd^{2+} species reduce at different temperatures. Some of their samples contained room temperature-reducible Pd^{2+} species; reduction of PdO species formed during calcination can be reduced at temperatures as low as -15^oC. Others possessed Pd^{2+} species reducible at about 90-100^oC along with another Pd^{2+} fraction that reduced at about 280-300 ^oC. The latter species was believed to be due to residual palladium (II) oxychloride, formed during calcination and not decomposed during thermal treatment.

It was postulated that oxygen pre-treatment immediately after the hydrogen pre-treatment of a PdO catalyst may result in the formation of a mixed PdO-Pd^0 phase in the catalyst with surface enriched PdO. Supported Pd^0 catalysts with surface-enriched PdO were found to be highly selective for the direct H_2O_2 formation because of their low H_2O_2 decomposition activity.

3.3.2 Comparison of Au-Pd/AwC and Au-Pd/C Calcined at 400 ^oC

To investigate the effect of Pd oxidation state further, a comparison of the Au-Pd/AwC and Au-Pd/C catalyst (both calcined at 400 ^oC) is required. The Au-Pd/C catalyst is stable and has activity for H_2O_2 hydrogenation corresponding to a lower H_2O_2 synthesis activity than Au-Pd/AwC as shown in Table 3.3.

Table 3.3 - Direct H_2O_2 synthesis and hydrogenation activities of Au-Pd/C and Au-Pd/AwC.

Sample	**Productivity ($molH_2O_2kg_{cat}^{-1}h^{-1}$)**		**Hydrogenation ($molH_2O_2kg_{cat}^{-1}h^{-1}$)**
	Initial activity	***Re-use activity***	
Au-Pd/C	110	110	120
Au-Pd/AwC	160	160	0

Detailed STEM measurements[10] have previously shown that the acid pre-treatment of the support does not appear to affect the morphology or dispersion of the metallic species in the catalysts, so eliminating the metal dispersion as a factor in this case. They both contain Au-rich nano-particles and a highly dispersed coverage of atomic and cluster-like Pd species, intermixed with small amount of atomically dispersed Au.

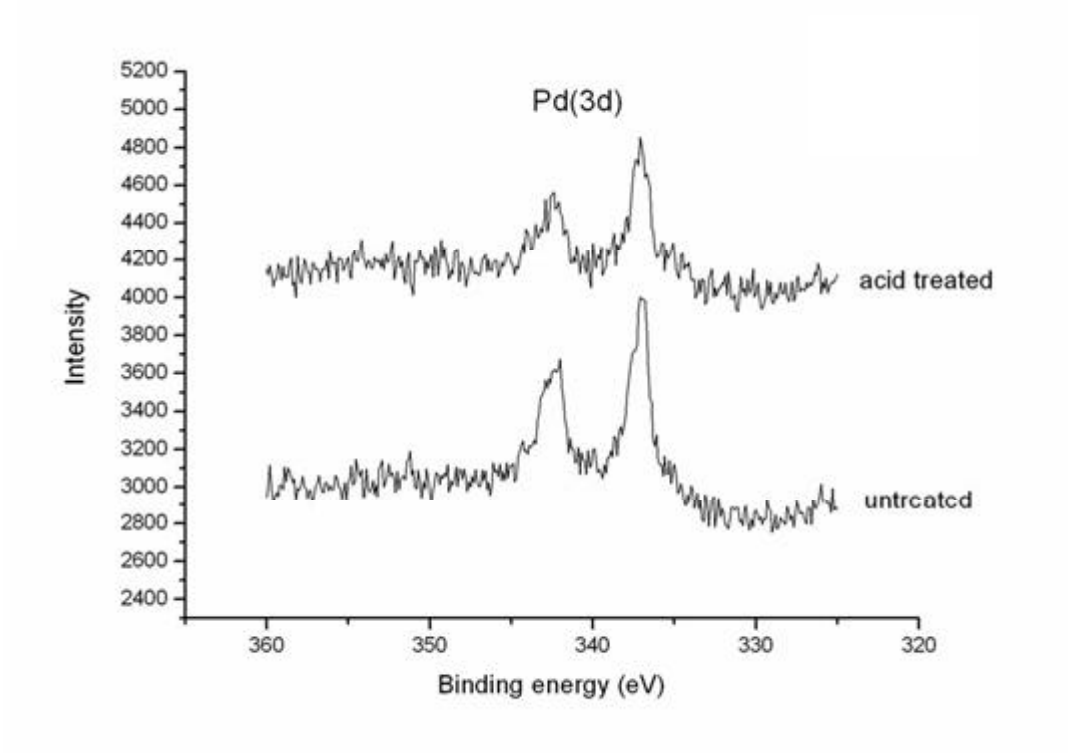

Figure 3.4 – XPS spectra comparing Au-Pd/AwC (acid pre-treated carbon) and Au-Pd/C (untreated carbon), calcined at 400°C.[10]

.

Table 3.4 - Quantified XPS data and H_2O_2 synthesis/hydrogenation data for stable Au-Pd/AwC (acid pre-treated carbon) and Au-Pd/C (untreated carbon) catalysts, calcined at 400°C.[10]

	XPS – Molar ratios			
	Pd/Au	(Pd + Au)/C (x100)	Cl/C (x100)	Pd^{2+} (%)
Acid pre-treated				
Calcined 400°C	4.2	0.50	0.42	>90
Untreated (°C)				
Calcined 400°C	1.4	0.63	0.44	68

The untreated carbon catalyst has a lower H_2O_2 productivity as a result of its activity towards H_2O_2 hydrogenation. Examining the quantified XPS data, it is clear the acid pre-treated sample has increased palladium at the surface, which is also in a different oxidation state. The presence of reduced palladium on the untreated carbon indicates that it has a higher reducing power.[14]

Firstly, the pre-treated sample has a higher Pd/Au ratio indicating changes in the relative size of the Pd and Au nano-particles leading to an apparently enhanced surface palladium concentration (the molar ratio for a nominal 2.5 wt%Au-2.5 w%Pd loading is 1.8). More highly dispersed Pd at the surface, of the catalyst, could explain the higher productivity of the acid pre-treated supported catalyst, as Pd has been shown to be the active component in the catalyst. Monometallic gold supported catalysts have relatively low activity compared to their monometallic Pd counterparts. The addition of Au to Pd to produce a bimetallic Au-Pd supported catalyst causes a synergistic effect on activity. This effect is probably achieved by Au altering the physical or electronic structure of Pd sufficiently to inhibit its hydrogenation ability. This is similar to observations by Goodman and co-workers[27] that Au promoted the synthesis of vinyl chloride monomer (VCM) for Au-Pd model catalysts. This effect was achieved through a slight alteration of the atomic spacing of Pd, which did not affect VCM synthesis but did inhibit its decomposition. It is also thought that gold has a unique ability in stabilising the hydroperoxy (OOH) species which is a precursor for H_2O_2 formation[28].

Secondly, the untreated supported catalyst, which is active for the H_2O_2 hydrogenation pathway, exhibits both Pd^{2+} and Pd^0 species, with a Pd^{2+} concentration of 68 %. This indicates that an acid pre-treatment of the support modifies the electronic state of the highly dispersed Pd, increasing H_2 selectivity by switching off the H_2O_2 hydrogenation pathway. The modification of the Pd could have been induced by Au and/or changes in the Cl^{x-} or O^{2-} species on the acid pre-treated support.

In order to investigate the effect of the palladium oxidation state on the performance of Au-Pd/AwC samples, a set of carefully controlled reduction-oxidation treatments were performed. Testing each material for the direct H_2O_2 synthesis and gathering quantified XPS data, the catalytic activity was investigated as a function of the palladium oxidation state.

3.4 Reduction – Oxidation Treatment of Au-Pd/Acid-Washed Carbon

Catalysts prepared by incipient wetness impregnation using standard conditions (calcined at 400 ^{o}C preceding deposition of the metals) were subjected to various reduction – oxidation treatments to elucidate the influence of the Pd oxidation state.

3.4.1 Direct H_2O_2 Synthesis and Hydrogenation

A Au-Pd catalyst, prepared on an acid pre-treated activated carbon support, that showed high activity towards the direct synthesis and some residual hydrogenation of hydrogen peroxide was selected as the baseline material. This was prepared by manipulation of the impregnation procedure as described previously[29]. A sample with some hydrogenation activity was needed to determine that the reduction-oxidation treatment had a negative or positive effect on hydrogenation activity.

3.4.1.1 Reduction

Firstly the baseline catalyst was subjected to a series of reduction procedures at various temperatures, using 5 %H_2/Ar. Their activities towards the direct synthesis and hydrogenation of hydrogen peroxide are shown in Table 3.5.

Table 3.5 - Effect of reduction at various temperatures on a 2.5 wt%Au-2.5 wt%Pd/AwC catalyst (pre-treated with 2 %HNO_3).

Sample	**Heat treatment**		**Productivity** ($molH_2O_2kg_{cat}^{-1}h^{-1}$)	**Hydrogenation** ($molH_2O_2kg_{cat}^{-1}h^{-1}$)
a	Initial catalyst		185	60
	Sample **a** + 5 %H_2/Ar treatment			
	Temperature (^{o}C)	*Time (h)*		
b	100	1	176	72
c	110	2	173	86
d	150	2	141	126
e	200	2	80	286

Increasing the temperature of the reduction treatment causes a decrease in the catalyst activity for the direct synthesis of hydrogen peroxide which corresponds to an increase in activity towards the hydrogenation pathway. After raising the temperature from 150 ^{o}C to 200 ^{o}C there is a sharp decrease in productivity and increase in hydrogenation.

3.4.1.2 *Direct oxidation*

Au-Pd/AwC was subjected to direct oxidation in pure O_2 (99 % as supplied by BOC) at various temperatures and times, after calcination in static air (400 ^{o}C, 3 h). The resultant catalytic activities towards the direct synthesis and hydrogenation of H_2O_2 are shown in Table 3.6.

Table 3.6 - Effect of oxidation at various temperatures and times on a 2.5 wt%Au-2.5 wt%Pd/carbon catalyst (pre-treated with 2 %HNO_3).

Sample	**Heat treatment**		**Productivity ($molH_2O_2kg_{cat}^{-1}h^{-1}$)**	**Hydrogenation ($molH_2O_2kg_{cat}^{-1}h^{-1}$)**
a	Initial catalyst		185	60
	Sample **a** + O_2 treatment			
	Temperature (^{o}C)	*Time (h)*		
f	200	3	179	13
g	200	5	165	13
-	300	3	117	15

The direct oxidation treatment at 200 ^{o}C for 3h (sample f) does not affect the H_2O_2 productivity activity significantly, although the hydrogenation drops considerably. Increasing the time or the temperature of the oxidation leads to a decrease in the direct synthesis activity; however, the hydrogenation activity remains virtually the same.

3.4.1.3 Re-oxidation of reduced sample

Au-Pd/AwC which was previously subjected to calcination (400 ^{o}C, 3 h) and reduction (5 %H_2/Ar, 200 ^{o}C, 2 h) at was re-oxidised in pure O_2 (99 %) at 100 ^{o}C and 200 ^{o}C; the resultant materials activities towards the direct synthesis and hydrogenation of H_2O_2 are shown in Table 3.7.

Table 3.7 - Effect of oxidation at various temperatures on a reduced 2.5 wt%Au-2.5 wt%Pd/AwC catalyst (pre-treated with 2 %HNO_3).

Sample	**Heat treatment**		**Productivity ($molH_2O_2kg_{cat}^{-1}h^{-1}$)**	**Hydrogenation ($molH_2O_2kg_{cat}^{-1}h^{-1}$)**
a	Initial catalyst		185	60
	Sample **a** + 5%H_2/Ar treatment			
	Temperature (^{o}C)	*Time (h)*		
e	200	2	80	286
	Sample **e** + O_2 treatment			
	Temperature (^{o}C)	*Time (h)*		
h	100	3	116	180
i	200	3	126	0

Increasing the temperature of the oxidation treatment causes an increase in the activity of the catalyst towards H_2O_2 formation, and decreases the hydrogenation activity. The Au-Pd/AwC catalyst reduced at 200 ^{o}C and then re-oxidised at 200 ^{o}C exhibits, very importantly, no activity towards the hydrogenation of hydrogen peroxide.

3.4.2 X-Ray Photoelectron Spectroscopy (XPS)

The Pd(3d) XP spectra for the Au-Pd catalysts, supported on acid pre-treated carbon, subjected to reduction and oxidation treatments are presented in Figure 3.5 and re-oxidised sample in Figure 3.6. The quantified XPS data is shown in Table 3.8.

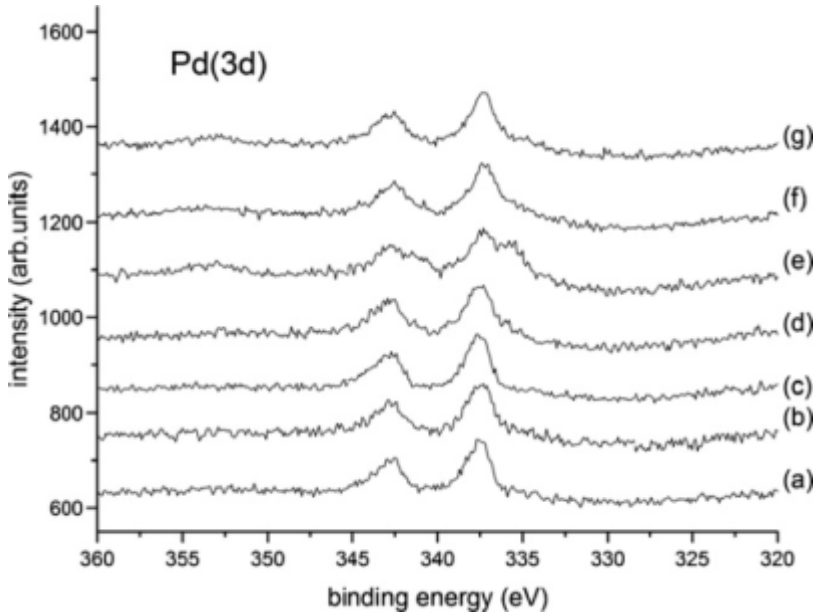

Figure 3.5 - Pd(3d) spectra observed for the 2.5 wt% Au-2.5 wt% Pd/AwC catalysts after sequential reduction and oxidation. (a) calcined under standard conditions; (b) reduced in H_2/Ar at 100 ^oC for 1 h, (c) reduced in H_2/Ar at 110 ^oC for 2 h; (d) reduced in H_2/Ar at 150 ^oC for 2 h; (e) reduced in H_2/Ar at 200 ^oC for 2 h; (f) oxidised at 200 ^oC for 3 h, and (g) oxidised at 200 ^oC for 5 h.

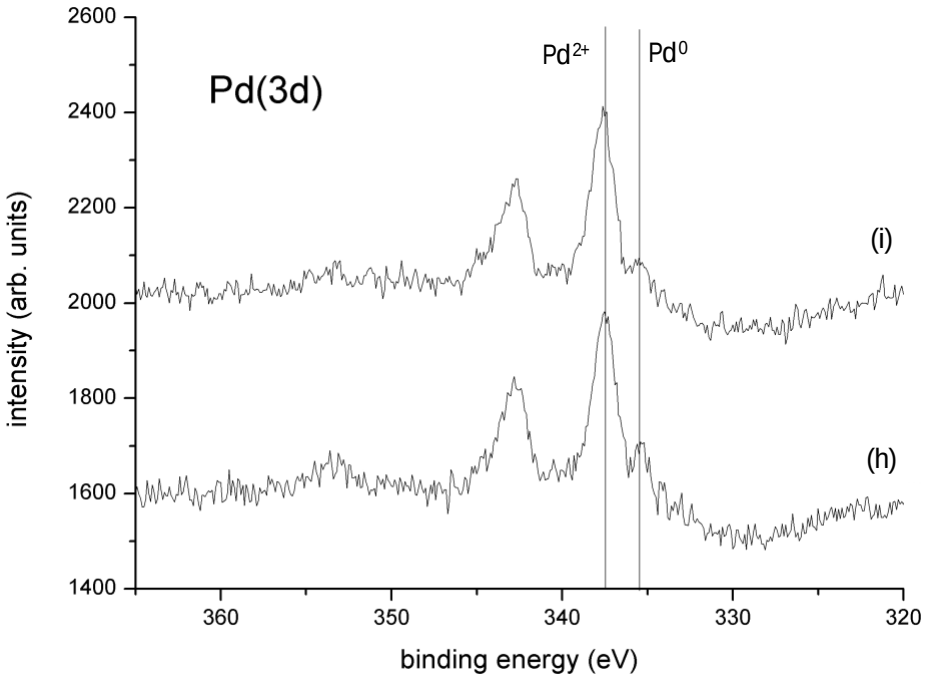

Figure 3.6 - Pd(3d) spectra observed for the 2.5 wt% Au-2.5 wt% Pd/AwC catalysts calcined at 400 ^oC in static air for 3 h, reduced at 200 ^oC in 5 %H_2/Ar for 2 h then subjected to 99 % O_2 at (h) 100 ^oC for 3 h and (i) 200 ^oC for 3 h.

Table 3.8 - Quantified XPS data resulting from figure 3.5 and 3.6, for the Au-Pd/AwC catalysts after different thermal treatments

Sample	Sample treatment	[Au] (at. %)	[Pd] (at. %)	Pd/Au*	Pd^{2+} (%)
a	Calcined in air at 400 ^{o}C 3h	0.061	0.268	3.9	>90
b	Reduced at 100 ^{o}C 1 h	0.054	0.252	4.1	>90
c	Reduced at 110 ^{o}C 2 h	0.062	0.267	3.8	>90
d	Reduced at 150 ^{o}C 2 h	0.068	0.291	3.7	87
e	Reduced at 200 ^{o}C 2 h	0.154	0.291	1.3	61
f	Oxidised in O_2 200 ^{o}C 3 h	0.12	0.27	1.6	>90
g	Oxidised in O_2 200 ^{o}C 5 h	0.16	0.33	1.7	>90
h	Re-oxidised in O_2 100 ^{o}C 3 h	0.132	0.292	1.7	86
i	Re-oxidised in O_2 200 ^{o}C 3 h	0.133	0.290	1.6	>90

*corrected for overlap of the Pd($3d_{5/2}$) and Au($4d_{5/2}$) components.

The greatest increase in H_2O_2 hydrogenation is seen with a reduction temperature of 200 ^{o}C, which corresponds to a dramatic decrease in the Pd/Au ratio from ca 3.9 to 1.3 due to an increase in the Au intensity. An increase in surface gold is usually linked with a decrease in H_2O_2 hydrogenation due to gold's ability to stabilise the H_2O_2. In this case the higher H_2O_2 hydrogenation is more likely to be explained by the increased surface Pd in the metallic state.

Directly oxidising the catalyst leads to a decrease in hydrogenation activity from 60 to 13 $mol_{H2O2}kg_{cat}^{-1}h^{-1}$, as well as a decreased Pd/Au ratio. In this case no changes in the oxidation state have been observed however it is likely the Pd is more oxidic. This linked with higher surface Au would explain the lower hydrogenation.

It is clear from Figure 3.6 that the re-oxidation of Sample e does not fully oxidise the Au-Pd/AwC material with a peak still present in the Pd^0 region. However, there is a significant increase in the Pd^{2+} %. The catalyst re-oxidised at 200 ^{o}C for 3h has >90 % of Pd^{2+} could explain the switching off of the H_2O_2 hydrogenation pathway. However the directly oxidised samples have similar XPS to this catalyst so the activity is more likely to be due to changes in the morphology or particle distribution from subsequent reduction-oxidation heat treatments.

Re-oxidation leads to a small increase in the Pd/Au ratio from 1.3 to 1.6. These effects are consistent with the activity of the catalyst and as has previously been indicated, the Pd/Au ratio is important in controlling the formation of H_2O_2. The level of interaction between Au and Pd is likely to be crucial to reducing and switching off H_2O_2 hydrogenation[28].

The Pd (3d) spectra were analysed to deduce the Pd^{2+} and Pd^0 content. These were obtained through curve fitting of the Pd (3d) spectra, although the process was complicated by the presence of the Au ($4d_{5/2}$) component under the Pd (3d) envelope. This is a particular problem here due to the significant surface gold content for the reduced and re-oxidised samples. Strict parameter constraints had to be used, some dependent on the measured values for the metal-oxide binding energy shift and the magnitude of the Au (4d) spin orbit splitting.

The Cl (2p), Au (4f) and O (1s) spectra (Figure 3.7) showed no significant changes in profile. There is no change in either the Au or Cl- electronic state, indicating the difference between the standard reduction potentials of Au^{3+} and Pd^{2+} cations. Also confirming significant interaction of Cl^- species with the support as discussed in section 3.2.4.

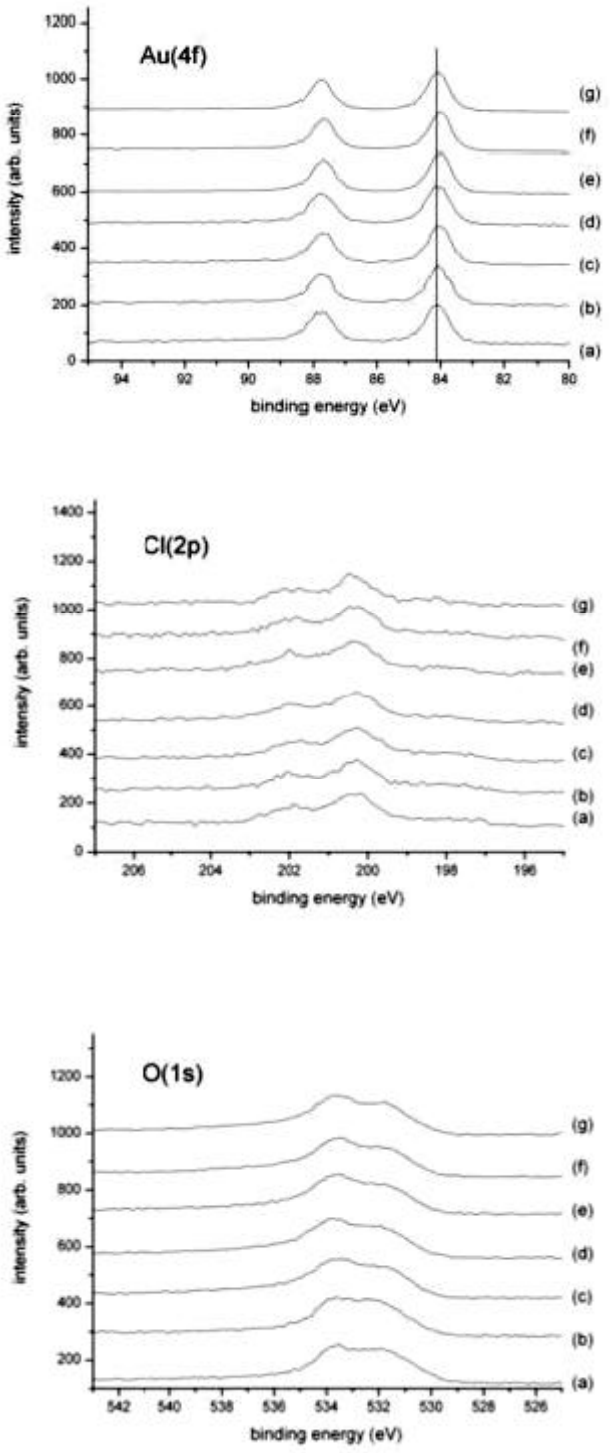

Figure 3.7 - Au(4f), Cl(2p) and O(1s) spectra observed for the 2.5 wt% Au-2.5 wt% Pd/AwC catalysts after sequential reduction and oxidation. (a) calcined under standard conditions; (b) reduced in H_2/Ar at 100 ^oC for 1 h, (c) reduced in H_2/Ar at 110 ^oC for 2 h; (d) reduced in H_2/Ar at 150 ^oC for 2 h; (e) reduced in H_2/Ar at 200 ^oC for 2 h; (f) re-oxidised at 100 ^oC for 3 h, and (g) re-oxidised at 200 ^oC for 3 h.

3.4.3 Electron Microscopy (EM)

A series of STEM-HAADF images of the Au-Pd catalysts, supported on acid pre-treated activated carbon support, subjected to the sequential reduction and oxidation conditions are shown in Figure 3.8.

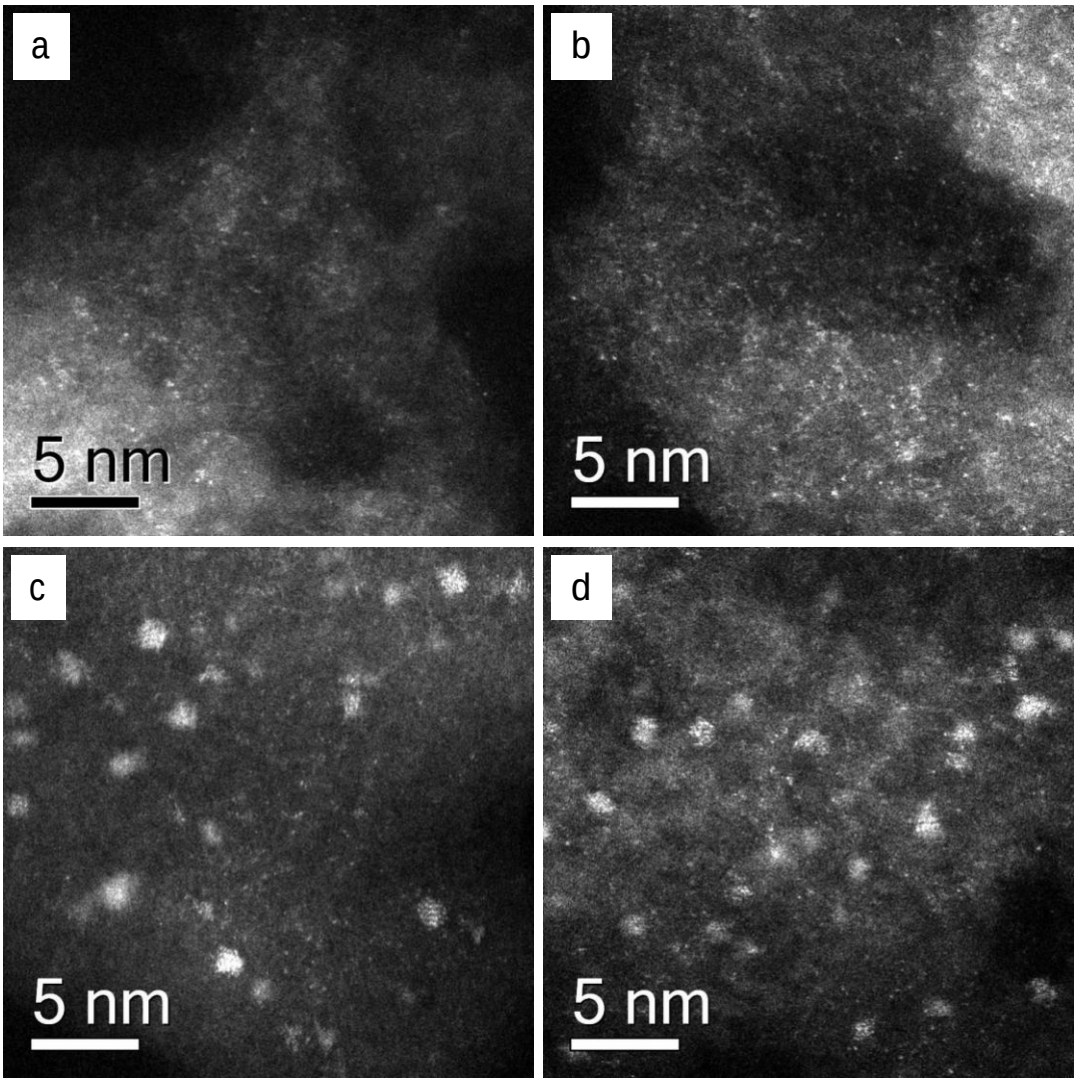

Figure 3.8 - STEM-HAADF images of the Au- Pd/AwC catalysts after sequential reduction and oxidation. (a) Sample calcined under standard conditions at 400 ^{o}C for 3 h; (b) shows sample (a) heated in O_2 at 200 ^{o}C for 3 h; (c) shows sample (a) reduced in 5% H_2/Ar at 200 ^{o}C for 2 h; and (d) shows sample (c) re-oxidised at 200 ^{o}C in O_2 for 3 h.

The baseline material, figure 3.8a, was the Au-Pd/AwC catalyst that had been calcined at 400^{o}C for 3 hours, which showed predominately atomically dispersed Pd species intermixed

with a small number of Au atoms. When this sample was heated in O_2 for 3 hours (direct oxidation) there was no observable change in the atomic dispersion of Pd and Au. Conversely, when the starting material was reduced in 5 %H_2/Ar for 2 hours, the majority of the atoms were found to have gathered up into 0.5-2.0 nm diameter metallic clusters. Upon re-oxidation of this reduced sample in O_2 for 3 hours, the cluster morphology was largely retained, although presumably the particles were now more oxidic in character, and had the effect of switching off the H_2O_2 hydrogenation as shown in table 3.6.

3.4.4 Discussion

The increase in Pd^0 is most notable for the Au-Pd/AwC sample reduced at 200 ^oC, which shows the highest hydrogenation activity; after this sample was re-oxidised, the concentration of Pd^0 decreased as shown in Figure 3.9.

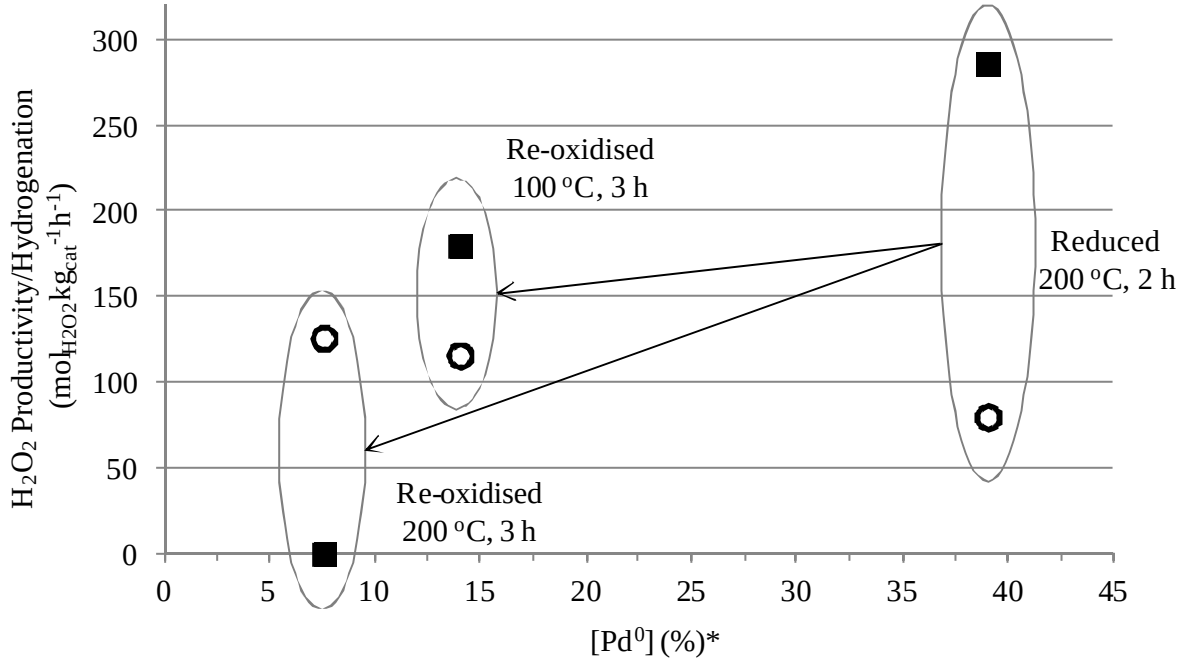

Figure 3.9 - Effect of surface Pd^0 concentration on the H_2O_2 synthesis (○) and H_2O_2 hydrogenation (■). *from XPS

During Pd reduction, to form Pd^0 species, a structural rearrangement may occur (Figure 3.10), leading to the formation of surface defects (more active sites), which could easily account for the improved hydrogenation performance responsible for the low H_2O_2 synthesis activity of the reduced materials. Upon re-oxidising the reduced species an oxidic layer could be forming stabilising the metal particles and protecting them from taking part in H_2O_2 hydrogenation.

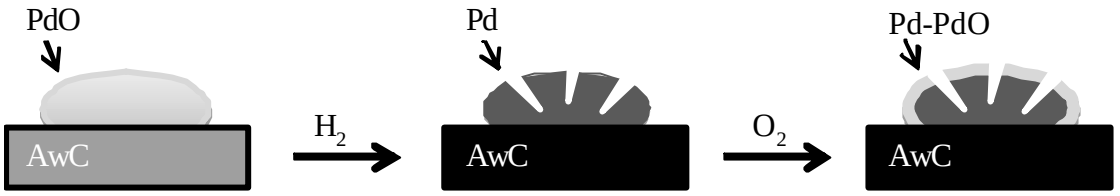

Figure 3.10 - Change in Pd particle structure from reduction – oxidation treatment; adapted from Melada et al.[26]

Another contributing factor could be the formation of ß-PdH from the dissolution of H_2 into Pd clusters during heat treatment under H_2. If ß-PdH is present on the catalyst surface it could account for the hydrogenation activity observed due to its high reduction potential. However, as ß-PdH decomposition is around 70 ^oC it is likely that reduction at 200 ^oC would cause re-dispersion of active metallic palladium species from its decomposition.[30] Reduction of a metal supported catalyst generally weakens the metal-support bond causing the metallic particles to become more mobile on the support surface. This accounts for the 'mopping up' of atomic species during reduction seen by STEM analysis and why direct oxidation doesn't have the desired effect of switching off H_2O_2 hydrogenation.

When preparing a sample by using the standard impregnation procedure, the addition of Au to Pd and an acid pre-treatment of activated carbon are required to produce a catalyst that does not hydrogenate H_2O_2.

To extend these studies and gain greater fundamental understanding of the scope of the reduction – oxidation treatment, the dependence on the addition of Au and the nature of the support for switching off H_2O_2 hydrogenation have been investigated in the following sections.

3.5 Reduction – Oxidation Treatment of Monometallic Pd/Acid-Washed Carbon

During the reduction – oxidation treatment of AuPd/AwC the Au oxidation state does not change. Therefore by excluding the Au and treating a monometallic Pd/AwC catalyst to a series of reduction – oxidation conditions; it is of interest to determine if it is possible to switch off H_2O_2 hydrogenation. Sequential reduction – re-oxidation conditions determined for the bimetallic material were applied to monometallic 5wt% Pd/AwC.

Note - when preparing 5wt% Pd a predetermined concentration of HCl was required to dissolve $PdCl_2$ (itself sparingly soluble in water) to form $PdCl_4^{2-}$ ions in solution. When adding $PdCl_2$ during preparation of a Au-Pd catalyst, Au does not induce a marked synergistic effect on the synthesis activity (refer to table 3.7).

Table 3.9 - Effect of sequential reduction – re-oxidation conditions on a 5 wt%Pd/AwC catalyst towards the direct synthesis of H_2O_2.

Sample	**Heat treatment**		**Productivity** ($mol H_2O_2 kg_{cat}^{-1} h^{-1}$)	**Hydrogenation** ($mol H_2O_2 kg_{cat}^{-1} h^{-1}$)
1	Initial catalyst		184	139
	Sample 1 + 5%H_2/Ar treatment			
	Temperature (^oC)	*Time (h)*		
2	200	2	53	729
	Sample 5 +O_2 treatment			
	Temperature (^oC)	*Time (h)*		
3	200	3	148	183
4	300	3	107	21

The initial reduction step resulted in a decrease in H_2O_2 productivity and an increase in hydrogenation similar to the bimetallic equivalent. Again this can be attributed to the increase of the concentration of surface Pd^0. However unlike the bimetallic material, when the reduced 5 %Pd/C is heated in O_2 the H_2O_2 hydrogenation activity is not deactivated. As the role of Au in enhancing H_2O_2 formation is related to its ability to limit the subsequent hydrogenation and decomposition of H_2O_2 formed, it is believed that the presence of Au is an essential component for switching off the hydrogenation under these heat treatment conditions.

3.6 Influence of the Support

Further investigation was required to determine the effect of the support in switching off H_2O_2 hydrogenation with reduction – oxidation treatments. This has been achieved by studying the effect of the sequential reduction–re-oxidation conditions on the activity of Au-Pd/C and Au-Pd/TiO_2 was investigated.

3.6.1 Sequential Reduction - Re-Oxidation of Au-Pd/C (Untreated Carbon)

A Au-Pd/C catalyst produced by impregnation was subjected to sequential reduction-re-oxidation treatment and tested for the direct synthesis of H_2O_2, table 3.10. The sequential heat treatment utilised has previously been shown to turn off H_2O_2 hydrogenation for a Au-Pd/AwC, in section 3.4.

Table 3.10 - Effect of sequential reduction – re-oxidation conditions on a Au-Pd/C (untreated carbon) catalyst towards the direct synthesis of H_2O_2.

Sample	**Heat treatment**		**Productivity** ($mol H_2O_2 kg_{cat}^{-1} h^{-1}$)	**Hydrogenation** ($mol H_2O_2 kg_{cat}^{-1} h^{-1}$)
1	Initial catalyst		108	98
	Sample 1 + 5%H_2/Ar treatment			
	Temperature (^oC)	*Time (h)*		
2	200	2	101	302
	Sample 2 +O_2 treatment			
	Temperature (^oC)	*Time (h)*		
3	200	2	99	139
4	200	3	82	31

Interestingly, the hydrogenation could not be switched off on Au-Pd/C, indicating significant differences based on support choice.

When the Au-Pd/C was subjected to the reduction conditions (sample 2), the productivity remains similar to the non-reduced sample whereas the hydrogenation increases dramatically.

This is believed to be due to reduction of the surface palladium, producing active sites which are responsible for H_2O_2 hydrogenation.

Re-oxidation at 200°C for 2 hours (sample 3) doesn't affect H_2O_2 productivity activity, however the hydrogenation approximately halves. This confirming an earlier conclusion that different active sites are responsible for the H_2O_2 productivity and hydrogenation.

Upon re-oxidation for 3 hours (sample 4) both the H_2O_2 productivity and hydrogenation decrease, indicating that the overall activity of the catalyst has dropped. However, the H_2O_2 hydrogenation hasn't been switched off. Decreased activity of the catalyst could be due to sintering of the Au and Pd nano-particles producing larger oxidised Au-Pd clusters (as seen in figure 3.8 for Au-Pd/AwC subjected to the same treatment), which have less activity, suggesting that re-oxidation for 3 hours is too long.

The Au-Pd/C samples were characterised using XPS, the Pd(3d) spectra is shown in Figure 3.11 with corresponding quantified XP data in Table 3.11.

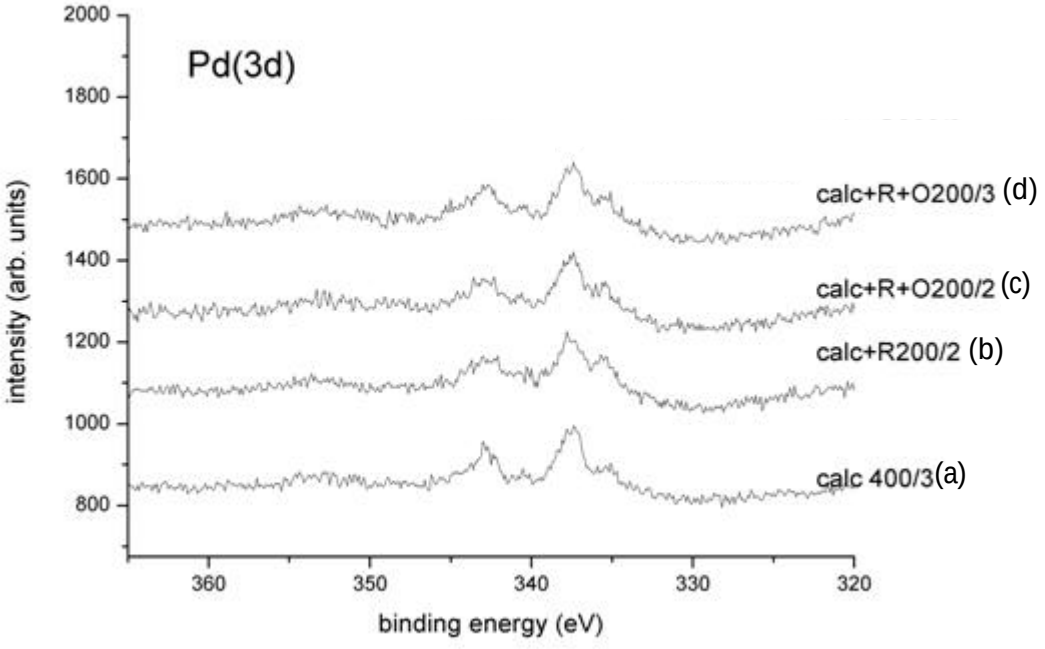

Figure 3.11 - Pd(3d) spectra observed for the 2.5 wt% Au-2.5 wt% Pd/C catalysts after sequential reduction and oxidation. **(a)** calcined under standard conditions (400 °C, 3 h); **(b)** reduced in H_2/Ar at 200 °C for 2 h; **(c)** (b) re-oxidised at 200 °C for 2 h and **(d)** (b) re-oxidised at 200 °C for 3 h.

Table 3.11 - Quantified XPS data for the Au-Pd/C catalysts after different thermal treatments

Sample treatment	**[Au] (at. %)**	**[Pd] (at. %)**	**Pd/Au***	**Pd^{2+} (%)**
(a) Calcined in air for 3 h at 400 ^{o}C	0.14	0.22	1.07	76
(b) Reduced at 200 ^{o}C 2 h	0.14	0.2	0.93	64
(c) Oxidised in O_2 200 ^{o}C 2 h	0.15	0.22	0.97	68
(d) Oxidised in O_2 200 ^{o}C 3 h	0.14	0.25	1.29	79

* corrected for overlap of the Pd($3d_{5/2}$) and Au($4d_{5/2}$) components.

The XPS spectra of Au-Pd/C, in Figure 3.11, subjected to the sequential reduction-re-oxidation treatment, indicate that Pd^{2+} and Pd^{0} species are present on the surface for all catalysts. An increase in formation of surface Pd^{0} upon reduction can be linked with the increase in H_2O_2 hydrogenation. Upon oxidation there is a decrease in Pd^{0}, corresponding to an increase in PdO.

Untreated activated carbon is believed to contain less oxygen-containing groups. These groups are also more basic in nature which both enhances the electrostatic attraction with the metal anion complex (e.g. CpH_3O^{+}-$PdCl_4^{2-}$) and diminishes the repulsion (e.g. COO^{-}-$PdCl_4^{2-}$), thus increasing the dispersion binding potential. Acid washing with HNO_3 can also change the nature of the binding groups, introducing/increase nitrogen groups. The characterisation of the nitrogen groups is difficult because oxygen and nitrogen functional groups in IR coincide however it is believed groups such as amides, imides and lactams are introduced.

3.6.2 Sequential Reduction - Re-Oxidation of Au-Pd/TiO_2

Au-Pd/TiO_2 produced by impregnation was subjected to sequential reduction - re-oxidation treatment and tested for the direct synthesis of H_2O_2. The results are shown in Table 3.12.

Table 3.12 - Effect of sequential reduction – re-oxidation conditions on the activity of a Au-Pd/TiO_2 catalyst towards the direct synthesis of H_2O_2.

Sample	**Heat treatment**		**Productivity ($molH_2O_2kg_{cat}^{-1}h^{-1}$)**	**Hydrogenation ($molH_2O_2kg_{cat}^{-1}h^{-1}$)**
1	Initial catalyst		67	221
	Sample 1 + 5%H_2/Ar treatment			
	Temperature (^oC)	*Time (h)*		
2	200	2	76	353
	Sample 2 +O_2 treatment			
	Temperature (^oC)	*Time (h)*		
3	200	3	82	47

Reduction of Au-Pd/TiO_2 preceding calcination (sample 2) is responsible for an increase in both the H_2O_2 productivity and the H_2O_2 hydrogenation, which is again believed to be due to an increase in surface Pd^0.

Re-oxidation (sample 3) dramatically decreases the hydrogenation corresponding to an increase in the H_2O_2 productivity.

The larger changes in activity could be due to less stable interaction between Pd-complexes and the surface increasing mobility and stability of the complex.

The nature of the support has previously been shown to be crucial to the activity of the catalysts towards direct H_2O_2 synthesis[1, 2, 9, 28, 31-33]. Reasons for this include differing reduction potentials of Au and Pd according to the chemical nature of the support as well as the concentration of oxygen-containing groups and their nature responsible for binding the metals are different.

Determination of the iso-electric point and surface acidity are considered important parameters in modifying the structure and activity of Au-Pd catalysts. While these techniques were not made available for this study, the specificity of the pre-treatment step with respect to concentration and acid species has an important effect.

3.7 Conclusion

In this chapter two ways of maintaining high synthesis rates while also switching off activity towards H_2O_2 hydrogenation have been shown. The acid-pre-treatment of the support prior to deposition of the metals, Au and Pd, drying and calcination at 400 ^oC for 3 h in static air presents one way of achieving this goal. And that a sequential reduction – re-oxidation treatment presents an alternative route to the same outcome. Further studies indicate that using acid-washed carbon and the presence of gold are essential to preparing a catalyst with zero H_2O_2 hydrogenation under standard conditions.

These experiments show that the oxidation state of Pd is crucial for determining not only the initial formation of H_2O_2, but also its sequential hydrogenation. It is clear that minimising the amount of Pd^0 is essential and the role of the Au and Pd^{2+} (as well as Cl^{x-}) could essentially be to isolate the residual Pd^0 so that the active sites required for synthesis persist, but those for hydrogenation are minimised. As H_2O_2 hydrogenation /decomposition can be switched off, as demonstrated by acid washing the support followed by an oxidation procedure, then it is clear that the sites for synthesis and hydrogenation of H_2O_2 are different. This is a logical conclusion since the sites for synthesis require the associative adsorption of O_2 followed by hydrogenation, whereas the sites for hydrogenation / decomposition will break the O-O bond. Isolating Pd^0 sites on the surface enables high rates of synthesis.

3.8 References

1. V. R. Choudhary and P. Jana, *Catalysis Communications*, 2008, **9**, 1624-1629.
2. J. K. Edwards, A. Thomas, A. F. Carley, A. A. Herzing, C. J. Kiely and G. J. Hutchings, *Green Chemistry*, 2008, **10**, 388-394.
3. J. K. Edwards, A. F. Carley, A. A. Herzing, C. J. Kiely and G. J. Hutchings, *Faraday Discussions*, 2008, **138**, 225-239.
4. A. A. Herzing, A. F. Carley, J. K. Edwards, G. J. Hutchings and C. J. Kiely, *Chemistry of Materials*, 2008, **20**, 1492-1501.
5. J. K. Edwards, B. E. Solsona, P. Landon, A. F. Carley, A. Herzing, C. J. Kiely and G. J. Hutchings, *Journal of Catalysis*, 2005, **236**, 69-79.
6. F. Menegazzo, P. Burti, M. Signoretto, M. Manzoli, S. Vankova, F. Boccuzzi, F. Pinna and G. Strukul, *Journal of Catalysis*, 2008, **257**, 369-381.
7. P. Landon, P. J. Collier, A. F. Carley, D. Chadwick, A. J. Papworth, A. Burrows, C. J. Kiely and G. J. Hutchings, *Physical Chemistry Chemical Physics*, 2003, **5**, 1917-1923.
8. A. F. Lee, C. J. Baddeley, C. Hardacre, R. M. Ormerod, R. M. Lambert, G. Schmid and H. West, *The Journal of Physical Chemistry*, 1995, **99**, 6096-6102.
9. J. K. Edwards, E. Ntainjua N, A. F. Carley, A. A. Herzing, C. J. Kiely and G. J. Hutchings, *Angewandte Chemie International Edition*, 2009, **48**, 8512-8515.

10. J. K. Edwards, B. Solsona, E. N. N, A. F. Carley, A. A. Herzing, C. J. Kiely and G. J. Hutchings, *Science*, 2009, **323**, 1037-1041.
11. J. K. Edwards, J. Pritchard, M. Piccinini, G. Shaw, Q. He, A. F. Carley, C. J. Kiely and G. J. Hutchings, *Journal of Catalysis*, 2012, **292**, 227-238.
12. D. P. Dissanayake and J. H. Lunsford, *Journal of Catalysis*, 2002, **206**, 173-176.
13. D. P. Dissanayake and J. H. Lunsford, *Journal of Catalysis*, 2003, **214**, 113-120.
14. P. A. Simonov, A. V. Romanenko, I. P. Prosvirin, E. M. Moroz, A. I. Boronin, A. L. Chuvilin and V. A. Likholobov, *Carbon*, 1997, **35**, 73-82.
15. N. E. Ntainjua, M. Piccinini, J. C. Pritchard, J. K. Edwards, A. F. Carley, J. A. Moulijn and G. J. Hutchings, *ChemSusChem*, 2009, **2**, 575-580.
16. E. Ntainjua N, M. Piccinini, J. C. Pritchard, Q. He, J. K. Edwards, A. F. Carley, J. A. Moulijn, C. J. Kiely and G. J. Hutchings, *ChemCatChem*, 2009, **1**, 479-484.
17. V. Choudhary, A. Gaikwad and S. Sansare, *Catalysis Letters*, 2002, **83**, 235-239.
18. V. R. Choudhary, S. D. Sansare and A. G. Gaikwad, *Catalysis Letters*, 2002, **84**, 81-87.
19. A. G. Gaikwad, S. D. Sansare and V. R. Choudhary, *Journal of Molecular Catalysis A: Chemical*, 2002, **181**, 143-149.
20. C. Samanta and V. R. Choudhary, *Applied Catalysis A: General*, 2007, **326**, 28-36.
21. C. Samanta and V. R. Choudhary, *Chemical Engineering Journal*, 2008, **136**, 126-132.
22. C. Samanta and V. R. Choudhary, *Applied Catalysis A: General*, 2007, **330**, 23-32.
23. V. V. Krishnan, A. G. Dokoutchaev and M. E. Thompson, *Journal of Catalysis*, 2000, **196**, 366-374.
24. S. Chinta and J. H. Lunsford, *Journal of Catalysis*, 2004, **225**, 249-255.
25. R. Burch and P. R. Ellis, *Applied Catalysis B-Environmental*, 2003, **42**, PII S0926-3373(0902)00232-00231.
26. S. Melada, R. Rioda, F. Menegazzo, F. Pinna and G. Strukul, *Journal of Catalysis*, 2006, **239**, 422-430.
27. M. Chen, D. Kumar, C.-W. Yi and D. W. Goodman, *Science*, 2005, **310**, 291-293.
28. V. R. Choudhary, C. Samanta and T. V. Choudhary, *Applied Catalysis A: General*, 2006, **308**, 128-133.
29. J. C. Pritchard, Q. He, E. N. Ntainjua, M. Piccinini, J. K. Edwards, A. A. Herzing, A. F. Carley, J. A. Moulijn, C. J. Kiely and G. J. Hutchings, *Green Chemistry*, 2010, **12**, 915-921.
30. M. W. Tew, J. T. Miller and J. A. van Bokhoven, *The Journal of Physical Chemistry C*, 2009, **113**, 15140-15147.
31. J. K. Edwards, A. Thomas, B. E. Solsona, P. Landon, A. F. Carley and G. J. Hutchings, *Catalysis Today*, 2007, **122**, 397-402.
32. N. N. Edwin, J. K. Edwards, A. F. Carley, J. A. Lopez-Sanchez, J. A. Moulijn, A. A. Herzing, C. J. Kiely and G. J. Hutchings, *Green Chemistry*, 2008, **10**, 1162-1169.
33. E. N. Ntainjua, M. Piccinini, J. C. Pritchard, J. K. Edwards, A. F. Carley, C. J. Kiely and G. J. Hutchings, *Catalysis Today*, 2011, **178**, 47-50.

- CHAPTER FOUR -

Catalysts Prepared by Physical Grinding

4.1 Introduction

As already described in Chapter 1, halides are often used in the reaction medium for the direct synthesis of H_2O_2 as promoters. Particularly, they are very effective for enhancing the catalytic activity of monometallic Pd supported catalysts by suppressing the unwanted and non selective H_2O_2 hydrogenation pathway.[1-8]

Hutchings *et al.*[9, 10] have investigated the effect of halide on bimetallic Au-Pd catalysts, prepared by impregnation, for the direct H_2O_2 synthesis. Although there was an initial promotion in activity in the presence of low halide concentrations (<0.0057 $mmolBr^- dm^{-1}$) they concluded that neither the addition of halide to the solvent[9], nor a pre-treatment of the catalyst with halide[10] are beneficial for bimetallic Au-Pd supported catalysts. The addition of halide to the solvent and halide pre-treatment both caused leaching of the metal from the catalyst during reaction, which could form active homogeneous species[11, 12] that are unsuitable for an industrial process. In these studies a Au-Pd catalyst was prepared by impregnation using tetrachloroauric acid and palladium chloride as the precursors. Even after calcination at 400 ^oC for 3 hours and washing the catalysts with water, a low chloride concentration (0.45 at%, determined by XPS) remains on the catalyst surface, which may affect the catalytic activity.

The presence of chloride during preparation has been found to increase the mobility of metal nano-particles on the support, leading to larger metal particles forming.[13] A method for limiting chloride levels, remaining in catalysts, involves tuning the pH during deposition precipitation, to ensure significant hydrolysis of the $HAuCl_4$ to $[Au(OH)_4]^-$, and minimise Cl^- deposition onto the support.[14] However, it is known that a pH that facilitates total hydrolysis (~pH 10) also results in a decrease in the target Au loading levels (around 67% of the metal is deposited).[14, 15] Au-Pd catalysts prepared by deposition precipitation have previously been shown to have low H_2O_2 productivity compared to impregnation catalysts.[16] An alternative

method of reducing chloride levels is by reduction (heat treatment in a H_2 rich atmosphere to remove Cl^- as HCl) of the catalyst, but unfortunately this causes metal particle agglomeration through sintering[14].

With a view to providing greater insight into the role the halide plays in Au-Pd catalysts for the direct synthesis of hydrogen peroxide, a rapid, solvent-less, and readily scalable method to prepare halide free Au-Pd supported nano-particles was developed. The technique, named here as physical grinding, consists of mixing gold and palladium acetate with a preformed support, followed by thermal treatment in an inert atmosphere to decompose the acetate salt. The absence of aqueous chloride ions from the preparation medium significantly decreases the volume of material used, ensuring that the catalyst preparation is completed in a greener manner and is readily scalable.

The catalysts produced using this methodology have been shown to be highly active for the direct H_2O_2 synthesis and the oxidation of benzyl alcohol, compared to previously reported impregnation catalysts. The origins of these effects are discussed in the following sections.

Note - Full details of experimental procedures and characterisation techniques are described in chapter two. The following reaction conditions have been utilised;

(a) Hydrogen Peroxide Synthesis catalyst (10 mg), 5% H_2/CO_2 (420 psi), 25% O_2/CO_2 (160psi), 5.6g MeOH and 2.9 H_2O as solvent, 2 ^oC, 1200 rpm, 30 minutes.

(b) Hydrogen Peroxide Hydrogenation catalyst (10 mg), 5% H_2/CO_2 (420 psi), 5.6g MeOH, 2.22 H_2O and 0.68g 50 wt% H_2O_2 as solvent, 2 ^oC, 1200 rpm, 30 minutes.

Au-Pd = 2.5 %Au-2.5% Pd. In the naming of catalysts PG is used for catalysts prepared by physical grinding and IMP is used for catalysts prepared by impregnation. For example PG-Au-Pd/C = 2.5 %Au-2.5%Pd supported on carbon prepared by physical grinding.

4.1.1 Thermal decomposition of metal acetates

Thermal decomposition, called pyrolysis in the absence of oxygen, of metal salts has been used extensively for the preparation of metal containing nano-particles and nanorods[17-22]. These are often performed in the presence of a reducing gas and/or solvent to obtain the fully reduced metal. Reports on direct salt decomposition in the presence of a suitable support material to produce a heterogeneous catalyst have been scarce[23-25]. Lin *et al.*[25] reported the auto-reduction of metal acetates *via* heat treatment, preceding physical grinding, to decorate carbon nano-tube supports. This included the use of the following metal acetates; Co, Cu, Au, Ag, Pd, Pt and Pb. In this chapter the preparation of bimetallic Au-Pd supported catalysts produced by the simultaneous thermal decomposition of the metal acetate salts is reported.

The synthesis of active metal nano-particles relies on thermal decomposition and/or combustion of metal salts. However, there is little understanding of the fundamental physical and chemical mechanisms that govern the complex decomposition of the metal acetates in oxygen-containing or oxygen-free systems. Thermal decomposition of individual metal acetate salts has been investigated by thermo-gravimetric analysis[26-31], as well as in line FT-IR and in situ X-ray diffraction (XRD). Typically, the decomposition of the acetate complex starts with melting and subsequent dehydration of the materials with evolved gas analysis (mass spectrometry) showing the formation of acetic acid during this initial stage. Acetic acid is considered to arise from partial hydrolysis of the acetate complex.

Pol and co-workers[32] concluded that for easily reducible metals such as copper, nickel and cobalt the acetate decomposition, in an oxygen free atmosphere, results in the autogenous reduction to the metal. In the case of less reducible elements such as manganese, zinc and iron, metal oxides are consistently formed. Based on obtained mass spectrometry data, they proposed the dissociation of acetates as follows:

$$M(CH_3COO)_2 \longrightarrow MCO_3 + CH_3COCH_3$$

$$MCO_3 \longrightarrow MO + CO_2$$

$$CH_3COCH_3 \longrightarrow CO + C_2H_6$$

$$MO + CO \longrightarrow M + CO_2$$

Where M = Cu, Ni, Co etc.

The formation of the first oxygenated product, acetone, occurs by equation 1. The metal carbonate which is a short lived intermediate, de-carboxylates to give a metal oxide at *ca.* 350 ^{o}C. Oxygenates, such as acetic acid, are known to decompose to hydrocarbon and further to carbon. Then the metal oxide, in the case of certain metals such as nickel (-0.25 eV at 25 ^{o}C), undergoes reduction by the evolved CO, while metals with lower reduction potential, such as Fe (-0.44 eV at 25 ^{o}C), prefer to stay as the oxide.[32] *Note* - The standard reduction potentials for Pd and Au are +0.92 eV and +1.52 eV respectively, for metal-metal ion equilibrium, therefore it is predicted their metal acetates will readily undergo reduction to the corresponding metal.

The decomposition is considered complex with other products including acetic acid and methane being produced. Judd et al.[27] observed that acetic acid was the primary component when a metal is formed; whereas, acetone is the primary component for decomposition that results in metal acetate. A kinetic study of the decomposition of nickel acetate, by Leicester and Redman,[33] showed that rates of decomposition are affected by sample mass due to a blanket of dense acetic acid formed from initial decomposition coating the sample. Arii and Kishi,[34] found that the humidity of the atmosphere had a dramatic effect on the decomposition of zinc acetate, with ZnO only being formed when water vapour was present in the atmosphere.

The thermal decomposition of bulk palladium acetate[31, 35] and gold acetate[30] have previously been studied. Gallagher and Gross[31] found that the ligand part CH_3COO^+ and CO_2 were the main decomposition products during TGA studies of palladium acetate to palladium metal. In an inert atmosphere the decomposition took place between 200-300 ^{o}C, which had observed activation energy of ca. 115 kJ mol^{-1} and enthalpy ca. 440$\pm$20 kJ mol^{-1}.[31] The decomposition of thin palladium acetate films using an excimer UV lamp (? = 222 nm) produced a number of fragments due to the high photon energy (540 kJ mol-1). The fragments, analysised by mass spectrometry, included CO^{2+}, CH_3CO^+, CH_3C^+, H_2O^+ and CH_3.[35]

Bakrania et al[30] studied the decomposition of gold acetate, using TGA in an inert atmosphere, and observed significant mass loss between 120-210 ^{o}C, with a DTG peak occurring at 170 ^{o}C. The same group examined the decomposition of gold acetate to be rapid and violent in air with the decomposition occurring at ca. 103$\pm$20 ^{o}C. They concluded that the highly exothermic nature of gold acetate and other metal acetates decomposition assists the

formation of nano-particles through fragmentation. Theses fragments can potentially be at much higher temperature than the decomposition temperature.[30] However, further investigation into the decomposition at a macro-scale and in the presence of a support is required to enable greater control over the architecture of the nano-particles.

4.2 Thermo-Gravimetric Analysis (TGA)

TGA records the weight loss of a material as the temperature is raised allowing the decomposition temperature of the metal acetates to be pinpointed. These were determined from the differential thermo-gravimetric (DTG) curve obtained at 5 ^{o}C min^{-1} in N_2 (refer to chapter two for full experimental procedures).

Gold and palladium acetate were investigated individually and together, both with and without supports. It is essential the thermal treatment temperature used is above the decomposition temperature required to produce the active metal catalyst.

4.2.1 Bulk Metal Acetates

Thermo-gravimetric analysis (TGA) was performed on the bulk acetates, palladium acetate Figure 4.1A and gold acetate, Figure 4.1B, and a 1:1 weight mixture of both, Figure 4.2.

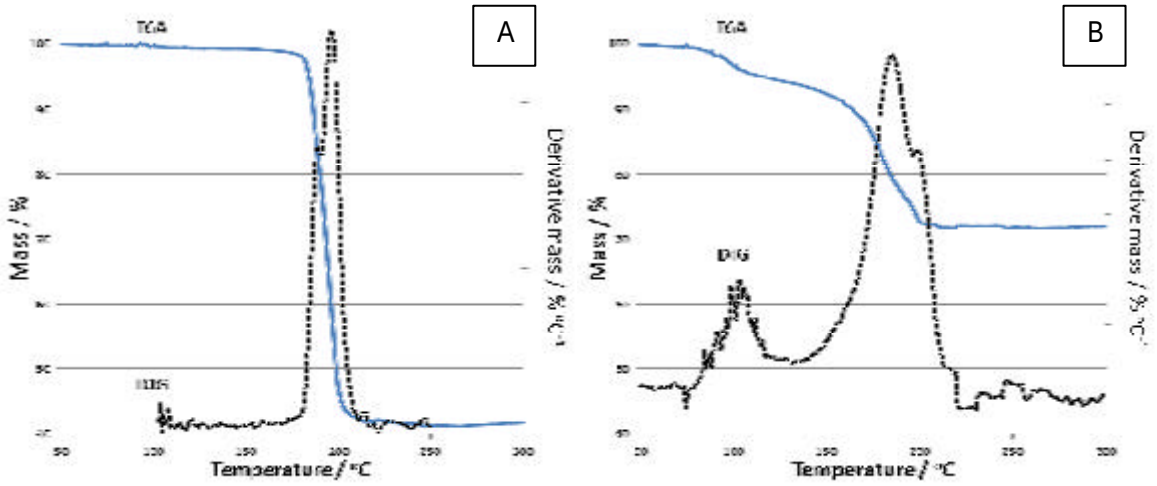

Figure 4.1 - TGA-DTG of metal acetate salts under flowing nitrogen with 5 ^{o}C min^{-1} ramp rate A) palladium (II) acetate, B) gold (III) acetate.

The decomposition temperatures of the palladium and gold salts corresponded well with those quoted in the literature[25, 30, 31], *ca.*190 ^{o}C and *ca.*180 ^{o}C respectively. Gold acetate had a low temperature weight loss around 100 ^{o}C associated with absorbed water. Both acetate DTG peaks have a slight shoulder at *ca.* 180 ^{o}C for palladium acetate and *ca.* 200 ^{o}C for gold acetate; suggesting that decomposition occurs in two separate steps, highlighting the complex nature of acetate decomposition.

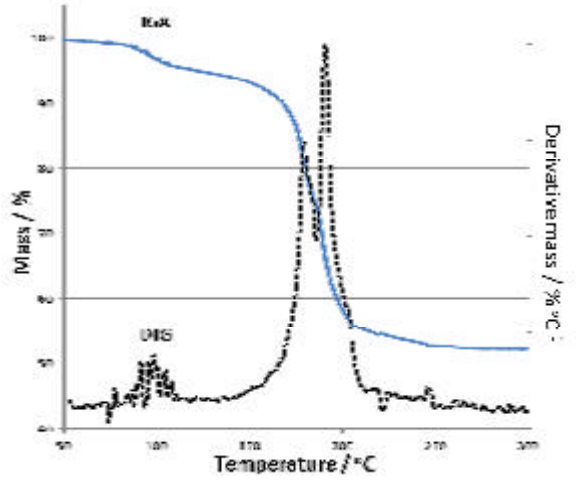

Figure 4.2 - TGA-DTG of a gold (III) acetate and palladium (II) acetate mixture, 1:1 by weight, under flowing nitrogen with 5 ^{o}C min^{-1} ramp rate.

When the salts were combined (with a 1:1 wt ratio) there was no obvious change in the decomposition profile or temperature of the gold and palladium acetates, *ca.*190 ^{o}C and *ca.*180 ^{o}C respectively. The close proximity of the two acetate decomposition temperatures may well be a beneficial factor for the formation of alloyed Au-Pd materials.

4.2.2 Metal Acetates With a Support

Following an understanding of the bulk acetates decomposition temperatures the effect of grinding the precursors with a carbon and oxide support was considered. The TGA-DTG graphs are shown in Figure 4.3.

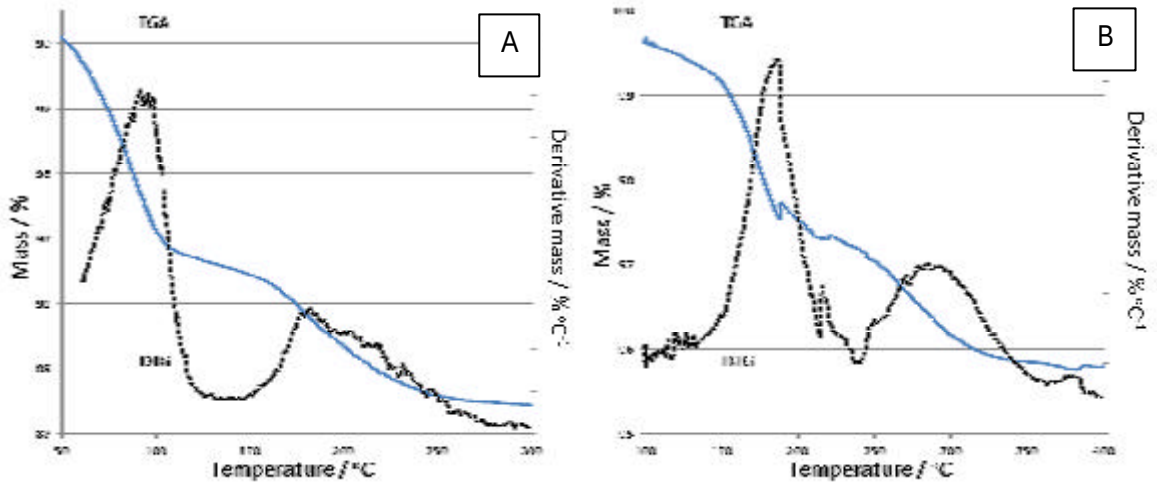

Figure 4.3 - TGA-DTG of a gold (III) acetate and palladium (II) acetate ground mixture, 1:1 by weight with, A) carbon and B) TiO_2 support, under flowing nitrogen with 5 ^oC min^{-1} ramp rate.

The addition of a support, carbon or TiO_2, slowed the rate of acetate decomposition as evident from the DTG peak occurring over a temperature range of ca. 150 – 250 ^oC on carbon (figure 4.3A) and 150 – 350^oC on titania (figure 4.3B). This compared to the sharp peak, observed in Figure 4.2, when no support is present implies an interaction exists between the supports and dispersed metal acetates. Reduced heat transfer rates, because of acetate dilution by the support material, could also be playing some role.

The salt decomposition starts at a slightly lower temperature in the presence of the carbon support, which can be attributed to the distribution of smaller salt particles on the support surface. The low temperature weight loss, at 100 ^oC, in Figure 4.3A is associated with adsorbed water.

In the presence of the TiO_2 support there is a distinct splitting of the metal acetate decomposition profiles into two distinct mass loss regions. The TGA-DTG of the blank support was performed to confirm these were due to metal precursor decomposition. The lower temperature (150-230 ^oC) mass loss correlates with the bulk salt decomposition; while the higher mass loss (230-350 ^oC) suggests the presence of an interaction between the salt and support and could be stable dispersed metal acetate salts.

4.3 Effect of Preparation Method on Catalyst Activity

Au-Pd (2.5 %Au-2.5 %Pd) catalysts on various supports (SiO_2, ZrO_2, CeO_2, C and TiO_2) were prepared by impregnation and physical grinding and tested for direct H_2O_2 synthesis and benzyl alcohol oxidation. The supports used have previously been shown to be effective supports for Au and Pd nano-particles, capable of generating excellent catalytic materials for both oxidation and reduction reactions[36].

4.3.1 Direct H_2O_2 Synthesis and Hydrogenation

IMP-Au-Pd and PG-Au-Pd catalysts were evaluated for the direct synthesis of H_2O_2 (Figure 4.4A) and the H_2O_2 hydrogenation pathway (Figure 4.4B) under standard reaction conditions.

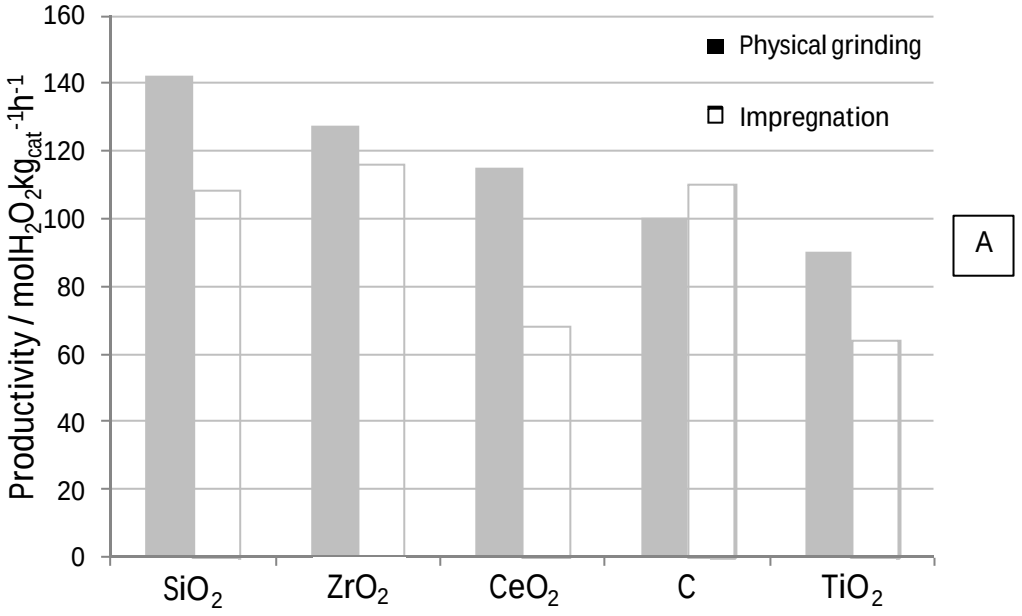

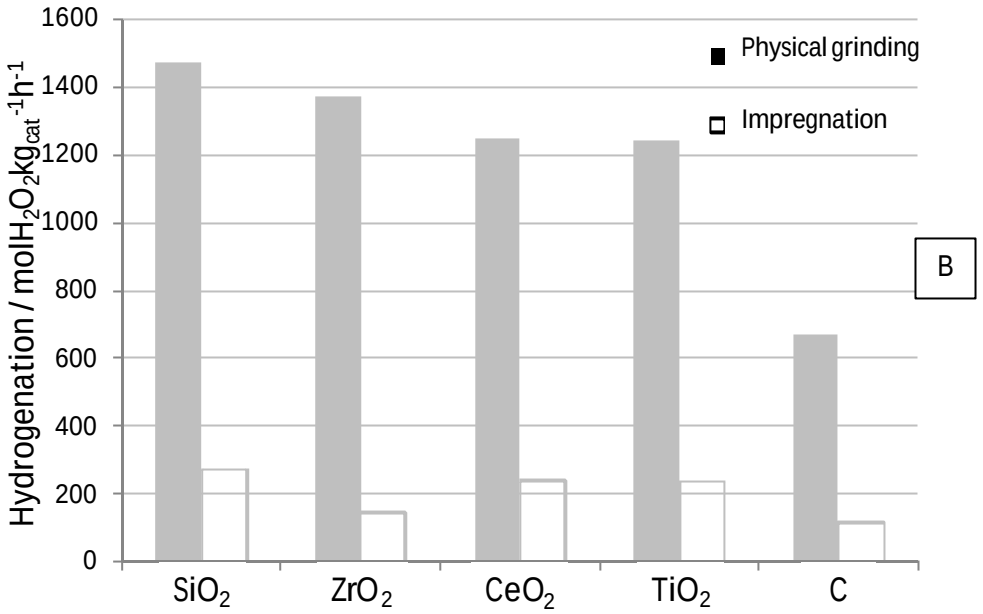

Figure 4.4 - Activity of Au-Pd supported catalysts prepared by physical grinding and impregnation for (A) H_2O_2 synthesis and (B) H_2O_2 hydrogenation.

All the physical grinding catalysts, with the exception of PG-Au-Pd/C, have higher activity towards H_2O_2 production when compared to analogous impregnation catalysts. The PG-Au-Pd/CeO_2 has approximately double the H_2O_2 productivity of the IMP-Au-Pd/CeO_2.

The lower H_2O_2 productivity of the PG-Au-Pd/C can be explained by its high activity towards H_2O_2 hydrogenation. In fact all the physical grinding catalysts have higher activity towards H_2O_2 hydrogenation. Ideally catalysts would not be active towards the hydrogenation pathway and the raised H_2O_2 hydrogenation for physical grinding catalysts may well be due to them being halide-free. However, investigation into the nature of the active particles and stability is required.

Pritchard et al.[37] utilised a colloidal method, sol immobilisation, to investigate the effect of particle size and morphology on catalytic activity. Interestingly, these catalysts contained no halide due to the nature of the preparation; formation of colloids by reduction of the chloride precursors in the presence of a stabiliser prior to deposition onto a support. Sol immobilisation Au-Pd catalysts were shown to be far more facile for H_2O_2 hydrogenation than the direct H_2O_2 synthesis. However, these catalysts were found to be unstable, leaching metal during the reaction and are, therefore, unsuitable for studying the effect of halide addition. Leached metallic species form homogenous catalysts affecting the direct H_2O_2

synthesis results[11, 12]. For this reason an investigation into the stability of the physical grinding catalysts is required.

4.3.2 Catalyst Stability

Reuse tests were performed on the physical grinding bimetallic supported catalysts in order to determine their stability for the direct synthesis of H_2O_2, Table 4.1.

Table 4.1 - Reuse data of physical grinding catalysts for the direct synthesis of H_2O_2

Catalyst	H_2O_2 Productivity ($mol_{H2O2}\ kg_{cat}^{-1} hr^{-1}$)	
	1st Use	2nd Use
2.5%Au 2.5%Pd / C	100	100
2.5%Au 2.5%Pd / TiO_2	90	90
2.5%Au 2.5%Pd / SiO_2	142	99
2.5%Au 2.5%Pd / CeO_2	115	60
2.5%Au 2.5%Pd / ZrO_2	127	81

The productivity of the PG-Au-Pd/C and TiO_2 catalysts displayed no decrease in activity upon second use, indicating stability. The comparable silica, zirconia and ceria supported catalysts, however, did show a decrease in productivity on second use, indicating that the metal particles are not stable on these particular supports. Previously, IMP-Au-Pd/SiO_2 catalysts have been shown to lack stability with a decreased H_2O_2 productivity on reuse.[38] It was concluded that the H_2O_2 productivity decrease was because of active metal leaching from the SiO_2 surface during the previous use, determined by atomic absorption spectroscopy (AAS) of the reaction medium. However, the Au-Pd zirconia and ceria supported catalysts prepared by impregnation are stable. In future, further investigation by AAS of the reaction medium and XPS of the catalyst after reaction, will be required to understand why physical grinding do not produce stable zirconia and ceria catalysts. A higher thermal treatment temperature or sequential treatments of the catalyst may aid the stability.

In subsequent tests only the stable PG-Au-Pd/C and TiO_2 catalysts have been used.

4.3.3 Benzyl Alcohol Oxidation

To gain a greater understanding of the differences between the techniques, the bimetallic materials that were stable for the direct synthesis of H_2O_2 (Au-Pd/C and TiO_2), were tested for the oxidation of benzyl alcohol at 140°C. The time-on-line data is shown in Figure 4.5 with corresponding turnover frequency (TOF – $mol_{Benzyl\ Alcohol\ converted}\ mol_{metal}^{-1}h^{-1}$), calculated at 0.5 hours, in Table 4.2.

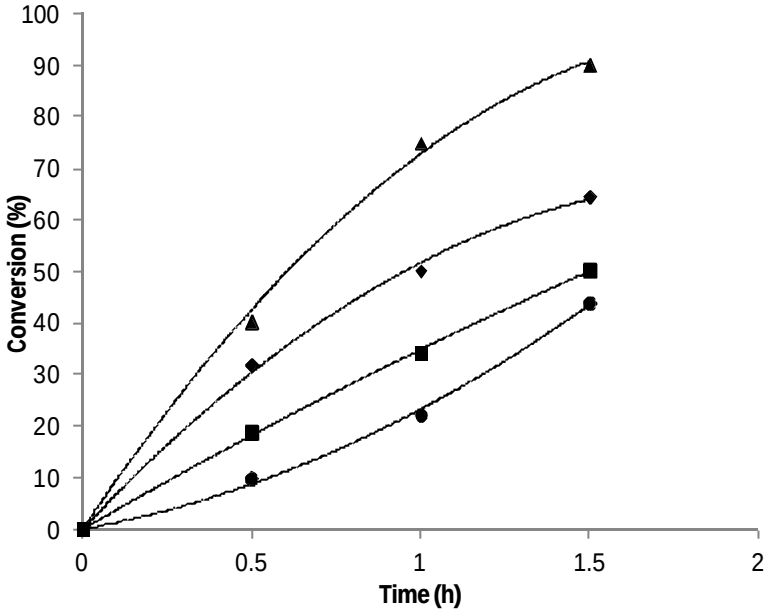

Figure 4.5 - Activity of bimetallic supported catalysts, prepared by impregnation and physical grinding, for the oxidation of benzyl alcohol. ● IMP-Au-Pd/C ▲ PG-Au-Pd/C, ■ IMP-Au-Pd/TiO_2, ◆ PG-Au-Pd/TiO_2

Table 4.2 - TOFs for the benzyl alcohol oxidation reaction over bimetallic titania- and carbon-supported catalysts prepared by impregnation and physical grinding.

Catalyst (2.5 wt% Au- 2.5 wt% Pd)	**TOF***
Carbon – Impregnation	8418
Titania – Impregnation	16008
Carbon – Physical grinding	34313
Titania – Physical grinding	27172

*Calculated at 0.5 hours.

The conversion and TOF (calculated after 0.5 h) of the PG-Au-Pd/C and PG-Au-Pd/TiO_2 are higher than the equivalent catalysts prepared by impregnation. Interestingly, when considering the methods separately, the IMP-Au-Pd/TiO_2 is the most active for impregnation; this trend is reversed for physical grinding catalysts; with the PG-Au-Pd/C having the highest conversion. The selectivity of each catalyst to benzaldehyde is shown in Figure 4.6.

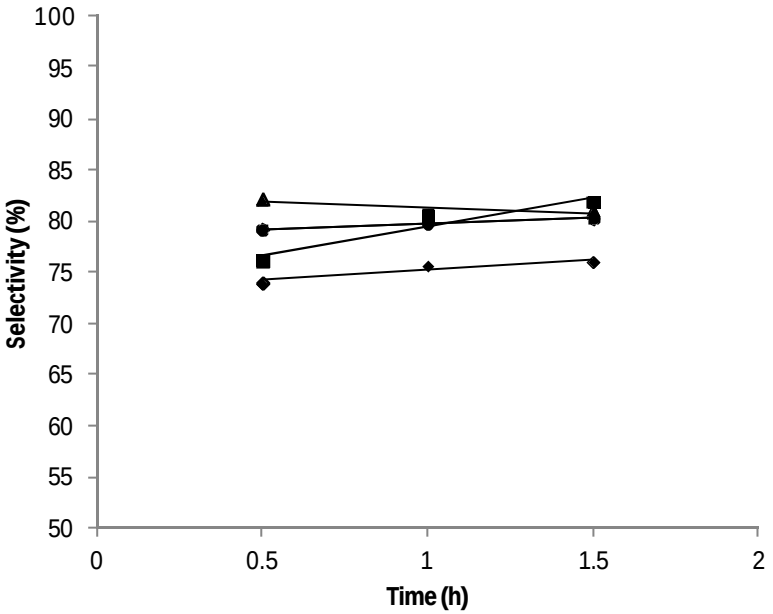

Figure 4.6 - Selectivity of bimetallic supported catalysts, prepared by impregnation and physical grinding, for the oxidation of benzyl alcohol to benzaldehyde. ● IMP-Au-Pd/C ▲ PG-Au-Pd/C, ■ IMP-Au-Pd/TiO_2, ◆ PG-Au-Pd/TiO_2

The selectivities towards benzaldehyde are similar for all catalysts, indicating that the preparation method used does not affect selectivity even though physical grinding catalysts are more active.

These results indicate that the removal of the chloride from the preparation step and therefore, from the final catalyst, leads to a significant enhancement in the activity as compared to previously reported impregnation catalysts. The origins of these effects are discussed in the following sections. The monometallic catalysts on carbon and titania have been prepared to elucidate if alloying is occurring in the analogous bimetallic Au-Pd, with XRD, STEM and

XPS being utilised to characterise the materials. Impregnation catalysts have previously been extensively characterised[16, 39-44].

4.4 Carbon Supported Au, Pd and Au-Pd Catalysts Prepared by Physical Grinding

4.4.1 Direct H_2O_2 Synthesis and Hydrogenation

A series of monometallic (Au and Pd) and bimetallic (Au-Pd) carbon supported catalysts were prepared by physical grinding and tested for H_2O_2 synthesis under standard reaction conditions. The data in Table 4.3 shows that both the monometallic and bimetallic materials have activity for the direct synthesis of hydrogen peroxide.

Table 4.3 - H_2O_2 synthesis data for monometallic and bimetallic catalysts prepared by physical grinding.

Catalyst	**Productivity ($molH_2O_2kg_{cat}^{-1}h^{-1}$)**	**Hydrogenation ($molH_2O_2kg_{cat}^{-1}h^{-1}$)**
2.5%Au / G60	3	44
5%Au / G60	5	60
2.5%Pd / G60	45	779
5%Pd / G60	48	1150
2.5%Au-2.5%Pd / G60	100	672

Although it can be seen the 5 %Au/C catalyst prepared by physical grinding generates H_2O_2 the rate of formation is considerably lower than the 5 %Pd containing catalysts. The addition of Au to Pd significantly enhances the catalytic performance for the synthesis of H_2O_2 (48 to 100 $molkg_{cat}^{-1}h^{-1}$); it also decreases the catalysts activity to the unwanted hydrogenation pathway. It has been reported that the incorporation of only a small amount of Au into a Pd-rich particle leads to a significant increase in the activity of the catalyst, suggesting alloying is being achieved here.[43]

To evaluate the synergy further monometallic (Au and Pd) catalysts with 2.5 wt% metal loading were prepared and tested. Again, the bimetallic Au-Pd supported catalyst has the superior activity (higher productivity, lower hydrogenation) further confirming the promotional effect of adding Au to Pd.

4.4.2 Benzyl Alcohol Oxidation

PG-5 %Au, PG-5 %Pd and PG-Au-Pd carbon supported catalysts have been tested for benzyl alcohol oxidation under standard conditions; the benzyl alcohol conversions are shown in Figure 4.7 and selectivity towards benzaldehyde in Figure 4.8.

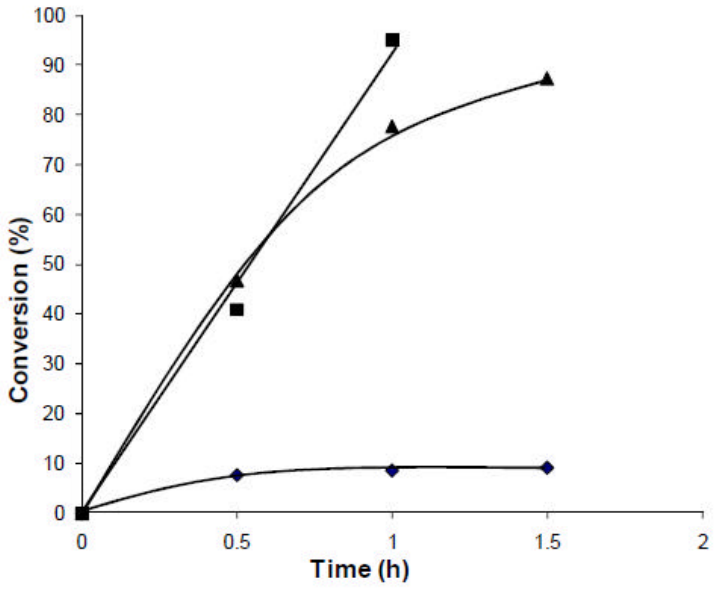

Figure 4.7 - Conversion of benzyl alcohol over mono and bimetallic carbon supported catalysts prepared by physical grinding. ▲ PG-Au-Pd/C ■ PG-5 %Pd/C ♦ PG-5 %Au/C

Figure 4.7 shows that monometallic and bimetallic carbon supported catalysts prepared by physical grinding are effective for the oxidation of benzyl alcohol. The Pd and Au-Pd catalysts had significantly higher activity than the Au catalyst. The bimetallic catalyst shows the highest initial activity, this is highlighted from the TOFs after 30 minutes in Table 4.4.

Again this indicates, as with the direct synthesis of H_2O_2 in section 4.4.1, that alloying between Au and Pd is being achieved.

Table 4.4 - TOFs for the benzyl alcohol oxidation reaction over mono and bimetallic carbon supported catalysts prepared by physical grinding.

Catalyst (5wt% total)	**TOF* (/h)**
Au	9340
Pd	26900
Au-Pd	39900

*calculated after 0.5 h

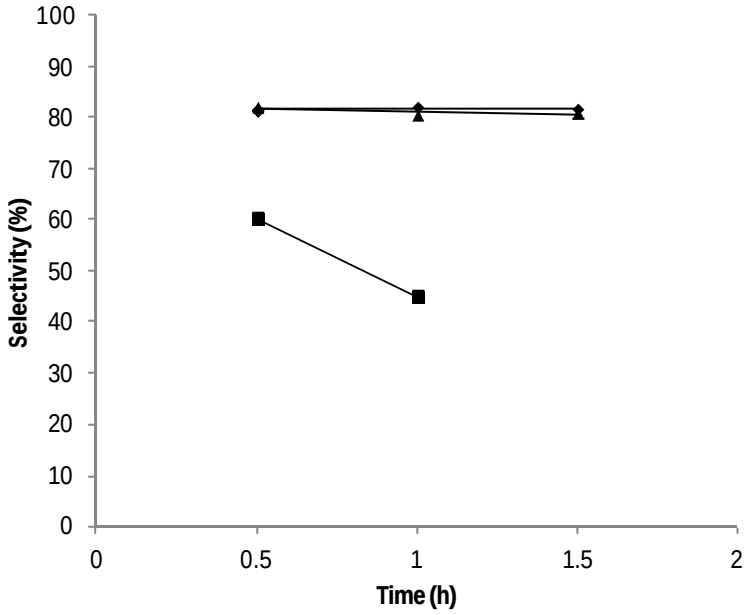

Figure 4.8 - Selectivity towards benzaldehyde during benzyl alcohol oxidation with mono and bimetallic carbon supported catalysts prepared by physical grinding. ▲ PG-Au-Pd/C, ■ PG-5 %Pd/C, ◆ PG-5 %Au/C

The Au-Pd catalyst has comparable selectivity to the monometallic Au catalyst; both are more selective towards benzaldehyde than monometallic Pd. The monometallic Pd catalyst

produces higher concentrations of further oxidation products such as benzoic acid and toluene. This is further evidence of synergy occurring on the addition of Au to Pd.

In order to investigate the origin of the synergistic effect, a number of characterisation techniques were employed to try to identify the nature of the nano-particles on activated carbon.

4.4.3 X-Ray Diffraction (XRD)

X-ray diffraction (XRD) analysis of the 5 %Au, 5 %Pd and Au-Pd carbon supported catalysts, produced by physical grinding, is shown in Figure 4.9.

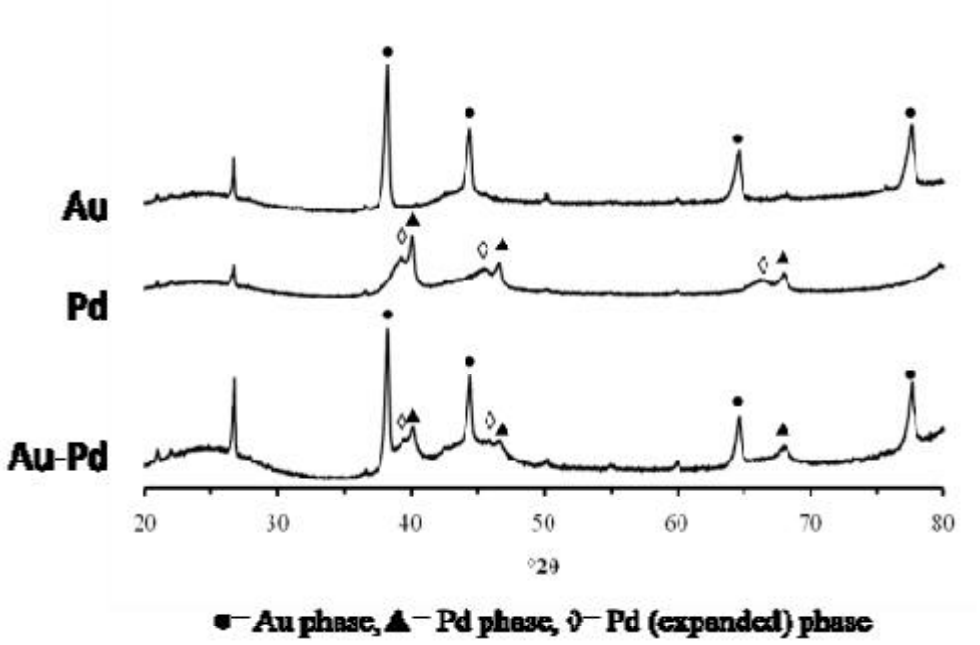

Figure 4.9 - XRD analysis of carbon supported 5 %Au, 5 %Pd and Au-Pd catalysts produced by physical grinding.

The average crystallite size of the monometallic Au on C, determined by Rietveld refinement of Figure 4.9 (refer to chapter two for further details), is significantly larger, at *ca.* 30 nm, than the monometallic Pd on C catalyst. However, the monometallic Pd supported on carbon showed two distinct metal Pd phases with different unit cell sizes and substantially

different crystallite sizes. The conventional Pd phase with a unit cell size of 59.40 $Å^3$ had the larger average crystallite size of 29±2 nm, while the phase with an expanded unit cell of 63.09 $Å^3$ had a smaller average crystallite size of 7 nm. The expanded unit cell is indicative of incorporation of additional species into the Pd unit cell, such as interstitial carbon[45-47]. As expected there was no evidence of interstitial carbon incorporation into the f.c.c Au phase, since these two components are known to be immiscible[48].

Au-Pd/C catalysts produced by acetate decomposition resulted in the distinct Au and Pd phases. The presence of the expanded Pd phase in the monometallic sample makes the identification of a Au-Pd alloy difficult to determine by XRD. Therefore, further characterisation is needed to explain the catalytic activities, in particular the synergistic effect, observed in the direct H_2O_2 synthesis results.

4.4.4 Electron Microscopy (EM)

Scanning transmission microscopy (STEM) - high-angle annular dark-field (HAADF) micrographs of Au (Figure 4.10), Pd (Figure 4.11) and Au-Pd (Figure 4.12) carbon supported material prepared by physical grinding are presented. X-ray energy-dispersive spectroscopy (XEDS) was used to analyse the composition of individual nano-particles.

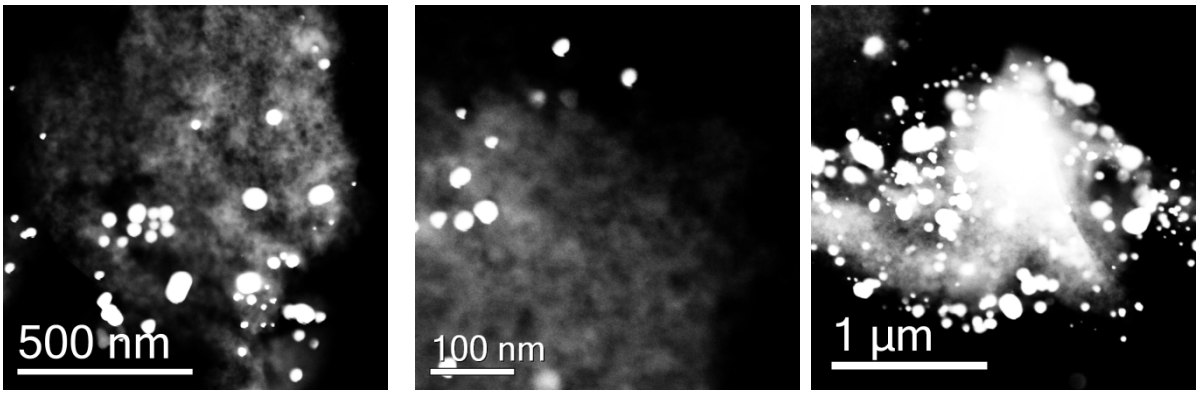

Figure 4.10 - Representative HAADF images of a carbon supported Au material prepared by physical grinding.

Analysis of the carbon supported Au material prepared by physical grinding, shown in Figure 4.10, confirmed the presence of both large >200 nm particles and a proportion of < 10 nm particles. The number of large particles indicates decomposition of gold acetate alone isn't achieving a high level of metal dispersion; this accounting for the low catalytic activity of PG-5 %Au/C.

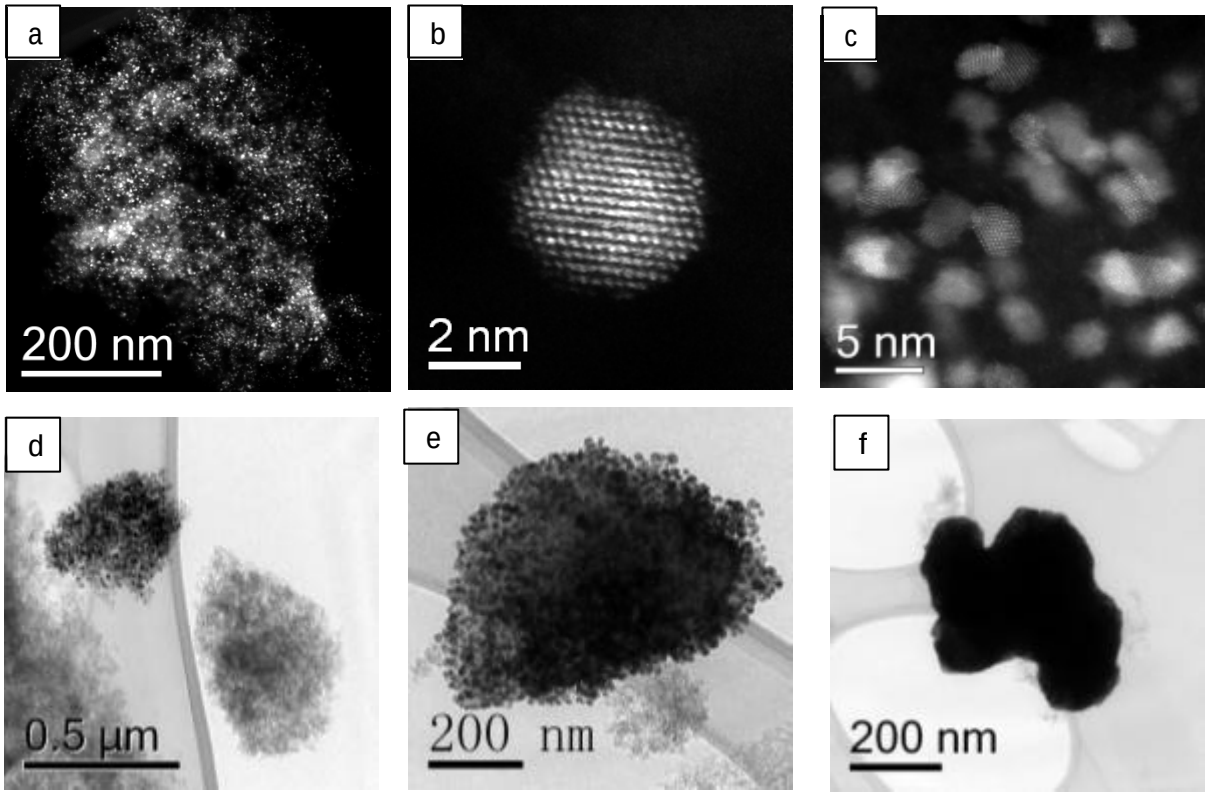

Figure 4.11 - Representative HAADF images (a-c) and BF-TEM (d-f) micrographs of a Pd carbon supported material prepared by physical grinding.

Analysis of the monometallic Pd images, in figure 4.11, indicates that there were three distinct morphologies present on the support surface. Firstly, there was a fine dispersion of sub 10 nm metallic Pd particles homogeneously dispersed over the support as represented by images a-c. Secondly, there were occasional micron-scale agglomerates of ~20 nm Pd particles held together in a carbonaceous matix, represented by images d and e. Thirdly there were also very occasional ~0.5 µm dense Pd particles (image f). Images d-f (Figure 4.11) corroborates the XRD findings for the presence of carbidic Pd species by showing large Pd-carbon masses on the surface of the support.

Also in agreement with XRD, is that there are significantly more small particles (sub 5 nm) in the monometallic Pd/C catalysts (figure 4.11 a-c) than the monometallic Au/C catalysts, indicating that Pd disperses far more successfully than Au on heat treatment. The high dispersion of Pd accounts for the high catalytic activity observed for monometallic Pd.

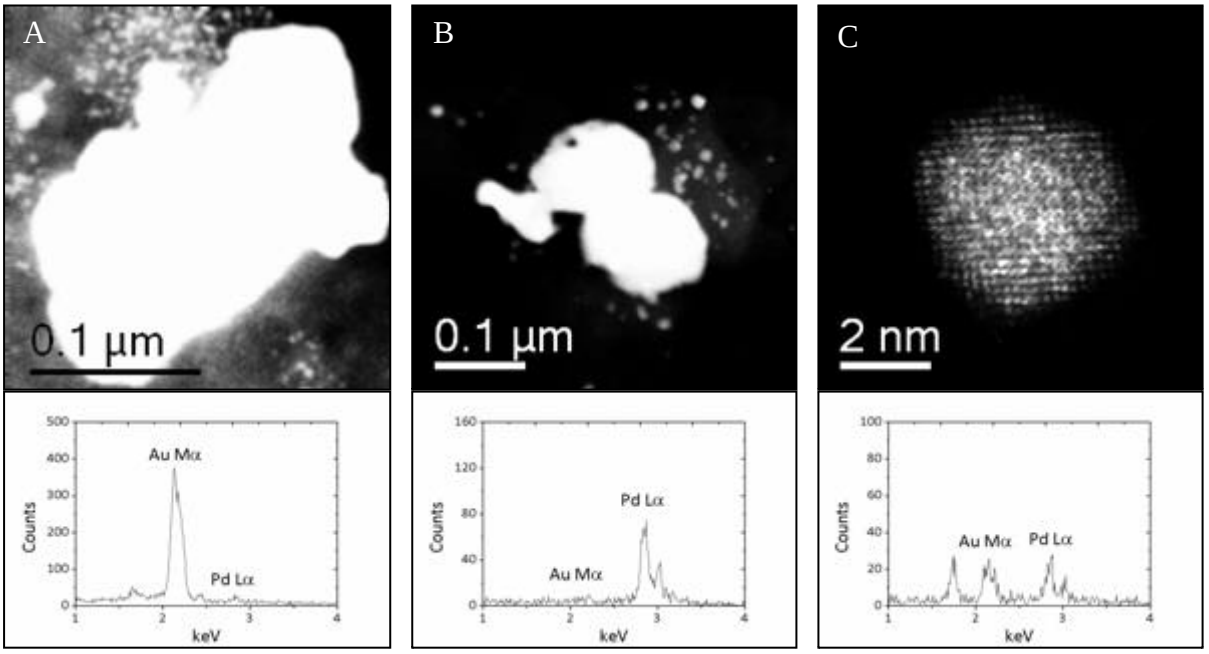

Figure 4.12 - Representative HAADF images and corresponding XEDS spectra from a Au-Pd carbon supported material prepared by physical grinding. (A) large *ca.* 200 nm gold, (B) large *ca.* 200 nm palladium and (C) Au-Pd alloy *ca.* 5 nm.

The HAADF images of PG-Au-Pd/C show a variety of metal particles. Firstly, it is apparent there are a number of large (*ca.* 0.2 µm) Au rich particles, represented in figure 4.12A, and large (*ca.* 0.2 µm) Pd rich particles, figure 4.12B. These particles are believed to be inactive, with active particles being less than 10 nm, and therefore a waste of expensive metal materials.

Analysis of higher resolution images shows the presence of sub 5 nm particles, represented by figure 4.12C, that are not observable by XRD analysis (Figure 4.12). Smaller, sub 5 nm, particles of monometallic and bimetallic nature were observed, with the alloying explaining the synergistic effect seen in the catalyst testing data. As seen in catalysts prepared by

impregnation, the bimetallic carbon supported catalysts exhibit Au-Pd bulk alloying.[43] The images are in agreement with an earlier postulation in section 4.2.1 that decomposing the metal acetates together may assist the formation of Au-Pd alloys. It appears that a higher level of metal dispersion, particularly gold, is being achieved due to simultaneous metal acetate decomposition, encouraging small (< 5 nm) Au-Pd alloys to form. However, sub 5 nm monometallic (unalloyed) particles were found on the carbon surface. It is likely that these Pd particles are responsible for the majority of the PG-Au-Pd/C catalysts H_2O_2 hydrogenation, due to the high H_2O_2 hydrogenation activity of PG-5 % Pd/C catalysts.

IMP-Au-Pd/C catalysts also comprise a broad size range of particles; mainly small particles that are ca. 2-10 nm, but also some larger particles, >10 nm.[43]

As well as varying composition, wide variations of sizes for the sub 10 nm particles were observed. A particle size distribution histogram is shown in Figure 4.13.

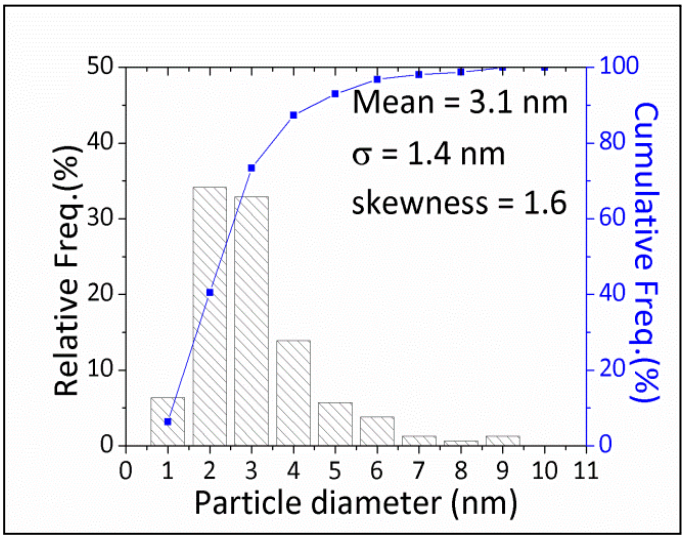

Figure 4.13 - Size distribution of sub-10 nm particles in carbon supported Au-Pd materials produced by physical grinding. *Note* - many much larger Au-rich and Pd-rich particles were also observed but are not included in this histogram.

Figure 4.13 indicates that PG-Au-Pd/C has mean particle size of 3.1 nm; this value is only for particles below 10 nm due to the high number of larger particles (>10 nm) making a particle size distribution graph for the whole particle range difficult.

Hutchings et al.[43] concluded when studying IMP-Au-Pd/C and TiO_2 catalysts that higher catalytic activity for stable catalysts (calcined at 400 ^oC) is associated with a higher number density of larger particles between 5 – 10 nm. This can be related to smaller particles that are <5 nm, having greater activity for the subsequent H_2O_2 hydrogenation pathway so the overall H_2O_2 formed is lower.

Concentrating on IMP-Au-Pd/C particles in the 1-10 nm range, Hutchings and co-workers found the majority of particles to be between 4 – 6 nm.[43] Indicating that the size distributions of the Au-Pd active particles are generally larger when prepared by impregnation than those prepared by physical grinding, where the majority of particles are between 2 - 4 nm. This could account for the greater activity of the physical grinding catalyst for the direct H_2O_2 synthesis observed in section 4.3. Imp-Au-Pd/C had a H_2O_2 productivity of 110 $mol_{H2O2}kg_{cat}^{-1}h^{-1}$ whereas PG-Au-Pd/C had a lower productivity of 100 $mol_{H2O2}kg_{cat}^{-1}h^{-1}$ due to a far higher hydrogenation activity.

In order to compare further the percentage of metal that is below 10 nm would be required; this would allow a more conclusive comparison between the H_2O_2 formations in terms of TOF (mol H_2O_2 per catalytic site per unit time).

4.4.5 X-ray Photoelectron Spectroscopy (XPS)

The surface of the PG-Au-Pd/C catalyst before and after heat treatment was analysised using XPS, as well as the monometallic PG-5 %Au/C and PG-5 %Pd/C catalysts; with the Pd(3d) spectra in Figure 4.14, Au(4f) spectra in Figure 4.15 and XPS quantification data in Table 4.5.

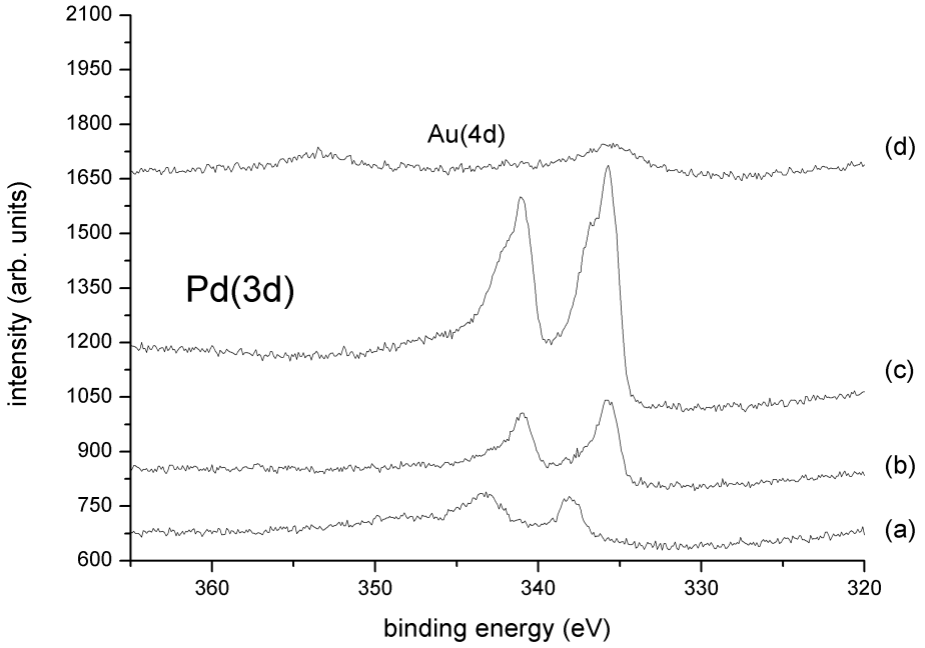

Figure 4.13 - Pd(3d) spectra for a carbon supported catalysts prepared by physical grinding, (a) Au-Pd before heat treatment, (b) Au-Pd after heat treatment, (c) 5 %Pd and (d) 5 %Au.

The Pd(3d) spectral region, Figure 4.13, for the carbon supported Au-Pd material shows a shift in the Pd($3d_{5/2}$) peak from 337.9 eV for the non-heat treated material to a doublet peak at 335.8 eV and 336.6 eV after heat treatment; the Pd($3d_{5/2}$) binding energy for metallic Pd is *ca*. 335.0 eV. The 336.6 eV peak is close to that expected for PdO generated by the decomposition of the acetate, but the presence of PdC must be considered, as seen by HR-TEM and XRD analysis of the sample.

The binding energy difference between Pd^{2+} in the acetate to the Pd^{2+} in PdO arises from a combination of different degrees of charge transfer between the Pd and ligand, and differences in the final state relaxation effects.

The two peaks in the Pd(3d) spectral region for the PG-5 %Pd/C are more pronounced at 335.3 and 336.6 eV, due to the higher palladium loading compared to the Au-Pd/C catalyst (2.5 wt%Pd).

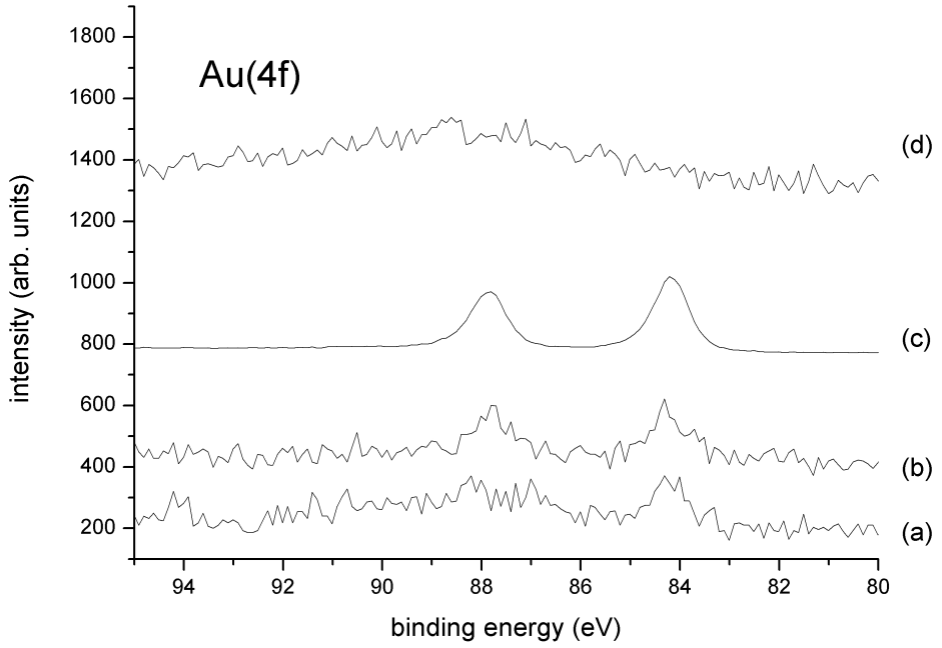

Figure 4.14 - Au(4f) spectra for a carbon supported catalysts prepared by physical grinding, (a) Au-Pd before heat treatment, (b) Au-Pd after heat treatment, (c) 5 %Au and (d) 5 %Pd.

The Au(4f) spectral region, Figure 4.14, indicates all the gold that is present on the surface is in the metallic state, by the peaks at ca. 84 eV. This highlights the higher reduction potential of gold compared to palladium.

Table 4.4 - Quantified XPS data for physical grinding catalysts, Au-Pd/C before and after heat treatment, Pd/C and Au/C.

PG-catalyst /C	**At%**				**Pd/Au[a]**	**Pd^{2+} (%)**
	Au	Pd	C	O		
Au-Pd Non heat-treated	0.04	0.52	94.34	5.1	12.50	nd
Au-Pd	0.04	0.47	95.22	4.27	11.25	22
Pd-only	-	1.47	92.06	6.47	-	46
Au-only	0.27	-	96.06	3.67	-	-

[a] Corrected for overlap of the Pd($3d_{5/2}$) and Au($4d_{5/2}$) components.

Quantification of the integrated peak intensities, in Table 4.4, shows that there is an excess of surface Pd over surface Au, prior and preceding heat treatment of the PG-Au-Pd/C catalyst. There is also a high metallic Pd content for both PG-Au-Pd/C (78 $\%Pd^0$) and PG-5 %Pd/C (54 $\%Pd^0$) preceding heat treatment, compared to Imp-Au-Pd/C which has 32 % surface Pd^0. A high surface Pd content in the metallic state would account for the high H_2O_2 hydrogenation activity of the physical grinding catalysts compared to the impregnation counterparts. Metallic Pd has previously been shown to be responsible for H_2O_2 hydrogenation, which has previously been investigated in Chapter Three.

4.4.6 Discussion

The characterisation, by XRD (figure 4.9) and STEM (figure 4.11 d-f), of the carbon supported material showed that carbidic species are present in the bulk and on the surface of the catalyst. This hasn't been observed previously for comparable impregnation catalysts, and the comparable selectivities to benzaldehyde of the physical grinding and impregnation derived catalysts suggest the carbidic species do not have an obvious effect on catalyst performance. However, when producing catalysts on a larger scale or lower metal content this may become an important issue. The presence of interstitial carbon has not been reported previously for carbon supported catalysts prepared by impregnation, so it is believed that the carbon exists as a result of acetate decomposition in an inert atmosphere. This carbon could be removed by calcination in oxygen; however the oxidation state will change and at high temperature the particles may sinter causing deactivation. Krishnankutty *et al.*[46] proposed a model, which is shown in Figure 4.15, in which a Pd/C catalyst could contain a mixture of particles, type A-D, with various extents of carbon coverage; each type could affect the catalyst performance differently.[46]

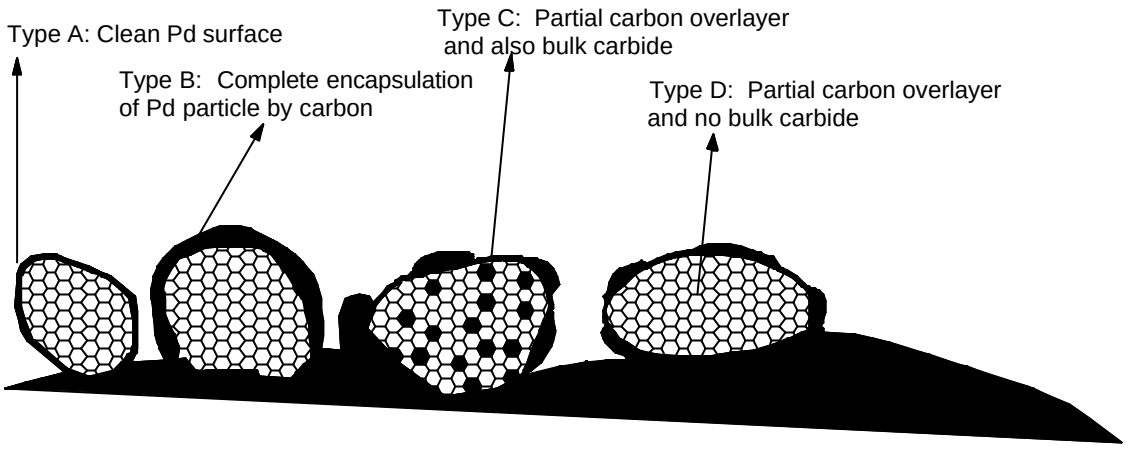

Figure 4.15 - Carbon deposits on Palladium which may affect the catalysts performance depending on the extent of coverage[46].

Type A, a clean Pd surface, would allow adsorption of the reactants to occur allowing the palladium particle to participate in the reaction to its full capacity. In contrast complete coverage of the Pd surface by carbon, type B, would deactivate the catalyst activity as there would be no active surface for the reactants to adsorb too. Partial carbon coverage, as in type C and D, would cause differing lower levels of reactant adsorption reducing the catalytic activity.

A number of differences between carbon and titania supported Au-Pd catalysts prepared by impregnation have previously been identified[43]. A particularly interesting observation is that the bimetallic titania supported particles form a core shell structure (Au core, Pd shell) upon calcination. In order to elucidate the extent and nature of Au-Pd alloying on titania when using physical grinding, monometallic Au, Pd and bimetallic Au-Pd catalysts were prepared, tested and characterised.

4.5 Titania Supported Au, Pd and Au-Pd Catalysts Prepared by Physical Grinding

4.5.1 Direct H_2O_2 Synthesis and Hydrogenation

A series of titania supported monometallic (Au and Pd) and bimetallic (Au-Pd) catalysts were prepared by physical grinding and tested for H_2O_2 synthesis under standard reaction conditions the results are shown in Table 4.5.

Table 4.5 - H_2O_2 synthesis data for monometallic and bimetallic titania supported catalysts prepared by physical grinding.

Catalyst	**Productivity ($molH_2O_2kg_{cat}^{-1}h^{-1}$)**	**Hydrogenation ($molH_2O_2kg_{cat}^{-1}h^{-1}$)**
5%Au / TiO_2	1	59
5%Pd / TiO_2	45	1416
2.5%Au-2.5%Pd / TiO_2	90	1243

In common with the carbon supported catalysts described earlier, the Pd and Au-Pd catalysts have significantly higher activity than the Au catalyst, with the bimetallic catalyst showing the highest productivity. The addition of Au to Pd also decreases the hydrogenation activity of the materials, indicating synergy. In order to investigate the origin of the synergistic effect, a number of characterisation techniques were employed to try to identify the nature of the nano-particles on TiO_2.

4.5.2 X-Ray Diffraction (XRD)

X-ray diffraction (XRD) analysis of the 5 %Au, 5 %Pd and Au-Pd titania supported catalysts, produced by physical grinding, with a comparable catalyst prepared by impregnation, is shown in Figure 4.16, with calculated parameters shown in Table 4.6 (refer to the experimental procedures in chapter 2 for further details).

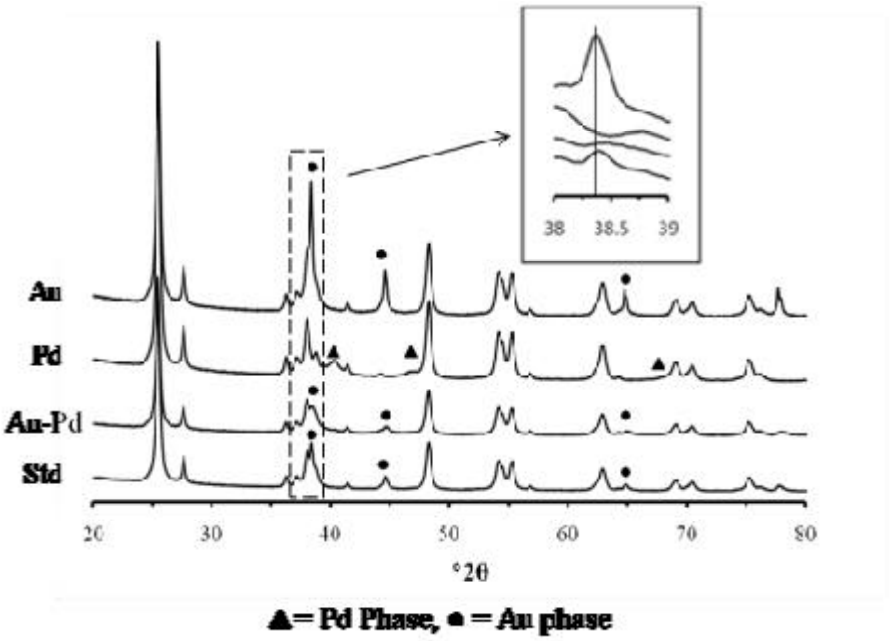

Figure 4.16 - XRD analysis of Au, Pd and Au-Pd titania catalysts produced by physical grinding and a comparable Au-Pd titania catalyst produced by impregnation (Std).

Table 4.6 – Calculated Au and Pd particle properties, for titania supported monometallic (Au, Pd) and bimetallic (Au-Pd) materials produced by physical grinding and a comparable Au-Pd catalyst prepared by impregnation (Std), from XRD[a].

Sample	Metal phase	Calculated unit cell volume (Å^3)	Average crystallite size (nm)	Weight contribution of phase (%)
Au	Au	67.79	57	4.4
Pd	Pd	59.03	7	4.7
Au-Pd	Pd	59.65	4	1.2
	Au	67.26	62	2.0
Std	Pd	n/a	n/a	n/a
	Au	67.70	34	2.2

[a] Errors: unit cell volume $\pm$0.1 Å^3, crystallite size $\pm$2 nm, weight fraction $\pm$0.5 %

Refinement of the monometallic XRD patterns showed metallic Au and Pd and provided agreement with interpretations of the crystallite size derived from catalytic testing. Suggesting the high activity of the monometallic Pd for the direct H_2O_2 synthesis being due to the presence of smaller particles, whereas, Au with the larger average particle size (57 nm) exhibited a lower H_2O_2 activity. The average Au crystallite size of 57 nm is considerably larger than the < 10 nm size required for an active particle.[49] The smaller average crystallite size (7 nm) of Pd particles produced by physical grinding indicates a far greater intrinsic ability of this metal to disperse over the support.

The PG-Au-Pd/TiO_2 catalyst showed reflections associated with two crystalline cubic phases, with unit cell volumes closely associated with Au and Pd. Both phases have an observable shift in unit cell volumes compared to the respective comparable monometallic systems. However no reflections associated with the unit cell size of a bulk 1:1 Au-Pd alloy (63.04 Å) were observed.[50] This suggests some limited alloying, with a small incorporation of one element into the bulk of the other. Though no reflections indicative of a homogeneous Au-Pd alloy were observed, as expected from the synergistic effect in catalyst activity, a proportion of nano-particles that are below the detectability limit of the XRD technique could be present. This is confirmed by the calculated weight contribution of the Pd and Au phases accounting for only 60 % of the metal loading (Table 4.6), implying the presence of sub 5 nm particles. Therefore, further characterisation is needed to explain the catalytic activities, in particular the synergistic effect, observed in the direct H_2O_2 synthesis results.

The lower Pd average particle size of 4 nm in the PG-Au-Pd/TiO_2 catalyst compared to 7 nm in the monometallic 5 % Pd catalyst indicates the decomposition of gold acetate aids the dispersion of Pd during the decomposition of $Pd(OAc)_2$. However, the higher Pd content in the monometallic 5 wt% Pd, compared to 2.5 wt% Pd in the bimetallic may be a factor. This increases the likelihood of metal sintering during heat treatment.

Titania supported Au-Pd catalysts produced by impregnation have previously been shown to form core shell structures by HR-TEM and XPS.[16] XRD of the impregnated sample shows reflections closely associated with a Au phase but with no observable Pd phase; making it difficult to compare the two techniques using this data. This is attributed to small monometallic Pd particles and the shell in the bimetallic particles having insufficient number of planes to provide observable reflections. However, what is evident is the larger average Au crystalline size of 62 nm in the PG-Au-Pd/TiO_2 catalyst than that seen in the comparable

impregnation catalyst, 34 nm. This illustrates the overall poorer dispersion of Au metal achieved by physical grinding over TiO_2.

4.5.3 Scanning Transmission Electron Microscopy (STEM)

STEM - high-angle annular dark-field (HAADF) micrographs of titania supported Au-Pd material prepared by physical grinding are presented in Figure 4.17. X-ray energy-dispersive spectroscopy (XEDS) was used to analyse the composition of individual nano-particles. Particle distribution was obtained for sub-10 nm particles and their distribution compared to the corresponding carbon supported catalysts.

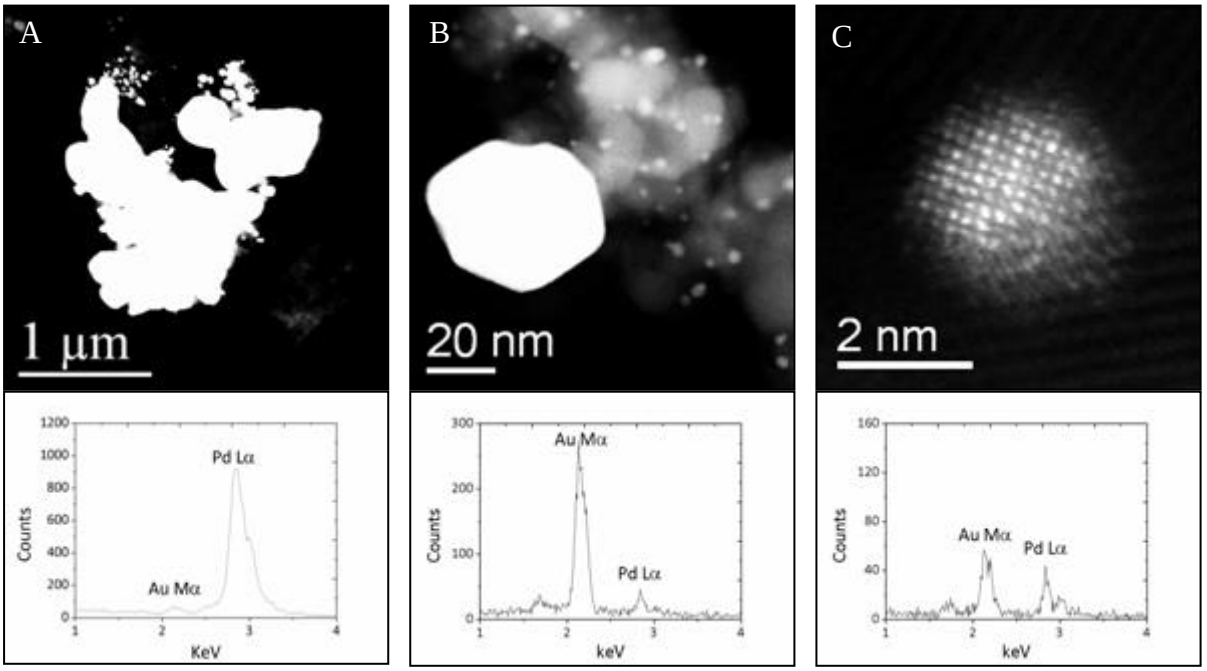

Figure 4.17 - Representative HAADF images and corresponding XEDS spectra from titania supported Au-Pd material prepared by physical grinding.

STEM-HAADF images of a titania supported Au-Pd catalyst prepared by physical grinding shows large Au and Pd particles on the titania surface. Smaller sub 5 nm particles can also be readily found and these appear to comprise of Au and Pd which indicates alloying. The alloying would explain the synergistic effect seen in the catalyst testing data.

There is no evidence from the STEM imaging that suggests the particles have core shell morphology as seen in Au-Pd titania materials prepared by impregnation.[16, 43] Here the particles appear to be Au-Pd random alloys, the same as the carbon supported material, of varying composition and size as shown in Figure 4.18.

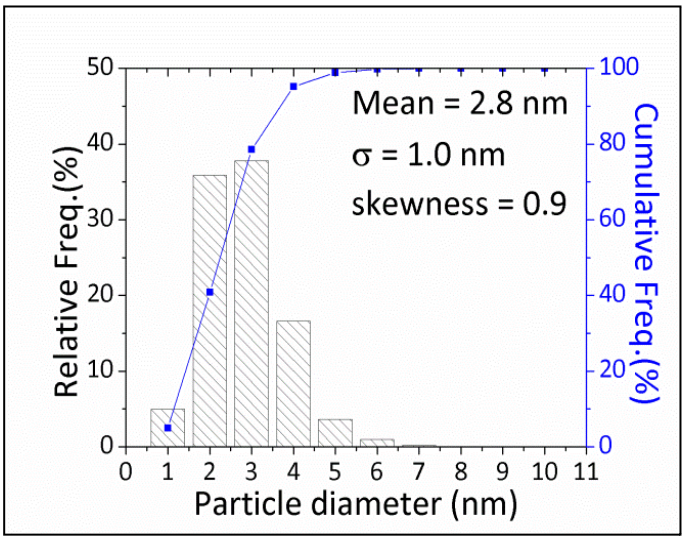

Figure 4.18 - Size distribution of sub-10 nm particles in titania supported Au-Pd materials produced by physical grinding. Note: many much larger (>10 nm) Au-rich and Pd-rich particles were also observed but are not included in this histogram.

The particle size distribution histogram, Figure 4.18, shows that the average particle size of the sub-10 nm particles is 2.8 nm; this is slightly smaller than the carbon supported counterpart (3.1 nm; Figure 4.13). The smaller average particle size could be a reason for the titania supported catalysts increased activity towards the H_2O_2 hydrogenation pathway as suggested previously by Hutchings *et al.*[43]

The small particles are more uniform in size on the titania support (skewness = 0.9) than on the carbon (skewness = 1.6). This trend has been seen previously for impregnation materials[43] and may be due to the more ordered structure of titania.

4.5.4 X-ray Photoelectron Spectroscopy (XPS)

The surface of Au-Pd titania supported material before and after heat treatment was analysised using X-ray photoelectron spectroscopy (XPS).

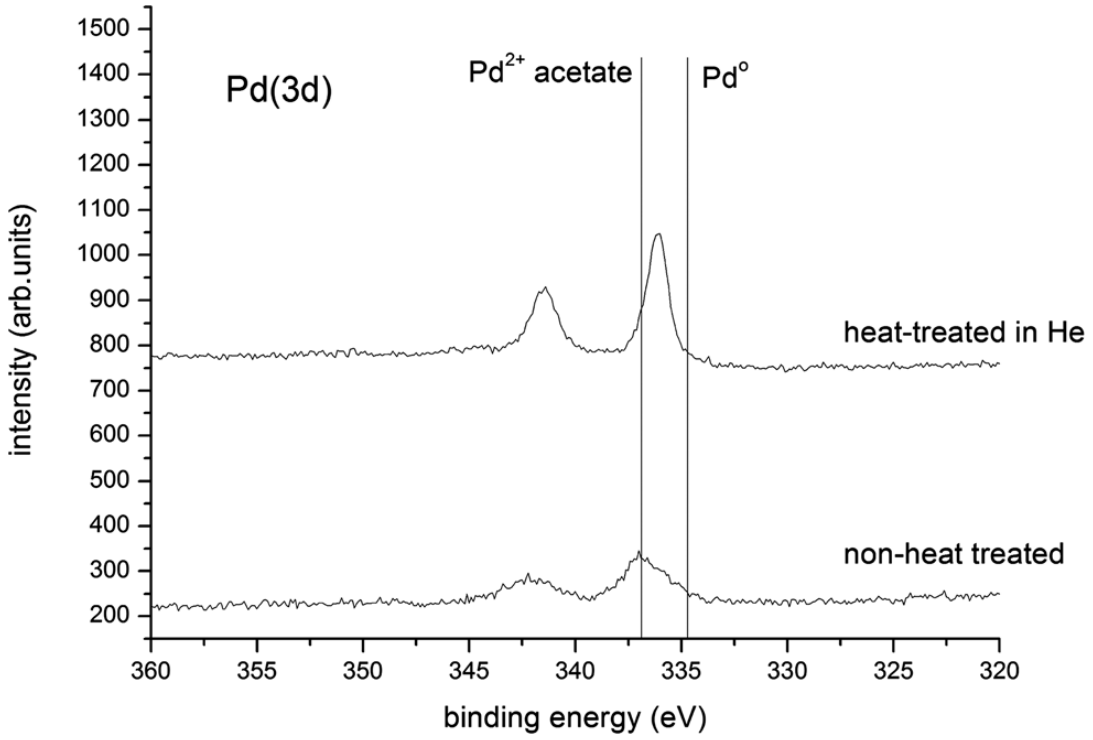

Figure 4.19 - Pd(3d) spectra for a titania supported Au-Pd material produced by physical grinding, before and after heat treatment.

The Pd(3d) spectral region, in Figure 4.19, for the titania supported Au-Pd material shows a shift in the Pd($3d_{5/2}$) peak from 336.9 eV for the non-heat treated material to 336.4 eV after heat treatment; the Pd($3d_{5/2}$) binding energy for metallic Pd is *ca*. 335.0 eV. The 336.4 eV peak is close to that expected for PdO generated by the decomposition of the acetate, but the presence of PdC must be considered, as seen for the carbon supported material. However, extensive analysis of the sample by HR-TEM did not show any presence of PdC; it was also not observed in the XRD analysis of the titania supported material.

As a result of the changes in the C(1s) profile from the different treatments, we have referenced all binding energies to the Ti($2p_{3/2}$) peak from the support, taken to be 458.2 eV[51]. The binding energy difference between Pd^{2+} in the acetate to the Pd^{2+} in PdO arises from a

combination of different degrees of charge transfer between the Pd and ligand, and differences in the final state relaxation effects.

Table 4.7 - Quantified surface compositions (at%) for the titania supported Au-Pd materials before and after heat treatment.

Catalyst	**At%**				**Pd/Au**[a]	**Pd^{2+} (%)**
	Au	Pd	Ti	O		
Non-heat treated	0.052	0.45	28.0	71.5	8.1	nd
Heat-treated	0.057	0.95	30.3	68.7	16.2	>90

[a] Corrected for overlap of the Pd($3d_{5/2}$) and Au($4d_{5/2}$) components.

Quantification of the integrated peak intensities in Table 4.7 shows that there is an excess of surface Pd over surface Au, especially after the heat treatment in He. This shows that the Pd disperses far more successfully than Au on heat treatment. Alternatively the high Pd surface contribution may indicate development of some core-shell morphology, although this was not observed in the corresponding STEM-HAADF imaging analysis.

Interestingly, the majority of the surface palladium on the heat treated sample is Pd^{2+} (>90 %). This is not what was expected due to the high hydrogenation activity of these materials (1243 $mol_{H2O2}kg_{cat}^{-1}h^{-1}$) and contradicts the findings for the PG-Au-Pd/C catalyst. However, there is double the palladium content on the titania surface (0.95 at%) compared to carbon (0.47 at%), which in this case could be responsible for the higher H_2O_2 hydrogenation activity. Further, indicating both the Pd/Au ratio and Pd^{2+} surface concentration play an important role.

Palladium disperses more efficiently on titania and is primarily in the Pd^{2+} oxidation state, whereas it is less dispersed with a higher metallic Pd content on carbon. This suggests that carbon aids the reduction of Pd^{2+} to Pd^{0}. And in conjunction with carboneous species only being observed when preparing physical grinding carbon supported catalysts indicates the support plays a vital role in the acetate decomposition.

4.6 Effect of Grinding Time

Physical grinding of the metal acetate precursor with the support provides improved macro-scale distribution of the precursors on the support, prior to the decomposition stage which is induced by the heat treatment step of the synthesis. This then leads to the observed mixture of Au, Pd and Au-Pd nano-particles. In order to ascertain the importance of the initial mixing of the support and metal acetate precursors, a series of Au-Pd/C catalysts were prepared with increasing grinding time. These catalysts were subsequently heat treated and tested for H_2O_2 formation as shown in Table 4.8.

Table 4.8 - The effect of grinding time on H_2O_2 productivity for a Au-Pd/C catalyst

Grinding time (min)	**Productivity ($molH_2O_2kg_{cat}^{-1}h^{-1}$)**
1	100
5	102
10	102
20	104

H_2O_2 synthesis tests showed similar productivity for all grinding times attempted. This indicates the most important redistribution of the metal occurs during the heat treatment stage rather than the grinding stage, once a certain level of basic mixing has been achieved.

4.7 Effect of Thermal Treatment Temperature

From TGA analysis, Figure 4.3A (section 4.2.2), the thermal decomposition of acetate on a carbon support starts at temperatures as low as 150 ^{o}C and is complete by 250 ^{o}C, suggesting that the use of lower thermal treatment temperatures might also be successful. The thermal treatment temperature has previously been shown to be a play off between activity and stability [16, 43], with catalysts calcined at lower temperature being more unstable but having higher activity. Thus, a series of experiments were performed for Au-Pd/C mixtures produced at 5 min grinding times, with the mixtures heated to 250 ^{o}C, 300 ^{o}C, 350 ^{o}C, and 400 ^{o}C, and then tested for H_2O_2 synthesis (Table 4.9). The heating rate and time were kept constant at 20 ^{o}C min^{-1} and 2 h.

Table 4.9 - The thermal treatment temperature on H_2O_2 productivity for a Au-Pd/C catalyst

Thermal treatment temperature (^{o}C)	**H_2O_2 Productivity ($mol_{H2O2}\ kg_{cat}^{-1} hr^{-1}$)**	
	1st Use	**2nd Use**
250	131	92
300	114	94
350	100	100
400	94	94

The catalytic testing data shown in table indicates that a temperature of 350 ^{o}C is required to produce a stable Au-Pd catalyst. It is likely that the higher temperature of 400 ^{o}C causes sintering of the nano-particles leading to deactivation of the catalyst. At lower temperatures (250 and 300 ^{o}C) the initial catalyst activity is higher; however the loss of activity on reuse indicates the nano-particles are not stable on the support surface. At the lower temperature TGA, Figure 4.3A, has shown the acetate not to be fully decomposed which would explain the lower activity and stability.

4.8 Effect of Chloride Addition

The objective of this study is to determine the role of halide in the catalyst; previous attempts to impregnate the catalyst with halide led to destabilising the material and leaching of active components into the reaction medium. Also the baseline catalyst already contained a significant concentration of halide, with the addition of extra halide leading to unselective catalyst poisoning[10].

A series of Au-Pd/C catalysts were prepared by physical grinding with varying concentrations of chloride, in collaboration with a colleague, Daniel Gaskell. The introduction of chloride was achieved by substituting amounts of $Pd(OAc)_2$ with $PdCl_2$ in the ratios shown in Table 4.10. Unfortunately the concentration of chloride has not been accurately measured here. In future the concentration of chloride in the bulk can be determined using inductively coupled plasma mass spectrometry (ICP). Results have been expressed as the theoretical weight percent if all chloride remains.

Table 4.10 - Au-Pd/C prepared by physical grinding using different precursor compositions.

$Pd(OAc)_2$: $PdCl_2$	**C (g)**	**$Au(OAc)_3$ (g)**	**$Pd(OAc)_2$ (g)**	**$PdCl_2$ (g)**	**Cl^- (wt %)**
100:0	0.475	0.025	0.026	0.0000	0.00
75:25	0.475	0.025	0.020	0.0053	0.42
50:50	0.475	0.025	0.013	0.0107	0.83
25:75	0.475	0.025	0.007	0.0160	1.25
0:100	0.475	0.025	0.000	0.0214	1.67

After heat treatment at 350 ^oC for 2 h in flowing He, the catalysts were tested for the direct H_2O_2 synthesis with a view of observing the effect on the hydrogenation activity. Here it should be noted that $PdCl_2$ does not decompose until *ca.* 680 ^oC; however, it is believed that the exothermic nature of $Au(OAc)_3$ decomposition may assist the decomposition of $PdCl_2$ and at a macro-scale particle size the temperature may be decreased. In order to elucidate the nature of the active metal particles, the catalyst prepared using exclusively $PdCl_2$ was characterised by STEM and XPS, the findings being compared to the characterisation, reported previously in Section 4.4, of the catalyst prepared using exclusively $Pd(OAc)_2$.

4.8.1 Direct H_2O_2 Synthesis and Hydrogenation

Figure 4.20 shows the activity of PG-Au-Pd/C catalysts, with varying concentrations of Cl^-, for the direct H_2O_2 synthesis. The H_2O_2 synthesis, hydrogenation and decomposition pathways have been investigated; full experimental procedures are outlined in chapter 2.

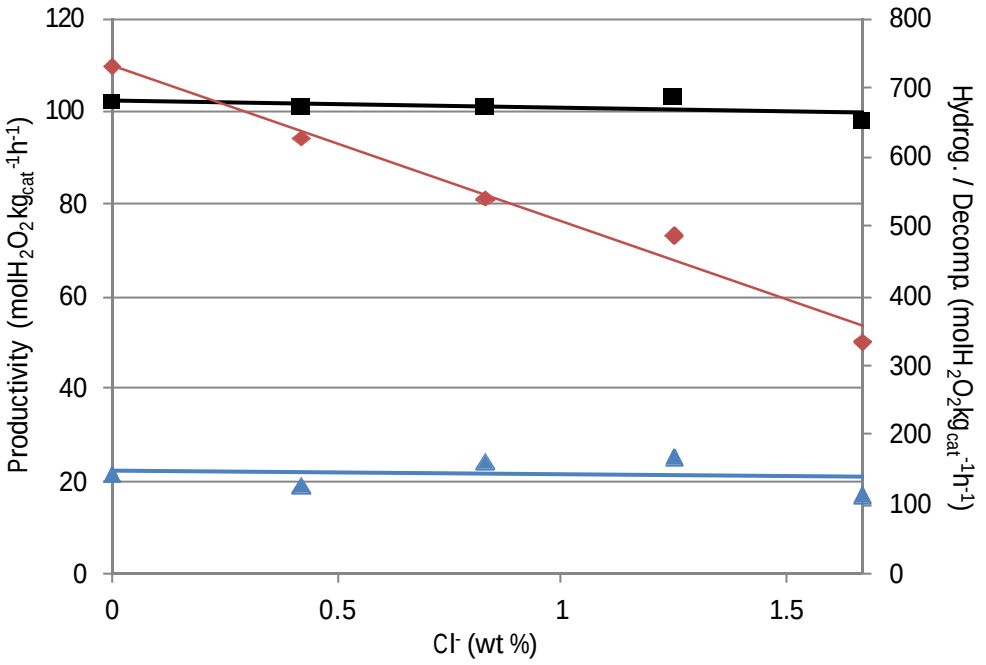

Figure 4.20 – Activity of catalysts with varying chloride concentration for the direct synthesis of H_2O_2: productivity, hydrogenation, decomposition

Increasing the concentration of chloride within the catalyst reduces the rate of hydrogenation, without affecting the total H_2O_2 produced. This indicates an improvement in the hydrogen selectivity with chloride preferentially blocking sites active for the H_2O_2 hydrogenation, while maintaining sites responsible for the direct H_2O_2 synthesis.

All the catalysts were active for H_2O_2 decomposition under the reaction conditions utilised. The rate of decomposition remained the same despite the chloride concentration, indicating surface chloride doesn't have a significant effect for the decomposition.

4.8.2 Scanning Transmission Electron Microscopy (STEM)

Scanning transmission electron microscopy (STEM) - high-angle annular dark-field (HAADF) micrographs of the Au-Pd/C catalyst prepared using $PdCl_2$ as the sole precursor (1.67 wt%Cl) are shown in Figure 4.21. The Au-Pd/C catalyst was prepared by physically grinding $PdCl_2$, $Au(OAc)_3$ and carbon prior to heat treatment at 350 ^oC in He for 2 h. X-ray energy-dispersive spectroscopy (XEDS) was used to analyse the composition of individual nano-particles. Particle distribution was obtained for sub-10 nm particles and their distribution compared to the corresponding PG-carbon material.

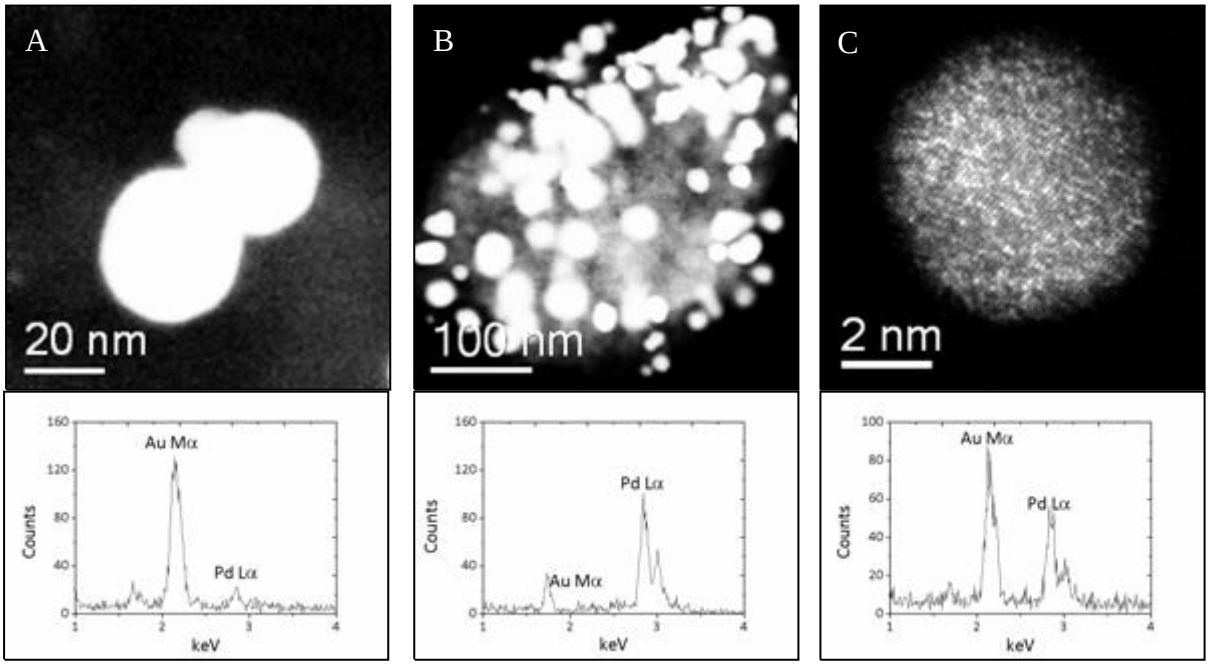

Figure 4.21 – Bright field imaging of PG-Au-Pd/C using $PdCl_2$ and $Au(OAc)_3$ precursors.

STEM showed that there was a larger proportion of large (*ca.* 50 nm) Au and Pd particles, suggesting the Pd is not dispersed as well when using $PdCl_2$ instead of $Pd(OAc)_2$. $PdCl_2$ has a decomposition temperature of 500 °C[52], and therefore does not undergo auto-reduction at the 350 °C, heat treatment temperature used here. The presence of a larger portion of Pd particles >50 nm could be a reason for the lower activity seen. There were also large Au particles present; however this is similar to PG-Au-Pd/carbon and titania-acetate only. Small

particles (<5 nm) were formed which contained both Au and Pd, and are thought to be the active species. The size distributuion of sub-10 nm particles is shown in Figure 4.22.

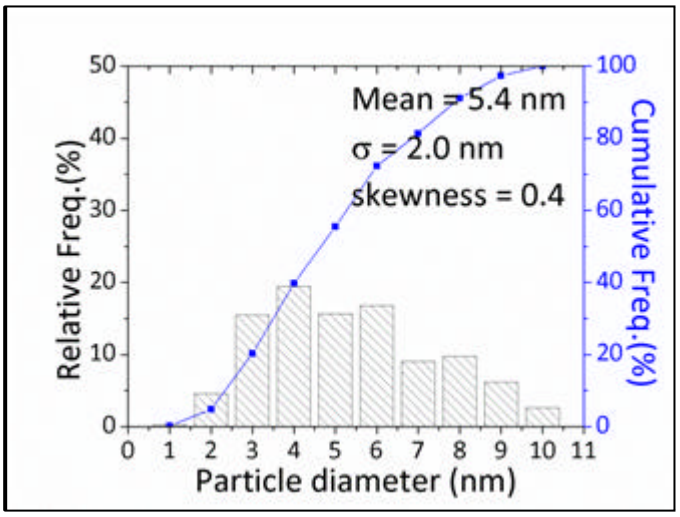

Figure 4.22 - Size distribution of sub-10 nm particles in Au-Pd/C ($PdCl_2$ precursor) produced by physical grinding. Note: many much larger Au-rich and Pd-rich particles were also observed but are not included in this histogram.

The average particle size of 5.4 nm, from Figure 4.22, is larger than for the PG-Au-Pd/carbon catalyst prepared with acetate only, of 3.1 nm in Figure 4.13 (section 4.4.4). In line with Hutching *et al* previous observation that a higher number density of larger particles (2-10 nm) is responsible for a high H_2O_2 producitvity due to lower H_2O_2 hydrogenation.[43] This may be the reason for the lower H_2O_2 hydrogenation activty observed for the catalyst prepared with $PdCl_2$. It also confirms an earlier postulation that the simultaneous decomposition of gold and palladium acetate may assist the decompositions in order to form more dispersed metal particles.

4.8.3 X-ray Photoelectron Spectroscopy (XPS)

The surface of Au-Pd carbon supported materials using $Pd(OAc)_2$ (Figure 4.23a) and $PdCl_2$ (Figure 4.23b) precursors, were analysised by XPS.

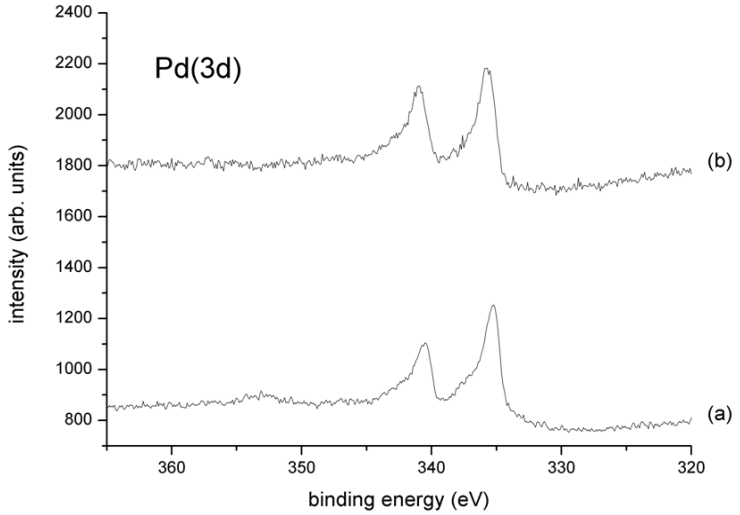

Figure 4.23 – Pd (3d) spectra observed for the PG-Au-Pd/C catalysts using different Pd precursors, (a) $PdCl_2$ and (b) $Pd(OAc)_2$.

The Pd(3d) spectral region, in Figure 4.23, of the physical grinding carbon catalysts are similar, when using $PdCl_2$ or $Pd(OAc)_2$ as the Pd metal precursor. Both spectra have a $Pd(3d_{5/2})$ peak at ca. 335.0 eV which corresponds to metallic Pd.

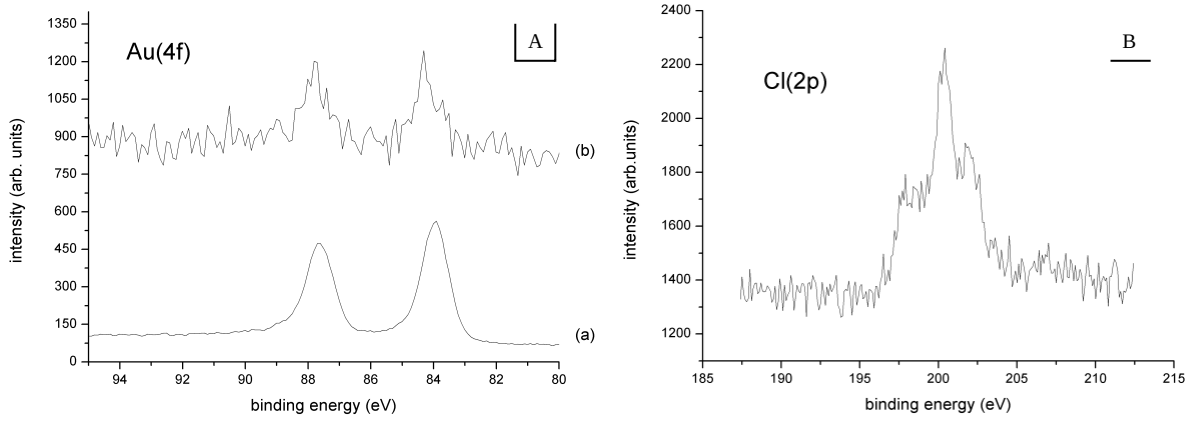

Figure 4.24 – [A] Au(4f) spectra observed for PG-Au-Pd/C catalysts using different precursors (a) $PdCl_2$ and (b) $Pd(OAc)_2$. [B] Cl(2p) spectra for PG-Au-Pd/C using $PdCl_2$.

The Au(4f) spectral region in Figure 4.24A indicates all the gold that is present on the surface is in the metallic state, by the peaks at ca. 84 eV. This highlights the higher reduction potential of gold compared to palladium.

The Cl(2p) spectra in Figure 4.24B, shows the presence of chloride on the surface of the PG-Au-Pd/C catalyst prepared with $PdCl_2$ precursor. Interestingly, a high binding energy (corresponding to more ionic, negatively charge Cl^{x-} species) is observed similar to stable IMP-Au-Pd catalysts (calcined at 400°C), represented by Figure 3.2 in Chapter Three. It can be postulated that a complex stable interaction between the support and Pd is occurring due to the stability of the catalyst during direct H_2O_2 synthesis which corresponds to lower H_2O_2 hydrogenation activity.

Table 4.11 - Quantified XPS data for PG-Au-Pd/C catalysts using different Pd precursors.

PG-Au-Pd/C	**At%**					**Pd/Au[a]**	**Pd^{2+} (%)**
Pd precursor	Au	Pd	C	O	**Cl**		
$Pd(OAc)_2$	0.04	0.47	95.22	4.27		11.25	22
$PdCl_2$	0.31	0.74	94.9	3.61	0.44	1.89	25

[a] Corrected for overlap of the Pd($3d_{5/2}$) and Au($4d_{5/2}$) components.

Quantification of the XPS in Table 4.11 indicates there is approximately 8 times the amount of gold on the surface as well as increased surface palladium, when the $PdCl_2$ precursor is utilised. This may mean a higher palladium and gold dispersion; however, this contradicts the STEM analysis so it is more likely to be simply due to a higher content of metal on the support surface i.e. less metal in the carbon pores. In this case unlike previously when it was postulated higher surface palladium causes higher H_2O_2 hydrogenation, on this occasion it corresponds to a lower Pd/Au ratio (1.89). Therefore, the decrease in H_2O_2 hydrogenation is likely to be due to a higher association between gold and palladium providing higher stability of the formed peroxide. This linked with chloride (0.44 at%) preferentially blocking active sites will be responsible for the lower H_2O_2 hydrogenation.

The Pd on the carbon surface, for both catalysts is mainly in the metallic state, indicating sufficient decomposition of the Pd precursor is being achieved, when $PdCl_2$ or $Pd(OAc)_2$ are utilised.

4.8.4 Discussion

Interestingly, XPS quantification of PG-Au-Pd/C prepared using $PdCl_2$ shows the presence of 0.44 at% on the carbon surface; this concentration is similar to that seen previously for stable IMP-Au-Pd/C catalysts, table. Table 4.12 compares quantified XPS data and direct H_2O_2 synthesis activities of PG-Au-Pd/C ($PdCl_2$ precursor) and IMP-Au-Pd/C.

Table 4.12 - Quantified XP data and H_2O_2 testing data for stable PG-Au-Pd/C ($PdCl_2$ precursor - 350°C in He) and IMP-Au-Pd/C (400°C in static air) catalysts.

	H_2O_2 Synthesis		XPS – Molar ratios						
	Prod	Hydrog	Au	Pd	C	O	Cl	Pd/Au	Pd^{2+} (%)
PG-$PdCl_2$									
350°C in He	98	335	0.31	0.74	94.9	3.61	0.44	1.89	25
***IMP*[10]**									
Calcined 400°C	110	120	0.17	0.38	93.7	5.3	0.45	1.7	68

It is clear from table, that the presence of halide on the catalyst surface is not solely responsible for the catalysts activity towards H_2O_2 hydrogenation and thus the synthesis of H_2O_2. This is shown by the PG-catalyst having a higher H_2O_2 hydrogenation activity of 335 $mol_{H2O2}kg_{cat}^{-1}h^{-1}$, than the IMP-Au-Pd/C 120 $mol_{H2O2}kg_{cat}^{-1}h^{-1}$, despite approximately the same surface halide concentration, 0.44 and 0.45 at% respectively. This indicates that although halide may be responsible for blocking some active sites for decreasing for H_2O_2 hydrogenation, halide is not solely responsible. The particle size distribution, palladium oxidation state and extent of Au-Pd alloying and all play vital roles.

The mean average particle size of particles <10 nm, believed to be active, is approximately the same 4-6 nm. They have both higher number densities of smaller particles compared to equivalent titania catalysts with higher hydrogenation. However, direct comparison between the mean particle sizes is difficult as values for the percentage of metal below 10 nm are unknown.

Examination of the palladium oxidation state indicates a higher surface Pd^{2+} concentration on the impregnation catalyst. This is as expected, as in order to stabilise the impregnation catalyst a heat treatment in an oxygen rich atmosphere (static air) and high temperature (400^oC) will partially oxidise the palladium. Whereas, to stabilise the physical grinding catalyst it is heated in an inert atmosphere to 350 ^oC causing the reduction of the precursor to the metal. In the previous chapter (Chapter Two) the presence of PdO has been shown to be crucial, by inhibiting the Pd^0 activity on a Au-Pd/AwC resulting in switching off H_2O_2 hydrogenation.

In Table 4.12, although the Pd/Au ratios are similar for the PG-Au-Pd/C and IMP-Au-Pd/C catalysts, the physical grinding catalyst has approximately double the metal content, Au and Pd. This may inhibit gold's ability to influence Pd and stabilise the O-O bond. Therefore, in this case, it can be postulated that double the metal in a higher metallic Pd concentration can be attributed to the higher H_2O_2 hydrogenation thus lower synthesis activity.

4.9 Conclusion

In conclusion, it has been shown that it is possible to prepare stable halide free Au-Pd catalysts on carbon and titania by physical grinding, a simple 'mix and heat' technique. Even though the catalysts had approximately six times higher activity towards the H_2O_2 hydrogenation pathway than previously reported impregnation catalysts the H_2O_2 productivities were similar in the case of Au-Pd/C or higher for oxide supported equivalents.

Characterisation of the materials showed there to be three types of particles present on the surface. The catalysts consistent of a significant amount of Au-Pd alloyed particles <5 nm. However, high H_2O_2 hydrogenation believed to be due to small (< 10 nm) monometallic Pd particles. The addition of halide in the form of Cl^- introduced by using $PdCl_2$ instead of $Pd(OAc)_2$ corresponds to a decreased H_2O_2 hydrogenation while retaining the catalysts H_2O_2 synthesis activity.

As well as small un-alloyed metal it was evident from STEM and XRD analysis that there was a significant amount of large metal particles (>10 nm) believed to be inactive for the H_2O_2 synthesis. Physical grinding could be improved by using this metal more efficiently, either by achieving control over the dispersion during heat treatment or using a lower content.

4.10 References

1. V. R. Choudhary, C. Samanta and P. Jana, *Applied Catalysis a-General*, 2007, **332**, 70-78.
2. V. R. Choudhary, Y. V. Ingole, C. Samanta and P. Jana, *Industrial & Engineering Chemistry Research*, 2007, **46**, 8566-8573.
3. V. R. Choudhary, C. Samanta and P. Jana, *Applied Catalysis A: General*, 2007, **317**, 234-243.
4. V. R. Choudhary, C. Samanta and P. Jana, *Industrial & Engineering Chemistry Research*, 2007, **46**, 3237-3242.
5. V. R. Choudhary and P. Jana, *Catalysis Communications*, 2008, **9**, 2371-2375.
6. S. Chinta and J. H. Lunsford, *Journal of Catalysis*, 2004, **225**, 249-255.
7. Y. F. Han and J. H. Lunsford, *Journal of Catalysis*, 2005, **230**, 313-316.
8. Q. S. Liu and J. H. Lunsford, *Journal of Catalysis*, 2006, **239**, 237-243.
9. N. E. Ntainjua, M. Piccinini, J. C. Pritchard, J. K. Edwards, A. F. Carley, J. A. Moulijn and G. J. Hutchings, *ChemSusChem*, 2009, **2**, 575-580.
10. E. Ntainjua N, M. Piccinini, J. C. Pritchard, Q. He, J. K. Edwards, A. F. Carley, J. A. Moulijn, C. J. Kiely and G. J. Hutchings, *ChemCatChem*, 2009, **1**, 479-484.
11. D. P. Dissanayake and J. H. Lunsford, *Journal of Catalysis*, 2002, **206**, 173-176.
12. D. P. Dissanayake and J. H. Lunsford, *Journal of Catalysis*, 2003, **214**, 113-120.
13. H. S. Oh, J. H. Yang, C. K. Costello, Y. M. Wang, S. R. Bare, H. H. Kung and M. C. Kung, *Journal of Catalysis*, 2002, **210**, 375-386.
14. H. H. Kung, M. C. Kung and C. K. Costello, *Journal of Catalysis*, 2003, **216**, 425-432.
15. F. Moreau, G. C. Bond and A. O. Taylor, *Journal of Catalysis*, 2005, **231**, 105-114.
16. J. K. Edwards, B. E. Solsona, P. Landon, A. F. Carley, A. Herzing, C. J. Kiely and G. J. Hutchings, *Journal of Catalysis*, 2005, **236**, 69-79.
17. C. Burda, X. Chen, R. Narayanan and M. A. El-Sayed, *Chemical Reviews*, 2005, **105**, 1025-1102.
18. Y. Wang and Y. Xia, *Nano Letters*, 2004, **4**, 2047-2050.
19. H. Guan, C. Shao, S. Wen, B. Chen, J. Gong and X. Yang, *Inorganic Chemistry Communications*, 2003, **6**, 1302-1303.
20. F. X. Redl, C. T. Black, G. C. Papaefthymiou, R. L. Sandstrom, M. Yin, H. Zeng, C. B. Murray and S. P. O'Brien, *Journal of the American Chemical Society*, 2004, **126**, 14583-14599.
21. R. Q. Song, A. W. Xu, B. Deng, Q. Li and G. Y. Chen, *Advanced Functional Materials*, 2007, **17**, 296-306.
22. C. J. Murphy, T. K. Sau, A. M. Gole, C. J. Orendorff, J. Gao, L. Gou, S. E. Hunyadi and T. Li, *The Journal of Physical Chemistry B*, 2005, **109**, 13857-13870.
23. L. Vovchenko, L. Matzui, M. Zakharenko, M. Babich and A. Brusilovetz, *Journal of Physics and Chemistry of Solids*, 2004, **65**, 171-175.
24. T. Ishida, N. Kinoshita, H. Okatsu, T. Akita, T. Takei and M. Haruta, *Angew Chem Int Ed Engl*, 2008, **47**, 9265-9268.
25. Y. Lin, K. A. Watson, M. J. Fallbach, S. Ghose, J. G. Smith Jr, D. M. Delozier, W. Cao, R. E. Crooks and J. W. Connell, *Acs Nano*, 2009, **3**, 871-884.
26. A. Obaid, A. Alyoubi, A. Samarkandy, S. Al-Thabaiti, S. Al-Juaid, A. El-Bellihi and E.-H. Deifallah, *Journal of Thermal Analysis and Calorimetry*, 2000, **61**, 985-994.
27. M. D. Judd, B. A. Plunkett and M. I. Pope, *Journal of thermal analysis*, 1974, **6**, 555-563.
28. K. C. Patil, G. V. Chandrashekhar, M. V. George and C. N. R. Rao, *Canadian Journal of Chemistry*, 1968, **46**, 257-265.
29. J. C. De Jesus, I. González, A. Quevedo and T. Puerta, *Journal of Molecular Catalysis A: Chemical*, 2005, **228**, 283-291.
30. S. D. Bakrania, G. K. Rathore and M. S. Wooldridge, *Journal of Thermal Analysis and Calorimetry*, 2009, **95**, 117-122.
31. P. K. Gallagher and M. E. Gross, *Journal of Thermal Analysis and Calorimetry*, 1986, **31**, 1231-1241.

32. S. V. Pol, V. G. Pol, I. Felner and A. Gedanken, *European Journal of Inorganic Chemistry*, 2007, **2007**, 2089-2096.
33. J. Leicester and M. J. Redman, *Journal of Applied Chemistry*, 1962, **12**, 357-366.
34. T. Arii and A. Kishi, *Thermochimica Acta*, 2003, **400**, 175-185.
35. J.-Y. Zhang, H. Esrom and I. W. Boyd, *Applied Surface Science*, 1996, **96–98**, 399-404.
36. M. Sankar, N. Dimitratos, P. J. Miedziak, P. P. Wells, C. J. Kiely and G. J. Hutchings, *Chemical Society Reviews*, 2012, **41**, 8099-8139.
37. J. Pritchard, L. Kesavan, M. Piccinini, Q. He, R. Tiruvalam, N. Dimitratos, J. A. Lopez-Sanchez, A. F. Carley, J. K. Edwards, C. J. Kiely and G. J. Hutchings, *Langmuir*, 2010, **26**, 16568-16577.
38. J. C. Pritchard, Cardiff University, 2012.
39. A. A. Herzing, M. Watanabe, J. K. Edwards, M. Conte, Z. R. Tang, G. J. Hutchings and C. J. Kiely, *Faraday Discussions*, 2008, **138**, 337-351.
40. J. K. Edwards, B. Solsona, E. N. N, A. F. Carley, A. A. Herzing, C. J. Kiely and G. J. Hutchings, *Science*, 2009, **323**, 1037-1041.
41. J. K. Edwards, E. Ntainjua N, A. F. Carley, A. A. Herzing, C. J. Kiely and G. J. Hutchings, *Angewandte Chemie International Edition*, 2009, **48**, 8512-8515.
42. J. K. Edwards, A. Thomas, A. F. Carley, A. A. Herzing, C. J. Kiely and G. J. Hutchings, *Green Chemistry*, 2008, **10**, 388-394.
43. J. K. Edwards, A. F. Carley, A. A. Herzing, C. J. Kiely and G. J. Hutchings, *Faraday Discussions*, 2008, **138**, 225-239.
44. N. N. Edwin, J. K. Edwards, A. F. Carley, J. A. Lopez-Sanchez, J. A. Moulijn, A. A. Herzing, C. J. Kiely and G. J. Hutchings, *Green Chemistry*, 2008, **10**, 1162-1169.
45. S. B. Ziemecki, G. A. Jones, D. G. Swartzfager, R. L. Harlow and J. Faber, *Journal of the American Chemical Society*, 1985, **107**, 4547-4548.
46. N. Krishnankutty, J. Li and M. Albert Vannice, *Applied Catalysis A: General*, 1998, **173**, 137-144.
47. M. Beck, M. Ellner and E. J. Mittemeijer, *Acta Materialia*, 2001, **49**, 985-993.
48. H. Okamoto and T. B. Massalski, *Bulletin of Alloy Phase Diagrams*, 1984, **5**, 378-379.
49. M. Haruta, N. Yamada, T. Kobayashi and S. Iijima, *Journal of Catalysis*, 1989, **115**, 301-309.
50. A. Maeland and T. B. Flanagan, *Canadian Journal of Physics*, 1964, **42**, 2364-2366.
51. www.cf.ac.uk/chemy/staffinfo/xpsaccess/database/tio2p25, Editon edn.
52. https://fscimage.fishersci.com/msds/17980.htm, Editon edn.

- CHAPTER FIVE -

Increasing Hydrogen Peroxide Concentration

5.1 Introduction – A Biphasic Solvent System for Direct H_2O_2 Synthesis

The direct synthesis of H_2O_2 is mainly carried out in water based solvents[1-9]. Water is not only desirable due to its non-toxicity but it is readily available and low cost compared with other solvents. Aqueous H_2O_2 can be directly used for a wide range of applications, including pulp/paper and textile bleaching, as a substitute for chlorine or chlorine-containing oxidants[10]. However a major drawback of using water is that H_2 and O_2, the reactant gases, have low solubility leading to low synthesis rates.[4, 6]

To overcome the gas solubility limitations of water various solvent systems have been investigated, including supercritical CO_2[11-16] and a biphasic mixture of water and fluorinated solvents as well as other halogenated hydrocarbon compounds[17-20], however low H_2O_2 synthesis rates were achieved.

The addition of water soluble organic additives proved more successful,[21] with low chain alcohol (methanol and ethanol) based solvents being extensively studied.[1-3, 22-25] The solubility of H_2 in alcohols is 4-5 times higher than in water, while that of O_2 may increase up to eightfold, as shown in Table 5.1, leading to higher H_2O_2 productivities[4].

Table 5.1 - H_2 and O_2 solubility's in low chain alcohols and water at 25°C[4]

Solvent	Solubility of H_2 (mg/l)(mM)	Solubility of O_2 (mg/L)(mM)
Water	1.62 (0.81)	40 (1.25)
Methanol	7.91 (3.96)	324 (10.12)
Ethanol	7.50 (3.75)	320 (10.0)

A miscible H_2O_2 alcohol solution would have direct applications in the chemical synthesis industry such as a source of oxygen for epoxidation reactions[26]. However, a major drawback of using a solvent that is highly miscible with H_2O_2 is catalysts active for the H_2O_2 synthesis are also active for its subsequent decomposition/hydrogenation reactions leading to low H_2 selectivities. The catalyst remains in close contact with the dissolved reagent gases and H_2O_2 during the direct synthesis reaction increasing the possibility of the subsequent hydrogenation and decomposition of H_2O_2 will occur. In fact, while H_2 combustion and H_2O_2 synthesis depend on H_2 and O_2 concentrations, subsequent hydrogenation and decomposition reactions also depend on H_2O_2 concentrations as shown in Figure 5.1.

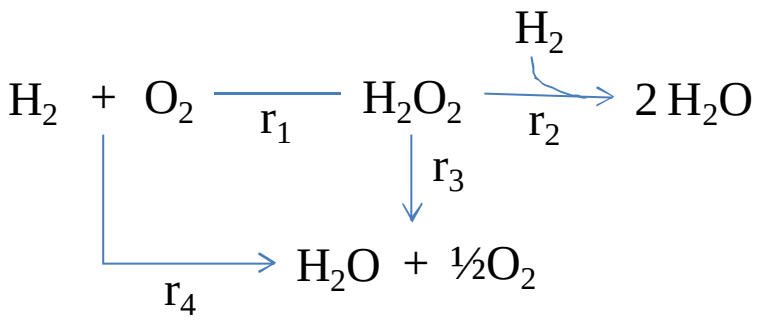

$$r_1 = k_1[H_2]^a[O_2]^b$$

$$r_2 = k_2[H_2]^c[H_2O_2]^d$$

$$r_3 = k_3[H_2O_2]^e$$

$$r_4 = k_4[H_2]^f[O_2]^g$$

Figure 5.1 - Hypothetical model of the kinetics involved in the direct H_2O_2 synthesis. H_2O_2 synthesis (r1) H_2O_2 hydrogenation (r2) H_2O_2 decomposition (r3) and H_2 combustion (r4).

Interestingly, Solvay® has postulated that using a biphasic solvent system consisting of a hydrophobic organic solvent and water, could present a way to produce high concentrations of H_2O_2. A schematic of the proposed system is shown in Figure 5.2.

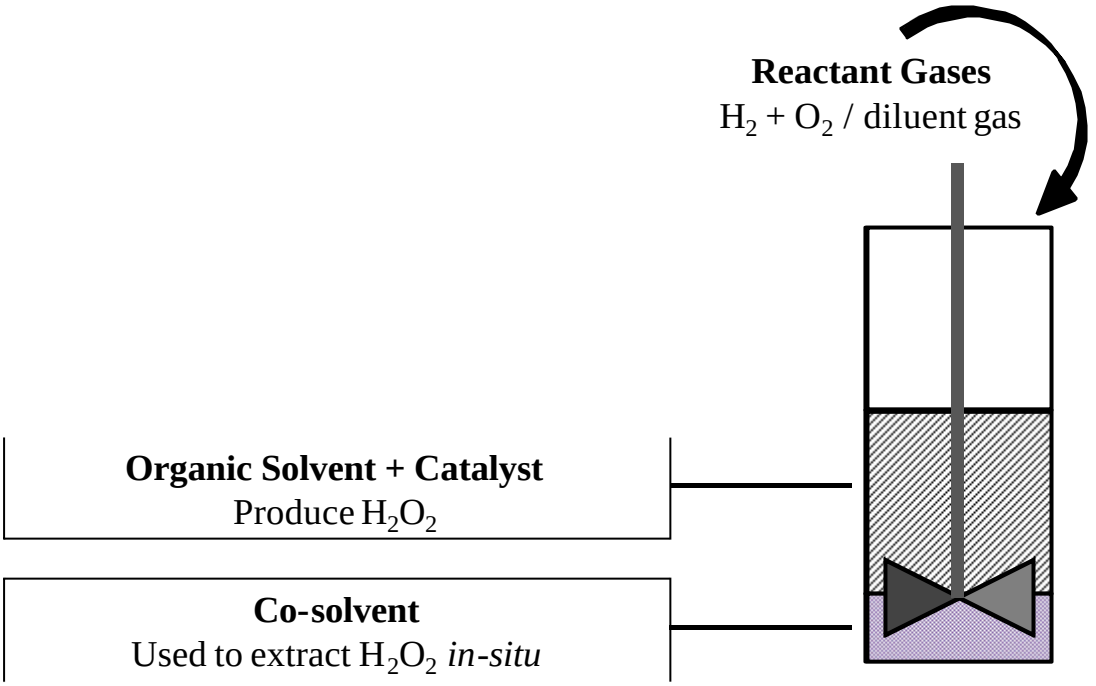

Figure 5.2 - A schematic highlighting the key features of the biphasic solvent system proposed.

In theory the catalyst would be held in the organic phase where the H_2O_2 would be formed. This is immediately extracted *in-situ* into the water phase due to the higher solubility of H_2O_2 in water than in the alcohol, therefore avoiding hydrogenation/decomposition. This allows a smaller target yield of H_2O_2. For example, if a solvent composition of 8 g organic solvent and 0.5 g immiscible co-solvent is used, then only 0.0425 g of H_2O_2 are required for 8.5 wt% H_2O_2 to be extracted from the immiscible phase. Whereas, if the same mass of H_2O_2 was produced in a one phase system (8.5 g) a solution of only 0.5 wt% H_2O_2 will be obtained.

In this chapter, the development of an innovative approach for the direct H_2O_2 synthesis based on a biphasic water/alcohol solvent system has been investigated in detail. The potential of such a system has been examined with a goal of producing a H_2O_2 concentration

of 3-8 wt%, which would be required for the direct synthesis to be industrially viable. Initial results were obtained in collaboration with a colleague, Marco Piccinini.

Note – Au-Pd = 2.5 %Au- 2.5 %Pd. All catalysts in this chapter have been prepared by impregnation and calcined at 400 ^{o}C, full procedures are described in Chapter Two. The reaction conditions utilised have been highlighted.

5.2 Choice of a Suitable Organic Solvent

When selecting a suitable candidate for the organic phase two key features are required, an ability to produce H_2O_2 in the solvent, and a low H_2O solubility. In order to narrow down the search for a suitable organic solvent only alcohols have been considered. However, in future further investigation into the solvent will be required. It should be noted water has been selected as the co-solvent due to it being low cost, readily available as well as having low H_2/O_2 solubility.

5.2.1 Direct H_2O_2 Synthesis

The ability of alcohols (no co-solvent) to produce H_2O_2 by the direct synthesis has been evaluated by evaluating their activity under H_2O_2 reaction conditions highlighted* using an impregnation Au-Pd/C catalyst calcined at 400^{o}C, Table 5.2.

Table 5.2 – H_2O_2 productivity in various alcohols as solvent

Solvent	**H_2O_2 productivity* ($mol_{H2O2}kg_{cat}^{-1}h^{-1}$)**	**[H_2O_2] (wt%)**
Methanol	50.1	0.094
Propan-1-ol	31.8	0.063
Butan-1-ol	26.1	0.030
Hexan-1-ol	4.4	0.008
Octan-1-ol	1.36	0.003
Decan-1-ol	0.84	0.0015

***Reaction conditions:** IMP-Au-Pd/C (10 mg), 5% H_2/CO_2 (420 psi), 25% O_2/CO_2 (160psi), 8.5 g solvent, 25 ^{o}C, 30 minutes.

Low concentrations of H_2O_2 have been produced regardless of the alcohol employed as the solvent. The activity decreases with increasing carbon chain length. This may be due to higher viscosity and surface tension as the carbon chain length increases. The success of the solvent being able to produce H_2O_2 strongly depends on the overall rate of mass transfer of gaseous reactants to the catalyst surface, highlighted in Figure 5.3.

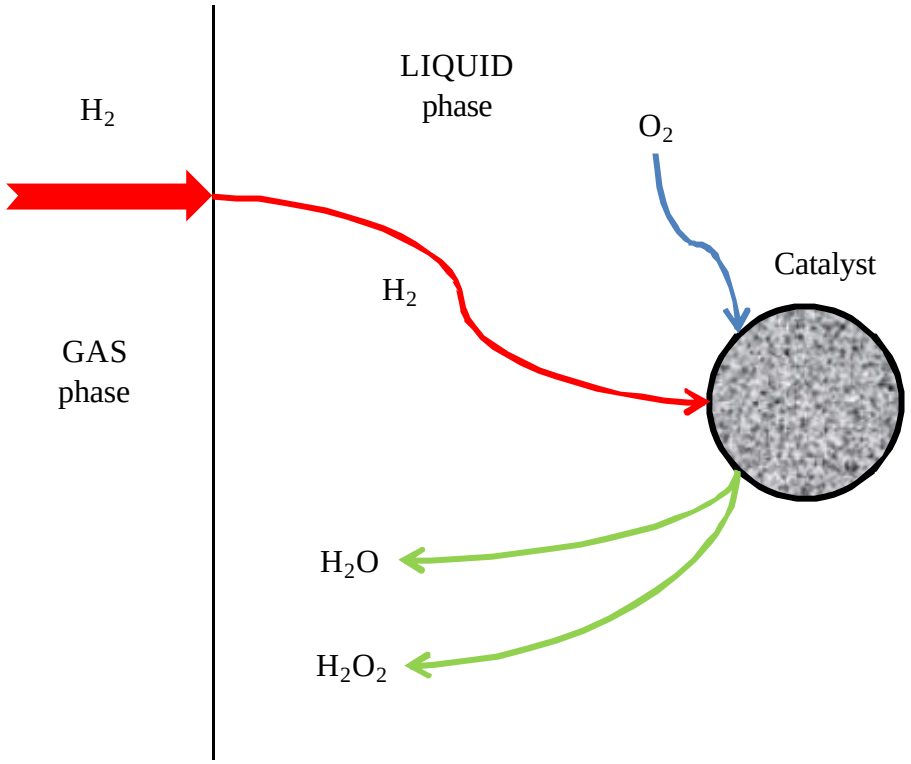

Figure 5.3 - Outline of the pathway of the reagent gas to the liquid phase then the catalyst surface to produce H_2O_2[27].

Here two mass transfer resistances are highlighted, dissolution of gases into the liquid phase and reactant transport in the liquid to the catalyst surface. Unfortunately it was not possible to measure solubility using the current reagent gases, 5 % H_2/CO_2 and 25 % O_2/CO_2, as the dissolution of H_2 and O_2 has to compete with the dissolution of CO_2 into the solvent. However, Francesconi *et al.* [28] and Wainwright *et al.*[29] have shown that hydrogen solubility in the C_{1-4} n-primary alcohol series increases with carbon chain length and therefore it is reasonable to expect hydrogen to be more miscible in decan-1-ol rather than methanol. Factors that will increase the mass transfer include: increasing the solubility of H_2 and O_2 by increasing reaction pressure; using solvents that have higher gas solubility; and using solvents with lower viscosity and surface tension.

5.2.2 H_2O Solubility

Another important consideration when selecting the organic solvent is the necessity for it to have low H_2O solubility in order to have a two phase system. Table 5.2 shows that methanol is the best solvent for the direct H_2O_2 synthesis. However, due to it being completely miscible with water, it is not a suitable solvent for this investigation. Higher carbon chain alcohols ($>C_6$) have low water solubility and the addition of excess water creates a two phase system. The saturation point of the alcohols has been determined experimentally by Karl Fischer titration with the results shown in Table 5.3.

Table 5.3 - Solubility of water in high chain alcohols

Solvent	**H_2O solubility (g_{H2O} dm^{-3})**
Hexan-1-ol	77
Octan-1-ol	44
Decan-1-ol	39

As chain length increases the H_2O solubility decreases, with decan-1-ol having the lowest saturation point. In this case it is desirable for a suitable industrial solvent to be hydrophobic so the concentration of alcohol in the final H_2O-H_2O_2 solution is minimal to decrease costs relating to purification through distillation. Hence, the only suitable candidate is decan-1-ol which was chosen as the ideal solvent candidate

It should be noted that although dodecan-1-ol has a lower saturation point, its melting point of 24 ^oC mean the direct H_2O_2 synthesis reaction would have to be run at higher temperatures than room temperature. H_2O_2 decomposition is much more facile at higher temperatures therefore this solvent was rendered unsuitable.

5.2.3 Stability of the Solvent

In order to ascertain the possible reactivity of decan-1-ol with the H_2O_2 synthesised during direct synthesis testing conditions, the working solution after reaction, with and without catalyst in the presence of H_2 and O_2, was filtered and then analyzed by 1H-NMR (spectra were recorded at room temperature on a Bruker DPX 500MHz Ultra-Shield NMR spectrometer (1H 500.13 MHz)), and compared to reference spectra ascertained from unused decan-1-ol in Figure 5.4. No differences were observed, indicating the decan-1-ol is stable towards the reaction conditions employed.

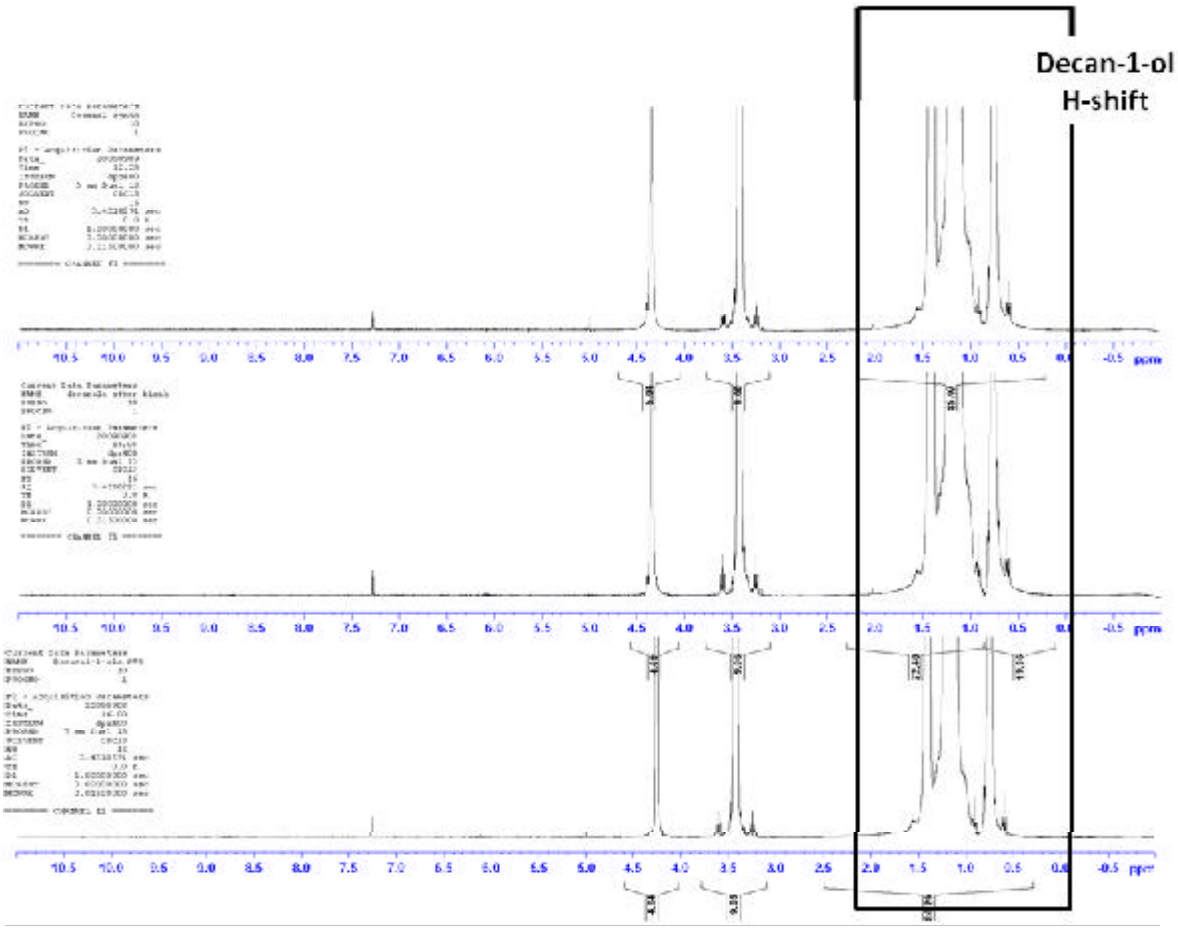

Figure 5.4 - ^{1}H-NMR spectra of decan-1-ol after a standard reaction with catalyst (A) and without catalyst (B), compared to un-used decan-1-ol (C). The H-shift due to decan-1-ol has been highlighted.

5.3 Determining the H_2O_2 Concentration in a Biphasic Solvent System

The separation of water from the organic solvent proved very time consuming and when less than ~0.3 g water in 8 g decan-1-ol was used separation was complicated as the organic solvent was saturated with water. Therefore, in all the cases reported in this chapter the overall H_2O_2 amount was determined by direct titration of the whole emulsion (decan-1-ol/H_2O) with acidified $Ce(SO_4)_2$ solution (*ca.*$8x10^{-3}$M), using ferroin as indicator. In order to determine the error when using this method compared to separation, three different experiments were performed with increasing masses of water. In each case, H_2O_2 concentration was ascertained using a direct titration of the whole emulsion and a titration of the separated water phase, the results are shown in Figure 5.5.

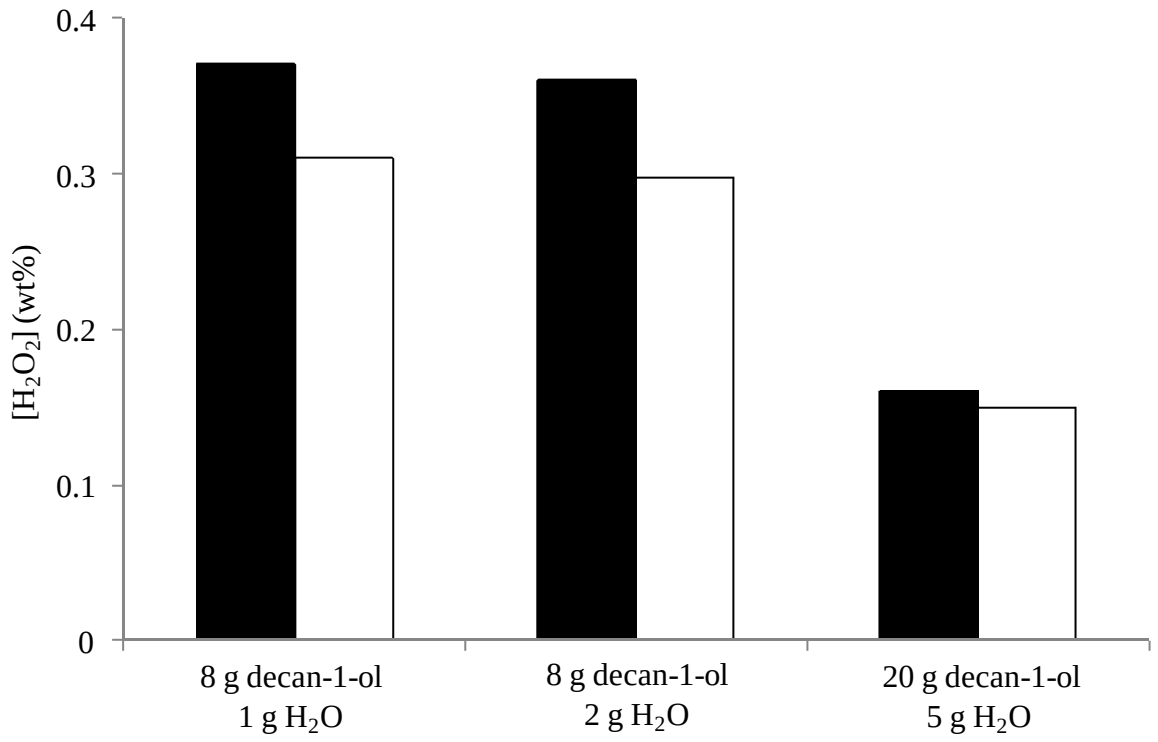

Figure 5.5 - Evaluation of the error of H_2O_2 determination; H_2O_2 concentration (■) calculated from titration of whole emulsion, (□) determined from water phase after separation.

Reaction conditions: IMP-Au-Pd/C (10 mg), 5% H_2/CO_2 (420 psi), 25% O_2/CO_2 (160psi), X g solvent, 1200 rpm, 25 ^oC, 30 minutes.

The error due to the over-estimation on the final concentration with titration of the whole emulsion is due to it not being a completely distinct two phase system as the decan-1-ol will contain 39 g_{H2O} dm^{-3}, therefore retain small amounts of H_2O_2. The error varies between ~20 % discrepancy for the first two experiments and ~6 % when 5 g water is added.

Although the assessment of H_2O_2 in the water phase is a more accurate way of determining H_2O_2 concentrations, the addition of more leads to less concentrated H_2O_2 solutions. In the following experiments the smallest amount of water will be added to the organic solvent to produce the highest H_2O_2 concentration possible. The influence of the addition of water has been studied in more detail in section 5.5.1. It is impossible to separate the 2 distinct phases if less than 39 g_{H2O} dm^{-3} is used

The H_2O_2 concentrations throughout this chapter will be expressed as $g_{H2O2}kg_{H2O}^{-1}$ (division by 10 is required to determine the H_2O_2 wt%). The value obtained represents the theoretical H_2O_2 concentration in water if neither H_2O nor H_2O_2 were soluble in the decan-1-ol. The H_2O_2 productivity ($mol_{H2O2}kg_{cat}^{-1}h^{-1}$) has also been provided where necessary to highlight trends.

5.4 Choice of a Suitable Catalyst

The choice of the catalyst is vital to the production of H_2O_2 and as previously recorded in this thesis many preparation methods have been used to produce supported Au-Pd catalysts. However within this chapter only Au-Pd catalysts prepared by impregnation are investigated. The supports have been varied due to their varying hydrophobicity. This was done to control the phase the catalyst was present in, to determine whether the presence in the aqueous or organic phase affected the H_2O_2 yield.

.

5.4.1 Direct H_2O_2 Synthesis

The activity of supported Au-Pd catalysts prepared by impregnation of different supports were evaluated for the direct synthesis of H_2O_2 in the new bi-phase solvent system described, the results are shown in Figure 5.6.

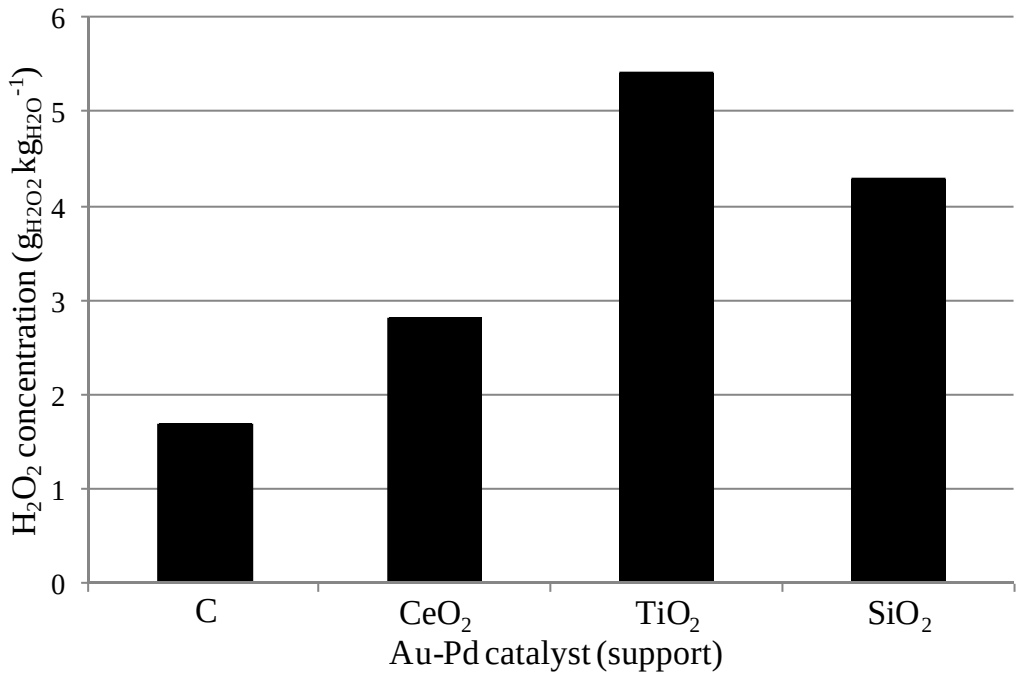

Figure 5.6 - H_2O_2 concentration produced in the biphasic solvent system described, using Au-Pd supported catalysts prepared by impregnation

Reaction conditions: IMP-Au-Pd/X (10 mg), 5 %H_2/CO_2 (420 psi), 25 %O_2/CO_2 (160 psi), solvent (8.17 g decan-1-ol, 0.33 g H_2O), 1200 rpm, 25 ^oC, 30 min.

Interestingly, the TiO_2 supported Au-Pd catalyst displayed the highest productivity in comparison to the other supported catalysts, with carbon having the lowest productivity. This is surprising as Au-Pd/TiO_2 has the lowest productivity, 64 $mol_{H2O2}kg_{cat}^{-1}h^{-1}$, and Au-Pd/C displays much higher activity, 110 $mol_{H2O2}kg_{cat}^{-1}h^{-1}$, in the standard water-methanol solvent system[22]. To investigate further the hydrogenation activities of the catalysts were evaluated in order to investigate whether H_2O_2 destruction was playing a vital role in the biphasic solvent system.

5.4.2 H_2O_2 Hydrogenation.

The activities of impregnation Au-Pd catalysts on various supports have been evaluated for the hydrogenation of H_2O_2 in the new biphasic solvent system. The results are given in Figure 5.7.

Note - The water phase was substituted with a 4 wt% H_2O_2 solution, the accuracy of this measurement being important because any small error in the titration would result in an unacceptable error in the final result. The reactions were run under hydrogenation conditions, 420 psi 5% H_2 /CO_2, full reaction conditions are highlighted*. The results have been expressed as the percent of H_2O_2 destroyed during 30 minutes.

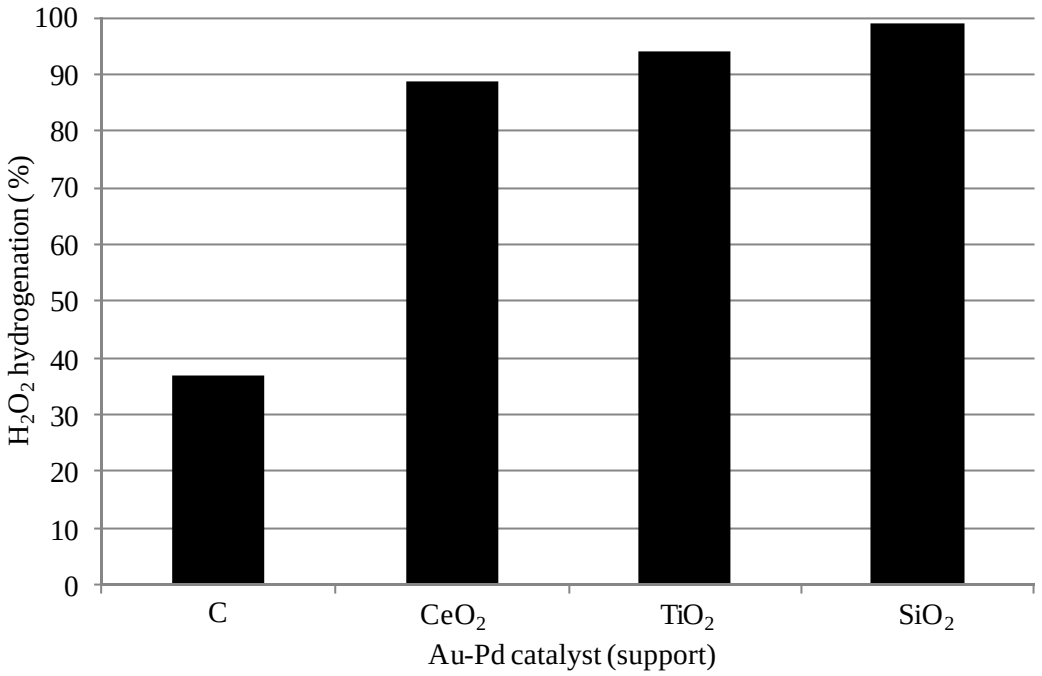

Figure 5.7 - % H_2O_2 destroyed by hydrogenation in the biphasic solvent system described, using impregnation Au-Pd supported catalysts.

***Reaction conditions:** IMP-Au-Pd/X (10 mg), 5% H_2/CO_2 (420 psi), solvent (8.17g decan-1-ol, 0.33 g 4 wt% H_2O_2), 1200 rpm, 25 ^oC, 30 min.

All the Au-Pd supported catalysts examined had extremely high hydrogenation activities, this is a major problem of this system which wasn't expected and in the future needs addressing. However, the Au-Pd/C catalyst has the lowest activity, whereas the Au-Pd oxide supported catalysts destroyed nearly all of the H_2O_2 present in the reaction medium.

5.4.3 Discussion

It is likely the direct synthesis of H_2O_2 results (productivity and hydrogenation) in the bi-phasic solvent system is due to varying amounts of interaction between the catalyst and the aqueous solvent. It is possible that if the catalyst is in the same phase as the H_2O_2 it is much more likely to hydrogenate the H_2O_2 In order to determine the phase in which the catalyst resides, the Au-Pd supported catalysts were added to separate vials which contained a mixture of decan-1-ol and water,. These results are shown in Figure 5.8.

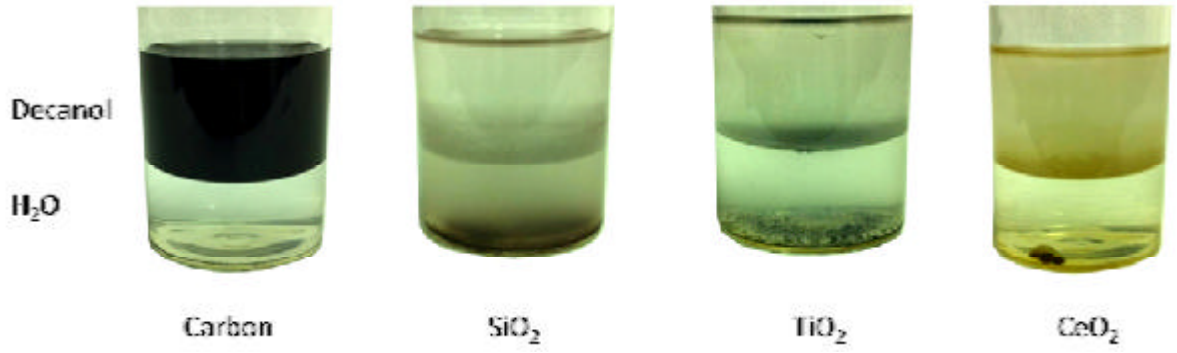

Figure 5.8 – Simple vial experiment to indicate which phase the catalyst resides.

The images in Figure 5.8 clearly demonstrate that the AuPd/carbon catalyst is the only material which resides entirely in the decan-1-ol phase; whereas the oxide supported catalysts have differing levels of interaction in the water phase. The Au-Pd/SiO_2 catalyst seems to be considerably hydrophilic as a large majority of the catalyst being held in the water phase. As a result of its hydrophilic nature SiO_2 has been used by scientists as it maintains a high water content, this enables the performance of proton exchange membrane fuel cells to be improved. This is achieved by SiO_2 addition improving the hydrophillicity, therefore conductivity of the cathode and preventing dehydration at high temperatures.[30, 31]

For the TiO_2 and CeO_2 supported catalysts it is more difficult to define their hydrophilicity; finely dispersed particles appeared to be retained in both the decan-1-ol and water phase. In the case of the ceria particles, in the water phase aggregation occurred forming a single large particle. The varying levels of water interaction may be explained by varying amounts of oxygen vacancies on the surface, which are favourable for water adsorption. In order to

improve the hydrophilicity a greater number of oxygen vacancies can be introduced by irradiation with UV light.[32] Comparing these results (figure 5.7) to the catalytic activities (figure 5.5 and figure 5.6) indicates that interaction between the catalyst support and water is crucial for producing higher H_2O_2 synthesis and hydrogenation activities.

However, Au-Pd/C is the only one that resides in the alcohol phase and also shows much reduced H_2O_2 hydrogenation activity, so was used in further studies. The H_2O_2 hydrogenation activity observed could be due to the catalyst being forced into the aqueous phase under the vigorous stirring conditions employed (1200rpm) when catalysts are evaluated under standard reaction conditions.

5.5 The Effect of Reaction Variables on H_2O_2 Concentration

In order for the biphasic solvent system to compete with the current commercially operated indirect process it is essential that a 3-8 wt% H_2O_2 solution can be obtained with high H_2 selectivity. Piccinini *et al.*[2, 3] have previously shown the performance of a catalyst, using a one phase solvent, can be significantly enhanced by understanding the effect of the key reaction parameters and by operating under optimised conditions.

In order to produce the highest H_2O_2 concentration possible in the decan-1-ol/water solvent system described the effect of key reaction variables have been investigated. An impregnation Au-Pd/C catalyst has been utilised with the decan-1-ol/H_2O ratio, solvent loading, catalyst mass, reaction time, stirring speed and pressure varied.

5.5.1 The Effect of Decan-1-ol/H_2O Ratio

The effect of decan-1-ol/water ratio on H_2O_2 synthesis was studied in detail by changing the ratio of decan-1-ol to water keeping the total solvent mass fixed at 8.5g, the results are shown in Figure 5.9.

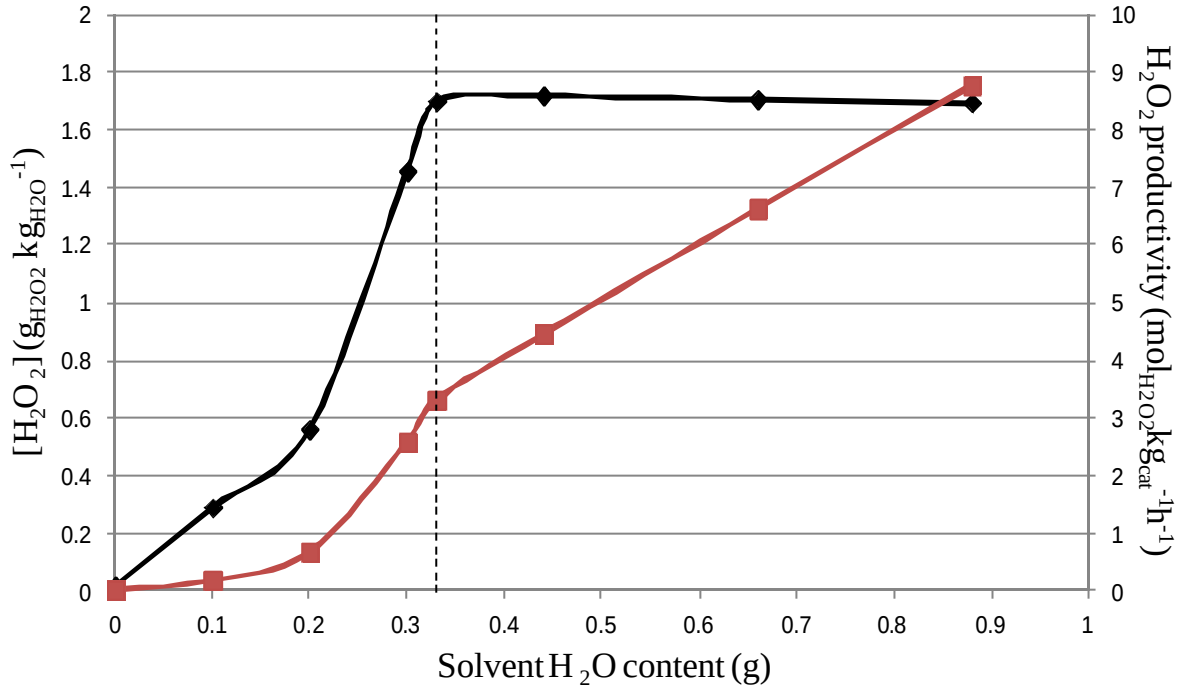

Figure 5.9 - H_2O_2 concentration and productivity as a function of water content. ◆ H_2O_2 concentration, ■ H_2O_2 productivity

Reaction conditions: IMP-Au-Pd/C (10 mg), 5% H_2/CO_2 (420 psi), 25% O_2/CO_2 (160psi), 8.5g solvent (8.5-X g decan-1-ol, X g H_2O), 1200 rpm, 25 ^oC, 30 min.

The greatest H_2O_2 concentration was achieved when the decan-1-ol was saturated (3.9 g_{H2O} dm^{-3}). The saturation point of decan-1-ol is shown by the dotted line. On the left of this line the solvent is in one phase with the water completely dissolved in the decan-1-ol. On the right a two phase system exists with a greater excess of water as shown.

Interestingly, water was found to be extremely beneficial to the productivity of H_2O_2. This is in agreement with the theory behind the biphasic solvent system, with the water acting as an

in-situ extractor. As the water mass is increased over the saturation point the H_2O_2 productivity increases almost linearly. This could be an indication of the catalyst mainly remaining in the decan-1-ol phase. The slow decrease in rate could be due to the amount of decan-1-ol decreasing meaning the overall amount of reagent gases, H_2 and O_2, dissolved in the solution will be less.

However, interaction between the catalyst Au-Pd/C and water cannot be ruled out. This would explain both the hydrogenation activity observed earlier in Figure 5.7 and the increase in H_2O_2 productivity of *ca.* 10 times when only 0.33 g of water in Figure 5.9. The addition of water to a methanol solvent system has previously been shown to improve direct H_2O_2 synthesis activities.[2, 3] Water addition has also been shown to promote other reactions such as CO oxidation. Date *et al.*[33] developed a reactor system to probe water concentration from 0.1 to 6000 ppm, clearly demonstrating the promotional effect of water on various supported catalysts. Very low moisture concentrations (~3 ppm) were shown to have rather large effects on activity. Goodman *et al.*[34] subsequently postulated that the promotional effects of water on CO oxidation were due to its effect on molecular oxygen adsorption and activation. Further study found that surface hydroxyl species may play the same promotional role as adsorbed water.

5.5.2 The Effect of Solvent Mass and Catalyst Loading

The effects of solvent mass and catalyst loading have been investigated in order to produce the maximum H_2O_2 concentration with a Au-Pd/C catalyst. Firstly, the mass of saturated decan-1-ol was varied keeping the catalyst loading at 10 mg, the results obtained are shown in Figure 5.10.

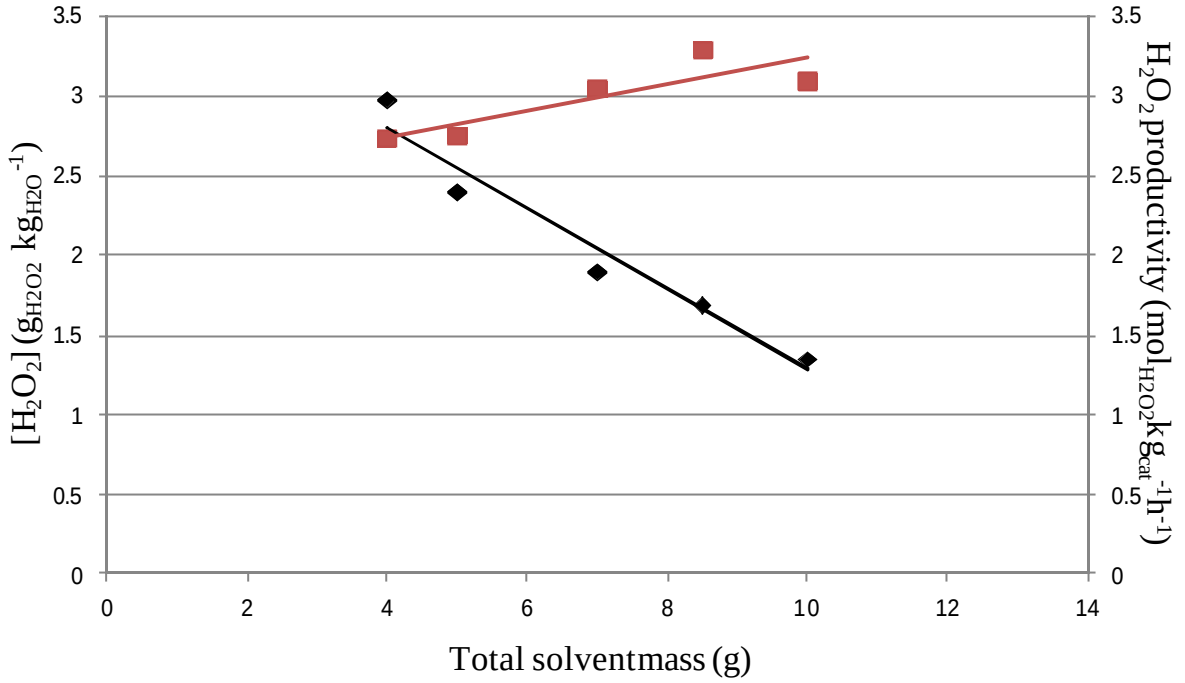

Figure 5.10 - H_2O_2 concentration and productivity as a function of solvent mass. ◆ H_2O_2 concentration, ■ H_2O_2 productivity

Reaction conditions: IMP-Au-Pd/C (10 mg), 5% H_2/CO_2 (420 psi), 25% O_2/CO_2 (160psi), X g solvent, 1200 rpm, 25 ^oC, 30 min.

The results show how it is possible to enhance the concentration of H_2O_2 by decreasing the solvent mass. Similar masses of H_2O_2 are produced by the horizontal trend of H_2O_2 productivity with solvent mass. This indicates that there are enough reagent gases dissolved in the decan-1-ol even when 4 g of solvent are used to not put kinetic restrictions on the system i.e. there is a high enough concentration of reagent in the solvent to allow the catalyst to work to its full capacity. However, the H_2O_2 is dissolved in a lower mass of H_2O hence the higher H_2O_2 concentration as the solvent mass is decreased.

Although it is theoretically possible to further decrease the amount of solvent, 4 g are the minimum that allows adequate stirring with the type of autoclaves used. Therefore the mass of catalyst loading was varied keeping the solvent mass constant at 4 g saturated decan-1-ol. The results are shown in Figure 5.11.

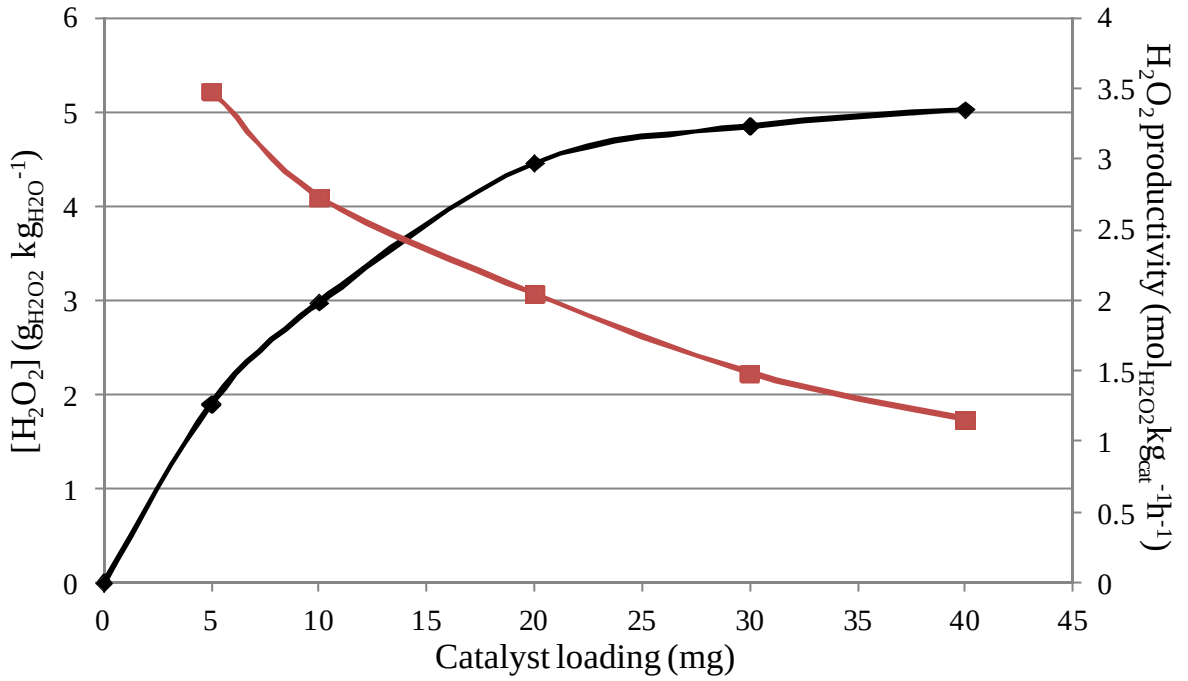

Figure 5.11 - H_2O_2 concentration and productivity as a function of catalyst loading. ◆ H_2O_2 concentration, ■ H_2O_2 productivity

Reaction conditions: IMP-Au-Pd/C (X mg), 5% H_2/CO_2 (420 psi), 25% O_2/CO_2 (160psi), solvent (3.84 g decan-1-ol, 0.16 g H_2O), 1200 rpm, 25 ^oC, 30 min.

Figure 5.11 shows that as the catalyst loading is increased, H_2O_2 concentration also increases. However, there is a decrease in H_2O_2 productivity which could be due to two reasons;

1) The decan-1-ol not being able to retain the catalyst forcing a higher concentration of catalyst into the water phase, increasing the hydrogenation contribution;

2) Not enough reagent gases being provided to the catalyst surface for it to work at maximum efficiency (kinetic restraints).

However, from 20- 40 mg the concentration of H_2O_2 is at its highest and remains similar as the catalyst loading is increased; therefore a catalyst: solvent ratio of >5 $mg_{cat}g_{solvent}^{-1}$ has been used in subsequent reactions.

5.5.3 The Effect of Reaction Time

The biphasic system should decrease/remove the contribution from the subsequent hydrogenation/decomposition reactions leading to higher H_2O_2 concentrations, so the H_2O_2 should increase linearly as a function of reaction time; this has been investigated and the results shown in Figure 5.12.

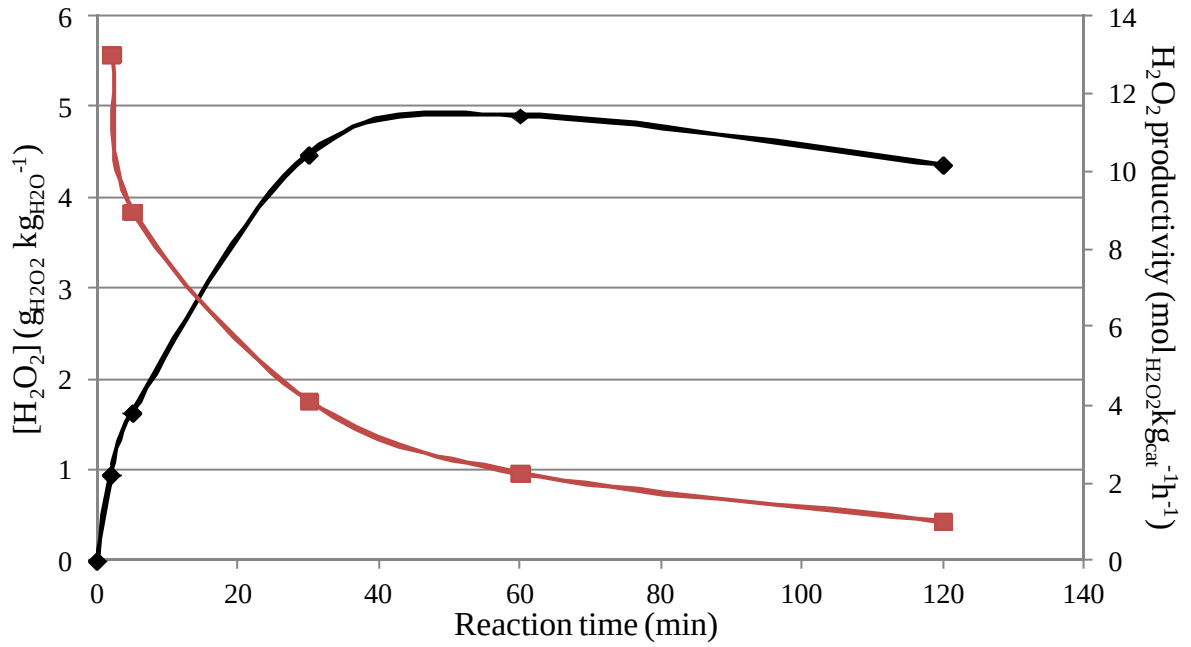

Figure 5.12 - H_2O_2 concentration and productivity as a function of reaction time. ◆ H_2O_2 concentration, ■ H_2O_2 productivity

Reaction conditions: IMP-Au-Pd/C (10 mg), 5% H_2/CO_2 (420 psi), 25% O_2/CO_2 (160psi), solvent (3.84 g decan-1-ol, 0.16 g H_2O), 1200 rpm, 25 ^oC, X min.

As time increases, up to 60 minutes, the concentration of peroxide in the reaction mixture also increases. The higher H_2O_2 concentration leads to faster H_2O_2 decomposition rates. Therefore, at higher residence time the hydrogenation rate is faster than synthesis leading to a net consumption of the H_2O_2. Also as time increases H_2 and O_2 concentration in the solvent decreases leading to slower H_2O_2 synthesis rates, so the H_2O_2 decomposition pathway becomes prevalent.

5.5.4 The Effect of Stirring Speed

The effect of stirring speed was evaluated whilst keeping all other variables unchanged, Figure 5.13.

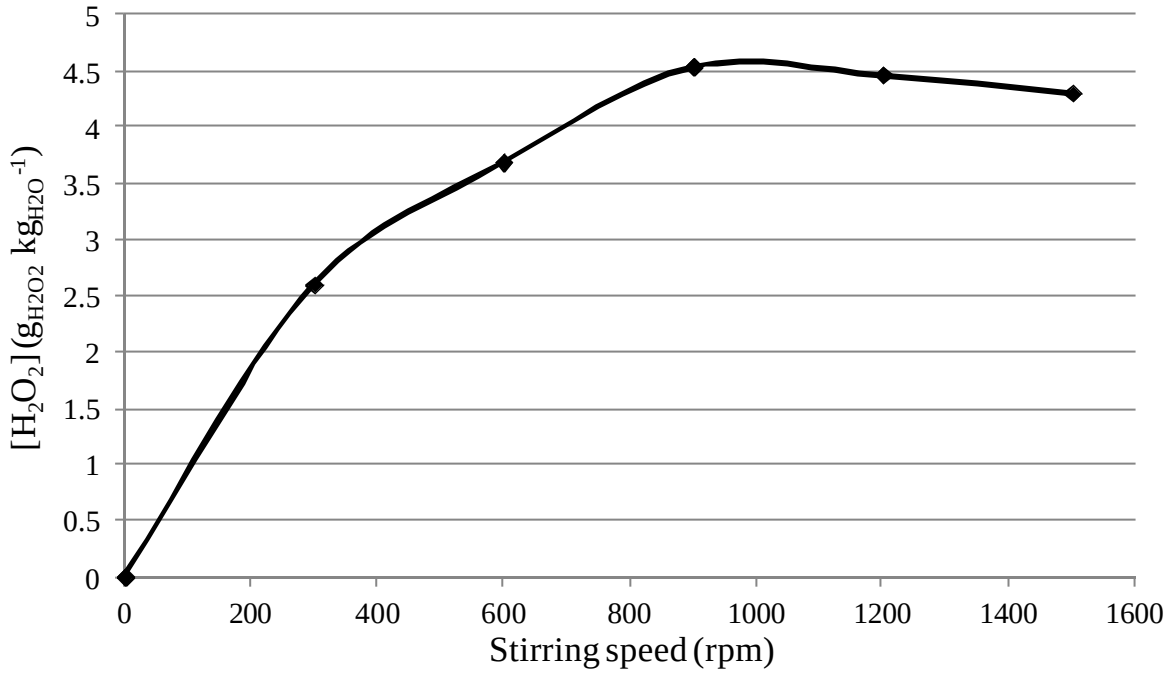

Figure 5.13 - H_2O_2 concentration as a function of stirring speed.

Reaction conditions: IMP-Au-Pd/C (10 mg), 5% H_2/CO_2 (420 psi), 25% O_2/CO_2 (160psi), solvent (3.84 g decan-1-ol, 0.16 g H_2O), X rpm, 25 ^oC, 30 min.

The maximum point most H_2O_2 was formed when a stirring speed of 900 – 1200 rpm, was employed. Below this point it can be considered the system is under kinetic constraints, i.e. dissolution of the reagent gases is low. Increasing above this stirring speed should be beneficial to enhancing the H_2O_2 concentration as a greater quantity of H_2 and O_2 should be in solution, instead a decrease in the H_2O_2 concentration is observed. This lower concentration could be due to higher H_2O_2 hydrogenation at higher stirring speeds due to increased H_2 in solution. Alternatively the intensity of the stirring could inhibit the H_2O_2 being removed from the alcohol phase.

Another explanation could be non-heterogeneous stirring, forcing the catalyst onto the reactor wall decreasing the active component in the decan-1-ol and so decreasing the H_2O_2 synthesis rate. High stirring speeds could also be responsible for forcing the catalyst into the aqueous phase increasing the hydrogenation / decomposition rate whilst decreasing the synthesis rate.

5.5.5 The Effect of Pressure

The effect of the total pressure was then evaluated keeping all the other reaction variables constant, Figure 5.14.

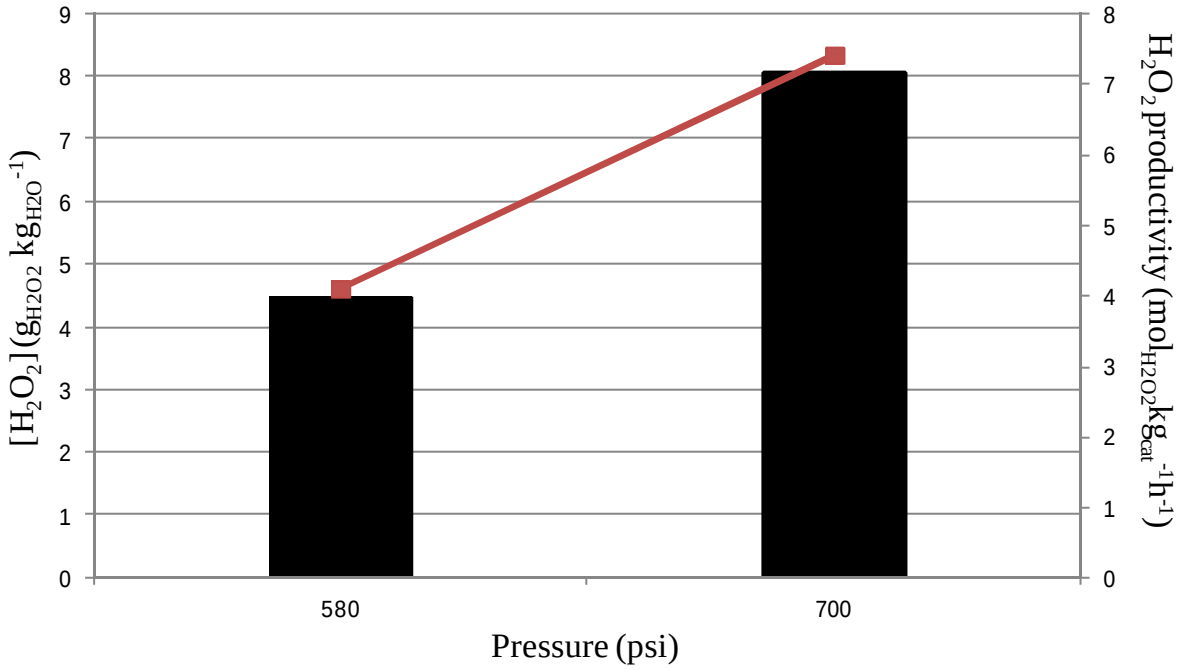

Figure 5.14 - H_2O_2 concentration and productivity as a function of pressure. ■ H_2O_2 concentration, ■ H_2O_2 productivity

Reaction conditions: IMP-Au-Pd/C (10 mg), 5% H_2/CO_2 + 25% O_2/CO_2 (X psi - H_2/O_2 = 0.525), solvent (3.84 g decan-1-ol, 0.16 g H_2O), X rpm, 25 ^oC, 30 min.

As expected, an enhancement in H_2O_2 concentration and productivity is observed with the pressure increase. At first sight the relationship observed could be considered to be

consistent with Henry's law, the rate of solute gas uptake by the liquid phase is related to the rate of change in pressure with the mole fraction of gas in solution.

$$p = k_H c$$

p = partial pressure of the gas above the solution

c = concentration of the gas in solution

k_H = Henry's law constant.

Therefore as the rate of H_2O_2 synthesis is controlled by the amount of H_2 and/or O_2 available for the reaction in solution, the rate equation can be written as;

$$r_{H2O2} = k_1 . pH_2^{nH2} . pO_2^{nO2}$$

r_{H2O2} = the rate of H_2O_2 synthesis

And the rate of hydrogenation can be written as follows;

$$r_{H2O} = k_2 . pH_2^{aH2} . [H_2O_2]^b$$

r_{H2O} = the rate of H_2O_2 hydrogenation

Therefore it can be postulated that, although increasing the pressure increases the rate of synthesis by increasing the concentration of reagents in solution. It will also increase the rate of H_2O_2 hydrogenation and decomposition as the concentration of hydrogen peroxide increases.

However, in this case the intercept of the line is just below zero. This could be due to higher solubility of CO_2 in the solvent, at 700 psi, having a positive effect on the H_2O_2 concentration. Hutchings *et al.*[1] have previously found that using CO_2 as the diluent gas increases peroxide stability attributed to it forming carbonic acid in solution. Unfortunately, the pressure could not be increased further due to the pressure of the 5 %H_2 / CO_2 and 25 %O_2 / CO_2 cylinders supplied by BOC which are restricted causing CO_2 liquefaction at room temperature at ~ 65 bar.

5.5.6 Discussion

Based on the set of reactions carried out it is possible to define a new set of reaction parameters, Table 5.4, required to produce the highest possible H_2O_2 concentration using a Au-Pd/C catalyst in the new biphasic solvent system described. Two parameters are missing and have not been examined in this study.

Firstly, the H_2 / O_2 ratio was not investigated; a ratio of 1 has previously been shown to give the highest H_2O_2 productivity[2, 3]. A ratio of 0.525 was used in this chapter where dissociation of H_2 is found to be the rate limiting step.

Secondly, the temperature, which was kept at room temperature (25 ^oC) throughout this study, any attempt to lower the temperature resulted in the decan-1-ol freezing and increasing the temperature is believed to be detrimental, due to higher H_2O_2 decomposition rates.

Table 5.4 - Optimum conditions to produce highest H_2O_2 concentration

Conditions	**Au-Pd/C**
Solvent decan-1-ol (wt% H_2O)	0.39
Solvent mass (g)	4
Catalyst loading (mg)	>20
Catalyst : solvent ratio ($mg_{cat}g_{sol}^{-1}$)	>5
Time (min)	30-60
Stirring speed (rpm)	1200
Total pressure (psi)	700

Using the optimum conditions in, Table 5.4, a H_2O_2 concentration of 8 $g_{H2O2}kg_{H2O}^{-1}$ (0.8 wt%) was achieved, thus highlighting the potential of using a biphasic system. The highest concentration achieved previously in the methanol-water solvent system is *ca.* 0.7 wt% using a Au-Pd/acid washed carbon supported catalyst that showed no H_2O_2 hydrogenation activity.

H_2O addition (section 5.5.1) indicates that the solvent system could be working as outlined in the theory; however it also indicates a definite interaction between catalyst and the water, which accounts for the hydrogenation seen in Figure 5.7. Varying the parameter using saturated decan-1-ol increased the concentration from 1.7 (0.17 wt%) to 8 $g_{H2O2}kg_{H2O}^{-1}$ (0.8 wt%).

The catalyst loading to solvent mass ratio has been highlighted in Table 5.4 and may be a crucial feature when looking to scale up the reaction. The retention of the catalyst in the organic solvent not only depends on the hydrophobic nature of the catalyst but also on the mass of catalyst the organic layer can hold under experimental procedures.

An important observation is a rise in the pressure by 20 % accounts for the H_2O_2 concentration approximately doubling. One of the simplest ideas to increase the H_2O_2 concentration further would be to increase the pressure. However, due to cylinder pressure restrictions this was not possible. High pressure is also unsuitable for an industrial process. Although it may be of interest at a later date to investigate the potential of the system further.

The key issue appears to be the H_2O_2 hydrogenation / decomposition due to catalyst coming into contact with the H_2O_2 solution which is limiting the biphasic system. To prevent this more hydrophobic solvents' and catalysts need to be investigated. Using a different solvent may be required in order to lower the reaction temperature which will allow H_2O_2 hydrogenation/decomposition to be decreased. Slow transfer of reagents through the solvent to the active surface in order to produce H_2O_2 is also paramount to the success of the system and will need investigating in future.

5.6 Increasing H_2O_2 Concentration Using Ceria Supported Catalysts

Ceria has been identified as an alternative support to carbon for producing active Au-Pd catalysts for the direct synthesis of H_2O_2. Section 5.4.1 indicates that Au-Pd/CeO_2 produces a higher concentration than Au-Pd/C and the catalyst mostly resides in the decan-1-ol phase. Solvay rendered TiO_2 unsuitable due to the formation of [Ti-H_2O_2] complexes when in contact with high H_2O_2 concentrations. Silica supported catalysts have been shown to be unstable[35] but require further investigation.

5.6.1 Ceria Supported Catalysts

Ceria supported catalysts have received considerable interest. Gold nano-particles supported on ceria have been identified to be active across a range of reactions including alcohol oxidation[36, 37] and carbon monoxide oxidation[38-42]. They have also been proved to be effective for other fuel-cell/automotive reactions such as water-gas shift (WGS) and preferential oxidation of CO in the presence of hydrogen (PROX). These results are of particular interest, since ceria is extensively employed in modern catalyst converters as the active component which is wash coated (deposited in a thin layer) on the walls of a monolith (cordierite). This is due to ceria's surface oxygen storage properties and capacity to undergo a rapid change in oxidation state upon changes in the redox potential of the exhaust gases.

Monometallic Pd/CeO_2 catalysts are also active for the water gas shift[43, 44] and CO oxidation[45-48] reactions. However, in the former, it suffers from rapid deactivation and in the latter low activity/selectivity in the presence of hydrogen (PROX) due to a change in the oxidation state of Pd (easily reducible).

Metsumura *et al.* have reported a monometallic Pd ceria catalyst to be effective for methanol synthesis from carbon monoxide and hydrogen[49-51]. They furthered this study by investigating Pd/CeO_2 catalysts for methanol decomposition[52], followed by the effect of X wt% Au addition to a 5 wt% Pd/CeO_2 catalyst on the decomposition at 180^{o}C with a significant promotional effect being observed[53]. Luo *et al.* have shown a promotional effect in the activity of Au-Pd/CeO_2 for partial oxidation of methanol compared to monometallic ceria catalyst[54].

CeO_2 supported Au-Pd catalysts have also been used for other selective oxidation and hydrogenation reactions including arabinose to arabinoic acid[55].

Tompos *et al.* produced tri-metallic ceria supported catalysts by the addition of Au and Pt to Pd/CeO_2. These materials had a higher conversion, than the equivalent Pd/CeO_2, for the temperature-programmed oxidation of methane over the whole temperature range examined[56].

Pritchard *et al.*[35, 57] prepared numerous ceria supported mono-metallic, bimetallic and tri-metallic catalysts by impregnation described in Experimental (Chapter Two). The metal loading was kept constant at 5 wt% with the metallic compositions varied accordingly. The addition of Au to Pd/CeO_2 catalysts was investigated on the rates of H_2O_2 synthesis and hydrogenation, using a methanol-water solvent system[57], before extending the study to tri-metallic Au-Pd-Pt/CeO_2[35]. The investigation of Pd-rich catalyst compositions resulted in the highest rates of H_2O_2 synthesis; the maximum of which was obtained using 0.20 wt% Au-4.60 wt% Pd - 0.20 wt% Pt (185 $mol_{H2O2}kg_{cat}^{-1}h^{-1}$).

5.6.2 Direct H_2O_2 Synthesis Using Bimetallic and Tri-metallic catalysts

A selection of bi-metallic and tri-metallic catalysts with Pd-rich compositions were tested for the direct synthesis of H_2O_2 using the biphasic solvent system previously described, the results are shown in Table 5.5.

Table 5.5 - Direct H_2O_2 synthesis using bi-metallic and tri-metallic ceria supported catalysts

Ceria catalyst (Metal composition wt %)	**H_2O_2 productivity ($mol_{H2O2}kg_{cat}^{-1}h^{-1}$)**	**H_2O_2 concentration ($g_{H2O2}kg_{H2O}^{-1}$)**
2.5 Au - 2.5Pd	4.2	4.6
1.2 Au - 3.8 Pd	6.8	7.4
0.4 Au - 4.6 Pd	9.3	10.1
0.6 Au - 0.6 Pt - 3.8 Pd	7.9	8.6
0.2 Au - 0.2 Pt - 4.6 Pd	11.5	12.5

Reaction conditions: 20 mg catalyst, 700 psi, H_2/O_2 = 0.525, 1200 rpm, 25 ^oC, solvent loading 4 g saturated decan-1-ol (0.16 g H_2O)

Interestingly, for the bi-metallic catalysts selected, when the Pd content is increased a higher H_2O_2 concentration is achieved; palladium is believed to be the active component with the addition of gold electronically promoting its activity. Previously, it has been shown that the optimum H_2O_2 productivity is achieved with a Au-Pd ratio of 1, however here it seems a lower Au content and higher Pd content causes a larger promotional effect.

When adding the third metal, Pt, a maximum concentration (12 $g_{H2O2}kg_{H2O}^{-1}$) was achieved with a metal composition of 0.2 wt% Au - 0.2 wt% Pt - 4.6 wt% Pd. Again the high palladium content is likely to be the crucial component. This represents a significant step forward towards producing H_2O_2 concentration of 3-8 wt%.

Interestingly, although Au-Pd ceria appeared initially to be a more active than Au-Pd/C Figure 5.6, however, under the 'optimum conditions' utilised carbon produces a higher concentration (0.8 v 0.46 wt%). This could be due to a higher retention of carbon in the organic phase hence lower H_2O_2 hydrogenation activity and/or the conditions utilised are not the optimum conditions for ceria catalysts.

Changing the metal compositions and the addition of a third metal both increased the H_2O_2 concentration, indicating the preparation of the catalyst will be crucial in future studies.

5.6.3 Effect of Reagent Reloading

In order to increase H_2O_2 concentration even further, it was decided to run top-up experiments, Figure 5.17. These experiments consist of the subsequent refilling of the autoclave with reagent gases for a determined number of times.

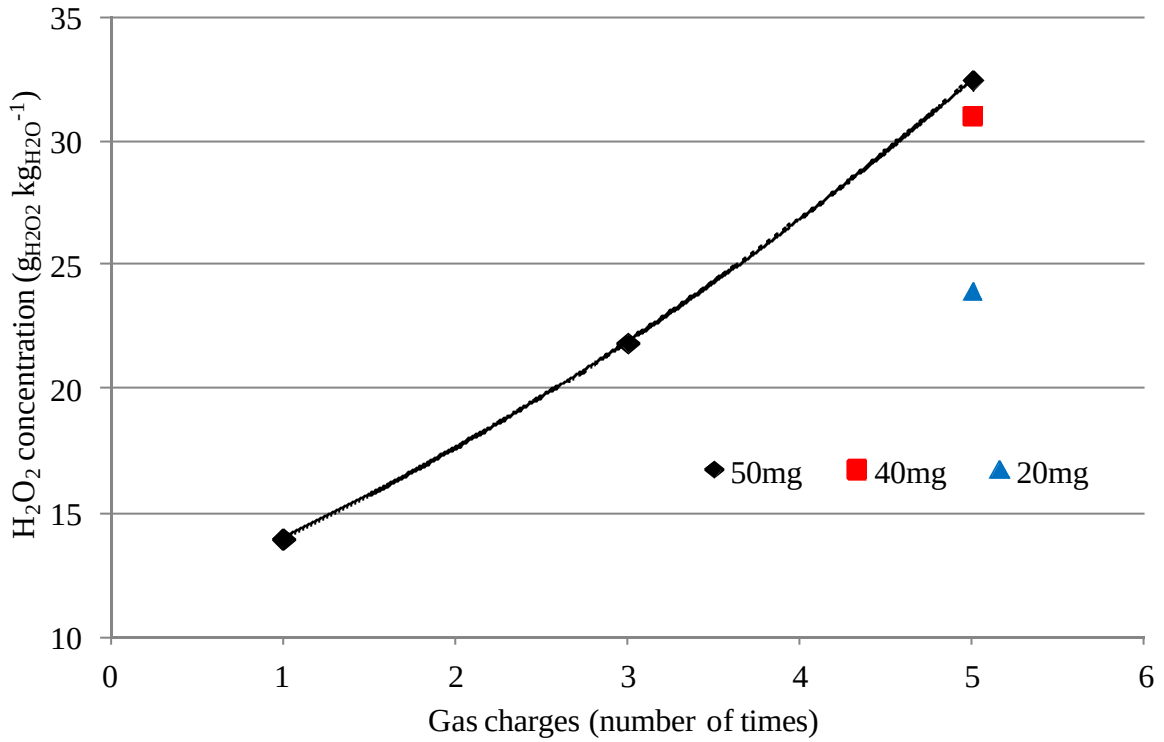

Figure 5.17 - H_2O_2 concentration as a function of reagent gas charges. Varying masses of 0.2Au0.2Pt4.6Pd/CeO_2 catalyst have been used.

Reaction conditions: **Each gas charge** = IMP-Au-Pd-Pt/CeO_2 (X mg), 5% H_2/CO_2 (507 psi), 25% O_2/CO_2 (193 psi), solvent (4.08 g decan-1-ol, 0.17 g H_2O), X rpm, 25 ^oC, 30 min.

The conditions, catalysts loading and working pressure used for this set of experiments were extremely drastic. However, the aim was to have an understanding of the reaction limits of this synthesis approach rather than fine tuning the reaction parameters.

Surprisingly, a H_2O_2 concentration > 3 wt% was achieved after 5 gas charges using 40 and 50 mg of catalyst. Decreasing the catalyst loading to 20 mg resulted in a decrease of H_2O_2

concentration to 2.4 wt%. The fact that H_2O_2 concentration achieved is almost the same for 40 and 50 mg agrees with previous results proving that kinetic limitations occur at catalyst loading > 30-40 mg.

Reagent reloading proved to be successful producing a H_2O_2 concentration >3 wt%, showing a biphasic solvent system has significant potential. Reagent reloading rejuvenates the H_2/O_2 concentration every 30 minutes in order to maintain a constant supply to the catalyst to produce further H_2O_2. As hydrogen is the limiting reagent, keeping the H_2 concentration constant and ensuring the catalyst is working at the highest efficiency possible, throughout the reaction may increase the H_2O_2 concentration further. This could be achieved by flowing reagent gases through the solvent using a semi-continuous flow reactor as described in the following sections of this chapter.

5.7 Introduction – Direct H_2O_2 Synthesis Using a Semi-Continuous Flow Reactor

There are a wide range of industrial reactors for heterogeneous reactions and generally scaled down versions of these are used for catalyst testing. The smallest of these is usually referred to as a micro-reactor, used in most academic laboratories, allowing a great number of results to be gathered in a relatively short period of time. Micro-reactors allow a variety of reaction conditions to be studied including temperature, pressure, solvents and catalysts. Numerous micro-reactors and reaction conditions[2, 3, 6, 24, 58-61], some of which are mentioned in Chapter One, have been used to measure the productivity of catalysts for the direct synthesis of hydrogen peroxide, making comparisons between research groups difficult.

Throughout this thesis a batch reactor has been utilised. However, the positive effect of subsequent reagent charges on H_2O_2 concentration for both the biphasic solvent system (Figure 5.17) and standard methanol-water solvent system[62] has led to increased interest in flow reactors.

Within this chapter a semi-continuous reactor is utilised allowing the reagent gases to flow continuously through a solvent-catalyst mixture under high pressure, which allows the reagent gas concentrations to be kept constant. The advantages of using such a reactor are the H_2O_2 synthesis rate is a function of the H_2 concentration:

$$v = k[H_2]^a[O_2]^b$$

v = rate of reaction

k = rate constant

a & b = stiochiometric coefficients

Since H_2 is the rate limiting reagent, it can be assumed that the reaction depends on the H_2 concentration. The difference between standard and semi-continuous can be better visualised in Figure 5.18.

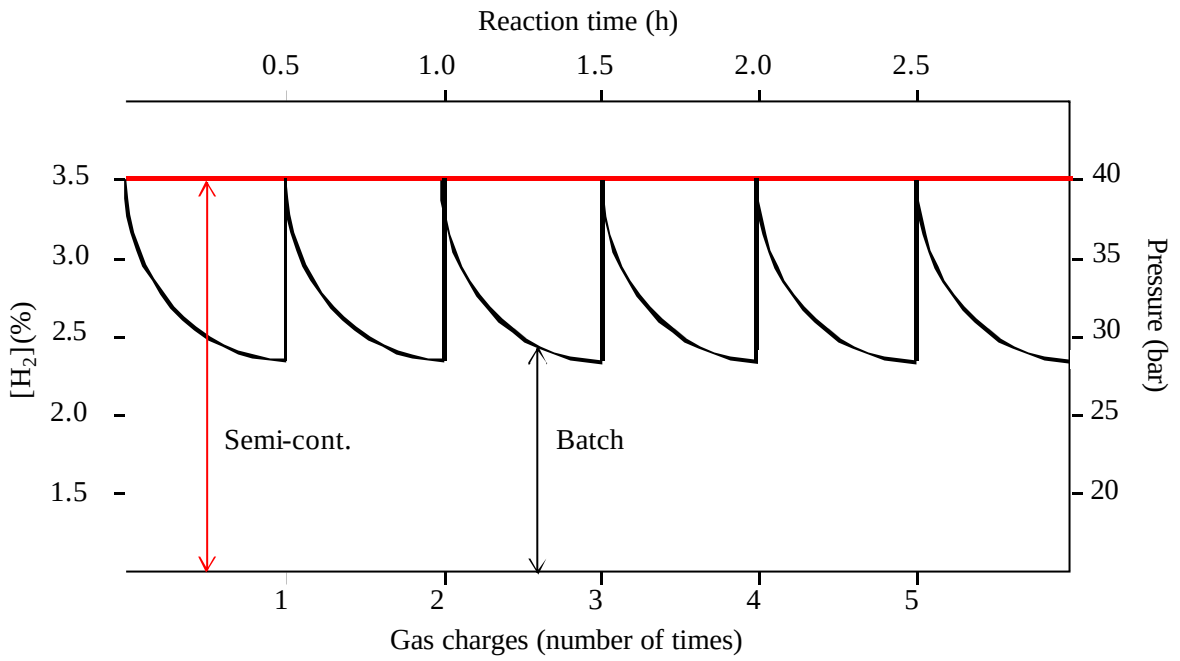

Figure 5.18 - Difference between reagent reloading in batch and semi-continuous flow conditions.

The semi-continuous reactor allows the H_2 concentration and pressure to be kept constant hence increasing the overall kinetic driving force. As the H_2O_2 concentration increases with the number of gas charges, flowing reagent gases should led to the same or a promotion in activity by simply increasing the reaction time.

A methanol-only solvent system has been utilised, which allows the water concentration to be measured using Karl Fischer titration as a function of time giving greater insight into the catalyst activity. A novel approach to investigating H_2O_2 decomposition has also been investigated using the procedure described.

5.8 Reactor Design and Working Conditions

Catalytic tests under a continuous flow of gas were performed inside a modified batch reactor detailed in Figure 5.19.

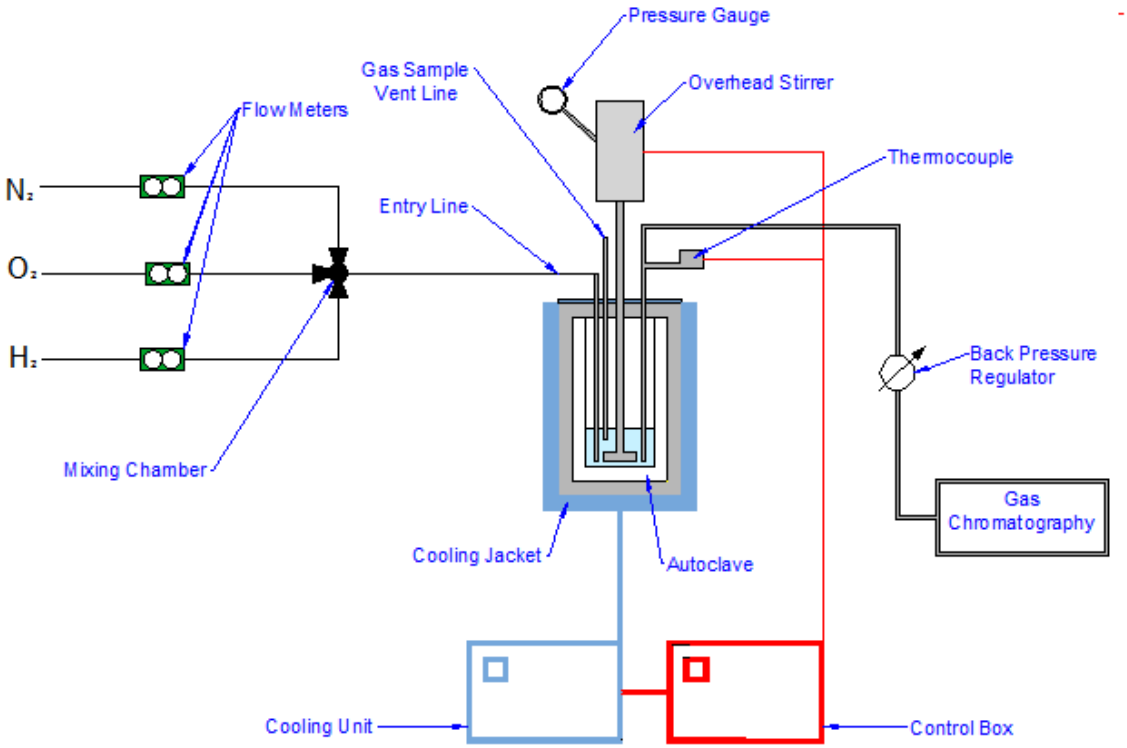

Figure 5.19 - Schematic of semi-continuous flow reactor for the direct synthesis of H_2O_2

Three flow meters, for, with the possibility to regulate the rate of O_2, H_2 and N_2 flows were installed. A mixing chamber with an internal volume of 150µm was positioned in order to make a homogenous combination of the three gases. At the exit of the reactor a back pressure regulator was installed to control the inlet pressure by balancing an adjustable spring force against the inlet gas flow, making it possible to work with a fixed pressure inside the autoclave. Finally a gas chromatographer (GC-14 B SHIMADZU) (GC) was installed on line to measure the concentration of gases coming out of the reactor.

5.8.1 Standard procedure

The standard procedure used to carry out catalytic tests in the semi-continuous flow is based on the batch conditions descried in chapter 2. However, a larger internal reactor volume of *ca.* 100ml allowed double the solvent mass to be used (17 ml). In order to keep the catalyst mass to solvent loading ratio constant the catalyst mass was doubled to 20 mg.

The reactor was charged with catalyst (0.02 g) and solvent (17 ml CH_3OH). Pre-mixed gas was injected inside the autoclave (N_2 180 ml min^{-1}, O_2 14 ml min^{-1} and H_2 7ml min^{-1}), giving a total flow of 201 ml min^{-1} and a H_2/O_2 ratio of 0.5. The H_2 concentration was monitored using the online GC, until the reaction pressure (580 psi) was obtained. When the H_2 concentration stabilised (~3.5 %) the stirring (1200 rpm) was started (t=0). Throughout the reaction (60 min), the gas concentrations were recorded every 6 minutes. The gas was evacuated and the solution filtered to separate the catalyst. The concentration of H_2O_2 was determined calorimetrically at ?=410 nm after mixing an aliquot (*ca.*0.1 g) of the reaction medium with $TiCl_4$ in 2 M H_2SO_4 (25 ml). Changes to these conditions have been highlighted where necessary.

5.8.2 Calculations

Under the continuous flow of gases the concentration of the gases following reaction were measured using the on-line GC, allowing the H_2 conversion to be measured as follows.

Note - The concentration of the inert gas N_2 was constant during the trial, because it does not take part in the reaction, so was used as an internal standard. As the H_2 concentration was measured, every 6 minutes using the on-line GC, H_2 conversion can be followed throughout the reaction.

1) $$H_2 \text{ conversion } (\%) = \frac{(\text{mol } H_2)_{t=0} - (\text{mol } H_2)_{t=t}}{(\text{mol } H_2)_{t=0}} \times 100$$

Where:

$$(\text{mol } H_2)_{t=0} = \frac{V\ (\text{ml\_}H_{2t=0} \times 10^{-3}) \times P\ (1 \text{ atm})}{R\ (0.08216 \text{ L atm mol}^{-1}\text{K}^{-1}) \times T\ (273.15 \text{ K})}$$

$$ml\_H_{2t=0} = \frac{[H_2]_{t=0}\ (\%)}{100} \text{ X total flow}_{t=0}\ (mlmin^{-1})\ (\text{flow } N_2 + \text{flow } O_2 + \text{flow } H_2)$$

and:

$$(\text{mol } H_2)_{t=t} = \frac{V\ (ml\_H_{2t=t} \text{ x } 10^{-3}) \text{ x P (1 atm)}}{R\ (0.08216 \text{ L atm mol}^{-1}K^{-1}) \text{ x T (273.15 K)}}$$

$$ml\_H_{2t=t} = \frac{[H_2]_{t=0}\ (\%)}{100} \text{X total flow}_{t=t}\ (mlmin^{-1})\ (\text{total flow}_{t=0} \text{ x} \frac{[N_2]_{t=0}\ (\%)}{[N_2]_{t=t}\ (\%)})$$

Following acquisition of the H_2O_2 concentration of in solution, the selectivity of H_2 consumption towards H_2O_2 can be measured. A high H_2 selectivity is of paramount importance to the success of the direct H_2O_2 synthesis becoming industrially viable due to the expense of using H_2 financially and economically. As well as the selectivity the H_2O_2 productivity and yield have been calculated.

2) H_2 selectivity (%) = $\frac{(\text{mol } H_2O_{2formed})_{t=t}}{(\text{mol } H_2)_{t=0} - (\text{mol } H_2)_{t=t}} \text{ X 100}$

3) H_2O_2 productivity $(mol_{H2O2} kg_{cat}^{-1} h^{-1})$ = $\frac{(\text{mol } H_2O_{2formed})_{t=t}}{t=t_h \text{ x } kg_{cat}}$

4) H_2O_2 yield (%) = $\frac{(\text{mol } H_2O_{2formed})_{t=t}}{(\text{mol } H_2)_{t=0}} \text{ X 100}$

5.9 Initial Results

5.9.1 Solvent Composition

The solvent composition was investigated using water-only, methanol-only and a methanol-water mixture with a ratio of 1.93 (66 wt% CH_3OH) keeping the total amount of solvent constant (Table 5.6). The latter is used by Edwards *et al.* for standard reactions[1]. The addition of water to methanol has previously been shown to be beneficial for direct H_2O_2 synthesis[2, 3].

Table 5.6 - Influence of solvent composition on catalyst activity.

Solvent	H_2O_2 Conc. *wt %*	Productivity $mol_{H2O2}kg_{cat}^{-1}h^{-1}$	Selectivity *%*	H_2 Conversion *%*	Yield
Methanol	0.49	245	45	29	13
$CH_3OH + H_2O$*	0.45	107	36	32	12
H_2O	0.07	20	11	16	2

*** 5.6 g MeOH + 2.9 g H_2O**

Reaction conditions: IMP-Au-Pd/C (10 mg), 3.5 %H_2, 7 %O_2, 89.5 %N_2, 201 ml min^{-1}, 40 bar, 8.5 g solvent, 2 ^oC, 60 min.

The highest H_2O_2 concentration, productivity and yield were obtained in pure-methanol. In methanol-only the IMP-Au-Pd/C catalyst also showed the highest H_2 selectivity towards H_2O_2. This has been likened to the development of surface formate when using methanol as solvent (acetate species when using ethanol) by reaction with oxygen on the Pd [110] surface thus preventing HO-OH bond breaking (HO-OH = 213 kJ mol^{-1}, H-O_2H = 369 kJ mol^{-1})[63].

The highest H_2 conversion was achieved with a mixture of CH_3OH and H_2O, indicating that the water is having a positive effect on the catalytic activity. Goodman *et al.*[34] have previously postulated the promotional effects of water on CO oxidation can be rationalised by its effects on molecular oxygen adsorption and activation. In this case water may be increasing the adsorption and activation of molecular oxygen and hydrogen, promoting the production of H_2O_2 and to a greater extent H_2O_2 hydrogenation. It is likely the lower concentration, productivity and selectivity is due to a higher rate of H_2O_2 hydrogenation/decomposition in this solvent mixture.

As expected water-only leads to the lowest catalytic activity which can be explained by the lower solubility of the reagent gases, H_2 and O_2, in water compared to methanol. The lower selectivity observed in H_2O-only indicates that H_2O_2 may not be as stable in H_2O as CH_3OH and is lost through either the H_2O_2 hydrogenation or decomposition pathway. Another explanation could be the combustion of H_2 is more prevalent in H_2O-only.

5.9.2 Influence of Catalyst Mass

The effect of increasing the amount of catalyst on the H_2O_2 concentration was investigated whilst keeping all the other reaction variables outlined in section 6.2 constant; the results are shown in Table 5.7.

Table 5.7 – Catalyst activity towards direct H_2O_2 synthesis as the catalyst mass is increased

Catalyst mass mg	**H_2O_2 Conc. wt %**	**Productivity $mol_{H2O2}kg_{cat}^{-1}h^{-1}$**	**Selectivity %**	**H_2 Conversion %**	**Yield**
10	0.49	245	45	29	13
20	0.83	208	53	42	22
40	1.05	131	50	55	28
60	1.09	91	51	56	29

Reaction conditions: IMP-Au-Pd/C (X mg), 3.5 %H_2, 7 %O_2, 89.5 %N_2, 201 ml min^{-1}, 40 bar, 8.5 g CH_3OH, 2 ^oC, 60 min.

Table 5.7 shows how the H_2O_2 concentration increases as the amount of catalyst is increased, with the highest concentration of 1.09 wt% H_2O_2, achieved using 60 mg of catalyst. Although there is a significant increase in concentration from 10 – 20 mg, the concentration increase plateaus as the catalyst mass is increased further. The fact that H_2O_2 productivity is the highest at lower catalyst masses suggests that at higher catalyst loadings the contribution of the subsequent H_2O_2 hydrogenation/decomposition reaction becomes more marked. However when 20 mg of catalyst is used the highest H_2 selectivity is achieved, indicating that mass transfer limitations, may also be playing a pivotal role when using higher catalyst loadings.

5.9.3 Flow Rate

The influence of flow rate was investigated keeping all other variables the same. Increasing the flow rate increases the amount of reagent gas available for the direct H_2O_2 synthesis to occur during the 60 minute reaction. The results are shown in Table 5.8.

Table 5.8 - Influence of the reagent gas flow rate on catalyst activity

Flow rate ml/min	**H_2 input mmol**	**H_2O_2 Conc. *wt %***	**Productivity $mol_{H2O2}kg_{cat}^{-1}h^{-1}$**	**Selectivity *%***	**H_2 Conversion *%***	**Yield**
201	19.0	0.83	208	53	42	22
313	29.7	0.86	215	48	30	14
402	37.7	0.89	224	43	28	12

Reaction conditions: IMP-Au-Pd/C (20 mg), 3.5 %H_2, 7 %O_2, 89.5 %N_2, X ml min^{-1}, 40 bar, 8.5 g CH_3OH, 2 ^oC, 60 min.

Increasing the flow rate increases the H_2O_2 concentration and productivity; however the increase is not proportional to the increase in H_2 input. This suggests that saturation of the solvent with H_2 is being achieved efficiently enough, at a flow rate of 201 ml min^{-1}, for the catalyst to work to full capacity.

H_2 conversion and more importantly selectivity decrease with increasing flow rate indicating that the excess flow of H_2 causes the H_2O_2 hydrogenation pathway to become more predominate.

5.9.4 Influence of the Diluent Gas

The influence of the 'inert' gas used to dilute H_2 and O_2 below the flammability limit (5-95 v/v% for H_2 in O_2) has been investigated keeping all other variables constant.

The use of N_2 as the diluent gas would be ideal due to its low cost and availability. However, CO_2 is more commonly used because it has a promotional effect on H_2O_2 productivity[1]. It was postulated that this is due to CO_2 forming carbonic acid *in situ* stabilising the formed peroxide. The results of using N_2 and CO_2 as diluent gas under semi continuous flow conditions are shown in Table 5.9.

Table 5.9 - Influence of diluent gas for the direct H_2O_2 synthesis.

Diluent Gas	**H_2O_2 Conc.** *wt %*	**Productivity** $mol_{H2O2}kg_{cat}^{-1}h^{-1}$	**Selectivity** *%*	**H_2 Conversion** *%*	**Yield**
N_2	0.83	208	53	42	22
CO_2	1.06	265	58	48	28

Reaction conditions: IMP-Au-Pd/C (20 mg), 3.5 %H_2, 7 %O_2, 89.5 %X, 201 ml min^{-1}, 40 bar, 8.5 g CH_3OH, 2 ^oC, 60 min.

As can be seen in Table 5.9, using CO_2 as the diluent gas improves the productivity of the catalyst and therefore a higher concentration of H_2O_2 is produced. Using CO_2 as the diluent gas causes an increase in the selectivity of the catalyst, which is explained by the earlier postulation that of *in-situ* carbonic acid formation stabilises the formed H_2O_2. However, what was not expected is the increase in H_2 conversion (42 – 48 %) when using CO_2 rather than N_2.

To investigate further when using N_2 and CO_2 as diluent gas for the direct H_2O_2 synthesis the pH of the working medium after the reaction was determined. The working solutions were also analysised for Au, Pd (Inductively-Coupled Plasma Mass Spectroscopy (ICP-MS)) and Cl^- (Ion Chromatography (IC)) as the addition of acid has previously been shown to destabilise supported metal nano-particles causing them to leach into the reaction medium[64], the results are shown in Table 5.10.

Table 5.10 - Analysis of the working solution after reactions using N_2 and CO_2.

Diluent gas used during reaction	**pH of reaction medium**	**Impurities (*μg/kg$_{solvent}$*) ****		
		Au	**Pd**	**Cl *(mg/L)***
(MeOH*)	6.1	1	0.9	<0.1
N_2	4.14	7	28	24
CO_2	3.5	22	34	22

*Before the reaction ** 1 μg/kg$_{solvent}$ = 0.034 % of original metal (2.5 wt%) leached

Under semi-continuous flow conditions the catalyst appears to be unstable, when using either N_2 or CO_2 as the diluent gas. This can be linked to the reaction medium becoming more acidic. The stability of the catalyst is decreased when using CO_2, where the reaction medium is most acidic, suggesting carbonic acid is being formed[1]. The increased metal content in the reaction medium when using CO_2 as the diluent may explain the previously unexplained trend of increased H_2 conversion (42 – 48 %). Dissanayake *et al.*[65, 66] have shown that leached Pd can form a homogeneous catalyst active for the direct H_2O_2 synthesis.

The increased acidity when using N_2 can be attributed to the slight acidity of the carbon support (~ 6) linked with the slight acidic nature of H_2O_2 in solution (*c.a.* 4.5 – 6.2 depending on concentration). Metal leached from the catalyst can form active homogeneous species[65, 66] and lead to significant deactivation in activity on catalyst reuse[67]. The leaching of chloride into the reaction medium can alter catalyst performance[68] and is not ideal for industrial use due to its corrosive nature.

After running the experiments with CO_2 as the diluent gas it was noted the gas flow rate was not steady. The fluctuation of the gas flow had a major effect on the final H_2O_2 concentration and it was not possible to acquire adequate reproducible data. The reason of this fluctuation was finally assigned to the gaseous CO_2 liquefying in the mass flow controllers. Therefore it was decided reactions were to be run using nitrogen as the diluent gas.

5.10 Influence of Reaction Time

Provision to extract a sample of the working solution was installed enabling the reaction to be run continuously with samples taken every 30minutes. The samples were analysised for water and hydrogen peroxide by volumetric Karl Fischer titration and UV-vis spectroscopy, respectively (refer to chapter 2 for further details). H_2 conversion was determined by online GC analysis as a function of time. This enabled the H_2O_2 productivity, selectivity and yield to be calculated using the equations shown in section 5.8.2. The standard experimental procedure in section 5.8.1 was utilised.

Note – In this section the following reaction conditions have been utilised:

Catalyst - IMP-Au-Pd/C (20 mg)

Gas composition - 3.5 %H_2, 7 %O_2, 89.5 %N_2

Flow rate - 201 ml min^{-1}

Pressure - 40 bar

Solvent mass - 17 g CH_3OH

Temperature - 2 ^oC

Reaction time - 60 min.

5.10.1 Hydrogen Peroxide and Water Concentration

The liquid phase was sampled every 30 minutes and the concentrations of H_2O and H_2O_2 were obtained as a function of time as shown in Figure 5.20.

The amount of liquid subtracted for each analysis was 0.8 ml, so that the total uptake never exceeded 25 % of the initial liquid volume. Errors on H_2O_2 and H_2O measurements were estimated analyzing a methanol solution with a known water and hydrogen peroxide content (0.8 % and 1.6 % respectively), sampled from the reactor under experimental conditions. Estimated error for H_2O_2 was 0.8 %, whereas for H_2O it was 2 %.

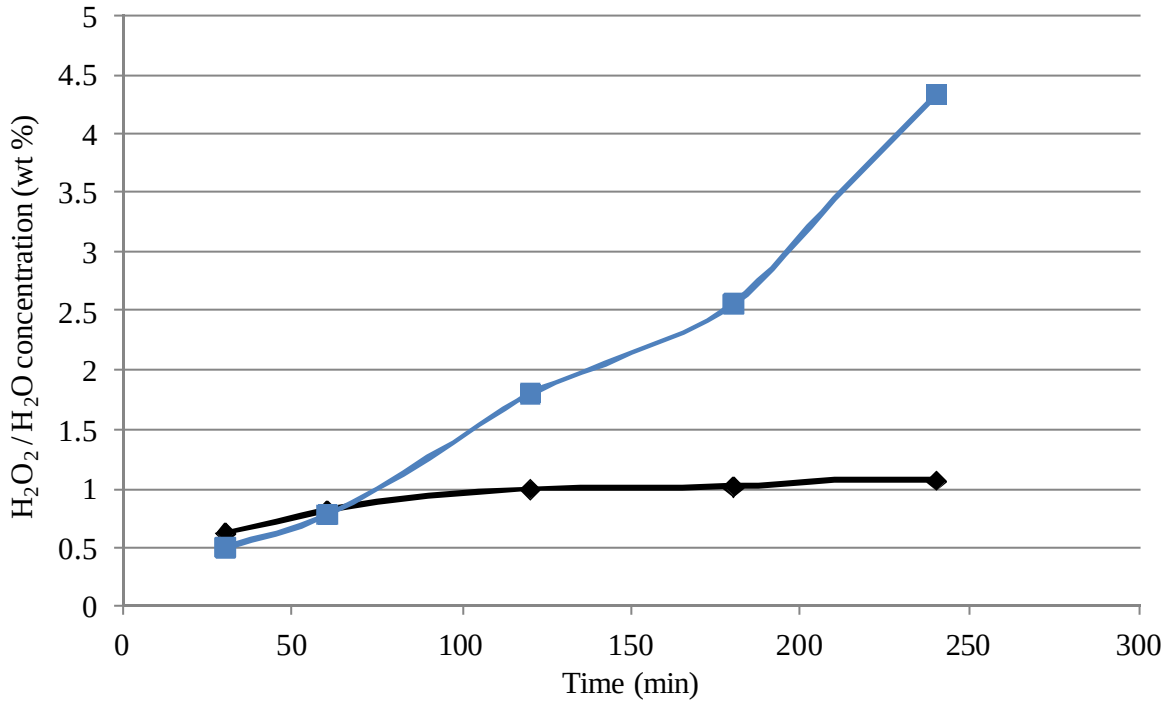

Figure 5.20 - Concentration of H_2O (■) and H_2O_2 (♦) as a function of time.

The H_2O_2 concentration steadily increases up to 120 minutes then plateaus for the remaining time investigated, whereas the H_2O concentration increases linearly with time. The apparent limit on the H_2O_2 concentration could be due to the rate of H_2O_2 production being equal to the rate of its destruction. This provides important information about the catalyst activity, with H_2O being the predominant product in the direct H_2O_2 synthesis after 60 minutes. H_2O can either be formed by H_2 combustion or subsequent hydrogenation/decomposition of H_2O_2. However, in this case, both may be dominating the H_2O_2 synthesis pathway.

5.10.2 Hydrogen Conversion

The H_2 concentration and conversions as a function of time are presented in Figure 5.21.

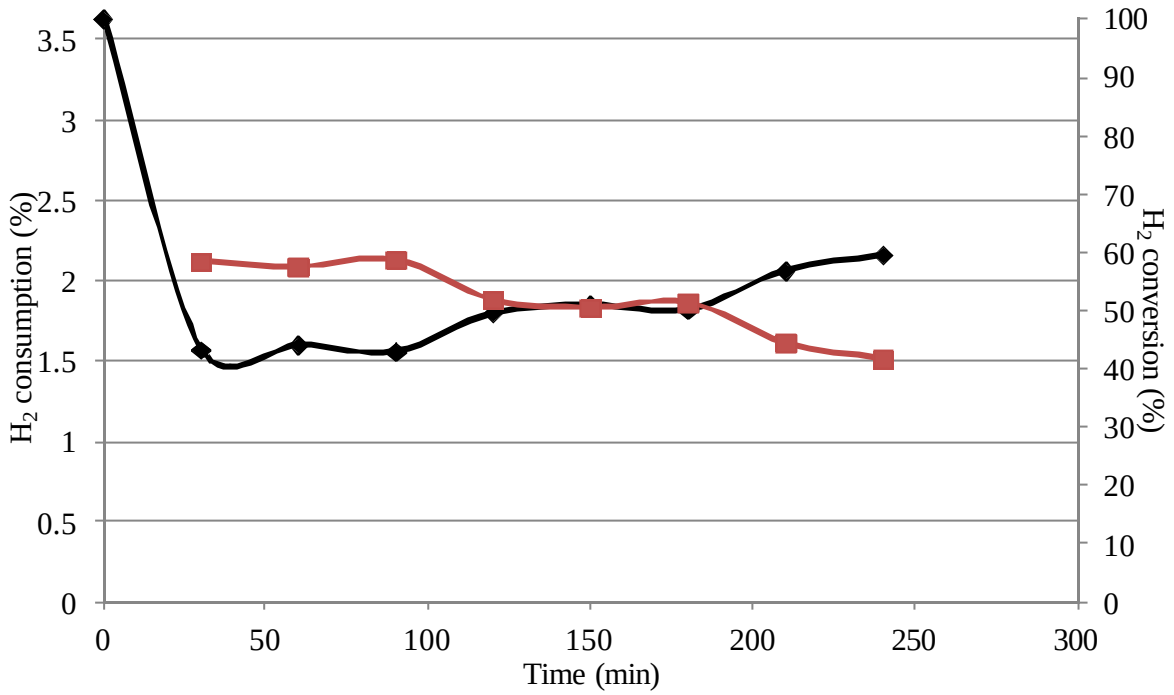

Figure 5.21 – Concentration of H_2 (◆) in the exit gas and the corresponding H_2 conversion (■) as a function of time.

Figure 5.21 indicates that H_2 conversion decreases slowly over time; this could be due to the loss of catalyst mass through sampling or the stability of the metal on the support surface. A lack of metal stability could cause a change in the metal oxidation state or even leaching of the metal from the support into the solvent; both of which would affect the catalysts performance. The IMP-Au-Pd/C catalyst utilised has been shown in section 5.9.4 to be unstable under semi-continuous flow conditions and the stability will need to be investigated further in future studies.

5.10.3 H_2O_2 Productivity, Selectivity and Yield

As the H_2O_2 concentration and H_2 conversion have been observed as a function of time the H_2O_2 productivity, selectivity and yield can be calculated using the equations in section 5.8.2. The obtained results as a function of time are presented in Figure 5.22.

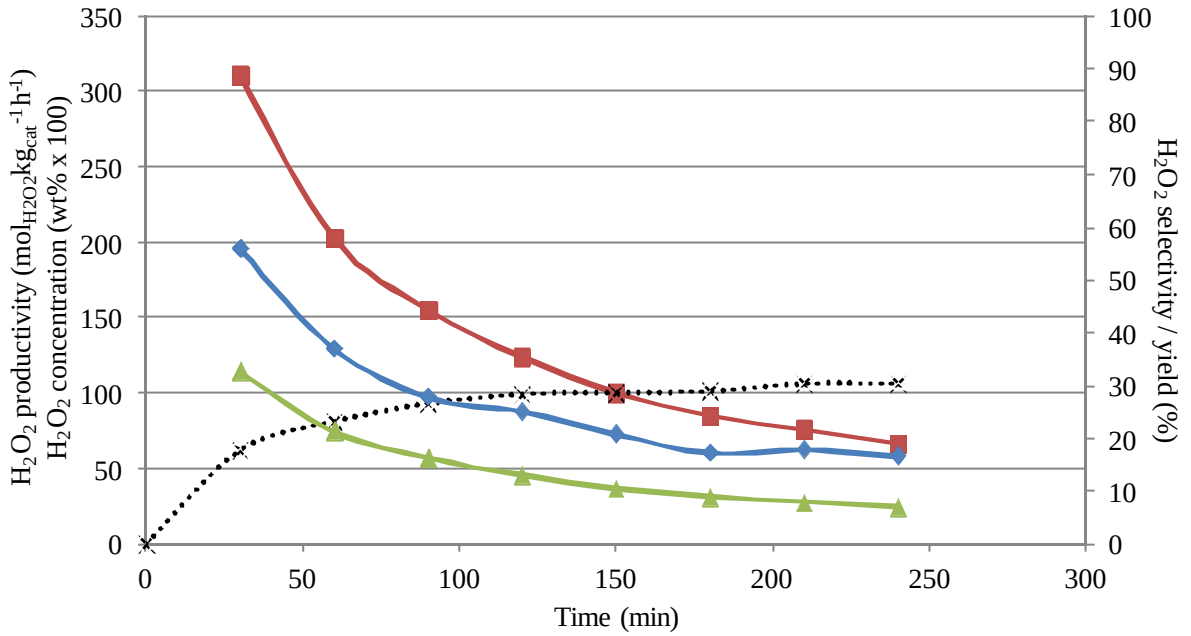

Figure 5.22 - H_2O_2 productivity (■), concentration (x), yield (▲) and selectivity (◆) as a function of time.

H_2 selectivity towards H_2O_2 decreases rapidly as a function of time this is likely to be due to increased rate of H_2O_2 hydrogenation/decomposition to water. This corresponds to a fast decrease in H_2O_2 productivity. It is likely H_2O_2 is being produced at similar rates due to similar H_2 conversions as a function of time. However, higher H_2O_2 concentration contributes to a greater rate of H_2O_2 hydrogenation/decomposition.

The rapid decrease in selectivity may well be linked with a change in surface Pd oxidation state which would, following reaction, require further analysis of the catalyst by XPS. However, it is likely that a loss of metal from the catalyst surface as observed in section 6.3.4, with colloidal Pd promoting the decomposition of H_2O_2 is the primary reason for the decrease.

5.10.4 Discussion

Making direct comparisons between the semi-continuous flow reactor and batch reactor is difficult due to variations to many of the conditions in order to make the flow reactor possible. However, comparing results obtained at 30 minutes under standard conditions for both reactors, batch and semi-continuous highlights the potential of a flow reactor compared to batch conditions, as shown in Table 5.11.

Table 5.11 - Comparison of catalytic activity under standard batch and standard semi-continuous flow reaction conditions at 30 minute reaction time.

	Batch	**Semi-Continuous**
Catalyst amount (mg)	10	20
Solvent loading (g)	8.5	17
Solvent type	$CH_3OH + H_2O$	CH_3OH
H_2 input (mmol)	4.5	9.5
O_2:H_2 ratio	0.525	0.5
Diluent gas	CO_2	N_2
H_2O_2 concentration (wt%)	0.22	**0.62**
H_2O_2 Productivity ($mol_{H2O2} kg_{cat}^{-1} h^{-1}$)	110	**310**
H_2 conversion (%)	41	**58**
H_2 selectivity (%)	*80*	56

Interestingly, even when using N_2 as the diluent gas with no added acid or water to the reaction medium (which have both been found to be beneficial), the semi-continuous flow reactor produces almost three times the H_2O_2 concentration and productivity of that achieved in the batch reactor. This corresponds to a greater conversion in the semi-continuous flow reactor, however the selectivity is decreased.

The beneficial effect of using a flow of the reagent gases can be linked to the H_2 concentration and pressure being kept constant throughout the reaction as shown in Figure 5.18, section 5.7. The reagent gases are constantly being replenished allowing the reaction to occur at similar rates over the reaction time; however even though this corresponds to a rise in the H_2O_2 produced it is also beneficial for the production of water.

5.11 References

1. J. K. Edwards, B. E. Solsona, P. Landon, A. F. Carley, A. Herzing, C. J. Kiely and G. J. Hutchings, *Journal of Catalysis*, 2005, **236**, 69-79.
2. M. Piccinini, E. Ntainjua N, J. K. Edwards, A. F. Carley, J. A. Moulijn and G. J. Hutchings, *Physical Chemistry Chemical Physics*, 2010, **12**, 2488-2492.
3. M. Piccinini, J. K. Edwards, J. A. Moulijn and G. J. Hutchings, *Catalysis Science & Technology*, 2012, **2**, 1908-1913.
4. V. V. Krishnan, A. G. Dokoutchaev and M. E. Thompson, *Journal of Catalysis*, 2000, **196**, 366-374.
5. V. R. Choudhary, S. D. Sansare and A. G. Gaikwad, *Catalysis Letters*, 2002, **84**, 81-87.
6. C. Samanta, *Applied Catalysis a-General*, 2008, **350**, 133-149.
7. S. Chinta and J. H. Lunsford, *Journal of Catalysis*, 2004, **225**, 249-255.
8. J. M. Campos-Martin, G. Blanco-Brieva and J. L. G. Fierro, *Angewandte Chemie International Edition*, 2006, **45**, 6962-6984.
9. Y. F. Han and J. Lunsford, *Catalysis Letters*, 2005, **99**, 13-19.
10. R. Hage and A. Lienke, *Angewandte Chemie International Edition*, 2006, **45**, 206-222.
11. P. Landon, P. J. Collier, A. J. Papworth, C. J. Kiely and G. J. Hutchings, *Chemical Communications*, 2002, 2058-2059.
12. P. Landon, P. J. Collier, A. F. Carley, D. Chadwick, A. J. Papworth, A. Burrows, C. J. Kiely and G. J. Hutchings, *Physical Chemistry Chemical Physics*, 2003, **5**, 1917-1923.
13. D. Hancu and E. J. Beckman, *Green Chemistry*, 2001, **3**, 80-86.
14. E. J. Beckman, *Green Chemistry*, 2003, **5**, 332-336.
15. Q. Chen and E. J. Beckman, *Green Chemistry*, 2007, **9**, 802-808.
16. D. Hâncu, J. Green and E. J. Beckman, *Industrial & Engineering Chemistry Research*, 2002, **41**, 4466-4474.
17. , 1982.
18. P. Li, C. He, S. Campestrini, B. Corain, W. Yuan and Y. F. Han, *Phys Chem Chem Phys*, 2010, **12**, 2170-2176.
19. I. T. Horváth, *Accounts of Chemical Research*, 1998, **31**, 641-650.
20. , 1994.
21. *US Pat.*, 2006.
22. J. K. Edwards, A. Thomas, B. E. Solsona, P. Landon, A. F. Carley and G. J. Hutchings, *Catalysis Today*, 2007, **122**, 397-402.
23. *US Pat.*, 2002.
24. Q. Liu, J. C. Bauer, R. E. Schaak and J. H. Lunsford, *Applied Catalysis A: General*, 2008, **339**, 130-136.
25. G. Blanco-Brieva, E. Cano-Serrano, J. M. Campos-Martin and J. L. G. Fierro, *Chemical Communications*, 2004, 1184-1185.
26. X. Liu, X. Wang, X. Guo and G. Li, *Catalysis Today*, 2004, **93–95**, 505-509.
27. N. Gemo, P. Biasi, P. Canu and T. O. Salmi, *Chemical Engineering Journal*, 2012, **207–208**, 539-551.
28. J. V. H. d'Angelo and A. Z. Francesconi, *Journal of Chemical & Engineering Data*, 2001, **46**, 671-674.
29. M. S. Wainwright, T. Ahn, D. L. Trimm and N. W. Cant, *Journal of Chemical & Engineering Data*, 1987, **32**, 22-24.
30. Y. Tominaga, I.-C. Hong, S. Asai and M. Sumita, *Journal of Power Sources*, 2007, **171**, 530-534.
31. Z. Miao, H. Yu, W. Song, D. Zhao, L. Hao, B. Yi and Z. Shao, *Electrochemistry Communications*, 2009, **11**, 787-790.
32. K.-s. Guan and Y.-s. Yin, *Materials Chemistry and Physics*, 2005, **92**, 10-15.

33. M. Daté, M. Okumura, S. Tsubota and M. Haruta, *Angewandte Chemie International Edition*, 2004, **43**, 2129-2132.
34. F. Gao, T. Wood and D. W. Goodman, *Catalysis Letters*, 2010, **134**, 9-12.
35. J. C. Pritchard, Cardiff University, 2012.
36. A. Abad, C. Almela, A. Corma and H. García, *Tetrahedron*, 2006, **62**, 6666-6672.
37. M. Alhumaimess, Z. Lin, W. Weng, N. Dimitratos, N. F. Dummer, S. H. Taylor, J. K. Bartley, C. J. Kiely and G. J. Hutchings, *ChemSusChem*, 2012, **5**, 125-131.
38. U. R. Pillai and S. Deevi, *Applied Catalysis A: General*, 2006, **299**, 266-273.
39. S.-Y. Lai, Y. Qiu and S. Wang, *Journal of Catalysis*, 2006, **237**, 303-313.
40. S. A. C. Carabineiro, A. M. T. Silva, G. Dražic, P. B. Tavares and J. L. Figueiredo, *Catalysis Today*, 2010, **154**, 21-30.
41. Z. Chen and Q. Gao, *Applied Catalysis B: Environmental*, 2008, **84**, 790-796.
42. S. D. Gardner, G. B. Hoflund, D. R. Schryer, J. Schryer, B. T. Upchurch and E. J. Kielin, *Langmuir*, 1991, **7**, 2135-2139.
43. S. Hilaire, X. Wang, T. Luo, R. J. Gorte and J. Wagner, *Applied Catalysis A: General*, 2004, **258**, 271-276.
44. X. Wang and R. J. Gorte, *Applied Catalysis A: General*, 2003, **247**, 157-162.
45. Marti, amp, x, A. nez-Arias, Hungri, A. B. a, G. Fernández, M. a, A. Iglesias-Juez, J. A. Anderson and J. C. Conesa, *Journal of Catalysis*, 2004, **221**, 85-92.
46. J. A. Wang, L. F. Chen, M. A. Valenzuela, A. Montoya, J. Salmones and P. D. Angel, *Applied Surface Science*, 2004, **230**, 34-43.
47. E. Bekyarova, P. Fornasiero, J. Kašpar and M. Graziani, *Catalysis Today*, 1998, **45**, 179-183.
48. O. Pozdnyakova, D. Teschner, A. Wootsch, J. Kröhnert, B. Steinhauer, H. Sauer, L. Toth, F. C. Jentoft, A. Knop-Gericke, Z. Paál and R. Schlögl, *Journal of Catalysis*, 2006, **237**, 17-28.
49. W. J. Shen, Y. Ichihashi, M. Okumura and Y. Matsumura, *Catalysis Letters*, 2000, **64**, 23-25.
50. Y. Matsumura, W.-J. Shen, Y. Ichihashi and H. Ando, *Catalysis Letters*, 2000, **68**, 181-183.
51. W.-J. Shen, Y. Ichihashi, H. Ando, Y. Matsumura, M. Okumura and M. Haruta, *Applied Catalysis A: General*, 2001, **217**, 231-239.
52. W.-J. Shen and Y. Matsumura, *Journal of Molecular Catalysis A: Chemical*, 2000, **153**, 165-168.
53. M. P. Kapoor, Y. Ichihashi, T. Nakamori and Y. Matsumura, *Journal of Molecular Catalysis A: Chemical*, 2004, **213**, 251-255.
54. Q.-b. Chen, L.-t. Luo and X. Yang, *Indian Journal of Chemistry - Section A*, 2008, **47A**, 1317-1322.
55. E. Smolentseva, B. T. Kusema, S. Beloshapkin, M. Estrada, E. Vargas, D. Y. Murzin, F. Castillon, S. Fuentes and A. Simakov, *Applied Catalysis A: General*, 2011, **392**, 69-79.
56. A. Tompos, J. L. Margitfalvi, M. Hegedus, A. Szegedi, J. L. Fierro and S. Rojas, *Comb Chem High Throughput Screen*, 2007, **10**, 71-82.
57. E. N. Ntainjua, M. Piccinini, J. C. Pritchard, J. K. Edwards, A. F. Carley, C. J. Kiely and G. J. Hutchings, *Catalysis Today*, 2011, **178**, 47-50.
58. V. R. Choudhary, C. Samanta and P. Jana, *Industrial & Engineering Chemistry Research*, 2007, **46**, 3237-3242.
59. P. Biasi, N. Gemo, J. R. Hernández Carucci, K. Eränen, P. Canu and T. O. Salmi, *Industrial & Engineering Chemistry Research*, 2012, **51**, 8903-8912.
60. P. Biasi, P. Canu, F. Menegazzo, F. Pinna and T. O. Salmi, *Industrial & Engineering Chemistry Research*, 2012, **51**, 8883-8890.
61. S. Chinta and J. H. Lunsford, *Journal of Catalysis*, 2004, **225**, 249-255.
62. M. Piccinini, Cardiff University, 2011.
63. S. Melada, F. Pinna, G. Strukul, S. Perathoner and G. Centi, *Journal of Catalysis*, 2006, **237**, 213-219.

64. N. E. Ntainjua, M. Piccinini, J. C. Pritchard, J. K. Edwards, A. F. Carley, J. A. Moulijn and G. J. Hutchings, *ChemSusChem*, 2009, **2**, 575-580.
65. D. P. Dissanayake and J. H. Lunsford, *Journal of Catalysis*, 2002, **206**, 173-176.
66. D. P. Dissanayake and J. H. Lunsford, *Journal of Catalysis*, 2003, **214**, 113-120.
67. J. K. Edwards, J. Pritchard, M. Piccinini, G. Shaw, Q. He, A. F. Carley, C. J. Kiely and G. J. Hutchings, *Journal of Catalysis*, 2012, **292**, 227-238.
68. V. R. Choudhary and C. Samanta, *Journal of Catalysis*, 2006, **238**, 28-38.

- CHAPTER Six -

Conclusion and Future Work

6.1 Conclusion

The aim and objectives of this research and the topic of this thesis are set out in chapter one. The anthraquinone auto-oxidation (AO) process currently used for the production of hydrogen peroxide suffers from requiring large amounts of energy and a continuous refill of the organic solvents due to unwanted side reactions, which makes it only economically viable on a large scale. Solvay have outlined that if certain requirements are met (H_2 selectivity > 90 %; [H_2O_2] > 8 wt %) the direct process would be able to challenge the AO process and allow H_2O_2 to be produced on site where required. As discussed in chapter one, many important developments in the research of the direct H_2O_2 synthesis, since the first patent in 1914, have already been achieved by research groups worldwide.

In this thesis a number of aspects of the direct synthesis of H_2O_2 were studied, by looking at the design of the catalyst (chapter 3-4) and varying reaction conditions together with the reactor (chapter 5). Conclusions have been recorded at the end of each chapter. It can be seen that the percentage of hydrogen peroxide produced has varied dependent on the conditions. However, although the requirements outlined by Solvay have not been achieved, the advantage of direct H_2O_2 synthesis to industry, the economy and the environment is so important that further study of variations in heterogeneous catalysis is necessary.

Specific lines of research were undertaken in an attempt to establish the active site responsible for the synthesis, hydrogenation and decomposition of H_2O_2 and to produce higher H_2O_2 concentrations. The most important results achieved within this thesis are highlighted, in Table 6.1, followed by a discussion of the results and an outline of future work.

Table 6.1 – Important results gained from this thesis

Chapter	Catalyst[e]	Reaction time (min)	H_2 input (mmol)	H_2O_2 productivity ($mol_{H2O2}kg_{cat}^{-1}h^{-1}$)	H_2O_2 hydrogenation ($mol_{H2O2}kg_{cat}^{-1}h^{-1}$)	H_2O_2 concentration (wt%)	H_2 selectivity (%)
Literature[a1]	Au-Pd/C	30	4.5	110	110	0.22	80
3[a]	Au-Pd/AwC[2]	30	4.5	160	**0**	0.32	-
3[a]	Au-Pd/AwC	30	4.5	126	**0**	0.252	-
4[a]	Au-Pd/C[f]	30	4.5	100	672	0.2	-
5[b]	Au-Pd/C	30	5.43	7	high[g]	0.8	-
5[c]	$AuPdPt/CeO_2$	150	5.43 x 5	8	high[g]	**3.2**	-
5[d]	Au-Pd/C	30	9.5	**310**	-	0.62	56
5[d]	Au-Pd/C	120	38	124	-	**1.0**	25

[a] Standard batch conditions – 10 mg catalyst, 2 ^oC, 580 psi, 5 $\%H_2/CO_2$ + 25 $\%O_2/CO_2$, H_2/O_2 = 0.525, 5.6 g CH_3OH + 2.9 g H_2O, 1200 rpm

[b] Biphasic solvent – 10 mg catalyst, 25 ^oC, 700 psi, 5 $\%H_2/CO_2$ + 25 $\%O_2/CO_2$, H_2/O_2 = 0.525, 3.84 g decan-1-ol + 0.16 g H_2O, 1200 rpm

[c] Reagent gases re-charged 5 times, biphasic solvent – 50 mg catalyst, 25 ^oC, 700 psi, 5 $\%H_2/CO_2$ + 25 $\%O_2/CO_2$, H_2/O_2 = 0.525, 3.84 g decan-1-ol + 0.16 g H_2O, 1200 rpm

[d] Semi-continuous flow reactor - 20 mg catalyst, 2 ^oC, 580 psi, total flow = 201 ml min^{-1}, 3.5 % H_2 + 7 $\%O_2$ + 89.5 $\%N_2$, H_2/O_2 = 0.5, 17 g CH_3OH, 1200 rpm

[e] Catalysts prepared by impregnation; Au-Pd = 2.5 %Au-2.5 %Pd, AuPdPt = 0.2 wt% Au-0.2 wt% Pt- 4.6 wt% Pd, AwC = acid-washed carbon.

[f] 2.5 %Au- 2.5 %Pd catalyst prepared by physical grinding

[g] Presumed based on initial results in section 5.4.

In Chapter Three two ways to turn off a Au-Pd/C supported catalyst's activity towards H_2O_2 hydrogenation/decomposition under standard reaction conditions have been discussed. Firstly, preceding acid washing the support and deposition of Au-Pd by impregnation a calcination of 400 ^oC for 3 h in static air is required. Higher activity was achieved with lower calcination temperature, but catalysts were unstable. Extensive characterisation by XPS of the series of catalysts calcined at different temperatures identified that the oxidation state of Pd maybe a crucial feature in achieving zero hydrogenation activity. In order to study this aspect further a number of controlled reduction and oxidation heat treatments were run. It was found that a sequential reduction (200 ^oC, 2 h) and oxidation (300 ^oC, 3 h) of a calcined Au-Pd/AwC catalyst also led to the switching off the hydrogenation pathway. This was linked to the formation of increased PdO on the surface isolating a minimum content of active Pd^0. Extended studies showed the presence of gold and acid-washing the carbon support, prior to deposition of the metals, are crucial features to switching off H_2O_2 hydrogenation. This goes some way to identifying what components of the catalyst are required in order to produce H_2O_2 without subsequent H_2O_2 hydrogenation and decomposition. This could be considered critical in future when designing catalysts to produce high H_2O_2 concentrations at high H_2 selectivities.

The presence of chloride on the surface even after extensive heat treatments, as shown in chapter 3, led to research into the effect of surface chloride. In current literature it has been shown a low concentration of halide has a beneficial effect on H_2 selectivity leading to greater H_2O_2 productivities. However, the presence of halide in the reaction medium is not ideal for industry and attempts to incorporate halide into a catalyst before or after metal deposition has proved unsuccessful, destabilising the supported metal. In Chapter Four, a very active stable catalyst produced for direct H_2O_2 synthesis, which contained no halide, was achieved by physical grinding metal acetates with a support and heated to produce the metal. The simple physical grinding technique produced small < 10 nm Au-Pd alloy particles and would be easily scalable for industrial use. The drawback of these materials was the 'wasted' metal in the form of large > 10 nm inactive particles and small non-alloyed particles as well as their high hydrogenation activities. At the end of the chapter it has been shown incorporating chloride into the physical grinding material led to a lowering of the hydrogenation activity. It is recommended future work concentrates on reducing the hydrogenation activity and using Au-Pd more efficiently without compromising the catalysts activity.

The potential of the batch reactor setup has previously been extensively examined by Picinini *et al.* using Au-Pd/TiO_2[3] and Au-Pd/C[4] by changing all reaction variables. However, methanol-water was used and is generally the solvent of choice in the literature. The potential of using a biphasic system of decan-1-ol and water is the decan-1-ol produces the H_2O_2 and the water extracts the H_2O_2 *in-situ* as outlined in chapter 5. The organic solvent retains the catalyst, serving to protect the H_2O_2 from decomposition /hydrogenation activity. It has been shown that at the saturation point when the solvent goes from one to two phases the highest H_2O_2 concentration is produced. The potential of this system has been examined by altering reaction variables to achieve the greatest H_2O_2 concentration possible with a Au-Pd/C catalyst. H_2O_2 concentrations approximately 8x higher were achieved than when reaction variables were not optimised. This has been extended by using the most active catalysts produced thus far, tri-metallic Au-Pd-Pt/CeO_2, where a H_2O_2 concentration of > 3 wt% was produced after reagent reloading. This value is closer to the 8 wt% industrial target set by Solvay®; however using the current reactor design H_2 selectivities were not measured. In the early stages of the research it was shown that H_2O_2 hydrogenation activities are high which in future will need to be investigated further.

Due to the promising results of reagent reloading in a batch reactor a semi-continuous flow reactor was set up as described in the latter part of Chapter Five. The flowing of reagent gases enables the pressure and maybe more importantly the H_2 concentration to be maintained throughout the reaction. Not only does this set-up allow the H_2 selectivities to be measured, it also proved to enhance the H_2O_2 concentration. Within this research Karl-Fischer titration was used to determine the water content proceeding reaction. A H_2O_2 concentration of 1 wt% was achieved with a standard Au-Pd/C catalyst, which is significantly higher than in the batch reactor (0.22 wt%) under standard conditions highlighted the potential of the flow reactor. The semi-continuous flow results indicated that a large excess of water was being produced over extended reaction time, this and the stability of the catalyst require further investigation. This study should be extended in order to provide a more in-depth understanding of the direct H_2O_2 synthesis using a larger set of catalysts.

Hopefully once greater understanding and refinement of the biphasic solvent system, described in the first part of Chapter Five, is achieved the semi-continuous flow reactor or a reactor based on it will provide the means to produce higher H_2O_2 concentrations. In future flow of both the gases and the solvent may be required. Interesting results using such a set up have already been achieved by some research groups.[5-11]

6.2 Future Work

A great deal of work prior to and throughout this thesis has involved solving the selectivity problem of H_2O_2 synthesis, which requires switching off catalyst activity towards the H_2O_2 hydrogenation and decomposition pathways. This would in turn allow for a greater H_2O_2 concentration to be produced. Although as concluded in chapter three this has been achieved under standard batch reaction conditions it is recommended further work concentrates on this particular problem under the various conditions used in the preceding chapters. To begin this study a greater understanding of the H_2 selectivity for a larger set of catalysts is required. This may be achieved by either online gas analysis, using the semi-continuous flow reactor outlined in the latter sections of Chapter Five, or by recording the water concentration before and after reaction using Karl Fischer titration.

Catalyst Design

- Detailed XPS analysis of a larger set of catalysts – Comparing characterisation results from chapter three with a larger number of catalysts prepared by different techniques and/or on various supports would give greater understanding/confirmation of the active components required for H_2O_2 synthesis and hydrogenation.
- Use metal more efficiently - Increase level of dispersion of larger >10 nm particles and achieve greater alloying of small particles. For physical grinding catalysts this may be achieved by altering the heat treatment conditions for example heating rate, heat treatment time or flow of inert gas or through the use of a ball mill. The latter would also allow the technique to be readily scalable for industrial use.
- Oxidation state of the Pd – A detailed investigation starting from a halide-free catalyst as outlined in chapter Four will allow greater understanding without halide being a factor. XPS data showed the majority of Pd, in physical grinding catalysts, was in the metallic state whereas Chapter Three showed a PdO state would be more selective to H_2O_2 production.
- Further investigation of halide addition – Addition of further halide to physical grinding catalysts may be required to lower the H_2O_2 hydrogenation. This investigation will give greater insight into the role of halide in direct H_2O_2 synthesis.

- Stability of the catalyst – The stability of using physical grinding to produce a Au-Pd/Ce_{O2} catalyst has been highlighted as an issue and investigation may lead to greater understanding of the preparation technique. The stability of ALL catalysts over extended reaction time and under more abrasive conditions requires investigation.
- The use of cheaper metals – Cheaper alternative metals, to replace gold and/or palladium, may prove to be more suitable for industrial use.

Biphasic Solvent System

- Hydrophilicity of the catalyst – a greater hydrophilicity will allow more of the catalyst to be retained in the organic phase throughout the reaction.
- Organic Solvent – A detailed investigation into the organic solvent in order to achieve greater H_2 dissolution and catalyst retention whilst still possessing low water solubility.
- Au-Pd(-Pt) particle compositions - It was noted that catalysts with higher Pd contents produced higher H_2O_2 concentration. Further investigation into ratios between the metals and their preparation will give greater understanding of the catalyst activity in order to achieve higher H_2O_2 concentrations.
- Reactor design – Investigation into the reactor design may allow for H_2O_2 to be produced at a higher concentration with greater selectivity. This maybe along the lines of the semi-continuous flow reactor outlined in the latter part of Chapter Five, as reagent reloading has already been shown to be beneficial.

If the hydrogenation/decomposition pathways cannot be switched off, a thorough investigation of *in-situ* H_2O_2 utilisation in a target reaction such as benzyl alcohol oxidation is recommended. To start such an investigation, knowledge of a materials activity towards H_2O_2 decomposition is desired. Although the H_2O_2 decomposition pathway is generally undesired for direct H_2O_2 synthesis, recent research has focussed on producing H_2O_2 *in-situ* for utilisation in oxidation reactions[12-14]. In this case H_2O_2 decomposition would be beneficial by activating the produced hydrogen peroxide in order to react further. Decomposition of hydrogen peroxide is a widely studied reaction, and a number of studies have been performed on the decomposition catalysed by palladium on a variety of supports[15-21]. However further investigation is required under the reaction conditions used in this thesis.

It has been a privilege to make a small contribution to hopefully an eventual successful outcome of further research. It is hoped that the work described in this thesis will provide a basis and prove to be helpful for anyone continuing studies in catalysis and the direct H_2O_2 synthesis.

References

1. J. K. Edwards, A. F. Carley, A. A. Herzing, C. J. Kiely and G. J. Hutchings, *Faraday Discussions*, 2008, **138**, 225-239.
2. J. K. Edwards, B. Solsona, E. N. N, A. F. Carley, A. A. Herzing, C. J. Kiely and G. J. Hutchings, *Science*, 2009, **323**, 1037-1041.
3. M. Piccinini, E. Ntainjua N, J. K. Edwards, A. F. Carley, J. A. Moulijn and G. J. Hutchings, *Physical Chemistry Chemical Physics*, 2010, **12**, 2488-2492.
4. M. Piccinini, J. K. Edwards, J. A. Moulijn and G. J. Hutchings, *Catalysis Science & Technology*, 2012, **2**, 1908-1913.
5. Y. Voloshin, R. Halder and A. Lawal, *Catalysis Today*, 2007, **125**, 40-47.
6. Y. Voloshin and A. Lawal, *Chemical Engineering Science*, 2010, **65**, 1028-1036.
7. Y. Voloshin and A. Lawal, *Applied Catalysis A: General*, 2009, **353**, 9-16.
8. T. Inoue, M. A. Schmidt and K. F. Jensen, *Industrial & Engineering Chemistry Research* , 2007, **46**, 1153-1160.
9. T. Inoue, K. Ohtaki, Y. Kikutani, K. Sato, M. Nishioka, S. Hamakawa, K. Mawatari, F. Mizukami and T. Kitamori, *Chemistry Letters*, 2009, **38**, 820-821.
10. X. Wang, Y. Nie, J. L. C. Lee and S. Jaenicke, *Applied Catalysis A: General*, 2007, **317**, 258-265.
11. J. F. Ng, Y. Nie, G. K. Chuah and S. Jaenicke, *Journal of Catalysis*, 2010, **269**, 302-308.
12. T. V. Choudhary and D. W. Goodman, *Topics in Catalysis*, 2002, **21**, 25-34.
13. G. Blanco-Brieva, M. C. Capel-Sanchez, M. P. de Frutos, A. Padilla-Polo, J. M. Campos-Martin and J. L. G. Fierro, *Industrial & Engineering Chemistry Research*, 2008, **47**, 8011-8015.
14. G. Li, J. Edwards, A. F. Carley and G. J. Hutchings, *Catalysis Communications*, 2007, **8**, 247-250.
15. V. R. Choudhary, S. D. Sansare and A. G. Gaikwad, *Catalysis Letters*, 2002, **84**, 81-87.
16. V. R. Choudhary, C. Samanta and P. Jana, *Applied Catalysis a-General*, 2007, **332**, 70-78.
17. V. R. Choudhary and C. Samanta, *Journal of Catalysis*, 2006, **238**, 28-38.
18. T. Moreno, J. García-Serna and M. J. Cocero, *The Journal of Supercritical Fluids*, 2011, **57**, 227-235.
19. I. Huerta, J. García-Serna and M. J. Cocero, *The Journal of Supercritical Fluids*, 2012.
20. Y. Voloshin, J. Manganaro and A. Lawal, *Industrial & Engineering Chemistry Research*, 2008, **47**, 8119-8125.
21. V. R. Choudhary, C. Samanta and P. Jana, *Applied Catalysis A: General*, 2007, **317**, 234-243.